

Copyright  
by  
Hsin-Yang Chung  
2004

**The Dissertation Committee for Hsin-Yang Chung Certifies that this is the  
approved version of the following dissertation:**

**FATIGUE RELIABILITY AND OPTIMAL INSPECTION  
STRATEGIES FOR STEEL BRIDGES**

**Committee:**

---

Lance Manuel, Supervisor

---

Karl H. Frank, Co-Supervisor

---

Joseph A. Yura

---

Michael D. Engelhardt

---

Carlos Torres-Verdin

**FATIGUE RELIABILITY AND OPTIMAL INSPECTION  
STRATEGIES FOR STEEL BRIDGES**

**by**

**Hsin-Yang Chung, B.S., M.S.**

**Dissertation**

Presented to the Faculty of the Graduate School of

The University of Texas at Austin

in Partial Fulfillment

of the Requirements

for the Degree of

**DOCTOR OF PHILOSOPHY**

**The University of Texas at Austin**

**May 2004**

UMI Number: 3143672

Copyright 2004 by  
Chung, Hsin-Yang  
All rights reserved.

UMI<sup>®</sup>

---

UMI Microform 3143672

Copyright 2004 ProQuest Information and Learning Company.  
All rights reserved. This microform edition is protected against  
unauthorized copying under Title 17, United States Code.

---

ProQuest Information and Learning Company  
300 North Zeeb Road  
PO Box 1346  
Ann Arbor, MI 48106-1346

## **Dedication**

To My Family

## **Acknowledgements**

The author would like to express his deepest appreciation to Dr. Lance Manuel and Dr. Karl Frank for their guidance, advice and support during the course of this research. Special thanks are also due to Dr. Joseph Yura, Dr. Michael Engelhardt, and Dr. Carlos Torres-Verdin for their review and invaluable suggestions regarding this dissertation.

The author would also like to acknowledge the financial support received by way of a research assistantship that was funded by the Texas Department of Transportation (TxDOT) Project 0-2135: Guidelines for Inspection of Fracture-Critical Steel Trapezoidal Girders.

# **FATIGUE RELIABILITY AND OPTIMAL INSPECTION STRATEGIES FOR STEEL BRIDGES**

Publication No. \_\_\_\_\_

Hsin-Yang Chung, Ph.D.

The University of Texas at Austin, 2004

Supervisors: Lance Manuel and Karl H. Frank

Structural reliability techniques can be employed to evaluate the fatigue performance of fracture-critical members in steel bridges. In this dissertation, two fatigue reliability formulations that can be applied for most details in steel bridges are developed. For details classified according to AASHTO fatigue categories, a limit state function related to the number of stress cycles leading to failure based on Miner's rule is used; for details not classified according to AASHTO fatigue categories, a limit state function based on linear elastic fracture mechanics and expressed in terms of crack size and growth rate is employed.

With the application of fatigue reliability analysis, a procedure for inspection scheduling of steel bridges is developed to yield the optimal (most economical) inspection strategy that meets an acceptable safety level through the planned service life. This inspection scheduling problem is modeled as an optimization problem with an objective function that includes the total expected cost of inspection, repair, and failure

formulated using an event tree approach, with appropriate constraints on the interval between inspections, and a specified minimum acceptable (target) safety level. With the help of several illustrations, it is shown that an optimal inspection scheduling plan can thus be developed for any specified fatigue details or fracture-critical sections in steel bridges.

A second optimal inspection scheduling procedure is formulated that takes into consideration crack detectability (or quality) of alternative nondestructive inspection techniques. This procedure based on Monte Carlo simulation of crack growth curves yields an optimal inspection technique and associated schedule for a given fracture-critical member in a steel bridge for minimum cost and a target safety level while also taking into account probability of detection (POD) data for candidate nondestructive inspection techniques.

Comparisons between the reliability-based procedure and the POD-based procedure for optimal inspection scheduling are discussed. Both scheduling strategies, when contrasted with ad hoc periodic inspection programs for steel bridges, are recommended because they are rational approaches that consider the actual fatigue reliability of the bridge member and account for economy as well as safety.



## Table of Contents

List of Tables .....	xii
List of Figures .....	xiv
Chapter 1: INTRODUCTION.....	1
1.1 RESEARCH BACKGROUND .....	1
1.2 RESEARCH OBJECTIVES AND SCOPE .....	4
1.3 ORGANIZATION .....	6
Chapter 2: LITERATURE REVIEW AND BACKGROUND ON METHODS FOR FATIGUE ANALYSIS .....	8
2.1 LITERATURE REVIEW .....	8
2.1.1 Fatigue Reliability Analysis.....	8
2.1.2 Reliability-Based Fatigue Inspection Scheduling.....	12
2.2 STRUCTURAL RELIABILITY ANALYSIS.....	16
2.2.1 Limit State Function .....	16
2.2.2 A Simple Load and Resistance Model.....	18
2.2.3 Reliability Index and Probability of Failure .....	20
2.2.3.1 First-Order Reliability Method (FORM) .....	21
2.2.3.2 Monte Carlo Simulation.....	22
2.3 DETERMINISTIC FATIGUE ANALYSIS FOR STEEL BRIDGES ...	24
2.3.1 Stress-Based Approach (S-N Curve Approach) .....	24
2.3.1.1 AASHTO LRFD Fatigue Design Specifications .....	28
2.3.1.2 The Fatigue Evaluation Model proposed by Moses et al. ....	30
2.3.2 Strain-Based Approach .....	33
2.3.3 Linear Elastic Fracture Mechanics (LEFM) Approach .....	34
2.4 CONCLUDING REMARKS.....	37

Chapter 3: MODELS FOR FATIGUE LOADING IN STEEL BRIDGES .....	38
3.1 INTRODUCTION .....	38
3.2 STRESS SPECTRUM ANALYSIS .....	39
3.3 ASSUMED DISTRIBUTION ANALYSIS.....	42
3.3.1 Rayleigh Distribution Analysis.....	42
3.3.2 Weibull Distribution Analysis .....	44
3.3.3 Beta Distribution Analysis.....	45
3.3.4 Polynomial Distribution.....	46
3.3.4 Lognormal Distribution .....	47
3.4 FATIGUE TRUCK ANALYSIS .....	48
3.4.1 Schilling’s Fatigue Truck Model .....	51
3.4.2 AASHTO Fatigue Truck Model .....	51
3.4.3 Moses’ Fatigue Truck Model.....	52
3.4.4 Laman’s Dual Fatigue Truck Model.....	54
3.5 CONCLUDING REMARKS.....	55
Chapter 4: FATIGUE RELIABILITY ANALYSIS FOR FRACTURE- CRITICAL MEMBERS IN STEEL BRIDGES .....	57
4.1 TARGET RELIABILITY .....	58
4.2 AASHTO FATIGUE RELIABILITY APPROACH.....	60
4.2.1 Limit State Function .....	60
4.2.2 Studies of Related Variables in the Limit State Function.....	62
4.2.2.1 Fatigue Detail Parameter, $A$ .....	62
4.2.2.2 Miner’s Critical Damage Accumulation Index, $\Delta$ .....	64
4.2.2.3 Accumulated Number of Stress Cycles, $N$ , and Number of Years in Service, $Y$ .....	64
4.2.3 Evaluation of the Fatigue Reliability Index, $\beta$ .....	66
4.2.4 Selection of the Target Reliability Index, $\beta_{\text{target}}$ .....	73
4.2.5 Example Study – Yellow Mill Pond Bridge .....	76
4.3 LEFM FATIGUE RELIABILITY APPROACH.....	80
4.3.1 Limit State Function .....	80
4.3.2 Studies of Related Variables in the Limit State Function.....	84

4.3.2.1 Initial Crack Size, $a_0$ .....	84
4.3.2.2 Critical Crack Size, $a_c$ .....	87
4.3.2.3 Fatigue Crack Growth Parameters, $C$ and $m$ .....	88
4.3.3 Evaluation of Fatigue Reliability .....	93
4.3.4 Example .....	94
4.4 SUMMARY .....	99
Chapter 5: RELIABILITY-BASED FATIGUE INSPECTION SCHEDULING FOR STEEL BRIDGES .....	103
5.1 INTRODUCTION .....	103
5.2 EVENT TREE ANALYSIS .....	107
5.3 LIKELIHOOD OF NEEDED REPAIR .....	110
5.3.1 AASHTO Approach .....	110
5.3.2 LEFM Approach .....	112
5.3.3 Repair Realizations in the Event Tree .....	113
5.4 COST FUNCTION .....	113
5.4.1 Cost of Inspections .....	114
5.4.2 Cost of Repairs .....	114
5.4.3 Cost of Failure .....	115
5.4.4 Total Cost .....	116
5.5 CONSTRAINTS .....	116
5.6 FORMULATION OF THE OPTIMIZATION PROBLEM .....	117
5.7 NUMERICAL EXAMPLES .....	118
5.7.1 Plate Girder Bridge Example .....	118
5.7.2 Box Girder Bridge Example .....	126
5.8 CONCLUDING REMARKS .....	143
CHAPTER 6: POD-BASED SELECTION OF NONDESTRUCTIVE INSPECTION TECHNIQUES FOR STEEL BRIDGES .....	146
6.1 INTRODUCTION .....	146
6.2 PROBABILITY OF DETECTION .....	147
6.2.1 Hit/Miss Method .....	149
6.2.2 Signal Response Method .....	150

6.3 FATIGUE CRACK GROWTH MODEL .....	152
6.4 SIMULATION OF CRACK PROPAGATION AND INSPECTION SCENARIOS .....	153
6.5 OPTIMAL NDI TECHNIQUE.....	159
6.5.1 Cost Function.....	159
6.5.2 Optimization Variables .....	161
6.5.3 Constraints .....	162
6.5.4 Formulation of Optimization Problem.....	162
6.6 NUMERICAL EXAMPLES.....	165
6.6.1 Box-Girder Example I.....	165
6.6.2 Box-Girder Example II .....	180
6.7 SUMMARY .....	184
Chapter 7: SUMMARY AND CONCLUSIONS .....	187
Appendix A.....	193
A.1 DERIVED PROBABILITY DISTRIBUTIONS FOR A FUNCTION OF RANDOM VARIABLES.....	193
Appendix B.....	195
B.1 RACKWITZ-FIESSLER ALGORITHM IN THE FIRST-ORDER RELIABILITY METHOD.....	195
Appendix C.....	197
C.1 RAINFLOW COUNTING METHOD FOR STRESS CYCLES .....	197
References.....	200
Vita .....	212

## List of Tables

Table 2.1:	Some Typical Values of Probability of Failure, $P_F$ , and Corresponding Reliability Index Values, $\beta$ .....	20
Table 2.2:	Fatigue Detail Constant, $A$ , and Fatigue Threshold, $(\Delta F)_{th}$ .....	29
Table 2.3:	Fraction of Truck Traffic in a Single Lane, $p$ .....	29
Table 2.4:	Number of Stress Range Cycles per Truck Passage, $C_s$ .....	30
Table 2.5:	Detail Constant, $K$ , and Limiting Stress Range, $S_{FL}$ , in the Model of Moses et al. (1987).....	32
Table 4.1:	Target Reliability Index Values for North Sea Jacket Structures (Onoufriou, 1999) .....	59
Table 4.2:	Regression Coefficients of the Fatigue Detail Parameter, $A$ , and Slope, $m$ .....	63
Table 4.3:	Mean Value, Standard Deviation, and Coefficient of Variation for the Fatigue Detail Parameter, $A$ .....	64
Table 4.4:	Pertinent Variables in the Three ADTT Models.....	72
Table 4.5:	Comparison of the Number of Stress Cycles ( $N_{target}$ ) until the Target Reliability is Reached with the AASHTO LRFD Fatigue Life ( $N_{LRFD}$ ) for Various Stress Ranges ( $S_R$ ) – Category E' Details.....	75
Table 4.6:	Fatigue Geometry Functions for some Common Details in Steel Bridges .....	83
Table 4.7:	Initial Crack Size Distributions from Various Sources.....	86
Table 4.8:	Fracture Toughness Statistics for A36, A588, and A514 Steels (Albrecht et al., 1986).....	88

Table 4.9:	Fatigue Crack Growth Parameter Statistics for Various Steels. ....	91
Table 4.10:	Fatigue Crack Propagation Parameter Statistics for Offshore Steels.....	92
Table 4.11:	Estimates of Mean and COV of $C$ and $m$ from Various References.	93
Table 5.1:	Three Inspection Schedules for an Example Detail.....	105
Table 5.2:	Related Random Variables for Center Crack in Bottom Flange.....	127
Table 6.1:	Four Possible Outcomes of NDI.....	148
Table 6.2:	POD Functions for Penetrant, Magnetic Particle, and Ultrasonic Inspections. ....	167
Table 6.3:	Optimal Results for the UI, MI and PI Techniques with the Constraint, $P_{nd,max} = 0.005$ . ....	174
Table A.1	Basic Random Variable Transformations for $Y = g(\mathbf{X})$ . ....	193

## List of Figures

Figure 2.1: Statistical Distributions of $R$ , $S$ , and $g(R,S)$ . .....	19
Figure 2.2: Illustration of the First-Order Reliability Method (FORM). .....	22
Figure 2.3: Flow Chart of Monte Carlo Simulation Method.....	23
Figure 2.4: Schematic S-N Diagram for a Typical Detail in the AASHTO Specifications (1990). .....	26
Figure 2.5: Schematic Strain-Life Curve.....	34
Figure 2.6: Crack Growth Rate versus Stress Intensity Factor Range. ....	36
Figure 3.1: Flow Chart of Equivalent Fatigue Truck Analysis for Steel Bridges. ....	50
Figure 3.2: Schilling's Fatigue Truck Model. ....	51
Figure 3.3: The AASHTO Fatigue Truck Model. ....	52
Figure 3.4: Moses' Fatigue Truck Model.....	53
Figure 3.5: The Laman's Three-Axle Fatigue Truck Model.....	55
Figure 3.6: The Laman's Four-Axle Fatigue Truck Model.....	55
Figure 4.1: Fatigue Reliability for Category A Details under Various Stress Range Levels. ....	69
Figure 4.2: Fatigue Reliability for Category C Details under Various Stress Range Levels. ....	69
Figure 4.3: Fatigue Reliability for Category E Details under Various Stress Range Levels. ....	70
Figure 4.4: Fatigue Reliability for a Category E Detail with $S_R = 5$ ksi based on Three Different ADTT Modeling Assumptions.....	71

Figure 4.5: Comparison of the Constant ADTT Model ( $ADTT=300$ ) with the ADTT Growth Model ( $ADTT_0=72, r = 5\%$ ).....	72
Figure 4.6: Comparison of the Number of Stress Cycles ( $N_{target}$ ) until the Target Reliability is reached with the AASHTO LRFD Fatigue Life (Category E' Details, with $S_R = 3$ ksi).....	75
Figure 4.7: Plan, Elevation, and Typical Cross Section of the Yellow Mill Pond Bridge (Fisher, 1984).....	77
Figure 4.8: Fatigue Cracks at Cover Plate Details in the Yellow Mill Pond Bridge (Fisher, 1984).....	77
Figure 4.9: The Chosen Cover Plate Detail for Analysis.....	78
Figure 4.10: Fatigue Reliability of a Cover Plate Detail in the Yellow Mill Pond Bridge.....	79
Figure 4.11: Elevation and Cross Section of the Lafayette Street Bridge (Fisher, 1984).....	95
Figure 4.12: Fatigue Crack in the Gusset Plate-Transverse Stiffener Detail (Fisher, 1984).....	95
Figure 4.13: The Gusset Plate-Transverse Stiffener Detail.....	96
Figure 4.14: Fatigue Reliability of Gusset Plate-Transverse Stiffener Detail with an Initial Crack Size, $a_0$ , of 0.39 in.....	98
Figure 4.15: Fatigue Reliability of Gusset Plate-Transverse Stiffener Detail with a Lognormal Initial Crack Size, $a_0$ , with a mean of $3.937 \times 10^{-3}$ in. and a COV of 0.2.....	98
Figure 4.16: Flow Chart for the AASHTO Fatigue Reliability Analysis Approach.....	101
Figure 4.17: Flow Chart for the LEFM Fatigue Reliability Analysis Approach.....	102
Figure 5.1: Fatigue Reliability for Three Illustrative Inspection Schedules.....	105



Figure 5.2: Representative Event Tree showing Inspection and Repair Realizations..	109
Figure 5.3: Brazos River Bridge showing (a) entire bridge in elevation; (b) a typical transverse section; and (c) a detail of interest for fatigue reliability.....	119
Figure 5.4: Fatigue Reliability of the chosen Category E Detail over 50 years.....	120
Figure 5.5: Optimal total cost as a function of the number of inspections for the chosen detail ( $K_I : K_R : K_F = 1 : 1.3 \times 10^2 : 4 \times 10^5$ ).....	122
Figure 5.6: Optimal inspection schedule ( $T_{min} = 0.5$ yrs, $T_{max} = 2$ yrs) for the repair cost case of $K_I : K_R : K_F = 1 : 1.3 \times 10^2 : 4 \times 10^5$ , $C_T = 162.7$ .....	122
Figure 5.7: Optimal inspection schedule ( $T_{max}$ unbounded) for the repair cost case of $K_I : K_R : K_F = 1 : 1.3 \times 10^2 : 4 \times 10^5$ , $C_T = 157.6$ .....	123
Figure 5.8: Optimal inspection schedule ( $T_{min} = 0.5$ yrs, $T_{max} = 2$ yrs) for the repair cost case of $K_I : K_R : K_F = 1 : 2.6 \times 10^2 : 4 \times 10^5$ , $C_T = 200.5$ .....	124
Figure 5.9: Optimal Inspection Schedule ( $T_{max}$ unbounded) for the repair cost case of $K_I : K_R : K_F = 1 : 2.6 \times 10^2 : 4 \times 10^5$ , $C_T = 195.0$ .....	125
Figure 5.10: Center-Notched Crack in the Box Girder Bridge Example. ....	126
Figure 5.11: Fatigue Reliability of the Detail with Center-Notched Crack over 80 years.....	127
Figure 5.12: Optimal Inspection Schedules with $T_{max} = 2$ yrs ( $C_T = 35.7$ ) and with unbounded $T_{max}$ ( $C_T = 19.3$ ) for Case (i): $K_I : K_R : K_F = 1 : 1 \times 10^1 : 1 \times 10^5$ .....	129
Figure 5.13: Optimal Inspection Schedules with $T_{max} = 2$ yrs ( $C_T = 59.0$ ) and with unbounded $T_{max}$ ( $C_T = 29.1$ ) for Case (ii): $K_I : K_R : K_F = 1 : 2 \times 10^1 : 1 \times 10^5$ .....	130
Figure 5.14: Costs of Various Optimized Inspection Schedules with $T_{max} = 2$ yrs for Case (i): $K_I : K_R : K_F = 1 : 1 \times 10^1 : 1 \times 10^5$ .....	132

Figure 5.15: Costs of Various Optimized Inspection Schedules with $T_{max} = 2$ yrs for Case (ii): $K_I : K_R : K_F = 1 : 2 \times 10^1 : 1 \times 10^5$ .....	132
Figure 5.16: Optimal Inspection Schedules with $T_{max} = 2$ yrs ( $C_T = 38.7$ ) and with unbounded $T_{max}$ ( $C_T = 26.4$ ) for Case (iii): $K_I : K_R : K_F = 1 : 1 \times 10^1 : 2 \times 10^5$ .....	133
Figure 5.17: Costs of Various Optimized Inspection Schedules with $T_{max}$ unbounded for Case (i): $K_I : K_R : K_F = 1 : 1 \times 10^1 : 1 \times 10^5$ .....	135
Figure 5.18: Costs of Various Optimized Inspection Schedules with $T_{max}$ unbounded for Case (iii): $K_I : K_R : K_F = 1 : 1 \times 10^1 : 2 \times 10^5$ .....	135
Figure 5.19: Fatigue Reliability for Various ADTT Models.....	136
Figure 5.20: Optimal Schedules with Constant and Lognormal ADTT Models.....	137
Figure 5.21: Costs of Various Optimized Inspection Schedules with $T_{max} = 2$ yrs with a Lognormal ADTT Model (mean=300 and COV=0.3).....	138
Figure 5.22: Normalized Costs for the Optimal Schedules with Various Lognormal ADTT Models.....	139
Figure 5.23: Optimal Total Cost as a Function of the Number of Inspections for the Butt-Welded Detail when $\beta_{target} = 3.7$ or $4.2$ for Case (i): $K_I : K_R : K_F = 1 : 1 \times 10^1 : 1 \times 10^5$ .....	141
Figure 5.24: Optimal Inspection Schedules with $\beta_{target} = 4.2$ ( $C_T = 22.3$ ) and with $\beta_{target} = 3.7$ ( $C_T = 19.3$ ) for Case (i): $K_I : K_R : K_F = 1 : 1 \times 10^1 : 1 \times 10^5$ .....	142
Figure 6.1: Probability of Detection Function, $POD(a)$ , Calculation in Signal Response Method (Berens, 1989).....	151
Figure 6.2: Probability of Detection Mapping. ....	153
Figure 6.3: Crack Growth Curves from Monte Carlo Simulations. ....	155
Figure 6.4: Crack Growth Models for $y_{cr} \leq y_1$ and $y_{cr} > y_1$ . ....	156

Figure 6.5: Monte Carlo Simulation Scenarios.....	158
Figure 6.6: Flow Chart of Optimization Procedure.....	164
Figure 6.7: Detail in the Fracture-Critical Member of the Box Girder Bridge. ....	166
Figure 6.8: Probability of Detection (POD) Curves for Penetrant, Magnetic Particle, and Ultrasonic Inspections.....	167
Figure 6.9: Probability Distribution of Time to Failure, $Y_{cr}$ , from 0 to 250 Years.....	168
Figure 6.10: Crack Growth Simulations (350 simulations; $a_{cr} = 2$ in.).....	169
Figure 6.11: Costs of Ultrasonic Inspections for Various Fixed-Interval Schedules for $K_{I,UI} : K_F = 1.5 : 2 \times 10^4$ .....	171
Figure 6.12: Costs of Magnetic Particle Inspections for Various Fixed-Interval Schedules for $K_{I,MI} : K_F = 1.2 : 2 \times 10^4$ .....	172
Figure 6.13: Costs of Penetrant Inspections for Various Fixed-Interval Schedules for $K_{I,PI} : K_F = 1.0 : 2 \times 10^4$ .....	172
Figure 6.14: Expected Probabilities of Failing to Detect the Growing Crack, $E(P_{nd})$ , for the UI, MI and PI Techniques Compared with the Maximum Acceptable Probability of Non-Detection, $P_{nd,max}$ .....	173
Figure 6.15: Cost Comparison of UI, MI and PI in Various Fixed-Interval Schedules for $K_{I,PI} : K_{I,MI} : K_{I,UI} : K_F = 1.0 : 1.2 : 1.5 : 2 \times 10^4$ with the Constraint, $P_{nd,max} = 0.005$ .....	173
Figure 6.16: Cost Comparison of UI, MI and PI in Various Fixed-Interval Schedules for $K_{I,PI} : K_{I,MI} : K_{I,UI} : K_F = 1.0 : 1.2 : 1.5 : 2 \times 10^4$ and with the Constraint $P_{nd,max} = 0.001$ .....	175
Figure 6.17: Costs of Ultrasonic Inspections for Various Fixed-Interval Schedules for $K_{I,UI} : K_F = 1.5 : 4 \times 10^4$ .....	176

Figure 6.18: Costs of Magnetic Particle Inspections for Various Fixed-Interval Schedules for $K_{I,MI} : K_F = 1.2 : 4 \times 10^4$ .....	177
Figure 6.19: Costs of Penetrant Inspections for Various Fixed-Interval Schedules for $K_{I,MI} : K_F = 1.2 : 4 \times 10^4$ .....	177
Figure 6.20: Cost Comparison of UI, MI and PI in Various Fixed-Interval Schedules for $K_{I,PI} : K_{I,MI} : K_{I,UI} : K_F = 1.0 : 1.2 : 1.5 : 4 \times 10^4$ with the Constraint $P_{nd \max} = 0.005$ .....	178
Figure 6.21: Cost Comparison of UI, MI and PI in Various Fixed-Interval Schedules for $K_{I,PI} : K_{I,MI} : K_{I,UI} : K_F = 1.0 : 1.2 : 1.5 : 4 \times 10^4$ with the Constraint $P_{nd \max} = 0.001$ .....	178
Figure 6.22: Total Costs of Various Fixed-Interval Schedules using the Reliability-Based Scheduling Method ( $K_{I,UI} : K_R : K_F = 1.5 : 10 : 10^5$ ).....	181
Figure 6.23: Total Cost Comparison of UI, MI and PI in Various Fixed-Interval Schedules using the POD-Based Scheduling Method for $K_{I,PI} : K_{I,MI} : K_{I,UI} : K_F = 1.0 : 1.2 : 1.5 : 10^5$ with the Constraint, $P_{nd \max} = 0.005$ .....	182
Figure C.1 Rainflow Counting Method for a Variable-Amplitude Stress History (Hoadley et al., 1982).....	198
Figure C.2 Modified Rainflow Counting Method for a Variable-Amplitude Stress History (Hoadley et al., 1982).....	199

## **Chapter 1: INTRODUCTION**

### **1.1 RESEARCH BACKGROUND**

Fatigue is one of the main forms of deterioration and can, potentially, be a failure mode in metal structures and mechanical systems. The American Society of Civil Engineers (ASCE) Committee on Fatigue and Fracture Reliability (1982) emphasized that 80-90% of failures in metallic structures are related to fatigue and fracture. In steel bridge engineering, fatigue problems caught the public's attention due to the unexpected collapse and fracture of the King's Bridge in Melbourne, Australia (1962), the Point Pleasant Bridge in West Virginia (1967) and the Yellow Mill Pond Bridge in Connecticut (1976). The failures of these bridges were all related to fatigue and caused great losses. Hence, in the United States, extensive fatigue tests were carried out in the 1960s and 1970s for various categories of details in steel bridges to establish stress range-fatigue life (S-N) relationships that form the basis for fatigue design. The derived S-N curves have been adopted in the present AASHTO fatigue specifications, and have become the foundation for the commonly used deterministic approach for estimating fatigue lives for details in steel bridges. It should be noted that significant variability is seen in the acquired fatigue life data used to establish the S-N curve for each AASHTO fatigue category. In fact, because of this variability, each AASHTO S-N curve corresponds to a conservative level where there is a 95% confidence of survival of at least 95% of all details in the corresponding category. It is not surprising too that the fatigue life evaluation of a detail based on the AASHTO S-N curves can often be considerably different from the actual realized fatigue life. In addition, the randomness of the nature of vehicle-induced fatigue loading, the variability in the make-up of the truck traffic, the

different environmental conditions as well as several other external factors increase the uncertainty in predictions of fatigue life.

The fatigue life calculation method proposed by Moses et al. (1987) and adopted in the AASHTO Guide Specifications for Fatigue Evaluation of Existing Steel Bridges (1990) is the most prevalent method of fatigue life evaluation in bridge engineering in the United States today. However, experience has shown that this fatigue life calculation method based on the AASHTO S-N curves often yields a conservative evaluation of the fatigue life for a detail. Combined with Paris' law, the linear elastic fracture mechanics (LEFM) method can be employed to develop an alternative deterministic approach for fatigue life evaluation. Due to the uncertainties in initial crack size estimation, material properties, detail geometry modeling, truck traffic, fatigue loading and other factors, the LEFM-based deterministic approach also has its own limitations in fatigue life evaluation. In summary, fatigue is a phenomenon that is very complex and subject to a great deal of uncertainty. The uncertainties introduced due to external factors, such as fatigue loading and environmental conditions, and internal factors such as the fatigue capacity of details make deterministic fatigue analyses less reliable in estimating the fatigue lives of details in steel bridges.

A program of regular inspection of bridges is the most effective way of preventing details susceptible to fatigue from bringing about failures. Such a program, though, demands experience and knowledge of the various inspection techniques and of the fatigue behavior of the detail in question. Deterministic fatigue approaches can provide only very limited information for cost-effective bridge inspections and scheduling strategies. In addition to actually aiding in the calculation of the fatigue life of a detail, the fatigue reliability approach can provide a useful index which quantifies the safety level of the detail. This index accounts for external and internal uncertainties that

affect the behavior of the detail and its likelihood to bring about failure due to fatigue. Fatigue reliability is modeled based on well-established structural reliability theories, and it has been successfully used in offshore applications to estimate the risk of fatigue failure of offshore structures (especially steel jacket platforms, Faber et al. (1992b)). Randomness and/or variability in loading and environmental stressors affecting offshore structures have also been accounted for when needed – some considerations have included randomness in wave loading and in the corrosive environment, variability in material properties and behavior of the structural system, variability in crack propagation at welds and in stress concentration, etc. The advantage of interpreting fatigue performance using reliability is that reliability is easily converted to or expressed in terms of the probability of fatigue failure. This then provides a useful framework for decision-making issues for bridge maintenance and inspection scheduling where safety is an important consideration.

For steel bridges, the Federal Highway Administration (FHWA) requires periodic inspections (every two years for fracture-critical inspections) to prevent fatigue failures. However, every steel bridge has its own specific structural type, geometry, design, and traffic conditions, and these characteristics may cause different fatigue performance for different bridges. In addition, even on the same bridge, details with different fatigue categorizations and different levels of stress ranges might experience different degrees of fatigue in the field. Therefore, due to these differences, the two-year periodic or any other fixed-interval inspections may not be adequate for the fatigue damage accumulation of all types of details in steel bridges. For example, some extremely fracture-critical members may require more frequent inspections (i.e. shorter intervals between inspections) than typical details, but some less critical details may require even fewer inspections than are implied by the two-year inspection schedule. Frequent inspections

increase the cost of bridge maintenance especially when expensive fracture-critical inspection methods are employed. From the owner's point of view, bridge safety is the first priority, and the limited bridge maintenance budget needs to be effectively managed. It is impossible and economically infeasible to perform frequent inspections for all fracture-critical members. The trade-off between bridge safety and cost of inspections for a steel bridge is an important issue. Two systematic methods for inspection scheduling, which are able to yield the most economical inspection strategy and at the same time guarantee an acceptable safety level through the planned service life for steel bridges are presented in this dissertation.

## **1.2 RESEARCH OBJECTIVES AND SCOPE**

There are two main objectives in this research. The first is to apply fatigue reliability analysis techniques to assess the performance of steel bridges that are subject to loading that could lead to fatigue failure. Then, with the help of a fatigue reliability index or measure that indicates the safety level of the specific detail on the bridge, our objective is to propose inspection schedules to minimize costs and maintain target safety levels. To meet this objective, bridge-specific and loading parameters such as material properties, stress ranges, crack types, crack sizes, crack geometry, etc. need to be well understood because they are an integral part of the overall reliability analysis. In this dissertation, two fatigue reliability approaches are demonstrated: the AASHTO approach and the LEFM approach. For details classified according to AASHTO fatigue categories, the AASHTO approach is used to evaluate fatigue reliability. A limit state function related to the number of stress cycles leading to failure based on Miner's rule is applied. For non-AASHTO type details, a limit state function related to crack size is employed in a LEFM approach for estimating fatigue reliability. In contrast with the



limited calculations of only remaining life in a deterministic approach, with a probabilistic approach, the derived fatigue reliability of a detail not only can be taken as a safety index for that detail, but it also can be applied in inspection scheduling for the detail.

The second main objective of this research is to develop a rational procedure that can be employed to yield the most economic inspection strategy and guarantee the safety of steel bridges against failure due to fatigue. Based on the fatigue reliability estimated by the AASHTO or the LEFM approaches and the assumption of ideal inspection quality, the scheduling of inspections can be modeled as an optimization problem with appropriate constraints on inspection intervals and on safety over the service life. The optimal schedule ensures that the fatigue reliability of the selected detail will be above the target reliability level during the service life and, at the same time, yields the lowest total cost among all possible inspection schedules. To consider the effect that imperfect inspection quality can have on scheduling of inspections, an alternative method based on the Probability of Detection (POD) of the chosen Nondestructive Testing (NDT) procedure for inspection is also proposed to help select both the optimal NDT procedure and the associated inspection schedule for details in steel bridges.

The research results presented in this dissertation focus on vehicle-induced high-cycle fatigue (HCF) problems in steel bridges. The goal is to find reliability-based solutions for fatigue evaluation and inspection planning. Fatigue is the only failure mode considered in this research, and failure in steel bridges due to other effects such as yielding (due to overloads), buckling, corrosion, and vehicular collision are not included. Vehicle passage, especially truck passage, on the bridges is assumed to be the only source of fatigue loading considered in this study. The details selected for the optimal inspection scheduling in this study are located in fracture-critical members meaning that

their failure would result in serious damage and consequences. Though this dissertation discusses only fatigue-related safety evaluations and inspection planning, the methodology proposed may be easily applied to other structural problems as well where damage accumulation or deterioration in performance occurs with time.

### **1.3 ORGANIZATION**

The dissertation is composed of seven chapters that are organized as follows.

Chapter 1 serves as an introduction to the study and provides the background, problem description, and the scope and objectives of this research.

Chapter 2 reviews the literature relevant to this research and briefly introduces structural reliability theory. Numerical procedures used in the probabilistic structural reliability approaches as well as in the deterministic fatigue approaches are discussed in order to understand how these approaches may be used in evaluating the performance of steel bridges against fatigue failure.

Chapter 3 describes the methods employed for modeling fatigue loads on steel bridges. These methods include stress spectrum analysis, assumed distribution analysis, and fatigue truck analysis. The objectives of all these methods are to derive equivalent stress ranges for the detail of interest in a steel bridge. The methods present alternative approaches to characterize the variability in the fatigue loading. The developed equivalent stress range is required in subsequent fatigue reliability analysis.

Chapter 4 presents two methods for evaluating fatigue reliability for fracture-critical members in steel bridges: the AASHTO fatigue reliability approach and the LEFM fatigue reliability approach. Based on statistical data from the AASHTO S-N curves, the AASHTO approach is proposed for estimating the fatigue reliability of all structural details that are classified according to the AASHTO fatigue categories. The

LEFM approach, derived by using Paris' law and a linear elastic fracture mechanics approach, is applicable for the fatigue reliability evaluations of all non-AASHTO type details (i.e., details not explicitly classified according to AASHTO categories).

Chapter 5 presents a reliability-based scheduling procedure for establishing schedules for fatigue inspections. By setting a target safety level and applying structural reliability methods, the planning of fatigue inspections for a given steel bridge detail over its service life becomes an optimization problem of searching for a set of feasible, non-uniform inspection intervals that can yield the minimum total cost and still meet the necessary safety requirements. Ideal inspection quality is assumed in this optimal inspection scheduling approach.

Chapter 6 provides an alternative probabilistic approach for selecting both the optimal nondestructive inspection (NDI) technique and associated inspection schedule for a given detail in a steel bridge when the (imperfect) quality of each candidate NDI technique is considered. Inspection quality is explicitly modeled in this approach.

Chapter 7 summarizes the key findings from this research study and after some discussion about the results and some concluding remarks; suggestions for future work in related areas are presented.

## **Chapter 2: LITERATURE REVIEW AND BACKGROUND ON METHODS FOR FATIGUE ANALYSIS**

In this chapter, a literature review of fatigue reliability analysis and reliability-based inspection scheduling methods is presented. A general background on probabilistic methods used in structural reliability theory as well as on more conventional deterministic analyses is presented since both these alternative approaches are used for fatigue analysis and are employed extensively in this research.

### **2.1 LITERATURE REVIEW**

Fatigue reliability analysis and reliability-based inspection scheduling methods have been widely applied in the offshore industry to address fatigue problems that occur especially for steel jacket platforms (Faber et al. (1992b)). Numerous publications and research studies have addressed these fatigue-related issues in the offshore area. In contrast, fatigue reliability analysis and reliability-based fatigue inspection scheduling for steel bridge maintenance are relatively new research areas. Some of the more significant publications in the field of reliability-based optimal inspection scheduling for fatigue are reviewed in the following sections.

#### **2.1.1 Fatigue Reliability Analysis**

In conventional fatigue analysis, two deterministic approaches are commonly employed for fatigue life evaluations. The well-known Miner's rule of S-N curve approach relating stress ranges (S) to the number of cycles (N) to failure was developed more than fifty years ago (Miner, 1945). This was later followed by the linear elastic fracture mechanics (LEFM) approach that accounts for loading condition and geometry

around a crack tip in a crack growth rate formulation used to estimate fatigue life (Paris and Erdogan, 1963). In probabilistic fatigue, too, these two approaches (using S-N curves or LEFM) may be used along with structural reliability theory to evaluate different types of components or details for fatigue failure.

Tang and Yao (1972) published one of the earliest papers on fatigue reliability analysis for structures. The analysis method they proposed was a simple approach based on Miner's rule in which the number of stress cycles leading to fatigue under various stress levels was treated as a random variable. This permitted calculations of the probability of fatigue failure for a given structural component. Later, Yao (1974) applied this fatigue reliability approach to the design of structural members with a specified acceptable probability of fatigue failure. Around the same time, Yang and Trapp (1974) proposed an LEFM-based reliability analysis for fatigue-sensitive aircraft structures. Their approach was based on random vibration theory and took into account random loadings for the aircrafts. Wirsching (1979 and 1980) proposed a fatigue reliability analysis procedure based on Miner's rule for offshore structures, especially for failure at welded joints under random wave loadings. In his studies, a Miner's rule fatigue damage index was first introduced in an S-N curve-based reliability analysis. Extensive statistical data were examined to characterize this fatigue damage index, which is now commonly used in fatigue reliability studies. Due to the anticipated widespread use of reliability techniques for fatigue problems in engineering, the ASCE Committee on Fatigue and Fracture Reliability (1982a-d) published a series of four papers in order to review the available fatigue reliability approaches, to discuss the statistical models used to describe random variables such as stress range and material properties, and to present possible applications of fatigue reliability analysis in the quality assurance, maintainability, and design of structural members. Based on the Miner's rule,

Wirsching (1984) employed a reliability format to establish a design rule for short-period offshore structures, and also proposed fatigue design criteria for tendons of tension leg platforms (TLPs) (Wirsching and Chen, 1987). Ortiz and Kiremidjian (1984) proposed an LEFM-based fatigue reliability analysis approach to evaluate tubular joints in offshore structures. This model was analyzed by the first-order reliability method (FORM) in order to estimate the probability of failure. Wirsching et al. (1987) also proposed an LEFM-based reliability model for fatigue problems but utilized Monte Carlo simulations to estimate the probability of failure. The chief difference between Wirsching's and Ortiz's LEFM models was in the formulation of the limit state function used in the reliability calculations. The variable explicitly included in the limit state function is crack size for the model by Ortiz and Kiremidjian (1984) whereas in Wirsching et al. (1987), the variable explicitly modeled is the number of stress cycles as derived from Paris' law. Jiao and Moan (1990) utilized component and system reliability analysis concepts to propose a method of updating of the fatigue reliability for structural details when additional information, such as the detection or non-detection of a crack, was available from inspections. Their proposed method improved on existing applications of fatigue reliability analysis by taking into consideration the findings from inspections. Thus, the fatigue reliability of a detail could be updated whenever new information was collected for that detail – this then resulted in a more accurate fatigue reliability estimate reflecting the true nature of the detail. In a similar way, Ximenes and Mansour (1991) discussed an LEFM-based approach for the system reliability of TLP tendons undergoing progressive fatigue damage at several joints, where reliability updating due to inspections was included in their analyses. Faber et al. (1992b) studied the fatigue reliability of tubular members in a North Sea jacket-type offshore structure using an LEFM-based approach in which a limit state function related to the stress intensity factor was

employed. Jiao (1992) extended the reliability updating procedure by setting a target reliability level so that after each inspection, this methodology was applied for scheduling future in-service inspections for TLP tethers. Hovde and Moan (1994, 1997) presented a procedure for estimating the fatigue reliability of a TLP system in which the effects of inspections and repairs were explicitly considered.

Thus, at least in the offshore industry and to some degree in the aerospace industry, the various studies carried out over the last thirty years have successfully used different approaches such as the S-N curve-based approach or an LEFM-based approach to evaluate the reliability of a detail, a component, or a structural system against fatigue failure. Additionally, several studies also sought to include findings from inspections as part of a reliability updating framework that took advantage of field inspections. Based on these initial studies, subsequent work on fatigue-related reliability analysis focused on two distinct directions. One direction led to developments related to the influence of nondestructive inspections on fatigue reliability analysis. Some examples of a focus on this direction include research studies by Hong (1997), Zheng and Ellingwood (1998), and Zhang and Mahadevan (2000, 2001). A second research direction essentially continued the approaches developed in the offshore and aerospace industry but began to focus on detailed modeling issues such as an examination of the rate of short crack growth relative to long crack growth for welded T-joints by Lanning and Shen (1996, 1997), consideration of inspections and repair in the fatigue reliability of ship hull structures by Garbatov and Soares (1997), and investigation of the use of alternative numerical computational models in probabilistic fracture mechanics with a focus on efficiency and accuracy by Liu et al. (1996).

For steel bridges, too, the application of fatigue reliability procedures has been proposed since the mid-1980s. However, compared to the offshore and aerospace

industries, studies of fatigue reliability for steel bridges have been far fewer. Yazdani (1984) and Yazdani and Albrecht (1987) describe an LEFM-based probabilistic procedure to estimate the risk of fatigue failure of steel highway bridges as a system reliability problem. They use Monte Carlo techniques and first-order bounds on the system reliability to estimate the bridge failure probability. Zhao et al. (1994a) employed both a Miner's rule approach (they refer to this as the AASHTO approach) as well as an LEFM-based approach in structural reliability computations of specific details on steel bridges. In addition, based on the initial work of Jiao (1992), Zhao et al. (1994b) applied reliability updating procedures to incorporate the findings from nondestructive inspections in evaluation of the fatigue reliability of details in steel bridges. Massarelli and Baber (2001) employed LEFM-based fatigue reliability analysis for details in steel highway bridges subjected to random, variable-amplitude traffic loads. Inspection data were also incorporated in their analyses. Righiniotis (2004) studied the effects of load restrictions, inspections, and repairs on the fatigue reliability of a typical welded joint in steel bridges. This study was based on a modified approach to the conventional Paris law and involved the use of a two-stage relation for the crack growth rate – one stage was termed the “near-threshold” stage, the other was the Paris crack growth region. Repair/invasive actions are also discussed following detection of a crack and are included in the analysis.

### **2.1.2 Reliability-Based Fatigue Inspection Scheduling**

One of the most important applications of fatigue reliability is in scheduling of inspections for structures. For a specified target reliability (or, equivalently, a minimum allowable safety level), the objective of such a reliability-based scheduling problem is to come up with an inspection program that is the most economical and also maintains the



fatigue reliability of the structural component or system above the target reliability. Costs, here, are assumed to include the cost of inspections, expected costs associated with any needed repairs, and expected costs associated with failure. (Note that even though failure probability is maintained at a target low level, it is not identically zero and hence, an estimate of costs of failure is required.)

This reliability-based scheduling problem for fatigue-sensitive structures has been studied extensively in the offshore industry particularly because of the large investments in offshore facilities, and because underwater inspections tend to be extremely expensive. In the North Sea because of the harsher marine environment there, in particular, there have been a large number of studies performed that relate to reliability-based fatigue inspection scheduling for offshore platforms.

Thoft-Christensen and Sorensen (1987) published one of the earliest papers in the area of reliability-based scheduling where they proposed a procedure for establishing an optimal schedule for inspection and repair of structural systems that were subjected to fatigue loading. The cost function employed in their approach only considered inspection and repair costs; expected system failure costs were not included. Following the work of Thoft-Christensen and Sorensen (1987), the Fifth International Conference on Structural Safety and Reliability (ICOSSAR '89) included the publication of several papers related to reliability-based optimal inspection scheduling for offshore structures. For example, Madsen et al. (1989) and Fujita et al. (1989) proposed optimal inspection scheduling procedures for fatigue-sensitive details in offshore structures and involved the use of LEFM-based fatigue reliability analyses, tree analysis (to represent inspection and repair scenarios), inclusion of failure costs in the overall cost function, and an optimization process that involved minimization of the total cost. The only difference in these two studies was in the formulation of the limit state function used to describe the

fatigue reliability. Wirsching and Tornig (1989) illustrated practical examples of the use of optimal strategies for design, inspection, and repair of structural systems. Cramer and Friis-Hansen (1992) applied these same reliability-based inspection scheduling procedures for homogeneous continuously welded structures containing hazardous material where prevention of leakage was critical.

The development of reliability-based inspection scheduling studies up this point in time employed tree analyses where at each branch point, only two events – “repair” or “no repair” – were considered when enumerating the scenarios to be considered in the optimization. Sorensen et al. (1991) and Faber et al. (1992a) extended the two-event type branches in the trees to allow for multi-event branches in component-level and system-level analyses by taking into consideration the possibility of several different repair effort choices that could exist in practical problems. In such approaches, however, numerous alternative repair scenarios in the event tree needed to be analyzed, and the proposed multi-event type tree analyses thus demanded an extensive amount of computations. To address this, a proposal to neglect all scenario branches that contributed very low costs was made so as to improve the computational efficiency of the optimization procedure.

Moan et al. (1993) utilized event tree techniques to include the effects of inspection and repair on fatigue reliability and further proposed a reliability-based fatigue design criterion for offshore structures. Several research studies (including those by Dharmavasan et al. (1994) and Lotsberg et al. (1999)) demonstrated how in-service inspection programs for offshore structures, sometimes involving both reliability analysis and knowledge-based computer systems, could be established that could provide rational schedules for safety and maintenance of offshore structures.

As a result of the successes in application of reliability-based inspection scheduling procedures in the offshore industry, other areas in civil engineering began to employ these procedures as well, particularly where deterioration mechanisms require some maintenance to avoid failure. For example, Sommer et al. (1993) proposed a reliability-based inspection strategy to address corrosion problems in steel girder bridges. Also, Frangopol et al. (1997) utilized the methodology to arrive at an optimal inspection and repair plan for reinforced concrete T-girders in a highway bridge to deal with possible reinforcement corrosion over time.

In summary, the development of a rational procedure for arriving at an optimal inspection scheduling program grew primarily out of the aerospace and offshore industries but has matured to the point where it has seen application in several areas of civil engineering where fatigue or some other deterioration mechanism may be present. One area that has not seen application of such optimal inspection scheduling procedures is that of fatigue inspection for steel bridges. This dissertation is focused on exactly this problem. The research here has benefited from the various previous studies cited in his literature review. Issues unique to fatigue in steel bridges, especially for fracture-critical members in these bridges, are developed in this research which will focus on event tree analyses and detailed structural reliability calculations reflecting variability in loading, material properties, and behavior. Additionally, one area that has been not addressed in most of the previous applications of the optimization procedure – namely accounting for imperfect quality of the inspections – will be taken up here and included in an alternative optimization framework to the most common one in use in most of the cited studies.

## 2.2 STRUCTURAL RELIABILITY ANALYSIS

The field of structural reliability analysis has been well developed over the last four decades and has been widely applied in many areas. In this section, general concepts of structural reliability and numerical techniques employed in this research are presented. The objective of structural reliability analysis for a structural member or system is to estimate its probability of failure (or its complement, the probability that there will not be a failure, i.e., the reliability) recognizing the role of resistance and load uncertainties in such calculations. It is convenient to construct a limit state function that differentiates between failed and safe states and can be mathematically expressed in terms of all of the known random variables. With well-established numerical techniques, it is then possible to estimate the probability of failure or reliability of the structural component or system under consideration.

### 2.2.1 Limit State Function

Defining a limit state function that can adequately describe the relationship between the capacity (or resistance) and the applied load (or demand) on a structural member is the first step in a structural reliability analysis. Hence, a limit state function can often be thought to be composed of a resistance-related measure,  $R$ , and a load-related measure,  $S$ . These two elements are generally described in terms of random variable(s) that can take into account various uncertainties in the material properties, the load, and the model used to describe the behavior of the structural component or system. In many engineering problems, a simple form for a limit state function may be given as follows:

$$g(R, S) = R - S \quad (2.1)$$

Note that in Equation 2.1, the resistance measure,  $R$ , and the load measure,  $S$ , will themselves need to be expressed in terms of other random variables.

In structural engineering problems, it is common to refer to different types of limit states based on the mode of failure of the structural component or system under consideration. Some common limit states include serviceability limit states, ultimate limit states, and fatigue (or damage accumulation) limit states. The following are examples of each of these limit state functions:

- (1) Serviceability limit state for mid-span deflection of a simple beam subjected to a uniformly distributed load:

$$g(L, w, E, I) = L/360 - 5wL^4/384EI \quad (2.2)$$

where  $L$  is the span length,  $L/360$  is the maximum allowable deflection,  $w$  is the uniformly distributed load,  $E$  is the Young's modulus for the material, and  $I$  is the moment of inertia of the cross-section of the beam.

- (2) Ultimate limit state for the bending moment capacity of a compact steel beam:

$$g(F_y, Z, M) = F_y \cdot Z - M \quad (2.3)$$

where  $F_y$  is the yield stress of the material (steel),  $Z$  is the plastic section modulus, and  $M$  is the applied bending moment at a position of interest along the beam.

- (3) Stability limit state associated with the buckling of an Euler column:

$$g(E, I, L, P, k) = \pi^2 EI / (kL)^2 - P \quad (2.4)$$

where  $E$  is the Young's modulus of the material;  $I$  is the moment of inertia of the column cross-section,  $kL$  is the effective length of the column accounting for support/boundary conditions, and  $P$  is the axial load on the column.

- (4) Fatigue limit state for a component subjected to cyclic loading:

$$g(A, \Delta, S_{RE}, m, N) = N_c(A, \Delta, S_{RE}, m) - N = \frac{A \cdot \Delta}{S_{RE}^m} - N \quad (2.5)$$

where  $N_c$  is a critical number of cycles which if exceeded will cause failure. Note that  $N_c$  depends on material properties,  $A$  and  $m$  as well as on an “equivalent” stress range,  $S_{RE}$ . Model uncertainty is described by the variable,  $\Delta$ , and  $N$  is the accumulated number of stress cycles that the component experiences.

After defining the limit state function,  $g(\mathbf{X})$ , it is possible to tell whether a component has failed by checking if  $g(\mathbf{X})$  is less than or equal to zero. Considering the likelihood of all combinations of random variables in  $\mathbf{X}$  where this is true yields the probability of failure,  $P_F$ :

$$P_F = P[g(\mathbf{X}) \leq 0] \quad (2.6)$$

where  $P[ ]$  signifies the probability of the event in brackets. The complementary probability,  $P_S$ , is then:

$$P_S = P[g(\mathbf{X}) > 0] \quad (2.7)$$

### 2.2.2 A Simple Load and Resistance Model

Consider a case where the resistance and load variables,  $R$  and  $S$ , are statistically independent normally distributed random variables with mean values,  $\mu_R$  and  $\mu_S$ , respectively, and standard deviations,  $\sigma_R$  and  $\sigma_S$ , respectively, as shown in Figure 2.1. The limit state function  $g(R, S)$  consists of the two random variables and is essentially a random variable as well. Since  $g(R, S)$  is a function of the independent random variables,  $R$  and  $S$ , it has mean,  $\mu_g$ , and standard deviation,  $\sigma_g$ , that may be calculated as follows (see Appendix A):

$$\mu_g = \mu_R + \mu_S \quad (2.8)$$

$$\sigma_g = \sqrt{\sigma_R^2 + \sigma_S^2} \quad (2.9)$$

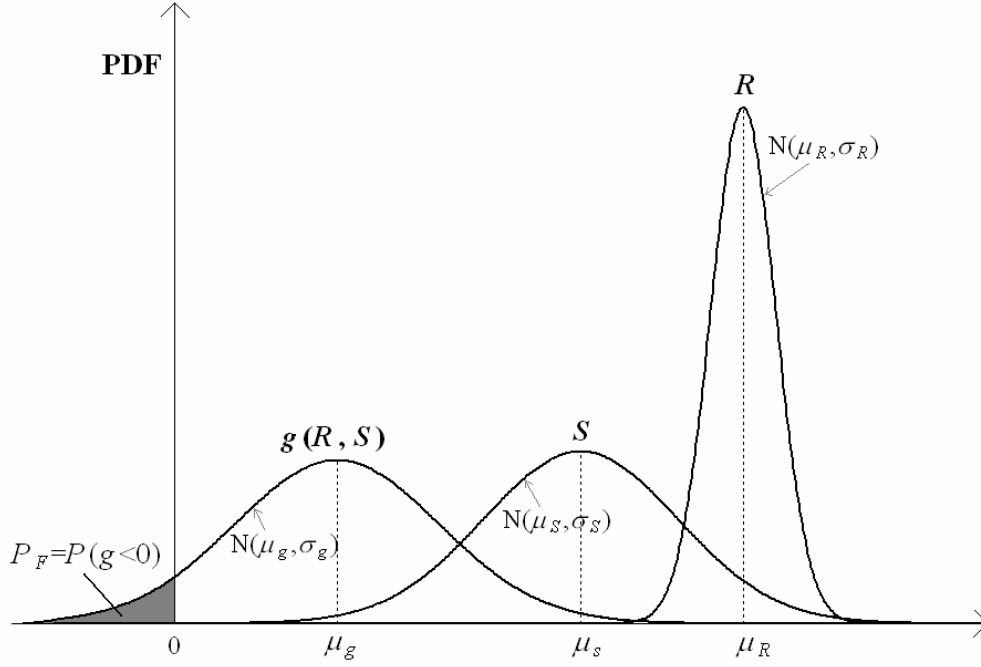


Figure 2.1: Statistical Distributions of  $R$ ,  $S$ , and  $g(R,S)$ .

The probability of failure can now be calculated as follows:

$$P_F = P(g \leq 0) = \Phi\left(\frac{0 - \mu_g}{\sigma_g}\right) = \Phi\left(\frac{\mu_S - \mu_R}{\sqrt{\sigma_S^2 + \sigma_R^2}}\right) \quad (2.10)$$

where  $\Phi(\cdot)$  is the cumulative distribution function (CDF) of a standard normal random variable. Correspondingly, the complementary probability  $P_S$  can be evaluated as:

$$P_S = P(g > 0) = 1 - \Phi\left(\frac{\mu_S - \mu_R}{\sqrt{\sigma_S^2 + \sigma_R^2}}\right) = \Phi\left(\frac{\mu_R - \mu_S}{\sqrt{\sigma_S^2 + \sigma_R^2}}\right) \quad (2.11)$$

More generally, for two dependent variables,  $R$  and  $S$ , with joint probability density function,  $f_{R,S}(r,s)$ , it is necessary to estimate the probability of failure in terms of a double integral over the entire failure domain. Thus, we have:

$$P_F = P[g(R,S) \leq 0] = \iint_{g(R,S) \leq 0} f_{R,S}(r,s) dr ds \quad (2.12)$$

The complementary probability  $P_S$  can then be defined as

$$P_S = P[g(R, S) > 0] = \iint_{g(R, S) > 0} f_{R, S}(r, s) dr ds = 1 - P_F \quad (2.13)$$

### 2.2.3 Reliability Index and Probability of Failure

It is convenient to define a reliability index,  $\beta$ , that is related to the probability of failure,  $P_F$  as follows:

$$\beta = \Phi^{-1}(1 - P_F) = -\Phi^{-1}(P_F) \quad (2.14)$$

or inversely as,

$$P_F = \Phi(-\beta) \quad (2.15)$$

This reliability index,  $\beta$ , increases as the probability of failure decreases. A set of  $P_F$  values and corresponding  $\beta$  values are shown in Table 2.1. In civil engineering applications, typical levels of acceptable probabilities of failure are around from  $10^{-3}$  to  $10^{-4}$ . The corresponding reliability index values then range from 3.72 to 4.27.

Table 2.1: Some Typical Values of Probability of Failure,  $P_F$ , and Corresponding Reliability Index Values,  $\beta$ .

Probability of Failure, $P_F$	Reliability Index, $\beta$
$10^{-1}$	1.28
$10^{-2}$	2.33
$10^{-3}$	3.09
$10^{-4}$	3.72
$10^{-5}$	4.27
$10^{-6}$	4.75
$10^{-7}$	5.20

When there are several random variables that are needed in the definition of the limit state function, a joint probability density function,  $f_{\mathbf{X}}(\mathbf{x})$ , for a vector,  $\mathbf{X} = \{ X_1,$



$X_2, \dots, X_n$  representing all  $n$  random variables may be used to compute the probability of failure as follows:

$$P_F = P[g(\mathbf{X}) \leq 0] = \int \cdots \int_{g(\mathbf{x}) \leq 0} f_{\mathbf{x}}(\mathbf{x}) d\mathbf{x} \quad (2.16)$$

The reliability index,  $\beta$ , can still be computed using Equation 2.14.

Though the probability of failure can be calculated using Equation 2.16, the integration implied by Equation 2.16 is rarely carried out. This is because the joint probability density function  $f_{\mathbf{x}}(\mathbf{x})$  is difficult to obtain. Also, the multi-dimensional integration needed in Equation 2.16 is formidable and generally difficult to compute with great accuracy due to the nature of the functions involved (and, especially, because rare failures and high reliability are associated with tails of probability distribution/density functions). As a result, several more efficient numerical procedures, such as the First-Order Reliability Method (FORM), the Second-Order Reliability Analysis (SORM), and various simulation techniques have been used for most structural reliability analyses. Two of these, FORM and Monte Carlo simulations, which are extensively employed in this research, are briefly reviewed next.

### ***2.2.3.1 First-Order Reliability Method (FORM)***

The First-Order Reliability Method (FORM) has been in used for structural reliability analyses since the 1970s following early work that included studies of Hasofer and Lind (1974) followed by Rackwitz and Fiessler (1978) among others who improved on the original development and formulation. The basic idea in FORM is to find the closest distance,  $\beta$ , from the origin in uncorrelated standard normal ( $\mathbf{U}$ ) space to a linearized form of the true limit state surface (separating the “safe” state from the “failed” state). The point on the limit state surface closest to the origin is commonly referred to as the “design point.” The probability of failure is estimated using the distance,  $\beta$ , using

Equation 2.15. The algorithm used in FORM to determine the closest distance from the origin in  $\mathbf{U}$  space to the linearized limit state surface is outlined in Appendix B.

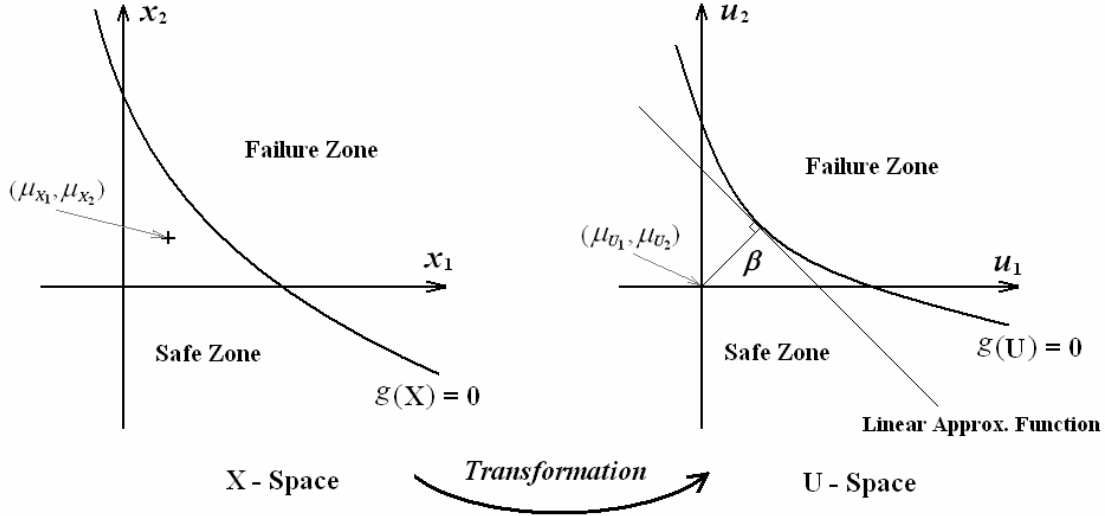


Figure 2.2: Illustration of the First-Order Reliability Method (FORM).

### 2.2.3.2 Monte Carlo Simulation

Monte Carlo simulation involves repeated drawing random samples of all random variables involved in the limit state function and simply checking whether a new “failure” or “non-failure” has resulted (or, equivalently, whether the limit state function had a value less than zero or not). This then offers an alternative way to carry out the numerical integration of Equation 2.16, which can be expressed as follows:

$$P_F = \int \dots \int I[g(\mathbf{X}) \leq 0] f_{\mathbf{X}}(\mathbf{x}) d\mathbf{x} \quad (2.17)$$

where  $I[g(\mathbf{X}) \leq 0] = 1$  if  $g(\mathbf{x}) \leq 0$  and  $I[g(\mathbf{X}) \leq 0] = 0$  otherwise;  $\mathbf{X} = \{X_1, X_2, \dots, X_n\}$  is a vector of  $n$  random variables;  $f_{\mathbf{X}}(\mathbf{x})$  is the joint probability density function of  $\mathbf{X}$ . Based on  $N$  simulations, Equation 2.17 can now be used to estimate  $P_F$  as follows:

$$P_F \approx \frac{1}{N} \sum_{k=1}^N I[g(X_i) \leq 0] \quad (2.18)$$

This computation is demonstrated pictorially in Figure 2.3.

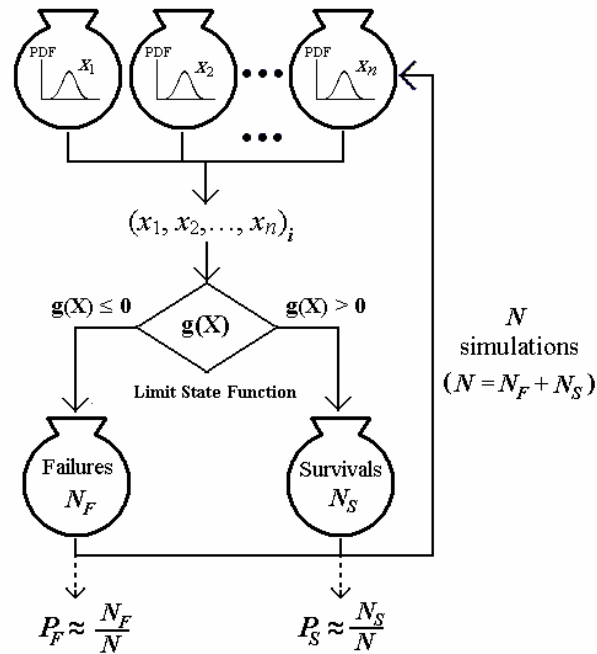


Figure 2.3: Flow Chart of Monte Carlo Simulation Method.

As can be seen in Figure 2.3, the Monte Carlo simulation procedure may be summarized by the following steps:

- (1) Represent all the basic random variables ( $X_1, X_2, \dots, X_n$ ) that occur in the limit state function by their probabilistic distributions;
- (2) Randomly sample each random variable. For example, the  $i^{\text{th}}$  simulation would yield  $(x_1, x_2, \dots, x_n)_i$ ;
- (3) Substitute this vector of values,  $(x_1, x_2, \dots, x_n)_i$ , into the limit state function to calculate the value of  $g(\mathbf{X}_i)$ ;
- (4) If  $g(\mathbf{X}_i) \leq 0$ , increase the number of failures ( $N_F$ ) by one;
- (5) Repeat Steps (2) to (4)  $N$  times (where  $N$  should be sufficiently large for good estimates of  $P_F$ );
- (6) Estimate the probability of failure as  $N_F/N$ .

Monte Carlo techniques are computationally expensive compared to other reliability analysis procedures such as FORM. Several other simulation-based procedures have been proposed to improve the efficiency of ordinary Monte Carlo simulations; these include the antithetic variates method, the control variates method, importance sampling, and Latin Hypercube sampling. For details related to these various methods, refer to Ang and Tang (1984); Iman and Conover (1980); Melchers (1989).

## **2.3 DETERMINISTIC FATIGUE ANALYSIS FOR STEEL BRIDGES**

In various engineering applications where structural components or structures are subjected to repeated fluctuating loads, deterministic analyses are often used in fatigue life estimation and in design for fatigue. There are three primary methods for deterministic fatigue analysis. These include stress-based approach, strain-based, and linear elastic fracture mechanics (LEFM) approaches. Stress-based and strain-based approaches are not related to the actual state of fracture of the detail or component nor on whether a crack of any size is actually present. The LEFM approach, however, is related to the stress field and rate of growth of a crack of a specific size with time. These three approaches and areas of application of each are briefly described next.

### **2.3.1 Stress-Based Approach (S-N Curve Approach)**

A stress-based approach for fatigue analysis is applicable to high-cycle fatigue (HCF) problems where stresses and strains are within the elastic range of the material and the structural components are assumed to be initially uncracked. High-cycle fatigue refers to cases where the number of cycles until failure is greater than a specified value,

ranging from 10 to  $10^5$ , depending on the material (Bannantine et al., 1990) but a number around 10,000 may be appropriate for application in steel bridges. For most structural components in steel bridges, the stresses and strains generated by repeated traffic loading are below the elastic limit of the structural steel. Since these structural components are expected to have long service lives; the only type of fatigue of concern is high-cycle fatigue. Hence, the stress-based approach is widely employed for deterministic fatigue analysis of steel bridges. This stress-based approach involves establishing an empirical relationship between stress range amplitudes ( $S_R$ ) and number of cycles to failure ( $N_f$ ) as follows:

$$N_f = A \cdot S_R^{-m} \quad (2.19)$$

where  $A$  and  $m$  are constants related to the material. Equation 2.19 describes a linear relationship between  $\log S_R$  and  $\log N_f$ . A large number of fatigue tests are needed to construct an S-N curve (describing the straight line relating  $\log S_R$  to  $\log N_f$ ). In the AASHTO specifications, each design S-N curve is defined conservatively (by specifying the value of  $A$  for the specific detail and assuming  $m$  is equal to 3 for steel) so that, based on the variability in the fatigue data, it represents the 95% confidence limit for 95% survival of all details in a given category (Barsom and Rolfe, 1999). Even though there is an implied probability of failure associated with the use of Equation 2.19, we refer to it as a deterministic approach because no reliability calculations based on the actual condition of the detail are carried out that either consider the variability in the loading or in the material properties/behavior.

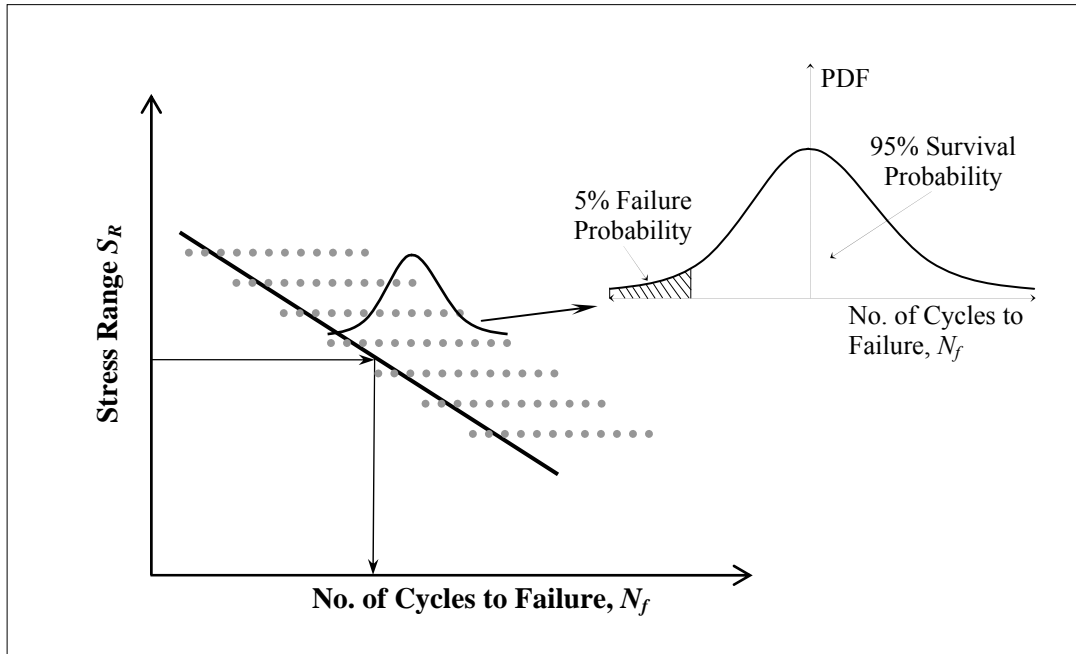


Figure 2.4: Schematic S-N Diagram for a Typical Detail in the AASHTO Specifications (1990).

Barsom and Rolfe (1999) discussed how the fatigue strength of components or details is affected by several factors that may be classified into three broad categories: stress, geometry/properties, and environment. The stress factors include the applied stress ranges, the mean stress, the stress ratio, whether the loading can be characterized as being of a constant- or variable-amplitude nature, the loading frequency, the maximum stress, and the residual stresses. The geometry and properties of the component/detail include stress concentration, size, stress gradient, surface finish, and metallurgical as well as mechanical properties of the base metal and any associated welds. Environmental factors include temperature as well as exposure to corrosion, oxidation, and other effects of the environment. In addition, several surface treatments such as nitriding, shot peening and cold rolling can influence fatigue behavior. Based on fatigue test results from numerous welded details in steel beams, Fisher et al. (1970) concluded that stress

range and the type of weld detail are the primary factors that influence the fatigue strength of details in steel bridges.

Miner (1945) proposed a linear damage accumulation rule to account for effects of fatigue on structural components or details subjected to variable-amplitude loading. Miner's damage accumulation index,  $D$ , is defined as follows:

$$D = \sum_{i=1}^k \frac{n_i}{N_{f,i}} \quad (2.20)$$

where  $n_i$  is the actual number of cycles associated with a specific stress range level,  $S_{R,i}$ , and  $N_{f,i}$  is the number of cycles until failure under a constant-amplitude stress range level,  $S_{R,i}$ . The detail under consideration is deemed to be safe if  $D < 1$ . Failure corresponds to situations where  $D \geq 1$ . This damage accumulation rule is commonly referred to as Miner's rule.

Combining Equation 2.19 with Miner's rule and setting the damage accumulation index,  $D$ , to unity, an equivalent stress range,  $S_{RE}$ , that accounts for the variable-amplitude nature of the loading may be derived as follows:

$$\sum \frac{n_i}{N_{f,i}} = \sum \frac{\gamma_i \cdot N}{A \cdot S_{R,i}^{-m}} = \frac{N}{A} \sum [\gamma_i \cdot S_{R,i}^m] = \frac{N}{A} S_{RE}^m = 1 \quad (2.21)$$

$$S_{RE} = \left[ \sum \gamma_i \cdot S_{R,i}^m \right]^{1/m} \quad (2.22)$$

where  $\gamma_i$  is the ratio of  $n_i$  to the total number of accumulated stress cycles,  $N$ , in the detail (i.e.,  $\gamma_i = n_i/N$ ), and  $S_{R,i}$  is as defined before. With the equivalent constant-amplitude stress range,  $S_{RE}$ , defined in Equation 2.22, the number of cycles until failure for any detail that is experiencing variable-amplitude loading may be estimated using a conventional S-N diagram.

Next, we describe two stress-based fatigue evaluation methods in common use for steel bridges in the United States. These are the AASHTO LRFD fatigue design specifications and the fatigue evaluation model proposed by Moses et al (1987) that was

adopted as part of the AASHTO Guide Specifications (1990). While there are differences in the approaches used to evaluate the fatigue life of a detail using these two methods, the design S-N curves for the two methods are identical and are based on the same data. Also, these design S-N curves were conservatively developed so as to assure with 95% confidence that 95% of all details would survive up to the design life implied by the Specifications.

### **2.3.1.1 AASHTO LRFD Fatigue Design Specifications**

In the AASHTO LRFD Specifications (1998), S-N curves are given for each of eight different categories of details in steel bridges for fatigue design. The AASHTO live load factor of 0.75 is employed with the HS20 design truck yielding an equivalent HS15 fatigue truck that is employed for steel bridges to evaluate live load stress ranges for any detail. Thus, for fatigue design, each detail needs to satisfy the following requirement:

$$\gamma \cdot (\Delta f) \leq (\Delta F)_n \quad (2.23)$$

where  $\gamma$  is the load factor equal to 0.75 for fatigue limit states;  $(\Delta f)$  is the live load stress range of the HS20 design truck;  $(\Delta F)_n$  is the nominal fatigue resistance which is defined as follows:

$$(\Delta F)_n = \left( \frac{A}{N} \right)^{\frac{1}{3}} \geq \frac{1}{2} (\Delta F)_{th} \quad (2.24)$$

for which

$$N = 365 \cdot 75 \cdot C_s \cdot ADTT_{SL} \quad (2.25)$$

where  $A$  is a constant specified for each of the eight fatigue categories for any detail and  $(\Delta F)_{th}$  is the constant-amplitude fatigue threshold for each category (given in Table 2.2). Also,  $ADTT_{SL}$  (the average number of trucks per day in a single lane) is related to  $ADTT$



(the average number of trucks per day) as shown in Table 2.3, and  $C_s$  is the number of stress range cycles per truck passage (given in Table 2.4), and These fatigue design provisions only need to be applied to (i) details that are subjected to a net applied tensile stress; or (ii) details where the compressive stress is less than twice the maximum tensile live load stress resulting from the specified fatigue live load combination. In Equation 2.24, the threshold stress,  $\Delta F_{th}$ , is multiplied by a factor of one-half to account for the possibility of the heaviest truck in 75 years being twice the weight of the fatigue truck used in calculating the stress range.

Table 2.2: Fatigue Detail Constant,  $A$ , and Fatigue Threshold,  $(\Delta F)_{th}$ .

Fatigue Category	Fatigue Detail Constant, $A$ (ksi <sup>3</sup> )	Fatigue Threshold, $(\Delta F)_{th}$ (ksi)
A	$250.0 \times 10^8$	24.0
B	$120.0 \times 10^8$	16.0
B'	$61.0 \times 10^8$	12.0
C	$44.0 \times 10^8$	10.0
C'	$44.0 \times 10^8$	12.0
D	$22.0 \times 10^8$	7.0
E	$11.0 \times 10^8$	4.5
E'	$3.9 \times 10^8$	2.6

Table 2.3: Fraction of Truck Traffic in a Single Lane,  $p$ .

Number of Lanes Available to Trucks	$p$
1	1.00
2	0.85
3 or more	0.80
$ADTT_{SL} = p \cdot ADTT$	

Table 2.4: Number of Stress Range Cycles per Truck Passage,  $C_s$ .

Longitudinal Members		Span Length	
		> 40.0 ft	≤ 40.0 ft
Simple-Span Girders		1.0	2.0
Continuous Girders	within 10% of the span length near interior support	1.5	2.0
	elsewhere	1.0	2.0
Cantilever Girders		5.0	
Trusses		1.0	
Transverse Members		Spacing	
		> 20.0 ft	≤ 20.0 ft
		1.0	2.0

According to the S-N curves provided in the AASHTO LRFD Specifications (1998) for the eight different categories, the fatigue life of a detail in one of these eight fatigue categories may be estimated using the following equation:

$$N_f = A \cdot (\Delta f)^{-3} \quad (2.26)$$

The conservatism in the design approach adopted by the AASHTO LRFD Specifications may arise from overestimation of the stress ranges or the conservative manner in which the design curves for each category were defined.

### ***2.3.1.2 The Fatigue Evaluation Model proposed by Moses et al.***

Moses et al. (1987) proposed a fatigue evaluation procedure for details in steel bridges that was adopted in the AASHTO Guide Specifications for Fatigue Evaluation of Existing Steel Bridges (1990). This procedure uses the same eight S-N curves that are

also used in the AASHTO LRFD Specifications. Additionally, however, reliability and safety factors are considered in this method in order to determine the remaining safe fatigue life or the remaining mean fatigue life. The remaining fatigue life of a detail in any of the eight AASHTO fatigue categories may be estimated as

$$Y_f = \frac{f \cdot K \times 10^6}{T_a \cdot C_s \cdot (R_s S_R)^3} - Y_a \quad (2.27)$$

where  $Y_f$  is the remaining fatigue life in years;  $Y_a$  is the present age of the bridge in years;  $K$  is a detail constant that depends on the fatigue category (see Table 2.5);  $T_a$  is the estimated lifetime average daily truck volume in the outer lane;  $C_s$  is the stress cycles per truck passage;  $f$  is a safety factor (taken to be 1.0 when calculating safe life and 2.0 when calculating mean life);  $R_s$  is a reliability factor associated with calculation of the stress range (taken to be 1.35 for redundant members and 1.75 for non-redundant members when calculating safe life; and taken to be 1.0 when calculating mean life);  $S_R$  is the stress range that can be obtained from a field stress-range histogram analysis, a HS15 fatigue truck analysis, or a field gross vehicle weight histogram analysis. The remaining fatigue life of a detail may be considered as infinite if (i) the factored stress range (i.e.,  $R_s \cdot S_R$ ) is less than the limiting stress range for infinite life,  $S_{FL}$  (see Table 2.5); or (ii) the compressive dead load stress in the detail is greater than two times the factored tensile portion of the live load stress range. The limiting stress range,  $S_{FL}$ , in Table 2.5 is equal to the fatigue threshold,  $\Delta F_{th}$ , (in Table 2.2) multiplied by a factor of 0.364. The factor of 0.364 was derived from a simplified reliability analysis by Moses et al. (1987) to provide a high probability that all of the stress ranges in the stress spectrum will be below the fatigue threshold,  $\Delta F_{th}$ .

Table 2.5: Detail Constant,  $K$ , and Limiting Stress Range,  $S_{FL}$ , in the Model of Moses et al. (1987).

Fatigue Category	Detail Constant, $K$ (ksi <sup>3</sup> )	Limiting Stress Range for Infinite Life, $S_{FL}$ (ksi)
A	68	8.8
B	33	5.9
B'	17	4.4
C	12	3.7
D	6.0	2.6
E	2.9	1.6
E'	1.1	0.9
F	2.9	2.9

In this model of Moses et al (1987), the value of the detail constant,  $K$ , multiplied by  $365 \times 10^6$  is the same as the other detail constant,  $A$ , in the AASHTO LRFD Bridge Design Specifications (1998) because both models are based on the same S-N curves. However, by incorporating the reliability factor,  $R_s$ , and the safety factor,  $f$ , the model proposed by Moses et al. (1987) is more conservative than the AASHTO LRFD model in evaluating fatigue life. For example, since the stress range in a non-redundant detail would be multiplied by the reliability factor,  $R_s$ , of 1.75, the fatigue life would be lowered by a factor of  $1.75^3$  (or approximately, 5.36) with Moses' model. This indicates the greater conservatism implied by Moses' model that has been employed in the AASHTO Guide Specifications (1990) as compared to the AASHTO LRFD Bridge Design Specifications (1998).

### 2.3.2 Strain-Based Approach

A strain-based approach for fatigue analysis is usually employed for low-cycle fatigue (LCF) problems where structural details experience very high stress levels and plastic strains contribute a considerable portion towards the total strain. Structural components and details are designed to sustain loads in the elastic range of materials. However, stress concentration and stress redistribution can often bring about plastic strain in structural components. A strain-based approach for fatigue analysis can be formulated using the Basquin-Coffin-Manson relation as follows:

$$\frac{\Delta\varepsilon}{2} = \frac{\sigma'_f}{E} (2N_{rev,f})^b + \varepsilon'_f (2N_{rev,f})^c \quad (2.28)$$

where  $\Delta\varepsilon/2$  is the total strain amplitude;  $N_{rev,f}$  is the number of reversals to failure (2 reversals = 1 cycle);  $E$  is the Young's modulus for the material;  $\sigma'_f$  is a fatigue strength coefficient;  $\varepsilon'_f$  is a fatigue ductility coefficient;  $b$  is a fatigue strength exponent; and  $c$  is a fatigue ductility exponent. The Basquin-Coffin-Manson formulation for evaluating fatigue is based on relating fatigue life to the number of stress amplitude cycles (Basquin, 1910) and to the number of plastic strain amplitude reversals (Coffin, 1954; Manson, 1954). The various material properties,  $\sigma'_f$ ,  $\varepsilon'_f$ ,  $b$ , and  $c$ , can be obtained from laboratory tests and the Basquin-Coffin-Manson relation can be understood by studying a log-log plot of strain amplitude versus load reversals as is shown in Figure 2.5. It can be seen that this strain-based curve approaches the elastic line when the total strain amplitude levels are low and it approaches the plastic line while the total strain amplitude levels are high.

Crack initiation often occurs at the plastic zone in details due to the formation of slip bands. The strain-based approach is frequently employed to estimate the initiation life for details.

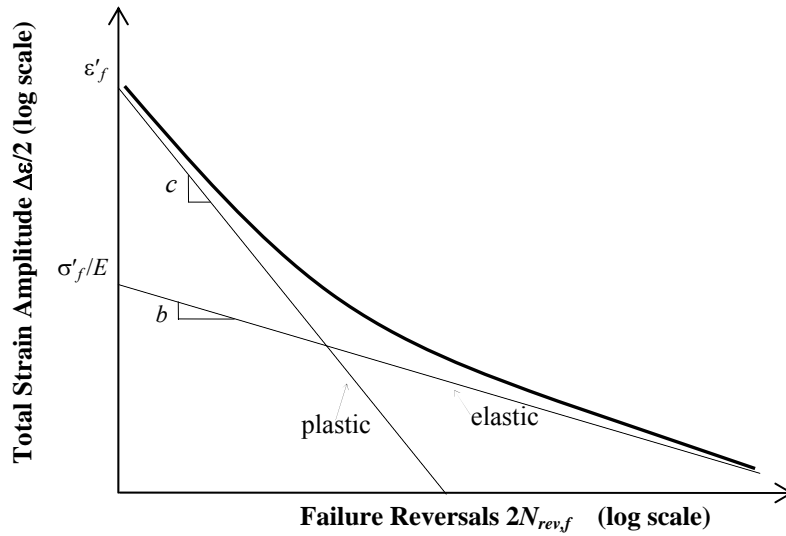


Figure 2.5: Schematic Strain-Life Curve.

### 2.3.3 Linear Elastic Fracture Mechanics (LEFM) Approach

In the stress- and strain-based approaches, uncracked structural components or details are assumed at the beginning of the fatigue analyses. The growth of cracks in components or details is not accounted for in these approaches. A fracture mechanics approach, on the other hand, can be employed to analyze fatigue in cracked components where the cracks might, for example, originate from material or welding flaws, or might have initiated during previous loadings. The linear elastic fracture mechanics (LEFM) approach is the most common fracture mechanics approach employed in engineering applications. This approach is based on the assumptions of small displacements, that the material is isotropic and linear elastic, and that a small plastic zone exists at the crack tip. According to LEFM, the stress intensity factor,  $K$ , around a crack tip may be expressed as follows:

$$K = F(a) \cdot \sigma \sqrt{\pi a} \quad (2.29)$$

where  $a$  is the size of the crack;  $F(a)$  is a function accounting for the shape of the specimen and the crack geometry;  $\sigma$  is the far-field stress resulting from the applied load on the component.

For metallic materials, the crack growth behavior due to fatigue loading may be represented as a sigmoidal curve on a  $\log da/dN$ – $\log \Delta K$  plot and can be divided into three regions as shown in Figure 2.6, where  $\Delta K$  is the stress intensity factor range in a stress cycle. In Region I, a threshold stress intensity factor,  $\Delta K_{th}$ , is shown below which crack growth cannot be detected. The closer the stress intensity factor range  $\Delta K$  is to  $\Delta K_{th}$ , the slower is the rate of crack growth. Below  $\Delta K_{th}$ , cracks do not grow under cyclic loading. In Region III, the crack growth rate is so high that cracks grow rapidly until the component fractures. Because cracks grow so fast in Region III, the crack growth behavior in this region does not significantly affect the total fatigue life. Region II is the most important region involving crack propagation that affects fatigue analysis. Paris and Erdogan (1963) proposed an empirical equation relating the rate of crack growth to the stress intensity factor range as follows:

$$\frac{da}{dN} = C \cdot (\Delta K)^m \quad (2.30)$$

where  $C$  and  $m$  are material properties obtained from data in Region II. The relationship described by Equation 2.30 is commonly referred to as Paris' law.

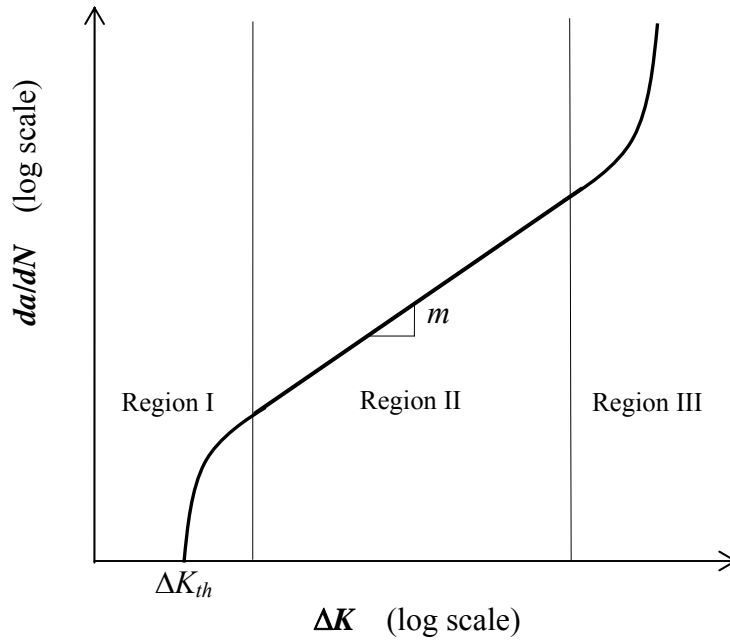


Figure 2.6: Crack Growth Rate versus Stress Intensity Factor Range.

Upon substitution of Equation 2.29 into Equation 2.30 and rearranging terms so as to compute the number of cycles to failure,  $N_f$ , it takes for a crack to grow from an initial crack size,  $a_i$ , to a failure crack size,  $a_f$ , it follows that:

$$N_f = \int_{a_i}^{a_f} \frac{da}{C \cdot [F(a) \cdot \Delta\sigma \cdot \sqrt{\pi a}]^m} \quad (2.31)$$

The number of cycles to failure,  $N_f$ , is very sensitive to the value of the initial crack size,  $a_i$ , and small changes to  $a_i$  can result in large variations in estimates of  $N_f$ . Generally, the initial crack size is not easily measured or estimated especially for details assumed to be “uncracked.” Determination of the size of a crack, when present, depends on the non-destructive evaluation (NDE) technique. In design calculations, the initial crack size is usually set at a conservative value so that the number of cycles to failure is not overestimated. In addition, for complicated details, it is not always easy to accurately



estimate stress intensity factors due to the complex geometric shapes that might be involved. In summary, limitations of the LEFM approach arise mostly due to difficulties in estimation of the initial crack size and due to geometric complexities associated with the detail being analyzed.

## **2.4 CONCLUDING REMARKS**

In this chapter, we have reviewed the relevant literature pertaining to fatigue reliability analysis and reliability-based inspection scheduling methods in various engineering applications. This provides useful background information and guidance for applying similar reliability analysis and inspection scheduling techniques with appropriate modification for use on steel bridges. Theories and procedures employed in probabilistic structural reliability analysis as well as in three different deterministic fatigue analysis approaches were reviewed in this chapter. Two deterministic fatigue approaches – the stress-based approach and the LEFM approach – will be used together with the fatigue load modeling procedures described in Chapter 3 in order to formulate fatigue reliability analysis approaches in Chapter 4 for dealing with two types of fracture-critical members (those categorized according to AASHTO and those not). Subsequent chapters demonstrate how these reliability analyses may then be used in inspection scheduling.

## **Chapter 3: MODELS FOR FATIGUE LOADING IN STEEL BRIDGES**

### **3.1 INTRODUCTION**

Fatigue calculations for steel bridges are generally developed based on loads arising from passing vehicles, especially single trucks. Due to the randomness of the actual traffic flow, vehicle-induced loads generate variable-amplitude stress ranges in bridge details. Most of the useful material properties for fatigue analysis, such as the fatigue details constant,  $A$ , in the S-N curve approach or the crack growth model parameters,  $C$  and  $m$ , in the Linear Elastic Fracture Mechanics (LEFM) approach are derived from fatigue tests under constant-amplitude stress cycles. It is important to be able to correctly model the irregular fatigue load cycles in steel bridges so that the material properties obtained from constant-amplitude fatigue tests can be employed for variable-amplitude fatigue analysis. In addition, the magnitude of the cyclic stress ranges is a principal parameter that controls the fatigue behavior of details in steel bridges. Estimation of these stress ranges also requires accurate modeling especially for steel bridges where fatigue evaluations leading to estimates of remaining life (in deterministic approaches) or of reliability (in probabilistic approaches) are influenced by the stress range raised to the third power. Thus, small errors in evaluating stress ranges can result in significant errors in results from these fatigue evaluations. Several methods have been proposed to model variable-amplitude fatigue loadings for fatigue analyses. The most practical of these methods is based on statistical modeling that can help to derive an equivalent stress range by using the statistical distribution of the full loading spectrum. Such an equivalent stress range can then be used to characterize the

variable-amplitude fatigue loadings as is commonly done for bridges and offshore structures. In bridge engineering, three statistical models – stress spectrum analysis, assumed distribution analysis, and fatigue truck analysis – are most often used in fatigue analyses. These three analysis methods are described in the following sections.

### **3.2 STRESS SPECTRUM ANALYSIS**

Before performing a stress spectrum analysis for a detail in a steel bridge, the first step is to obtain a representative stress range spectrum for the detail. The stress range spectrum, also known as a stress range histogram, is a statistical summary that shows the frequency of occurrence of all stress ranges experienced by the detail during its life. These various stress ranges result from the various possible fatigue loadings that are induced by passing trucks. Generally, either stress history data collected for the detail or summaries based on cycle-counting approaches are needed in order to establish the representative stress range spectrum for the detail.

In order to accurately reflect the fatigue loading due to the of actual truck traffic, the most reliable method is to collect sufficient stress data (stress histories) directly from the field. Field measurements, however, can be expensive. Schilling et al. (1978) suggested two alternatives. One option is to collect field data on truck traffic on the bridge and relate these data to the stress spectrum by suitable models; the other is to estimate the stress spectrum directly from field data on similar bridges. Since stress range spectra for bridges are strongly site-specific (Laman and Nowak, 1996), field measurements provide the best stress range data for bridge details.

After collecting sufficient stress data from the field, a proper cycle-counting method is needed to process the irregular stress histories and store the data in an appropriate and manageable number of stress range bins. Dowling (1993) suggested

that the rainflow cycle-counting method, developed by Matsuishi and Endo (1968), or other similar methods that take into consideration the closed hysteresis loops for complicated loading processes are the best methods to use for counting cycles. To avoid yielding half cycles in the cycle-counting process, the stress history of a detail can be modified by moving the segment of the stress history that occurs before the absolute maximum stress to the end of the stress history so that the counting can begin and end at the greatest stress value. A review of the rainflow cycle-counting procedure is presented in Appendix C.

The objective of a stress spectrum analysis is to derive an equivalent stress range from the representative stress range spectrum for a specified detail. The equivalent stress range is defined as the constant-amplitude stress range that can yield the same fatigue life as the variable-amplitude stress range spectrum for a detail. An expression for the equivalent stress range can be derived separately for the two deterministic fatigue approaches – the stress-based approach and the LEFM approach.

In the stress-based approach, the equivalent stress range,  $S_{RE}$ , representing a total of  $N$  variable-amplitude stress cycles, is derived using the S-N relation and Miner's rule as follows:

$$S_{RE} = \left( \sum_{i=1}^N \alpha_i \cdot S_{R,i}^m \right)^{1/m} \quad (3.1)$$

where  $S_{R,i}$  is the value at the mid-point of the  $i^{\text{th}}$  stress range interval;  $\alpha_i$  is the occurrence frequency of the stress ranges in the  $i^{\text{th}}$  stress range interval; and  $m$  is the material constant defined in Equation 2.19 for the S-N curve. Thus, the equivalent stress range represents the combined effect of all of the variable-amplitude fatigue loading cycles on the detail and can be treated as a constant-amplitude stress range to be applied in the stress-based fatigue analysis.

For the fracture mechanics approach, the equivalent stress range is derived using Paris' law given by Equation 2.30, according to which, the crack size increment,  $\Delta a_i$ , in a single cycle (say the  $i^{\text{th}}$  cycle) is:

$$\Delta a_i = C \cdot (\Delta K_i)^m \quad (3.2)$$

After  $N$  stress cycles, the crack is assumed to grow by an amount  $a_N$  that can be expressed as follows:

$$a_N = \sum_{i=1}^N \Delta a_i = \sum_{i=1}^N C \cdot (\Delta K_i)^m = C \sum_{i=1}^N (\Delta K_i)^m \quad (3.3)$$

An average crack growth rate can be defined in terms of the total number of stress cycles,  $N$ , and the corresponding total change in crack size,  $a_N$  as follows:

$$\left( \frac{da}{dN} \right)_{\text{avg}} = \frac{a_N}{N} = \frac{C \sum_{i=1}^N (\Delta K_i)^m}{N} = C \cdot \left\{ \left[ \sum_{i=1}^N \alpha_i \cdot (\Delta K_i)^m \right]^{1/m} \right\}^m = C (\Delta K_E)^m \quad (3.4)$$

where  $\Delta K_E$  is defined below and Equation 2.29 is used to relate stress intensity factor ranges to stress ranges

$$\Delta K_E = \left[ \sum_{i=1}^N \alpha_i \cdot (\Delta K_i)^m \right]^{1/m} = F(a) \sqrt{\pi a} \left[ \sum_{i=1}^N \alpha_i \cdot S_{R,i}^m \right]^{1/m} = F(a) \sqrt{\pi a} \cdot S_{RE} \quad (3.5)$$

where  $F(a)$  is the geometry function for the crack as defined in Equation 2.29 and  $\alpha_i$  is the occurrence frequency of the stress ranges in the  $i^{\text{th}}$  stress range interval whose mid-point value is  $S_{R,i}$ .

Finally, the equivalent stress range in the LEFM-based fatigue analysis can be expressed as

$$S_{RE} = \left( \sum_{i=1}^N \alpha_i \cdot S_{R,i}^m \right)^{1/m} \quad (3.6)$$

It may be noted that the expression for the equivalent stress range in the stress-based approach and the fracture mechanics approach are identical (see Equations 3.1 and 3.6). This expression of is sometimes referred to as Miner's equivalent stress range. By setting  $m$  equal to 2, the root-mean-square (RMS) equivalent stress range proposed by

Barsom (1973) is obtained. Schilling et al. (1978) compared the Miner's and RMS equivalent stress ranges and found that the Miner's range provided a more conservative estimate than the RMS range in fitting variable-amplitude data to constant-amplitude regression lines representing S-N curves.

### **3.3 ASSUMED DISTRIBUTION ANALYSIS**

Upon examination of sufficient stress range data collected from the field, the random and variable-amplitude fatigue loadings in steel bridges will usually reveal some regularity and the stress spectra might follow some recognizable probability distributions. After years of analyses by several researchers, a few probability distributions have been proposed for modeling the stress spectra on details in bridges. The ASCE Committee on Fatigue and Fracture Reliability (1982a-d) discussed possible use of the Rayleigh, Weibull, Beta, Polynomial, and lognormal distributions for fatigue analysis. A closed-form expression for the equivalent stress range can be easily derived using any of these assumed probability distributions and can then be used in the modeling of random fatigue loadings on steel bridges. Derivations of the equivalent stress range for the various assumed distributions are presented in the following sections.

#### **3.3.1 Rayleigh Distribution Analysis**

On the basis of the analysis of 51 sets of stress range spectrum data on bridges from six sources including Interstate and U.S. routes in semi-rural and metropolitan locations, Schilling et al. (1978) showed that the Rayleigh distribution can provide a reasonable model for the stress range spectrum of some details in steel bridges. The

Rayleigh probability density function (PDF),  $f_{S_R}(s_R)$ , and cumulative distribution function (CDF),  $F_{S_R}(s_R)$ , for stress ranges,  $S_R$ , can be expressed as:

$$f_{S_R}(s) = \left( \frac{s}{S_{R0}^2} \right) \cdot \exp \left[ -\frac{1}{2} \left( \frac{s}{S_{R0}} \right)^2 \right] \quad (3.7)$$

$$F_{S_R}(s) = 1 - \exp \left[ -\frac{1}{2} \cdot \left( \frac{s}{S_{R0}} \right)^2 \right] \quad (3.8)$$

where  $S_{R0} = \sqrt{\frac{2}{\pi}} \cdot E[S_R]$ . The mean value,  $E[S_R]$ , and variance,  $Var[S_R]$ , of the stress range are given as follows:

$$E[S_R] = \sqrt{\frac{\pi}{2}} \cdot S_{R0} \quad (3.9)$$

$$Var[S_R] = \left( 2 - \frac{\pi}{2} \right) \cdot S_{R0}^2 \quad (3.10)$$

A closed-form expression for the  $m^{\text{th}}$  moment of  $S_R$  with the Rayleigh distribution can be given as:

$$E[S_R^m] = \left( \sqrt{2} S_{R0} \right)^m \Gamma \left( \frac{m}{2} + 1 \right) = \sum \gamma_i \cdot S_{R,i}^m \quad (3.11)$$

where  $\Gamma()$  is the gamma function and  $\gamma_i$  represents the fraction of cycles that had stress range,  $S_{R,i}$ .

The equivalent stress range,  $S_{RE}$ , derived from the variable-amplitude stress range spectrum with the assumed Rayleigh distribution can be obtained as:

$$S_{RE} = \left\{ \left( \sqrt{2} S_{R0} \right)^m \Gamma \left( \frac{m}{2} + 1 \right) \right\}^{1/m} \quad (3.12)$$

where  $S_{R0}$  can be computed using Equation 3.9 and an estimate of the mean stress range alone.

### 3.3.2 Weibull Distribution Analysis

Nolte and Hansford (1976) proposed a Weibull distribution to model the long-term stress range spectrum. The two-parameter Weibull probability density function (PDF) and cumulative distribution function (CDF) can be written as:

$$f_{S_R}(s) = \left(\frac{\nu}{\eta}\right) \cdot \left(\frac{s}{\eta}\right)^{\nu-1} \cdot \exp\left[-\left(\frac{s}{\eta}\right)^\nu\right] \quad (3.13)$$

$$F_{S_R}(s) = 1 - \exp\left[-\left(\frac{s}{\eta}\right)^\nu\right] \quad (3.14)$$

where  $\eta$  is a scale parameter and  $\nu$  is a shape parameter. These two parameters can be obtained using the method of moments along with estimates of the mean and variance from the stress range data. This is possible because the mean value,  $E[S_R]$ , and variance,  $Var[S_R]$ , of the stress range with a Weibull distribution may be expressed as follows:

$$E[S_R] = \eta \cdot \Gamma\left(\frac{1}{\nu} + 1\right) \quad (3.15)$$

$$Var[S_R] = \eta^2 \cdot \left\{ \Gamma\left(\frac{2}{\nu} + 1\right) - \left[ \Gamma\left(\frac{1}{\nu} + 1\right) \right]^2 \right\} \quad (3.16)$$

A closed-form expression for the  $m^{\text{th}}$  moment of  $S_R$  with the Weibull distribution can be given as:

$$E[S_R^m] = \eta^m \cdot \Gamma\left(\frac{m}{\nu} + 1\right) = \sum \gamma_i \cdot S_{R,i}^m \quad (3.17)$$

The equivalent stress range,  $S_{RE}$ , derived from the variable-amplitude stress range spectrum with the assumed Weibull distribution can be obtained as:

$$S_{RE} = \left\{ \eta^m \cdot \Gamma\left(\frac{m}{\nu} + 1\right) \right\}^{1/m} \quad (3.18)$$

where  $\eta$  and  $\nu$  are obtained using Equations 3.15 and 3.16. Note that by setting  $\nu$  equal to 2, it can be seen that the Rayleigh distribution is actually a special case of the Weibull



distribution. The Weibull distribution, though, has greater flexibility in modeling data than the Rayleigh distribution in part because it involves two parameters.

### 3.3.3 Beta Distribution Analysis

Ang and Munse (1975) suggested that the Beta distribution could be applied to model fatigue loadings on highway bridges. The probability density function (PDF) and cumulative distribution function (CDF) of stress ranges with the Beta distribution can be written as:

$$f_{S_R}(s) = \frac{1}{B(q, r)} \cdot \frac{s_R^{q-1} (s_0 - s)^{r-1}}{s_0^{q+r-1}} \quad \text{where } B(q, r) = \int_0^1 t^{q-1} (1-t)^{r-1} dt \quad (3.19)$$

$$F_{S_R}(s) = \frac{\int_0^{s/s_0} t^{q-1} (1-t)^{r-1} dt}{B(q, r)} \quad (3.20)$$

where  $0 \leq s_R \leq s_0$ ; while  $q$  and  $r$  are parameters of the distribution; and  $s_0$  is an upper bound on the stress range. The mean value,  $E[S_R]$ , and variance,  $Var[S_R]$ , of the stress range with a Beta distribution may be expressed as:

$$E[S_R] = \frac{q \cdot s_0}{(q + r)} \quad (3.21)$$

$$Var[S_R] = \frac{q \cdot r \cdot s_0^2}{(q + r)^2 (q + r + 1)} \quad (3.22)$$

A closed-form expression for the  $m^{\text{th}}$  moment of  $S_R$  with the Beta distribution can be given as:

$$E[S_R^m] = \frac{s_0^m \cdot \Gamma(m + q) \cdot \Gamma(q + r)}{\Gamma(q) \cdot \Gamma(m + q + r)} = \sum \gamma_i \cdot s_{R,i}^m \quad (3.23)$$

The equivalent stress range,  $S_{RE}$ , derived from the variable-amplitude stress range spectrum with the assumed Beta distribution can be obtained as:

$$S_{RE} = \left\{ \frac{s_0^m \cdot \Gamma(m + q) \cdot \Gamma(q + r)}{\Gamma(q) \cdot \Gamma(m + q + r)} \right\}^{1/m} \quad (3.24)$$

where  $s_0$  can be taken to be the maximum applied or anticipated stress range and the parameters,  $q$  and  $r$ , can be estimated using Equations 3.21 and 3.22.

### 3.3.4 Polynomial Distribution

Yamada and Albrecht (1976) collected 106 published stress range spectra from 29 highway bridges in the United States and proposed the Polynomial distribution model for the stress ranges on highway bridges. All of the 106 stress range spectra were reduced to a non-dimensional form before the analysis. The probability density function (PDF) and cumulative distribution function (CDF) of the non-dimensional stress range variable,  $X$ , can be written as:

$$f_X(x) = \begin{cases} 0 & 0 \leq x < 0.25 \\ -12(x-1)^3 + 0.07 & 0.25 \leq x \leq 1.0 \\ 0 & x > 1.0 \end{cases} \quad (3.25)$$

$$F_X(x) = \begin{cases} 0 & 0 \leq x < 0.25 \\ 1 - 3(x-1)^4 + 0.07(x-1) & 0.25 \leq x \leq 1.0 \\ 1 & x > 1.0 \end{cases} \quad (3.26)$$

where  $X = S_R/S_{\max}$ , and  $S_{\max}$  is the maximum stress range measured in the stress range spectrum. The mean value and variance of  $X$  and  $S_R$  with the Polynomial distribution can be obtained as follows:

$$E[X] = 0.4125 \quad (3.27)$$

$$Var[X] = 1.893 \times 10^{-2} \quad (3.28)$$

$$E[S_R] = 0.4125 \cdot S_{\max} \quad (3.29)$$

$$Var[S_R] = 1.893 \times 10^{-2} \cdot S_{\max}^2 \quad (3.30)$$

A closed-form expression for the  $m^{\text{th}}$  moment of  $S_R$  with the Polynomial distribution can be given as:

$$E[S_R^m] = S_{\max}^m \cdot \left\{ \frac{(7m^3 + 63m^2 + 182m + 7368) \cdot (10^{-2})}{(m+1)(m+2)(m+3)(m+4)} - \frac{(2053m^3 + 20502m^2 + 68903m + 79422) \cdot (6.25 \times 10^{-4})}{4^m (m+1)(m+2)(m+3)(m+4)} \right\} \quad (3.31)$$

The equivalent stress range,  $S_{RE}$ , derived from the variable-amplitude stress range spectrum with the assumed Polynomial distribution can be obtained as:

$$S_{RE} = S_{\max} \left\{ \frac{(7m^3 + 63m^2 + 182m + 7368) \cdot (10^{-2})}{(m+1)(m+2)(m+3)(m+4)} - \frac{(2053m^3 + 20502m^2 + 68903m + 79422) \cdot (6.25 \times 10^{-4})}{4^m (m+1)(m+2)(m+3)(m+4)} \right\}^{1/m} \quad (3.32)$$

### 3.3.4 Lognormal Distribution

The ASCE Committee on Fatigue and Fracture Reliability (1982a-d) discussed the lognormal distribution model for variable-amplitude stress ranges. The probability density function (PDF) and cumulative distribution function (CDF) of stress ranges with the lognormal distribution can be written as:

$$f_{S_R}(s_R) = \frac{1}{\sqrt{2\pi} \zeta_{S_R} \cdot s_R} \exp \left[ -\frac{1}{2} \left( \frac{\ln s_R - \lambda_{S_R}}{\zeta_{S_R}} \right)^2 \right] \quad (3.33)$$

$$F_{S_R}(s_R) = \Phi \left( \frac{\ln s_R - \lambda_{S_R}}{\zeta_{S_R}} \right) \quad (3.34)$$

where  $\lambda_{S_R}$  and  $\zeta_{S_R}$  are distribution parameters that can be estimated from the mean ( $\mu_{S_R}$ ) and the coefficient of variation ( $\delta_{S_R}$ ) of the stress range data as follows:

$$\lambda_{S_R} = \ln(\mu_{S_R}) - 0.5 \zeta_{S_R}^2 \quad (3.35)$$

$$\zeta_{S_R} = \sqrt{\ln(1 + \delta_{S_R}^2)} \quad (3.36)$$

A closed-form expression for the  $m^{\text{th}}$  moment of  $S_R$  with the lognormal distribution can be given as:

$$E[S_R^m] = \mu_{S_R}^m (1 + \delta_{S_R}^2)^{m(m-1)/2} \quad (3.37)$$

The equivalent stress range,  $S_{RE}$ , derived from the variable-amplitude stress range spectrum with the assumed lognormal distribution can be obtained as:

$$S_{RE} = \mu_{S_R} (1 + \delta_{S_R}^2)^{(m-1)/2} \quad (3.38)$$

### 3.4 FATIGUE TRUCK ANALYSIS

Since single truck passings are a major source of variable-amplitude stress ranges on steel bridges, one practical approach for modeling truck-induced fatigue loadings is to create an equivalent fatigue truck that when passed over the bridge will generate the equivalent stress ranges in details identified for fatigue analysis. The fatigue damage caused by a certain number of passages of trucks of different weights on the bridge is thus identical to the fatigue damage caused by an equal number of passages of the equivalent fatigue truck on the same bridge. The equivalent fatigue truck, which is analogous to the equivalent stress range derived from the variable-amplitude stress range spectrum, can be estimated from the gross vehicle weight (GVW) spectrum as follows:

$$W_E = \left( \sum \alpha_i \cdot W_i^m \right)^{1/m} \quad (3.39)$$

where  $W_E$  is the equivalent fatigue truck weight;  $W_i$  is the value at the mid-point of the  $i^{\text{th}}$  truck weight interval in the GVW spectrum;  $\alpha_i$  is the occurrence frequency of trucks in the  $i^{\text{th}}$  truck weight interval; and  $m$  is the material constant defined in Equation 2.19 for the S-N curve. The GVW spectra for bridges can be obtained from field measurements, such as weigh-in-motion data or weigh station data. Due to the different sources of GVW data, several equivalent fatigue truck models have been proposed in the past to model truck-induced cyclic loadings on steel bridges. The analysis procedures for generating an equivalent stress range from a fatigue truck in plate girder bridges and box

girder bridges are demonstrated in Figures 3.1 and 3.2, respectively. Because most of the equivalent fatigue truck models are developed for design purposes, the equivalent stress ranges derived from the equivalent fatigue truck analysis are usually conservative compared to the equivalent stress ranges derived from a stress spectrum analysis. The various available equivalent fatigue truck models are described next.

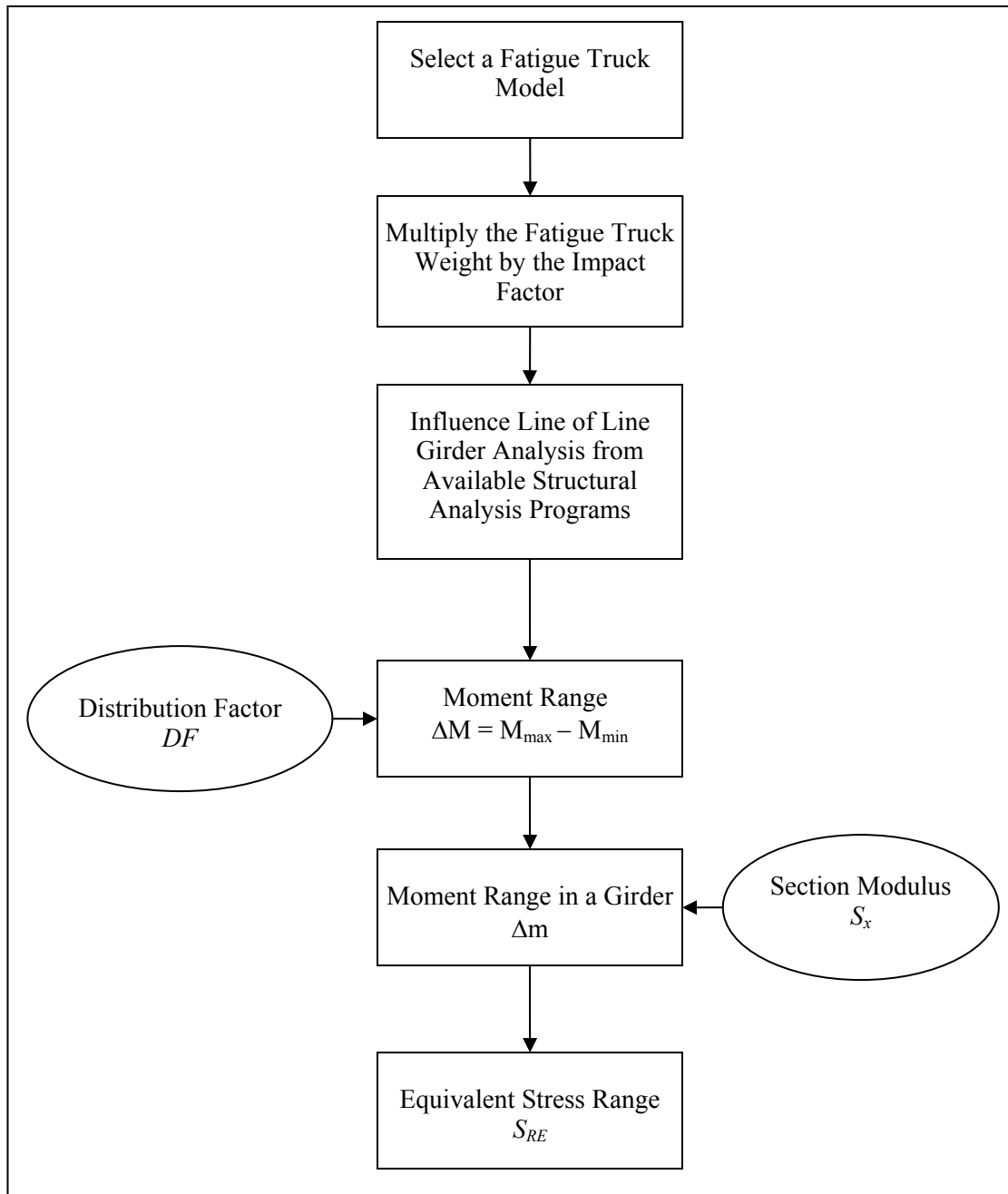


Figure 3.1: Flow Chart of Equivalent Fatigue Truck Analysis for Steel Bridges.

### 3.4.1 Schilling's Fatigue Truck Model

Based on the Federal Highway Administration 1970 nationwide loadmeter survey, Schilling et al. (1978) suggested a fatigue truck model for highway bridge design. The gross vehicle weight (GVW) spectrum analysis of the loadmeter data showed that the equivalent gross weight of the fatigue truck calculated from Equation 3.39, by setting  $m$  equal to 3, was 50 kips, which is about 70% of the weight of AASHTO HS20 design truck. Schilling's fatigue truck model distributes the 50 kips truck weight according to the same axle configuration as the AASHTO HS20 live load design truck (see Figure 3.2).

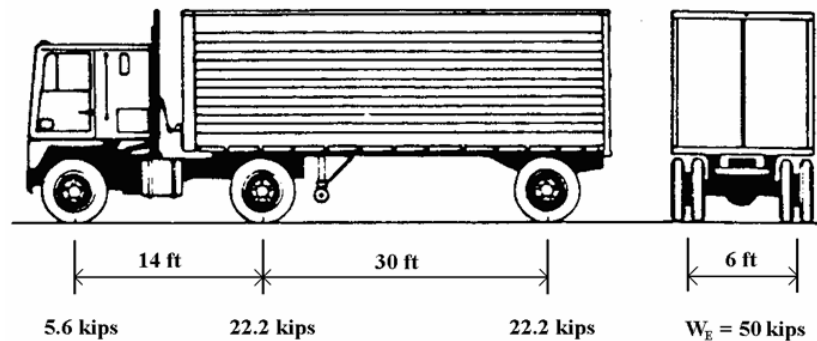


Figure 3.2: Schilling's Fatigue Truck Model.

### 3.4.2 AASHTO Fatigue Truck Model

The fatigue truck model in the AASHTO specifications is based on the gross vehicle weight (GVW) spectrum from the weight-in-motion (WIM) research conducted by the Federal Highway Administration (FHWA) in 1981 (Snyder et al., 1985). This research study considered 30 sites in the United States and recorded data from more than 27,000 trucks. The FHWA research proposed a fatigue truck model with a gross vehicle

weight of 54 kips and, for convenience, the same axle spacing and axle load distribution as the AASHTO live load design truck HS20 (weight = 72 kips) were employed. Because this equivalent fatigue truck is three-quarters of the vehicle weight of the HS20 design truck, the AASHTO fatigue truck is also referred to as the HS15 truck in bridge engineering. The configuration of the HS15 truck is shown in Figure 3.3. The weight difference between the AASHTO fatigue truck and Schilling's fatigue truck might be explained in two ways. One explanation is that the WIM measuring system (used in development of the AASHTO fatigue truck model) can detect more overweight trucks which was not done in the FHWA loadmeter data from fixed weigh stations (and used in development of Shillings' model). An alternative explanation might be that truck traffic load sizes increased from 1970 to 1981.

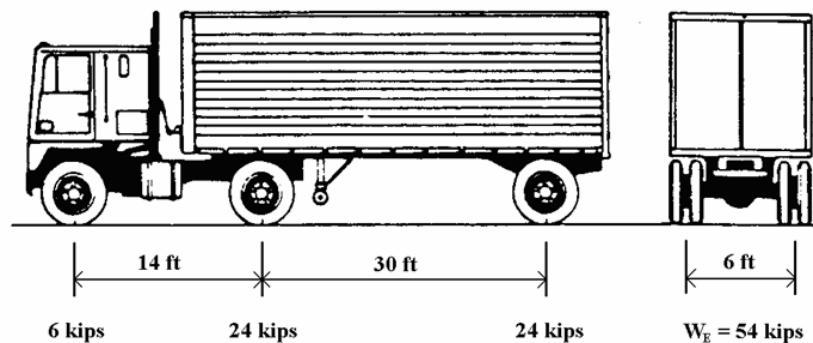


Figure 3.3: The AASHTO Fatigue Truck Model.

### 3.4.3 Moses' Fatigue Truck Model

Since the GVW spectra for bridges are strongly site-specific, Moses et al. (1987) proposed an adaptive fatigue truck model for steel bridges that was adapted in the AASHTO Guide Specifications for Fatigue Evaluation of Existing Steel Bridges (1990).



- Four methods are suggested to obtain the equivalent gross vehicle weight,  $W_E$ :
- (1) Adjust the gross weight of the fatigue truck based on judgment supported by the knowledge of truck traffic at the site;
  - (2) Construct a GVW spectrum from weigh station data and apply Equation 3.39 to calculate the equivalent gross vehicle weight;
  - (3) Construct a GVW spectrum from weigh-in-motion data and apply Equation 3.39 to calculate the equivalent gross vehicle weight;
  - (4) Collect traffic survey data that include the percentages of various types of trucks in the traffic and use Equation 3.39 to calculate the equivalent gross vehicle weight.

Note that the truck data in Methods (2), (3), and (4) above exclude panel, pickup, and other 2-axle/4-wheel trucks. The estimated equivalent gross vehicle weight is distributed in accordance with the same axle weight proportions as the HS20 design truck (Figure 3.4).

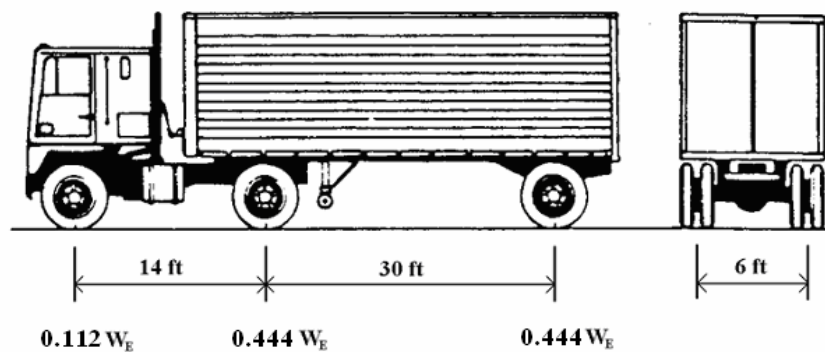


Figure 3.4: Moses' Fatigue Truck Model.

### 3.4.4 Laman's Dual Fatigue Truck Model

Laman and Nowak (1996) studied weigh-in-motion (WIM) data from five steel bridges in Michigan, which included 22,000 truck files each containing GVW, axle weights, and axle spacing. Because the state of Michigan permits heavier trucks on bridges than in other states, a single fatigue truck model was not sufficient to model the fatigue damage in the five bridges studied. Hence, a dual fatigue truck model was proposed to provide a more accurate fatigue damage evaluation method for steel bridges under normal truck traffic. The fatigue damage caused by the passages of all trucks with 2 to 9 axles was felt to be equivalent to the fatigue damage caused by the same number of passages of the proposed 3-axle fatigue truck (see Figure 3.5), while a 4-axle fatigue truck (see Figure 3.6) was proposed to model the fatigue damage caused by trucks with 10–11 axles. WIM data, with more detailed information about the percentage of trucks of different axles, are needed in order to use this dual fatigue truck model. The equivalent stress range,  $S_{RE}$ , for the dual fatigue truck model can be expressed as:

$$S_{RE} = \left[ \gamma_3 \cdot S_{RE3}^m + \gamma_4 \cdot S_{RE4}^m \right]^{1/m} \quad (3.41)$$

where  $\gamma_3$  is the fraction of 2-9 axle trucks in *ADTT*;  $\gamma_4$  is the fraction of 10-11 axle trucks in *ADTT*;  $S_{RE3}$  is the equivalent stress range generated by the proposed 3-axle fatigue truck; and  $S_{RE4}$  is the equivalent stress range generated by the proposed 4-axle fatigue truck. According to the study by Laman and Nowak (1996), the AASHTO fatigue truck model might overestimate the fatigue damage of bridges with a simple span shorter than 40 to 60 feet and underestimate the fatigue damage for bridges with longer spans. The dual fatigue truck model is site-specific and needs to be characterized by the load spectra for the bridge.

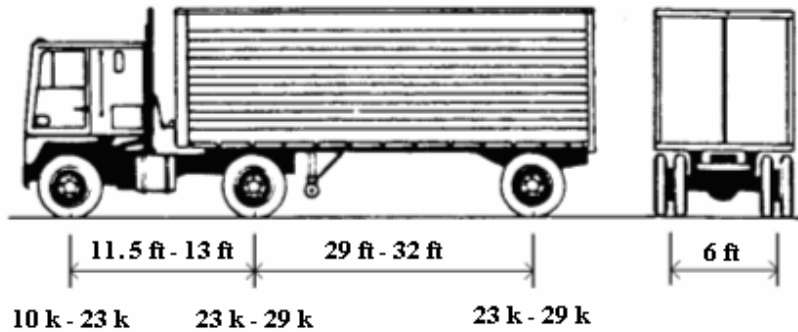


Figure 3.5: The Laman's Three-Axle Fatigue Truck Model

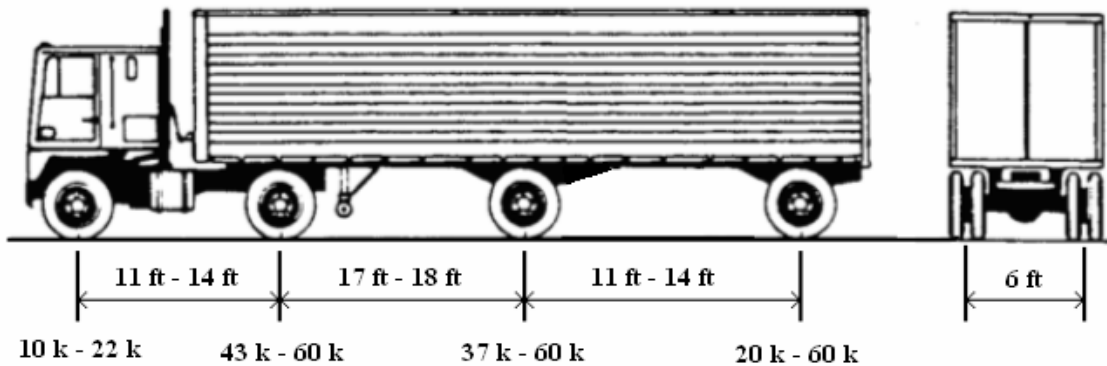


Figure 3.6: The Laman's Four-Axle Fatigue Truck Model

### 3.5 CONCLUDING REMARKS

Three methods for modeling fatigue loadings in steel bridges were presented in this chapter. The objective of each of these three methods is to derive the equivalent stress range for a given bridge detail. The stress spectrum analysis can provide the most accurate evaluation of the equivalent stress range for the detail of interest. However, collecting stress data using strain gages is costly as well as difficult or restrictive for

complex details. One way to circumvent this problem is to convert the stress data collected from one detail to other details that have no strain gages installed, but this conversion may lead to large errors. With limited statistical information, the equivalent stress range for a detail can also be obtained using the assumed distribution analysis. The ASCE Committee on Fatigue and Fracture Reliability (1982a-d) suggested use of the Rayleigh, Weibull, Beta, Polynomial, and lognormal distributions for fatigue analysis. Closed-form expressions for the equivalent stress range derived from these assumed distributions were presented in this chapter. Fatigue truck analysis provides a simple and convenient method for acquiring the equivalent stress range for a bridge detail. However, from the collected field data in Michigan studied by Laman and Nowak (1996), it was found that the fatigue truck model was site-specific due to the traffic variability at different sites. Hence, though the AASHTO fatigue truck model gives a suitable equivalent stress range for design purposes, for fatigue analysis, more accurate evaluation of equivalent stress ranges might likely come from analysis using Moses' fatigue truck model (Moses et al, 1987), which was built on GVW spectrum analyses from field vehicle data.

## **Chapter 4: FATIGUE RELIABILITY ANALYSIS FOR FRACTURE-CRITICAL MEMBERS IN STEEL BRIDGES**

The objective of this chapter is to apply structural reliability theory to evaluate the safety of fracture-critical members or details in steel bridges under fatigue loadings over the course of the service life of the bridge. Structural reliability analysis and fatigue load modeling to establish equivalent stress ranges are employed in the development of a systematic approach for evaluating the fatigue reliability of details in steel bridges. For those details that are standard enough so as to be classified according to the AASHTO fatigue categories, the AASHTO fatigue analysis approach that applies a limit state function based on Miner's Rule (with an empirical S-N curve relation based on fatigue test results) is used to evaluate the fatigue reliability. For those details not conveniently identified as representative of any AASHTO fatigue category, the LEFM-based fatigue reliability approach that applies a limit state function related to crack size and based on a damage accumulation function proposed by Madsen et al. (1985) is used. A decrease in fatigue reliability with an increase in the cumulative number of stress cycles experienced by the fracture-critical member will thus be modeled. This decreasing reliability can then be compared with the prescribed target reliability level (or, equivalently, with the prescribed minimum acceptable level of structural safety for the bridge) and can provide useful information needed in inspection scheduling. If the fatigue reliability of the detail is higher than the target reliability over the entire service life, periodic routine inspections, such as visual inspections, may be sufficient. However, if the fatigue reliability falls below the target reliability at any time during the service life, refinements in both the type of inspection techniques and in the frequency (with a possibly non-periodic inspection schedule) may be necessary to ensure adequate safety.

#### 4.1 TARGET RELIABILITY

The target reliability index,  $\beta_{\text{target}}$ , is defined as the minimum safety level approved and accepted for a specific application. In the present situation, this value can be applied as a standard against which one might measure safety of the bridge from the point of view of fatigue failure that initiates at a specified detail on the bridge. The target reliability index,  $\beta_{\text{target}}$ , can be expressed in terms of the inverse of the cumulative distribution function of a standard Gaussian random variable,  $\Phi^{-1}(\cdot)$ , and a maximum acceptable probability of failure,  $P_F$ :

$$\beta_{\text{target}} = \Phi^{-1}(1 - P_F) \quad (4.1)$$

Note that the use of the target reliability index,  $\beta_{\text{target}}$ , is only done for convenience in describing results in this study. It is possible to establish and use a maximum acceptable probability of failure instead without affecting the formulation of the reliability analyses or the optimal inspection scheduling procedures to be described. The use of  $\beta_{\text{target}}$  as a starting point is in fact often tied to notions of probability (such as requiring  $\beta_{\text{target}}$  to be such that there is only a small probability of failure, such as 1 in 10,000).

It is important to note that the higher the target reliability index employed for a detail, the safer that detail will be over the service life. At the same time, however, it will be more expensive to maintain this higher safety level due to possible additional inspections and repairs that might be necessary for the detail. Hence, there is a tradeoff between the value of the target reliability index and the costs involved. Skjong and Bitner-Gregersen (2002) suggested that selection of a target reliability index should depend on failure consequences, should calibrate against known cases that are felt to be acceptable in the industry, and should be based on accepted decision analysis techniques. Several studies have been conducted on this topic in the offshore industry; however, there

are very few similar studies for bridges. By performing a series of redundancy analyses, Onoufriou (1999) proposed several target reliability index values associated with different failure consequences for offshore structures (see Table 4.1). These estimates are considered to be conservative for North Sea jacket structures.

For offshore structures, life loss is generally considerably smaller and financial losses considerably larger than for steel bridges. The criticality of a bridge and its degree of redundancy in a transportation network will greatly influence the selection of a target reliability index as will the available budget, the traffic, and the consequences of a failure. In this dissertation that deals with steel bridges, a target reliability index value of 3.7 which corresponds to a probability of failure of  $10^{-4}$  is employed in most of the numerical studies.

Table 4.1: Target Reliability Index Values for North Sea Jacket Structures (Onoufriou, 1999).

Failure Consequence	Target Reliability Index $\beta_{\text{target}}$	Failure Probability $P_F$
Very Serious	4.27	$10^{-5}$
Serious	3.72	$10^{-4}$
Not Serious	3.09	$10^{-3}$
Local Effect	2.33	$10^{-2}$
Negligible Effect	1.28	$10^{-1}$

## 4.2 AASHTO FATIGUE RELIABILITY APPROACH

The AASHTO fatigue reliability analysis approach is proposed for all structural members or details that are classified according to AASHTO fatigue categories. This approach is based on the AASHTO S-N curves, Miner's damage accumulation rule, and statistical information collected from numerous fatigue tests conducted in the 1970s when fatigue design provisions were being established in the United States. The AASHTO fatigue reliability approach is not applicable for analyzing AASHTO category details that contain cracks or flaws because of the limitation of the employed limit state function which does not take into consideration crack propagation in the analysis. The LEFM fatigue reliability approach, discussed in Section 4.3, can help in evaluating the fatigue reliability of flawed or cracked details that are classified according to AASHTO fatigue categories. It can also help in evaluation of any non-AASHTO category details.

### 4.2.1 Limit State Function

The limit state function employed in the AASHTO fatigue reliability approach is defined as follows:

$$g(\mathbf{X}) = N_c - N \quad (4.1)$$

where  $N_c$  is the critical number of stress cycles it takes for the specified detail to achieve fatigue failure, and  $N$  is the total accumulated number of stress cycles applied on the detail. By definition,  $g(\mathbf{X}) > 0$  implies that the detail has not failed due to fatigue; failure is assumed to occur when  $g(\mathbf{X}) \leq 0$ . It can be seen that the limit state function, given by Equation 4.1, is directly related to the number of stress cycles.



Combining the AASHTO S-N relation (Equation 2.19) and Miner's damage accumulation rule (Equation 2.20) for fatigue details under variable-amplitude stress ranges, the following expression can be obtained.

$$D = \sum \frac{n_i}{N_{c,i}} = \sum \frac{\gamma_i \cdot N}{A \cdot S_{R,i}^{-m}} = \frac{N}{A} \sum [\gamma_i \cdot S_{R,i}^m] = \frac{N}{A} S_{RE}^m \quad (4.2)$$

where  $D$  is Miner's damage accumulation index;  $n_i$  is the actual number of stress cycles associated with the stress range level,  $S_{R,i}$ ;  $N_{c,i}$  is the critical number of stress cycles that the detail can sustain under the constant-amplitude stress range,  $S_{R,i}$ ;  $\gamma_i$  is the ratio of  $n_i$  to the total number of accumulated stress cycles,  $N$ , in the detail;  $A$  is a fatigue detail constant parameter in the AASHTO S-N relation;  $m$  is the fatigue exponent in the S-N curve (see Equation 2.19); and  $S_{RE}$  is the Miner's equivalent stress range defined from the stress spectrum for the specified detail as discussed in Chapter 3.

According to Miner's rule (1945), fatigue failure occurs when the damage accumulation index,  $D$ , reaches a critical value,  $\Delta$ .

$$D \geq \Delta \quad (4.3)$$

where  $\Delta$  (Miner's critical damage accumulation index) has a value approximately equal to 1.0 for metallic materials. Combining Equations 4.2 and 4.3, the critical number of stress cycles,  $N_c$ , needed for fatigue failure under variable-amplitude loading with equivalent stress range,  $S_{RE}$ , can be expressed as:

$$N_c = \frac{A \cdot \Delta}{S_{RE}^m} \quad (4.4)$$

Hence, the limit state function for the AASHTO fatigue reliability approach can be rewritten as:

$$g(\mathbf{X}) = \left( \frac{A \cdot \Delta}{S_{RE}^m} \right) - N \quad (4.5)$$

Since the fatigue detail parameter,  $A$ , and Miner's critical damage accumulation index,  $\Delta$ , are obtained from experiments, they can be treated as random variables with

statistical characteristics estimated from fatigue tests. The equivalent stress range,  $S_{RE}$ , can be obtained by any suitable method described in Chapter 3. The accumulated number of stress cycles,  $N$ , is related to the traffic volume, particularly truck traffic volume, passing over the bridge and can be transformed into the number of years in service,  $Y$ ; however, the transformation from  $N$  to  $Y$  must, in general, account for uncertainty in the traffic. Fatigue reliability analysis can be implemented using the limit state function (Equation 4.5) when the related variables are completely described. A description of all of these related variables is presented next.

## **4.2.2 Studies of Related Variables in the Limit State Function**

### **4.2.2.1 Fatigue Detail Parameter, $A$**

When the AASHTO S-N relation (Equation 2.19) is expressed in logarithmic form or in a plot of  $\log_{10}N_f$  versus  $\log_{10}S_R$ , the fatigue detail parameter,  $A$ , is seen to be the  $\log_{10}N_f$ -axis intercept and  $m$  is the magnitude of the slope of this line, since we have:

$$\log_{10} N_f = -m \cdot \log_{10} S_R + \log_{10} A \quad (4.6)$$

Keating and Fisher (1986) studied extensive fatigue data of 800 full-sized and welded steel bridge details that were tested over a period of 6 years from 1966 to 1972 in the United States. Through regression analyses, they estimated the parameters,  $\log_{10}A$  and  $m$ , for the different fatigue categories. Results from this study are summarized in Table 4.2.

Table 4.2: Regression Coefficients of the Fatigue Detail Parameter,  $A$ , and Slope,  $m$ .

AASHTO Fatigue Category	Intercept, $\log_{10} A$		Slope $m$
	Mean Value ( $\mu_{\log_{10} A}$ )	Standard Deviation ( $\sigma_{\log_{10} A}$ )	
A	11.121	0.221	3.178
B	10.870	0.147	3.372
C	10.085	0.158	3.097
C'	10.038	0.063	3.250
D	9.664	0.108	3.071
E	9.292	0.101	3.095
E'	9.166	0.194	3.200

In addition, Fisher et al. (1970) studied fatigue test data from 374 steel beams and concluded that  $\log_{10} N_f$  can be assumed to follow a normal distribution. Hence,  $\log_{10} A$  is also assumed to follow a normal distribution and  $A$  therefore follows a lognormal distribution. The mean value,  $\mu_A$ , standard deviation,  $\sigma_A$ , and coefficient of variation,  $\delta_A$ , of the parameter,  $A$ , are calculated in Table 4.3 using the following transformation:

$$\mu_A = e^{(\lambda_A + \zeta_A^2 / 2)} \quad (4.7)$$

$$\sigma_A = \sqrt{\mu_A^2 \cdot (e^{\zeta_A^2} - 1)} \quad (4.8)$$

$$\delta_A = (\sigma_A / \mu_A) \quad (4.9)$$

where:

$$\lambda_A = \mu_{\ln A} = \ln 10 \cdot \mu_{\log_{10} A} \quad (4.10)$$

$$\zeta_A = \sigma_{\ln A} = \ln 10 \cdot \sigma_{\log_{10} A} \quad (4.11)$$

$$\ln A = \ln 10 \cdot \log_{10} A \quad (4.12)$$

Table 4.3: Mean Value, Standard Deviation, and Coefficient of Variation for the Fatigue Detail Parameter,  $A$ .

Fatigue Category	Mean Value $\mu_A$	Std. Deviation $\sigma_A$	COV $\delta_A$
A	$1.50 \times 10^{11}$	$8.18 \times 10^{10}$	0.54
B	$7.85 \times 10^{10}$	$2.74 \times 10^{10}$	0.35
C	$1.30 \times 10^{10}$	$4.89 \times 10^9$	0.38
C'	$1.10 \times 10^{10}$	$1.61 \times 10^9$	0.15
D	$4.76 \times 10^9$	$1.20 \times 10^9$	0.25
E	$2.01 \times 10^9$	$4.74 \times 10^8$	0.24
E'	$1.62 \times 10^9$	$7.63 \times 10^8$	0.47

#### 4.2.2.2 Miner's Critical Damage Accumulation Index, $\Delta$

In order to study Miner's critical damage accumulation index,  $\Delta$ , at fatigue failure for steel structures, Wirsching et al. (1987) and Wirsching and Chen (1988) surveyed the fatigue test data from Schilling et al. (1974), Schütz (1979), Berge and Eide (1981), Holmes and Kerr (1982), Shin and Lukens (1983), and Gurney (1983) and found that a lognormal distribution with a mean value,  $\mu_\Delta$ , of 1.0 and coefficient of variation,  $\delta_\Delta$ , of 0.3 is a reasonable model to describe Miner's critical damage accumulation index,  $\Delta$ . This represents the uncertainty associated with the use of Miner's rule. A lognormal distribution model for  $\Delta$  has been extensively applied in offshore and other engineering applications dealing with fatigue problems involving variable-amplitude stress ranges.

#### 4.2.2.3 Accumulated Number of Stress Cycles, $N$ , and Number of Years in Service, $Y$

In Equations 4.1 and 4.5, the limit state function there is defined in terms of the accumulated number of stress cycles,  $N$ , directly. Generally, however, we are more

interested in the fatigue reliability associated with a specified number of years in service. Therefore, a relationship between the accumulated number of stress cycles,  $N$ , and the corresponding number of years in service,  $Y$ , needs to be developed.

The passage of single trucks on steel bridges is the primary source of cyclic loading that can generate stress cycles and can cause fatigue damage (Moses et al., 1987). In addition, the support structure and the span length also influence the number of stress cycles produced by the passage of a single truck across the bridge. Truck passages and number of years in service are related to the accumulated number of stress cycles as follows:

$$N(Y) = 365 \cdot ADTT_{SL} \cdot C_s \cdot Y \quad (4.13)$$

where  $ADTT_{SL}$  is the single-lane average daily truck traffic on the bridge;  $C_s$  is the stress cycles per truck passage for the bridge span where the detail of interest is located; and  $Y$  is the number of years in service for the bridge. The parameter,  $C_s$ , can be obtained from the AASHTO specifications, as was shown in Table 2.4. According to the AASHTO LRFD Specifications (1998), the  $ADTT_{SL}$  (in Equation 4.13) for a bridge can be estimated by multiplying the average daily truck traffic ( $ADTT$ ) by  $p$ , a factor that accounts for the number of lanes available to trucks, as shown in Table 2.3. The  $ADTT$  of the bridge can be obtained from site surveys of the bridge, typically collected by the bridge authority.

Both  $ADTT$  and  $C_s$  can be taken as random variables in the fatigue reliability analysis. Moses et al. (1987) suggested that  $ADTT$  and  $C_s$  can be treated as lognormally distributed random variables with coefficients of variation of 0.1 and 0.05 for  $ADTT$  and  $C_s$ , respectively. Mean values for  $ADTT$  and  $C_s$  are estimated by the methods described in the previous paragraph.

If allowance for the growth of truck traffic with time is to be considered, a growing ADTT model can be formulated and a relationship between the accumulated number of stress cycles ( $N$ ) and the number of years in service ( $Y$ ) can be expressed as follows:

$$ADTT(Y) = ADTT_0 \cdot (1+r)^Y \quad (4.14)$$

$$N(Y) = 365 \cdot C_s \cdot \int_0^Y ADTT(y) dy = 365 \cdot C_s \cdot ADTT_0 \cdot \left[ \frac{(1+r)^Y - 1}{\ln(1+r)} \right] \quad (4.15)$$

where  $ADTT_0$  is the average daily truck traffic in the first year in service and  $r$  is the annual truck traffic growth rate. Both  $ADTT_0$  and  $r$  can be taken as random variables in the fatigue reliability analysis when data on truck traffic growth for the bridge are available.

The influence of ADTT modeling assumptions on the evaluation of fatigue reliability will be discussed in the following section.

### 4.2.3 Evaluation of the Fatigue Reliability Index, $\beta$

With the limit state function defined in Equations 4.1 and 4.5 for the AASHTO fatigue reliability approach, the fatigue failure event of a detail is defined by cases where:

$$g(\mathbf{X}) \leq 0 \quad (4.16)$$

The probability of fatigue failure,  $P_F$ , for the detail in question can then be evaluated and related to a fatigue reliability index,  $\beta$ , using the following relationship:

$$P_F = P(g(\mathbf{X}) \leq 0) = \Phi(-\beta) \quad (4.17)$$

where  $\Phi(\ )$  is the cumulative distribution function of a standard normal random variable. Similarly, the fatigue reliability index for a given probability of fatigue failure may be expressed as:

$$\beta = \Phi^{-1}(1 - P_F) = \Phi^{-1}[1 - P(g(\mathbf{X}) \leq 0)] \quad (4.18)$$

where  $\Phi^{-1}(\cdot)$  is the inverse cumulative distribution function of a standard normal random variable.

Employing lognormal distribution models for  $A$  and  $\Delta$  in the limit state function (Equation 4.5), and applying random variable transformations (see Appendix A), the fatigue reliability index,  $\beta$ , can be directly expressed as:

$$\beta = \frac{(\lambda_{\Delta} + \lambda_A) - m \cdot \ln(S_{RE}) - \ln(N)}{\sqrt{\zeta_{\Delta}^2 + \zeta_A^2}} \quad (4.19)$$

where the parameters,  $\lambda_{\Delta}$ ,  $\lambda_A$ ,  $\zeta_{\Delta}$ , and  $\zeta_A$  are given in terms of the mean value and the coefficient of variation of  $A$  and  $\Delta$  as follows:

$$\lambda_A = \ln(\mu_A) - \zeta_A^2/2 \quad (4.20)$$

$$\lambda_{\Delta} = \ln(\mu_{\Delta}) - \zeta_{\Delta}^2/2 \quad (4.21)$$

$$\zeta_A = \sqrt{\ln(1 + \delta_A^2)} \quad (4.22)$$

$$\zeta_{\Delta} = \sqrt{\ln(1 + \delta_{\Delta}^2)} \quad (4.23)$$

Equation 4.19 represents the fatigue reliability index of a detail under the condition that no repairs and inspections are performed during the service life while stress cycles are being experienced. Hence, for a given equivalent stress range  $S_{RE}$ , and for given values of the mean and COV of  $A$  and  $\Delta$ , one can easily express the fatigue reliability of a detail as a function of the number of stress cycles accumulated.

Substituting the values of the mean and COV of  $A$  and  $\Delta$  as described in Sections 4.2.2.1 and 4.2.2.2 into Equation 4.19, Figures 4.1 to 4.3 can be drawn so as to demonstrate the changing fatigue reliability versus accumulated number of stress cycles (ranging from 0 to  $10^7$  cycles) under various constant-amplitude stress range levels for the details defined by AASHTO fatigue categories, A, C, and E. The influence of three factors – the number of stress cycles, the stress range level, and the fatigue category – on fatigue reliability is evident in the figures. It can be seen that fatigue reliability is a non-

increasing function of the accumulated number of stress cycles; the larger the number of stress cycles, the lower is the fatigue reliability and the higher is the probability of fatigue failure. For each fatigue category, higher stress range levels lead to a decrease in the fatigue reliability. In addition, the more severe the fatigue category (category severity:  $E > C > A$ ), the lower is the fatigue reliability for any stress range level.

In this dissertation, a target reliability ( $\beta_{\text{target}}$ ) value of 3.7, which corresponds to a probability of failure of  $10^{-4}$ . This target level is shown in all of the plots in Figures 4.1 to 4.3. The actual fatigue reliability of a specified fracture-critical member will generally be compared with this target reliability to yield information that can help in scheduling of inspections. If the fatigue reliability of the selected detail is higher than the target reliability during the entire service life, only routine inspections are needed. However, if the fatigue reliability of the detail falls below the target reliability level during the service life, carefully scheduled and detailed inspections may be required. For those details whose fatigue reliability falls below the target reliability during the service life, an option is to apply optimal fatigue inspection scheduling to keep the safety above the acceptable level during the entire service life. Details related to reliability-based optimal inspection scheduling method are presented in Chapter 5.



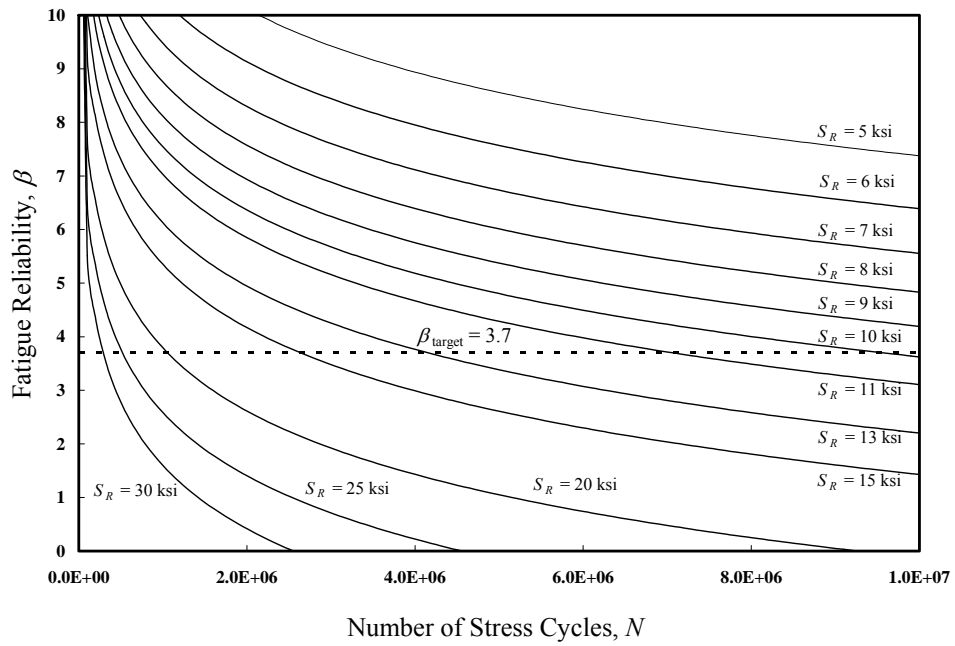


Figure 4.1: Fatigue Reliability for Category A Details under Various Stress Range Levels.

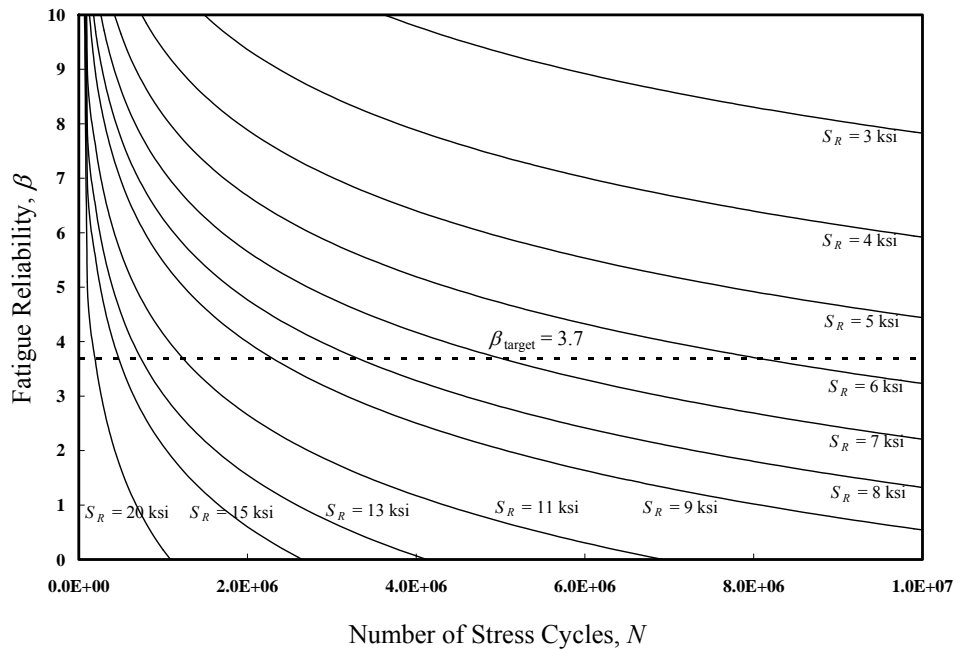


Figure 4.2: Fatigue Reliability for Category C Details under Various Stress Range Levels.

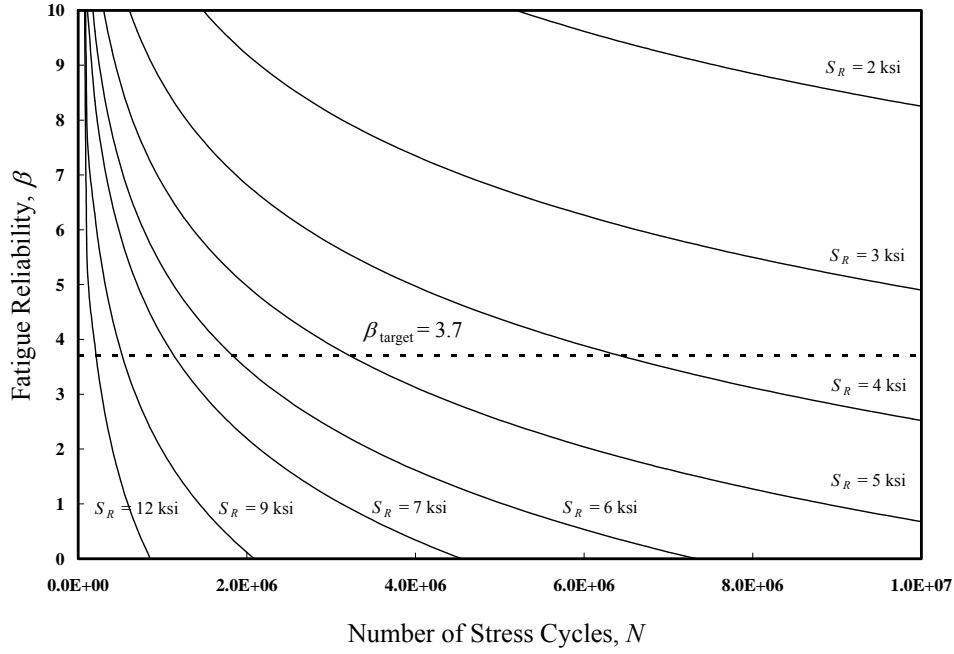


Figure 4.3: Fatigue Reliability for Category E Details under Various Stress Range Levels.

If  $ADTT$  and  $C_s$  in Equation 4.13 are considered as lognormally distributed random variables, as was described in Section 4.2.2.3, and used to model the relationship between the accumulated number of stress cycles,  $N$ , and the number of years in service,  $Y$ , a closed-form expression for the fatigue reliability index can be derived as follows:

$$\beta = \frac{(\lambda_A + \lambda_{\Delta} - \lambda_{C_s} - \lambda_{ADTT}) - m \cdot \ln(S_{RE}) - \ln(365) - \ln(Y)}{\sqrt{\zeta_A^2 + \zeta_{\Delta}^2 + \zeta_{C_s}^2 + \zeta_{ADTT}^2}} \quad (4.24)$$

where the parameters,  $\lambda_{ADTT}$ ,  $\lambda_{C_s}$ ,  $\zeta_{ADTT}$ , and  $\zeta_{C_s}$ , are given as follows:

$$\lambda_{ADTT} = \ln(\mu_{ADTT}) - \zeta_{ADTT}^2 / 2 \quad (4.25)$$

$$\lambda_{C_s} = \ln(\mu_{C_s}) - \zeta_{C_s}^2 / 2 \quad (4.26)$$

$$\zeta_{ADTT} = \sqrt{\ln(1 + \delta_{ADTT}^2)} \quad (4.27)$$

$$\zeta_{C_s} = \sqrt{\ln(1 + \delta_{C_s}^2)} \quad (4.28)$$

For a given slope  $m$ , a given equivalent stress range level,  $S_{RE}$ , and for given values of the mean and COV of  $A$ ,  $\Delta$ ,  $ADTT$  and  $C_s$ , the fatigue reliability of a detail can be described as a function of the number of years in service.

If the ADTT growth model defined in Equation 4.14 is employed to describe the relationship between the accumulated number of stress cycles,  $N$ , and the number of years in service,  $Y$ , a closed-form expression for  $\beta$ , as was possible in Equation 4.24, cannot be obtained due to the nature of the limit state function. The First Order Reliability Method (FORM) or a Monte Carlo simulation scheme can, however, be utilized in order to numerically estimate  $\beta$  or  $P_F$ .

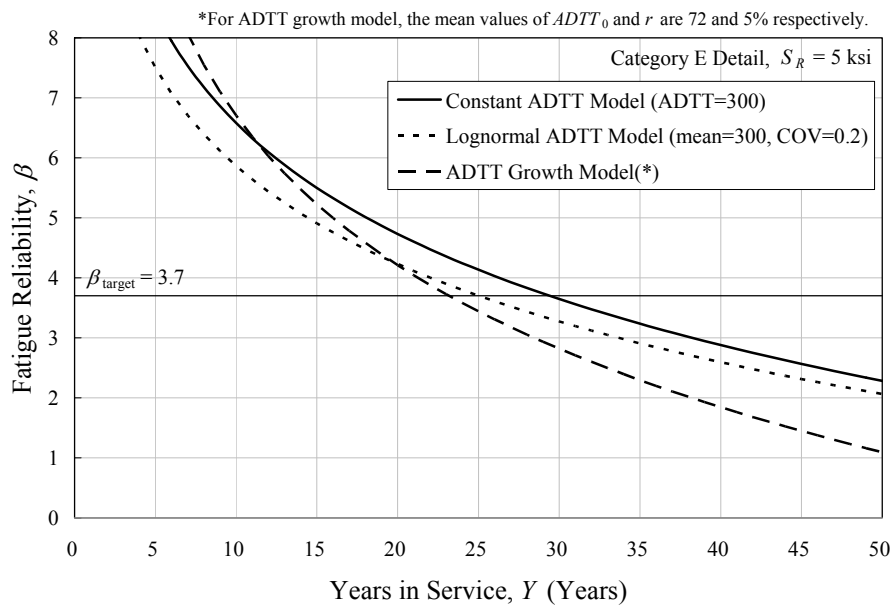


Figure 4.4: Fatigue Reliability for a Category E Detail with  $S_R = 5$  ksi based on Three Different ADTT Modeling Assumptions.

Figure 4.4 shows fatigue reliability curves for a category E detail with a stress range of 5 ksi obtained by employing three different ADTT models – a constant ADTT model, a lognormal ADTT model, and an ADTT model that includes a growth factor.

Both the constant and the lognormal ADTT models utilize Equation 4.13 to describe the relationship between  $N$  and  $Y$ . The ADTT growth model employs Equation 4.14 to describe a growing ADTT with time, and assumes that the initial ADTT value,  $ADTT_0$ , and the annual truck traffic growth rate,  $r$ , can be modeled as random variables. Pertinent information for all the variables in the three ADTT models is summarized in Table 4.4.

Table 4.4: Pertinent Variables in the Three ADTT Models.

	Variable	Variable Type	Mean	COV
Constant ADTT Model	$ADTT$	constant	300	–
Lognormal ADTT Model	$ADTT$	lognormal	300	0.3
ADTT Growth Model	$ADTT_0$	lognormal	72	0.3
	$r$	normal	5%	0.3

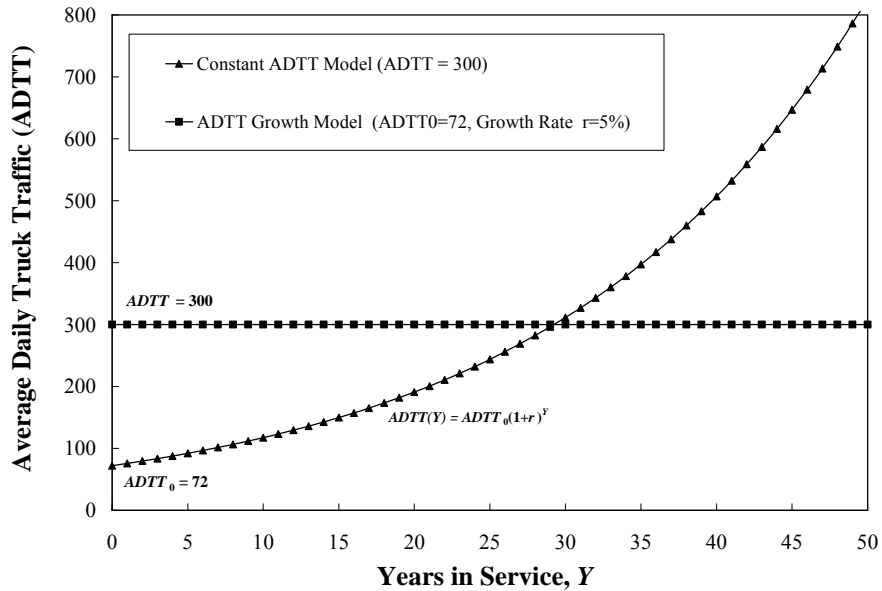


Figure 4.5: Comparison of the Constant ADTT Model ( $ADTT=300$ ) with the ADTT Growth Model ( $ADTT_0=72$ ,  $r = 5\%$ ).

Figure 4.5 compares a constant ADTT model ( $ADTT = 300$ ) with an ADTT growth model where the initial ADTT value ( $ADTT_0$ ) is constant and an annual truck traffic growth rate ( $r$ ) is assumed. It is noted that both models experience the same accumulated number of truck passages after 50 years in service. The three fatigue reliability curves described as a function of years in service,  $Y$ , are based on the same fatigue reliability curves described as a function of the number of stress cycles,  $N$ , as shown in Figure 4.3. In the lognormal ADTT model, the fatigue reliability curve is lower than the fatigue reliability curve for the constant ADTT model, which means that uncertainty in ADTT decreases the fatigue reliability. In the ADTT growth model, the fatigue reliability is higher than the fatigue reliability of the constant ADTT model in the first few years in service due to the lower initial ADTT value, but the increasing ADTT and truck passage accumulation in the ADTT growth model accelerate the decrease in fatigue reliability with time and cause the fatigue reliability in the ADTT growth model to fall below the fatigue reliability for the constant ADTT model after 12 years in service. As can be seen in Figure 4.4, it is the ADTT model, which establishes a relationship between  $N$  and  $Y$ , that affects how the fatigue reliability varies as a function of number of years in service,  $Y$ . Note that the ADTT model simply works with the same fatigue reliability curves defined based on the AASHTO category and expressed as a function of the number of stress cycles,  $N$ ; differences in fatigue reliability expressed as a function of  $Y$  result only because each ADTT model relates  $N$  to  $Y$  differently.

#### **4.2.4 Selection of the Target Reliability Index, $\beta_{\text{target}}$**

Considering Figures 4.1 to 4.3, one can see that in many instances, especially at the higher stress range levels, the reliability curve reaches the target reliability index,  $\beta_{\text{target}}$ , in a finite number of stress cycles,  $N_{\text{target}}$ . Thus,  $N_{\text{target}}$  can be thought of as a

warning point in the life of the detail of interest. Immediate and detailed inspections should be implemented at this time to detect any existing cracks because the fatigue reliability of the detail has become unacceptable from a safety viewpoint after  $N_{\text{target}}$  cycles have occurred. In the  $\beta$  versus  $N$  diagrams, the intersection of the reliability curve with the horizontal target reliability line helps to determine  $N_{\text{target}}$ . Typically, the higher the target reliability ( $\beta_{\text{target}}$ ), the smaller will be the number of stress cycles,  $N_{\text{target}}$ , it takes to reach this target reliability. In this dissertation, the target reliability is selected to be 3.7, which corresponds to a probability of failure of  $10^{-4}$ . With this target reliability, it is possible to compare the values of  $N_{\text{target}}$  for each fatigue category under various stress ranges with the implied fatigue life,  $N_{\text{LRFD}}$ , based on an AASHTO LRFD S-N analysis to see if this target reliability provides realistic values of  $N_{\text{target}}$ . Based on the AASHTO S-N curves,  $N_{\text{LRFD}}$  can be obtained as follows:

$$N_{\text{LRFD}} = \frac{A}{S_{RE}^3} \quad (4.29)$$

where  $A$  is the fatigue detail parameter as given in the AASHTO LRFD Specifications and presented in Table 2.2.

The values of  $N_{\text{target}}$  associated with a target reliability index of 3.7 for details in fatigue category E' under various stress range levels are compared with  $N_{\text{LRFD}}$  in Table 4.5. A representative  $\beta$  versus  $N$  diagram for details in fatigue category E' showing a comparison between  $N_{\text{target}}$  and  $N_{\text{LRFD}}$  is presented in Figure 4.6. Figure 4.6 and Table 4.5 reveal that the  $N_{\text{target}}$  value for fatigue category E' is always smaller than  $N_{\text{LRFD}}$ . This same conclusion was drawn based upon analysis for all of the other fatigue categories – namely, A, B, C, C', D, and E. Hence, since the fatigue life estimated from an AASHTO LRFD S-N curve analysis is regarded as a conservative lower bound of the detail's actual fatigue life, the number of stress cycles that it takes to reach the target reliability index of 3.7 can be considered as a warning point in the life of the fatigue

detail in any category. Preventive measures taken at this time can help to avoid failures due to fatigue. It should be remembered that the time until  $N_{\text{target}}$  cycles are completed or while the fatigue reliability is above the target reliability does not correspond to a period when the detail is unlikely to fail due to fatigue. Rather, it means that during this period, the probability of fatigue failure is lower than the target probability of failure, i.e., lower than  $\Phi(-\beta_{\text{target}})$ . Routine inspections are still needed during this period to detect cracks or flaws that could lead to subsequent failure.

Table 4.5: Comparison of the Number of Stress Cycles ( $N_{\text{target}}$ ) until the Target Reliability is Reached with the AASHTO LRFD Fatigue Life ( $N_{\text{LRFD}}$ ) for Various Stress Ranges ( $S_R$ ) – Category E' Details.

$S_R$ (ksi)	$N_{\text{target}}$ (cycles)	$N_{\text{LRFD}}$ (cycles)	$N_{\text{target}} < N_{\text{LRFD}}$ ?
2	2.11E+07	4.88E+07	Yes
4	2.30E+06	6.09E+06	Yes
6	6.28E+05	1.81E+06	Yes
8	2.50E+05	7.62E+05	Yes
10	1.22E+05	3.90E+05	Yes

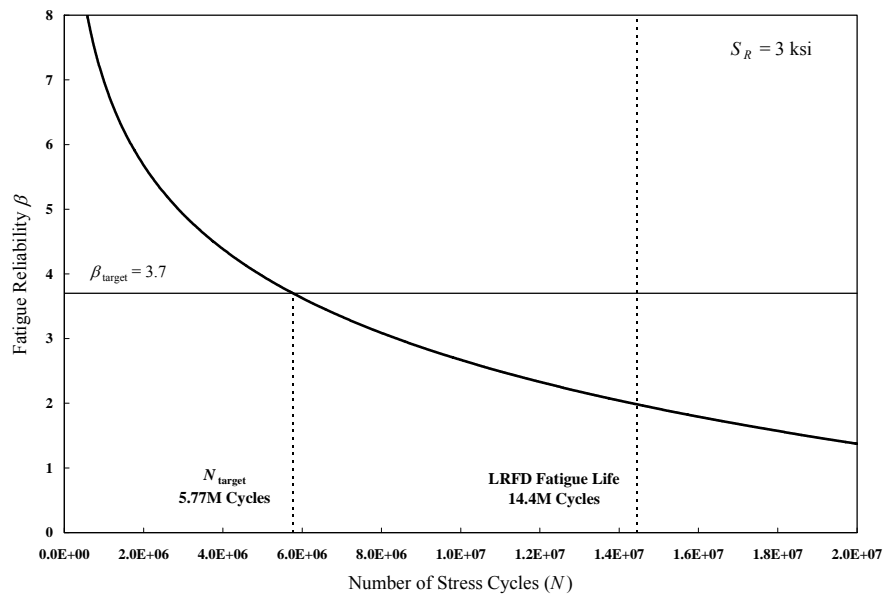


Figure 4.6: Comparison of the Number of Stress Cycles ( $N_{\text{target}}$ ) until the Target Reliability is reached with the AASHTO LRFD Fatigue Life (Category E' Details, with  $S_R = 3$  ksi).

#### 4.2.5 Example Study – Yellow Mill Pond Bridge

A cover plate detail in the Yellow Mill Pond Bridge in Connecticut studied by Fisher (1984) is utilized here as an example to demonstrate the AASHTO fatigue reliability approach. The Yellow Mill Pond Bridge complex, opened to traffic in January 1958, consists of 14 consecutive simple span cover-plated steel and concrete composite beam bridges crossing the Yellow Mill Pond Channel at Bridgeport in Connecticut. The plan, elevation, and a typical cross section of the bridge are shown in Figure 4.7. In June 1976, non-destructive inspections including visual, magnetic particle, dye penetrant, and ultrasonic techniques were employed to monitor fatigue cracking in the cover-plate details in the eastbound and westbound bridges of Span 10. Twenty-two out of forty cover plate details were discovered to have fatigue cracks with crack lengths ranging from 0.25 in. to 12 in. (see Figure 4.8).

A cover plate detail (see Figure 4.9) in Span 10 was analyzed by Fisher (1984) to explain the occurrence of cracks in these details on the Yellow Mill Pond Bridge. Field surveys showed that the equivalent stress range ( $S_{RE}$ ) in the detail, evaluated from the stress range spectrum, was 1.9 ksi. This variable stress spectrum corresponded to 1.8 cycles per truck passage, with a total of approximately 35 million trucks crossing the span between 1958 and 1976. As a result, the accumulated total number of stress cycles on the detail until 1976 was estimated at about 63 million. This cover plate detail falls under fatigue category E' according to the AASHTO fatigue categories; hence, the AASHTO LRFD fatigue life,  $N_{LRFD}$ , for this detail would have been evaluated as:

$$N_{LRFD} = \frac{3.9 \times 10^8}{1.9^3} = 56,859,601 \approx 57 \times 10^6 \text{ (cycles)} \quad (4.30)$$

The “safe” fatigue life,  $N_{Moses}$ , based on Moses et al. (1987) for this detail would have been evaluated as:



$$N_{\text{Moses}} = \frac{1 \times 1.1 \times 10^6 \times 365}{(1.35 \times 1.9)^3} = 23,791,589 \approx 24 \times 10^6 \text{ (cycles)} \quad (4.31)$$

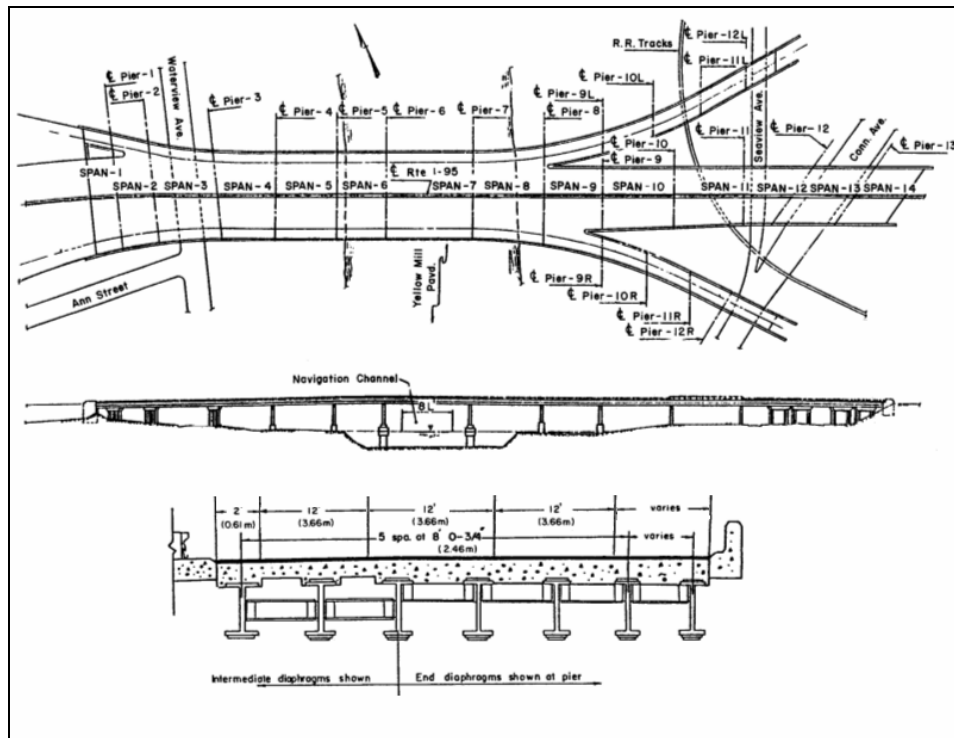


Figure 4.7: Plan, Elevation, and Typical Cross Section of the Yellow Mill Pond Bridge (Fisher, 1984).



Figure 4.8: Fatigue Cracks at Cover Plate Details in the Yellow Mill Pond Bridge (Fisher, 1984).

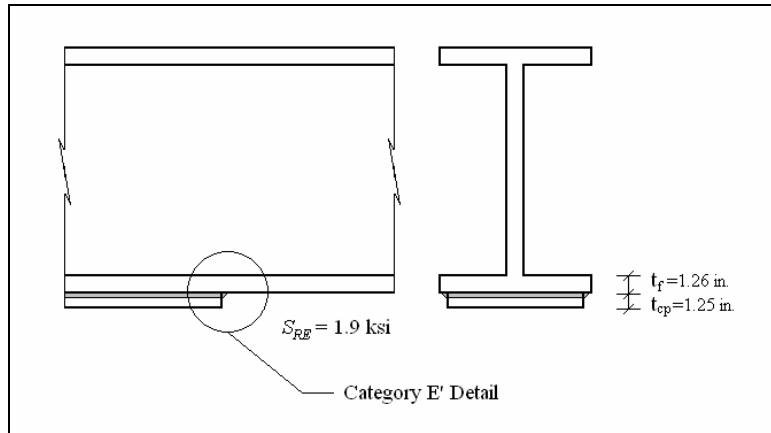


Figure 4.9: The Chosen Cover Plate Detail for Analysis.

Based on the field survey information, the fatigue reliability of this cover plate detail was evaluated using Equation 4.19 and is illustrated in Figure 4.10 as a function of the number of stress cycles. It can be seen that, for this detail, the number of stress cycles that it takes to reach the target reliability index of 3.7 is 29 million, which is greater than Moses' fatigue life (24 million cycles) but less than the AASHTO LRFD fatigue life (57 million cycles) and the actual total number of accumulated stress cycles until 1976 (63 million). Thus, the point in time when  $N_{\text{target}}$  cycles have been accumulated can serve as a point after which meticulous inspections may be warranted so as to detect any fatigue cracks or flaws before the detail develops a much deeper fatigue crack or even has a fatigue fracture. In fact, a large amount of funds was spent in 1981 at the Yellow Mill Pond Bridge to retrofit 427 cracked cover plate details by peening, gas tungsten arc remelting, or use of bolted splices. If these cover plate details had been carefully inspected after  $N_{\text{target}}$  cycles had been accumulated, the cracks might have been detected at an earlier stage and far less funds would have been needed to repair these details.

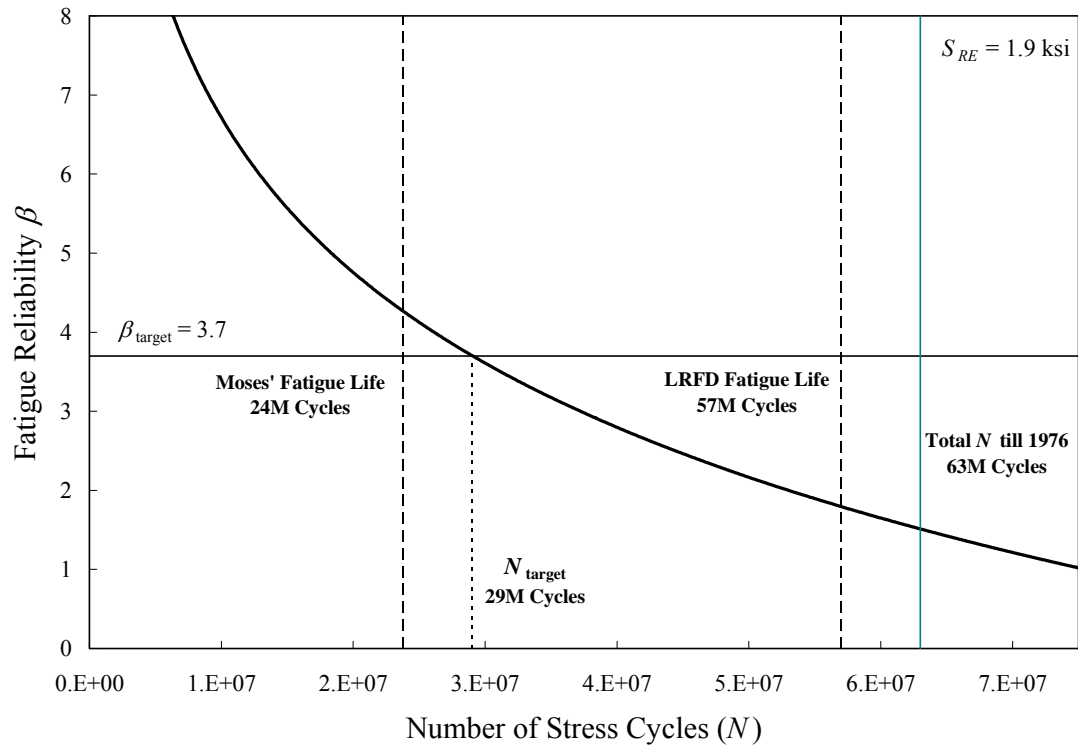


Figure 4.10: Fatigue Reliability of a Cover Plate Detail in the Yellow Mill Pond Bridge.

### 4.3 LEFM FATIGUE RELIABILITY APPROACH

A linear elastic fracture mechanics (LEFM) reliability analysis approach is proposed in order to address shortcomings of the AASHTO fatigue reliability approach which does not take into account the sizes of any existing cracks. For details that do not clearly belong to any of the eight AASHTO fatigue categories or for AASHTO fatigue category details where cracks are known to be present, the LEFM approach provides a convenient method for evaluating the fatigue reliability of a detail. This reliability approach is based on linear elastic fracture mechanics principles and employs Paris' law to describe fatigue crack propagation. Material properties for describing Paris' law, crack geometry functions for evaluating the stress intensity factor, as well as initial and critical crack sizes at the detail being studied need to be provided in order to employ this fatigue reliability analysis approach.

#### 4.3.1 Limit State Function

Madsen et al. (1985) proposed a fatigue limit state function that was developed using Paris' Law and linear elastic fracture mechanics (LEFM) principles. On the basis of results from numerous metal fatigue experiments, Paris and Erdogan (1963) proposed a relationship (see Equation 2.30) between the rate of crack growth and the stress intensity range as follows:

$$\frac{da}{dN} = C \cdot (\Delta K)^m \quad (4.32)$$

where  $a$  is the crack size;  $N$  is the number of stress cycles;  $C$  and  $m$  are material properties affecting fatigue; and  $\Delta K$  is the stress intensity range which can be expressed as Equation 4.33 (similar to Equation 2.29 presented earlier) using linear elastic fracture mechanics:

$$\Delta K = F(a) \cdot S_{RE} \cdot \sqrt{\pi a} \quad (4.33)$$

where  $F(a)$  is a function accounting for the shape of the specimen and the crack geometry and  $S_{RE}$  is the far-field equivalent stress range on the detail.

By substituting Equation 4.33 into Equation 4.32 and rearranging terms, it is possible to relate the accumulated number of stress cycles (from an initial number,  $N_0$ , to a final number,  $N_f$ ) to a corresponding change in crack size of the detail from  $a_0$  to  $a_f$ :

$$\int_{a_0}^{a_f} \frac{da}{[F(a) \cdot \sqrt{\pi a}]^m} = C \cdot S_{RE}^m \cdot (N_f - N_0) \quad (4.34)$$

In Equation 4.34,  $a_0$  and  $a_f$  are the initial and final crack sizes while  $N_0$  is the number of accumulated stress cycles it takes to for a crack to grow to a size,  $a_0$ , and  $N_f$  is the number of stress cycles it takes for the crack to grow to a size,  $a_f$ .

Using the left hand side of Equation 4.34, Madsen et al. (1985) defined a damage accumulation function  $\psi(a_1, a_2)$  that accounts for fatigue damage related to change in crack size from  $a_1$  to  $a_2$ :

$$\psi(a_1, a_2) = \int_{a_1}^{a_2} \frac{da}{[F(a) \sqrt{\pi a}]^m} \quad (4.35)$$

Therefore,  $\psi(a_0, a_c)$  represents the fatigue damage accumulation associated with crack growth from an initial size,  $a_0$ , to a critical size,  $a_c$ , while  $\psi(a_0, a_N)$  corresponds to fatigue damage accumulation from  $a_0$  to a crack size,  $a_N$ , after  $N$  stress cycles. For a specified crack geometry and material,  $a_c$  represents a limit associated with fracture; hence,  $\psi(a_0, a_c)$  is a critical damage accumulation level for the material and detail. The limit state function proposed by Madsen et al. (1985) employed  $\psi(a_0, a_c)$  as a resistance (or capacity) term and  $\psi(a_0, a_N)$  as a loading term as follows:

$$g(\mathbf{X}) = \psi(a_0, a_c) - \psi(a_0, a_N) \quad (4.36)$$

where using Equation 4.34, we can express  $\psi(a_0, a_c)$  and  $\psi(a_0, a_N)$  as follows:

$$\psi(a_0, a_c) = \int_{a_0}^{a_c} \frac{da}{[F(a)\sqrt{\pi a}]^m} \quad (4.37)$$

$$\psi(a_0, a_N) = C \cdot S_{RE}^m \cdot (N - N_0) \quad (4.38)$$

Hence, the limit state function for the LEFM fatigue reliability approach can be rewritten as follows:

$$g(\mathbf{X}) = \int_{a_0}^{a_c} \frac{da}{[F(a)\sqrt{\pi a}]^m} - C \cdot S_{RE}^m \cdot (N - N_0) \quad (4.39)$$

where, as always, failure in fatigue is assumed to occur when  $g(\mathbf{X}) \leq 0$ .

In terms of the number of years,  $Y$ , in service during which the accumulated number of stress cycles increased from  $N_0$  to  $N_f$ , we have:

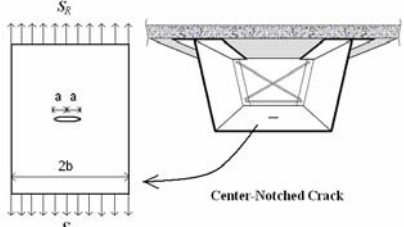
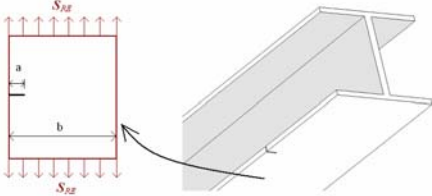
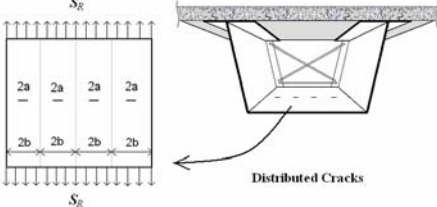
$$g(\mathbf{X}) = \int_{a_0}^{a_c} \frac{da}{[F(a)\sqrt{\pi a}]^m} - C \cdot S_{RE}^m \cdot (365 \cdot ADTT_{SL} \cdot C_s \cdot Y) \quad (4.40)$$

The geometry function,  $F(a)$ , of the detail in question can be obtained from several sources, including specifications or handbooks discussing stress intensity factors. Alternatively, one can use the following equation to directly compute a generalized stress intensity factor as was suggested by Albrecht and Yamada (1977):

$$K = F_e \cdot F_s \cdot F_w \cdot F_g \cdot \sigma \sqrt{\pi a} \quad (4.41)$$

where  $K$  is the stress intensity factor;  $F_e$  is a crack shape correction factor;  $F_s$  is a free surface correction factor;  $F_w$  is a finite width correction factor; and  $F_g$  is a stress gradient correction factor. Numerous exact and empirical solutions for these correction factors can be found in the literature. For more complex details,  $F(a)$  can be determined by employing various fracture mechanics modeling approaches, including the finite element method and other numerical models. Table 4.6 shows geometry functions for some common details in steel bridges.

Table 4.6: Fatigue Geometry Functions for some Common Details in Steel Bridges.

Crack Pattern	Geometry Function $F(a)$
 <p style="text-align: center;">Center-Notched Crack</p>	$F(a) = \left[ 1 - 0.025(a/b)^2 + 0.06(a/b)^4 \right] \cdot \sqrt{\sec \frac{\pi a}{2b}}$
 <p style="text-align: center;">Single-Edged Crack</p>	$F(a) = \sqrt{\frac{2b}{\pi a} \tan \frac{\pi a}{2b}} \cdot \left[ \frac{0.752 + 2.02(a/b) + 0.37 \left( 1 - \sin \frac{\pi a}{2b} \right)^3}{\cos \frac{\pi a}{2b}} \right]$
 <p style="text-align: center;">Distributed Cracks</p>	$F(a) = \left[ \frac{2b}{\pi a} \tan \left( \frac{\pi a}{2b} \right) \right]^{0.5}$

## **4.3.2 Studies of Related Variables in the Limit State Function**

### **4.3.2.1 Initial Crack Size, $a_0$**

Generally, a statistical distribution for the initial crack size,  $a_0$ , of a specified fatigue detail can be obtained by either a Non-Destructive Evaluation (NDE) method or the Equivalent Initial Flaw Size (EIFS) method. Both methods are commonly applied for offshore structures and steel bridges.

NDE techniques for steel bridges mentioned in the FHWA Bridge Inspector's Training Manual (Hartle et al. (1995)) include Ultrasonic Testing (UT), Magnetic Particle Testing (MT), Penetrant Testing (PT), Radiographic Testing (RT), Acoustic Emission Testing (AET) and Visual Testing (VT). Each technique has certain specific details, materials, and operating environments where it is best suited for use. Also, each technique has its own detectability limits related to the minimum crack size it will detect. Selecting an appropriate NDE technique is very important in estimating the initial crack size on a detail. Due to uncertainties associated with crack detection, the crack size measurement from each test of a specified detail will in general not be the same. Hence, a statistical distribution of the initial crack size for the detail has to be obtained based on the NDE test data.

For details with initial crack sizes smaller than the detectability limits of the employed NDE technique, the EIFS method provides an alternative way to estimate the initial crack size. This method has been discussed in studies by Rudd and Gray (1977), Shinozuka (1979), Yang (1980), Rudd et al. (1982a-c), Yang et al. (1985), and Manning et al. (1986) for fatigue analysis. An equivalent initial crack size obtained from the EIFS method is an assumed crack size in a fatigue detail, prior to being put into service, as defined by Yao and Furuta (1986). The equivalent initial crack size can be obtained



by back-solving for the  $a_0$  value in Equation 4.31 assuming a known critical crack size ( $a_f$ ), material parameters ( $C$  and  $m$ ), an equivalent stress range ( $S_{RE}$ ), an initial number of stress cycles ( $N_0$ ), and a total number of stress cycles to fatigue failure ( $N_f$ ). In fact, this solution procedure calibrates the initial crack size so that the LEFM fatigue analysis and the S-N fatigue analysis will lead to the same fatigue life in a deterministic fatigue analysis. The fatigue test data sets utilized to establish the S-N curve for a specific detail can be employed to obtain the statistical distribution of the equivalent initial crack size for the detail. Yazdani (1984) analyzed such fatigue test data that were used to establish the S-N curves for the AASHTO fatigue categories, A, B, C, E, and E', and obtained initial crack size distributions for these different category details. The mean and coefficient of variation values of the initial crack size for various details collected are presented in Table 4.7. These results include crack size statistical information from both the NDE method and the EIFS method.

Table 4.7: Initial Crack Size Distributions from Various Sources

Detail	Initial Crack Size $a_0$			Reference
	Distribution	Mean (in)	COV	
Weld Toe Undercut in Butt Weld	Exponential	4.331E-3	1.00	Bokalrud and Karlsen (1982)
Fillet Welded Joint	Lognormal	4.900E-3	0.34	Engesvik and Moan (1983)
HSLA Rolled Beam	Lognormal	1.276E-3	0.45	Yazdani (1984)
HSLA Welded Beam	Lognormal	3.472E-2	0.36	
HSLA Transverse Stiffener	Lognormal	1.741E-2	0.71	
HSLA Cover Plate	Lognormal	1.084E-2	0.80	
HSLA Thick Cover Plate	Lognormal	1.843E-2	0.28	
QT Rolled Beam	Lognormal	5.100E-5	1.78	
QT Welded Beam	Lognormal	9.159E-3	0.47	
QT Transverse Stiffener	Lognormal	5.280E-3	0.57	
QT Cover Plate	Lognormal	1.700E-4	0.19	
Tubular Joint	Exponential	4.331E-3	1.00	
TLP Joint	Lognormal	2.874E-2	1.07	Kountouris and Baker (1989)
Tubular Joint	Lognormal	2.874E-2	1.07	Shetty and Baker. (1990)
Tubular Joint	Exponential	4.331E-3	1.00	Pedersen et al. (1992)
Butt Weld	Lognormal	2.000E-2	0.50	Zhao et al. (1994a)
Cover Plate	Lognormal	2.000E-2	0.50	Zhao and Haldar (1996)
Stiffener to Bottom Flange	Lognormal	2.362E-2	0.10	Cremona (1996)
30 North Sea Jackets	Exponential	3.701E-2	1.00	Moan et al. (1997)
Stiffener to Bottom Flange	Lognormal	4.921E-3	0.36	Lukic and Cremona (2001)
Butt Weld	Lognormal	7.874E-3	0.50	Zhang and Mahadevan (2001)
Butt Weld	Lognormal	7.874E-3	0.20	Righiniotis and Chryssanthopoulos (2003)
Cover Plate	Lognormal	2.362E-2	0.40	Righiniotis and Chryssanthopoulos (2003)
Gusset Plate	Lognormal	3.937E-3	0.20	Righiniotis and Chryssanthopoulos (2003)
Butt Weld at a Hole	Lognormal	3.937E-3	0.20	Righiniotis and Chryssanthopoulos (2003)

#### 4.3.2.2 Critical Crack Size, $a_c$

The critical crack size,  $a_c$ , is the crack size above which fatigue failure is assumed to result. In practical applications, this critical crack size,  $a_c$ , can be determined by using either a fracture mechanics criterion or a serviceability criterion (Zhao, 1995).

With the fracture mechanics criterion, the critical crack size,  $a_c$ , is directly related to the fracture toughness,  $K_c$ , of the material employed and can be estimated by setting  $K$  equal to  $K_c$  in Equation 4.38. Fracture toughness is a material property commonly determined from Charpy V-notch Impact (CVN) tests on simple specimens. Due to uncertainties in the laboratory tests,  $K_c$  may be considered to be a random variable. Yazdani (1984) analyzed fracture toughness and Charpy V-Notch Impact test data of A36, A588, and A514 steels collected by Rippling and Crosley (1983) and proposed a truncated normal distribution model to describe  $K_c$  for these steels. The mean and coefficient of variation (COV) values of fracture toughness for these steels are summarized in Table 4.8. In addition, fracture toughness for a given material may be affected by service temperature, loading rate, and constraint condition (Barsom and Rolfe, 1999). Shetty (1992) suggested that these factors should be considered in developing a probability distribution model for fracture toughness. Suwan et al. (2003) analyzed data on plates made of A572 and A588 steels supplied by six steel mills in North America and found that variability in CVN test data varied with plate thickness and with test temperature. This would imply that resulting critical crack sizes determined from toughness estimates would have similar variability. Suwan (2002) also studied critical crack sizes of A572 and A588 plates of different thicknesses for with through-thickness cracks, edge cracks, and surface cracks and reported on the variability of critical crack sizes in each case.

With the serviceability criterion, the critical crack size can be defined as a specific crack size at which the fatigue detail fails to meet serviceability requirements. Usually, the critical crack size defined based on the serviceability criterion is more conservative than that based on the fracture mechanics criterion. Zhao (1995) suggested that the thickness or width of a detail can be taken as its critical crack size in many cases. For offshore structures, the Health and Safety Executive (UK) Offshore Technology Report 061 (Aker Offshore Partner, 1999) suggested that wall thickness be taken as the critical crack size for steel tubes in fatigue analysis.

Table 4.8: Fracture Toughness Statistics for A36, A588, and A514 Steels (Albrecht et al., 1986).

Steel Type	Mean (ksi $\sqrt{\text{in}}$ )	COV
A36	40.0	0.18
A588	45.1	0.19
A514	70.1	0.24

#### **4.3.2.3 Fatigue Crack Growth Parameters, $C$ and $m$**

Due to the large variability in data from fatigue experiments, the two crack propagation parameters,  $C$  and  $m$ , in Paris' law are usually treated as random variables and their statistical characteristics can be estimated using regression analyses with available fatigue test data. Table 4.9 represents a compilation of available regression estimates of  $C$  and  $m$  from numerous fatigue tests on various structural steels in the United States. It is satisfactory to treat  $m$  as fixed but to retain the uncertainty in  $C$  (as is done in several references including Aker Offshore Partner (1999) as well as all of the

references mentioned in the table) because the nature of Paris' law is such that it results in a high negative correlation ( $\approx -0.95$ ) between  $C$  and  $m$ . Accordingly, Table 4.9 presents estimates of mean values for both  $C$  and  $m$ , but it presents COV estimates only for  $C$ .

Based on the test data from Klingerman and Fisher (1973), Hirt and Fisher (1973), Barsom and Novak (1977), Mayfield and Maxey (1982), and Roberts et al. (1986); Yazdani and Albrecht (1989) summarized the crack growth parameters,  $C$  and  $m$ , for Paris' law (Equation 4.29). for several different uses, as follows:

For mild and high strength low alloy (HSLA) steels in an air environment:

$$\frac{da}{dN} = (8.291 \times 10^{-11}) \cdot (\Delta K)^{3.344} \quad (4.42)$$

For mild and high strength low alloy steels (HSLA) in an aqueous environment:

$$\frac{da}{dN} = (2.231 \times 10^{-10}) \cdot (\Delta K)^{3.279} \quad (4.43)$$

For quenched and tempered steels in air:

$$\frac{da}{dN} = (1.174 \times 10^{-9}) \cdot (\Delta K)^{2.534} \quad (4.44)$$

For quenched and tempered steels in an aqueous environment:

$$\frac{da}{dN} = (2.975 \times 10^{-9}) \cdot (\Delta K)^{2.420} \quad (4.45)$$

where the  $C$  and  $m$  values in Equations 4.42 through 4.45 are their mean values. The table shows that the environment and steel type affect fatigue crack propagation in a direct manner. For the same stress intensity range, an aqueous environment results in a higher fatigue growth rate than that in air. Quenched and tempered steels have a higher crack growth rate than HSLA steels.

Table 4.10 shows statistics of the crack propagation parameters,  $C$  and  $m$ , for offshore steels collected from Europe. Note that a two-stage linear relationship for crack growth rate ( $da/dN$ ) and stress intensity range ( $\Delta K$ ) is employed in the British

Standard PD6493 (BSI, 1991). This fatigue crack growth model includes the near-threshold stage (Stage 1) and the Paris crack growth stage (Stage 2). For conservatism, estimates of  $C$  and  $m$  from Stage 2 can be applied for the LEFM fatigue reliability approach.

Table 4.11 shows some additional mean and COV estimates for  $C$  and  $m$  that have been collected from various other sources not mentioned in Tables 4.8 and 4.9.

Table 4.9: Fatigue Crack Growth Parameter Statistics for Various Steels.

Steel Type	Environment	$C$		$m$	Reference
		mean	COV		
A36 ( $n=89$ )	Air	9.476E-11	0.221	3.183	Klingerman and Fisher (1973)
A36, A588 ( $n=260$ )	Air	7.831E-11	0.076	3.523	Barsom and Novak (1977)
Martensitic	Air	4.650E-09	–	2.250	Barsom and Rolfe (1999)
Ferrite-Pearlite	Air	*3.600E-10	–	3.000	Barsom and Rolfe (1999)
Austenitic	Air	*3.000E-10	–	3.250	Barsom and Rolfe (1999)
X52 ( $n=321$ )	Air	5.183E-10	0.140	3.725	Mayfield and Maxey (1982)
A36, A588 ( $n=724$ )	Air	9.344E-11	0.200	3.202	Roberts et al. (1986)
HSLA steel ( $n=1394$ )	Air	8.291E-11	0.226	3.344	Yazdani and Albrecht (1989)
A36, A588 ( $n=505$ )	Aqueous	2.231E-10	0.150	3.279	Yazdani and Albrecht (1989)
A514 ( $n=372$ )	Air	2.794E-11	0.088	3.026	Barsom and Novak (1977)
A514 ( $n=499$ )	Air	1.324E-11	0.187	2.456	Roberts et al. (1986)
QT ( $n=871$ )	Air	1.174E-09	0.167	2.534	Yazdani and Albrecht (1989)
QT ( $n=484$ )	Aqueous	2.975E-09	0.156	2.420	Yazdani and Albrecht (1989)
1020 (HR)	Air	2.960E-10	–	3.070	Hertzberg (1995)
4130 (QT)	Air	3.730E-10	–	2.590	Hertzberg (1995)
<p><math>n</math>: number of test data                      *: upper bound                      The units of <math>C</math> assume units of inches for crack size and ksi <math>\sqrt{\text{in}}</math> for <math>\Delta K</math>                      HSLA: high strength low alloy steel                      QT: quenched and tempered steel                      HR: hot rolled steel                      Aqueous Environment: 3% solution sodium chloride in distilled water</p>					

Table 4.10: Fatigue Crack Propagation Parameter Statistics for Offshore Steels.

Environment	C		m	Reference
	mean	COV		
Air	2.587E-10	0.55	3.10	DNV Classification Notes No. 30.2 (1984)
Air	3.319E-10	0.77	3.50	
Air	7.031E-10	0.55	3.10	DNV-RP-404 (1988)
Air	3.319E-10	0.77	3.50	
Air	1.360E-09	0.10	3.30	Bokalrud and Karlsen (1982)
Air	2.271E-10	0.1	3.10	Cortie and Garrett (1988)
Air	2.418E-10	0.3	3.30	Aaghaakouchak et al. (1989)
Air	3.343E-10	0.25	3.00	Shetty and Baker (1990)
Air, R~0.1	2.478E-10	0.35	3.00	BSI PD 6493 (1991)
Air, R>0.5	4.130E-10	0.37	3.00	
Air, R~0.1 Stage 1	1.786E-15	1.31	8.16	
Air, R~0.1 Stage 2	4.295E-10	0.35	2.88	
Air, R>0.5 Stage 1	1.365E-11	1.69	5.10	
Air, R>0.5 Stage 2	6.324E-10	0.60	2.88	
Seawater, R~0.1 Stage 1	2.199E-10	0.93	3.42	
Seawater, R~0.1 Stage 2	5.037E-07	0.26	1.30	
Seawater, R>0.5 Stage 1	3.937E-10	1.10	3.42	
Seawater, R>0.5 Stage 2	1.146E-06	0.16	1.11	
Air	4.130E-10	0.54	3.00	

The units of C assume units of inches for crack size and ksi  $\sqrt{\text{in}}$  for  $\Delta K$



Table 4.11: Estimates of Mean and COV of  $C$  and  $m$  from Various References.

$C$		$m$		Reference
Mean	COV	Mean	COV	
1.888E-10	0.50	3.0	0.10	Cramer and Friis-Hansen (1992)
2.271E-10	0.50	3.1	0.20	Jiao (1992)
2.271E-10	0.51	3.1	0.00	Moan et al. (1993)
2.050E-10	0.63	3.0	0.10	Zhao et al. (1994a)
4.120E-10	0.10	2.9	0.05	Cremona (1996)
2.591E-10	0.55	3.1	0.00	Hovde and Moan (1997)
6.323E-10	0.14	2.9	0.00	Lotsberg et al. (1999)
4.135E-10	0.37	3.0	0.01	Lukic and Cremona (2001)
4.130E-10	0.54	3.0	0.00	Righiniotis (2004)
The units of $C$ assume units of inches for crack size and $\text{ksi}\sqrt{\text{in}}$ for $\Delta K$				

### 4.3.3 Evaluation of Fatigue Reliability

The probability of fatigue failure,  $P_F$ , and the fatigue reliability index,  $\beta$ , can be obtained by using the limit state function given by Equations 4.36 or 4.39 and by evaluating the probability that  $g(\mathbf{X}) \leq 0$  using Equation 4.17. A closed-form expression for  $\beta$ , as was possible with the AASHTO approach, cannot be obtained due to the nature of the limit state function in the LEFM approach. A Monte Carlo simulation scheme or the First Order Reliability Method (FORM) needs to be employed in order to numerically estimate  $\beta$  or  $P_F$ .

#### 4.3.4 Example

A gusset plate-transverse stiffener detail in the Lafayette Street Bridge over the Mississippi River in St. Paul, Minnesota, studied by Fisher (1984) is adopted as an example to demonstrate the LEFM fatigue reliability approach. The elevation and cross section of the Lafayette Street Bridge are shown in Figure 4.11. The bridge was opened to traffic in November 1968. Due to fatigue resulting from vehicular loads, a long crack in the main girder of Span 10 was discovered in May 1975. This fatigue crack originated in the weld between the gusset plate and the transverse stiffener and propagated into the girder web. Because of the high residual tensile stresses at the cracked web location, the stress intensity at that location reached the fracture toughness of the material and resulted in a cleavage crack growing up to within 7.5 in. of the top flange and fracturing the whole bottom flange (see Figure 4.12).

The gusset plate-transverse stiffener detail considered in the analysis is shown in Figure 4.13. Field surveys showed that the equivalent stress range ( $S_{RE}$ ) in the detail evaluated from the stress range spectrum was 2.0 ksi. It is also known that a total of approximately 3.3 million trucks crossed the span prior to the time the crack was discovered (i.e., between 1968 and 1975). The gusset plate-transverse stiffener detail is not clearly identified as being in any one of listed AASHTO fatigue categories. Hence, the LEFM approach is adopted for the fatigue reliability analysis. The geometry function for the detail analyzed by Fisher (1984) is expressed as:

$$Y(a) = 2.829 \cdot \sqrt{\sec\left(\frac{\pi a}{2t}\right)} \cdot \left[ 1 - 3.215\left(\frac{a}{t}\right) + 7.897\left(\frac{a}{t}\right)^2 - 9.288\left(\frac{a}{t}\right)^3 + 4.086\left(\frac{a}{t}\right)^4 \right] \quad (4.46)$$

where  $a$  is the crack size and  $t$  is the web thickness, which is equal to 0.5 in. for the detail studied.

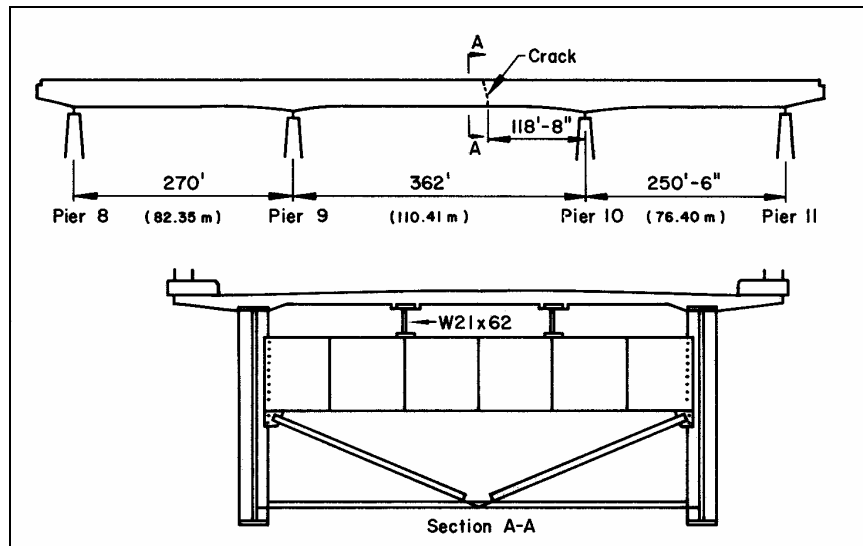


Figure 4.11: Elevation and Cross Section of the Lafayette Street Bridge (Fisher, 1984).

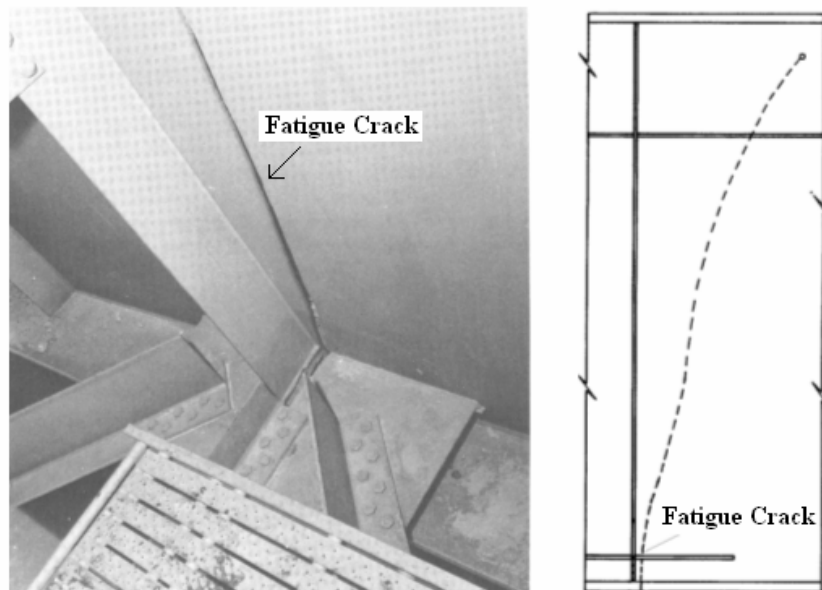


Figure 4.12: Fatigue Crack in the Gusset Plate-Transverse Stiffener Detail (Fisher, 1984).

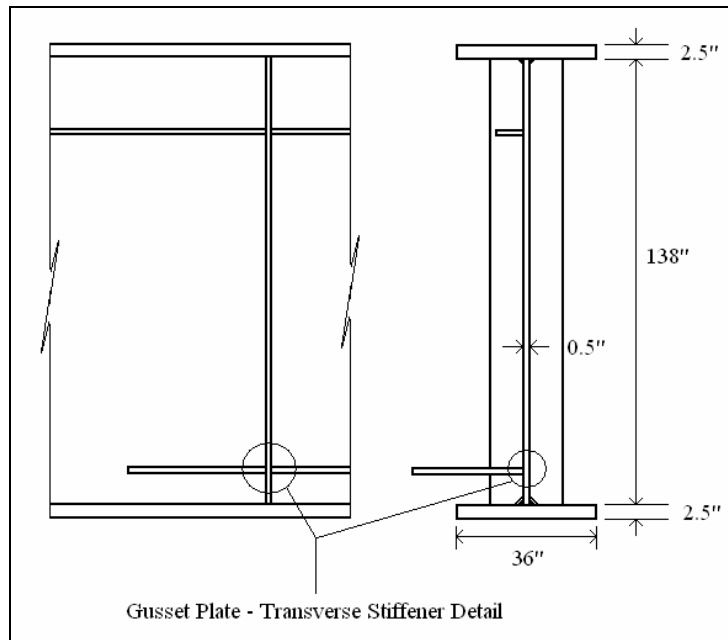


Figure 4.13: The Gusset Plate-Transverse Stiffener Detail.

Based on the crack examination by Fisher (1984), the initial crack size,  $a_0$ , due to the lack of fusion weld in the detail was 0.39 in. The critical crack size,  $a_c$ , is determined to be 0.5 in., which is equal to the web thickness, based on the serviceability criterion. In fact, due to the high residual tensile stresses at the web-stiffener-gusset location, this critical crack size of 0.5 in. is very close to the critical crack size defined based on the fracture mechanics criterion. Employing statistical information obtained by Fisher (1984), the crack growth parameter,  $C$ , is taken to be a lognormally distributed random variable with a mean of  $2.05 \times 10^{-10}$  (with units consistent with crack size in inches and  $\Delta K$  in  $\text{ksi-in}^{1/2}$ ) and a COV of 0.63; while the crack growth exponent,  $m$ , is taken to be a normally distributed random variable with a mean and COV of 3.0 and 0.3, respectively. With these parameters, the LEFM fatigue reliability analysis for the gusset plate-transverse stiffener detail is carried out using the First Order Reliability Method

(FORM). The computed the fatigue reliability versus number of stress cycles for the detail is shown in Figure 4.14. It can be seen that the number of stress cycles,  $N_{\text{target}}$ , that it takes to reach the target reliability index of 3.7 for the detail is 0.17 million, which is almost twenty times less than the total number of stress cycles to failure (3.3 million). Hence, the  $N_{\text{target}}$ , if used for planning detailed inspections of such a gusset plate-transverse stiffener detail might help prevent a fatigue crack from growing as long as it did in this case (7.5 inches).

The initial crack size of 0.39 in. was observed by Fisher (1984) from examining the fractured portion of the detail after the failure. In most cases, the initial crack size of the detail being studied is uncertain and should be treated as a random variable. If the initial crack size, for this detail, were assumed to be lognormally distributed with a mean value of  $3.937 \times 10^{-3}$  in. and a COV of 0.2 suggested by Righiniotis et al. (2003) for gusset plate welds (see Table 4.7) and all the other parameters affecting reliability remained the same, a revised fatigue reliability curve is obtained as shown in Figure 4.15. Because the mean value of this new assumed initial crack size is almost 100 times smaller than the initial crack size of 0.39 in. assumed earlier based on Fisher (1984), it is seen that the fatigue reliability curve associated with this smaller mean initial crack size is higher than before (compare Figure 4.15 with Figure 4.14). As a result, the  $N_{\text{target}}$  value is 2.6 million cycles now compared to 0.17 million cycles in Figure 4.14. This  $N_{\text{target}}$  value of 2.6 million could still provide a timely warning point to prevent the growth of such long fatigue cracks as were found here. As is clear from Figures 4.14 and 4.15, the initial crack size affects the fatigue reliability of a detail in a direct manner. The larger the initial crack size is, the lower will be the fatigue reliability over the service life, which will in turn lead to a smaller  $N_{\text{target}}$  value. Without accurate information on the initial crack size, an assumed initial crack size distribution for the given detail from available

references can still yield an estimate of the fatigue reliability so as to suggest detailed inspections of the detail once  $N_{\text{target}}$  stress cycles have been accumulated.

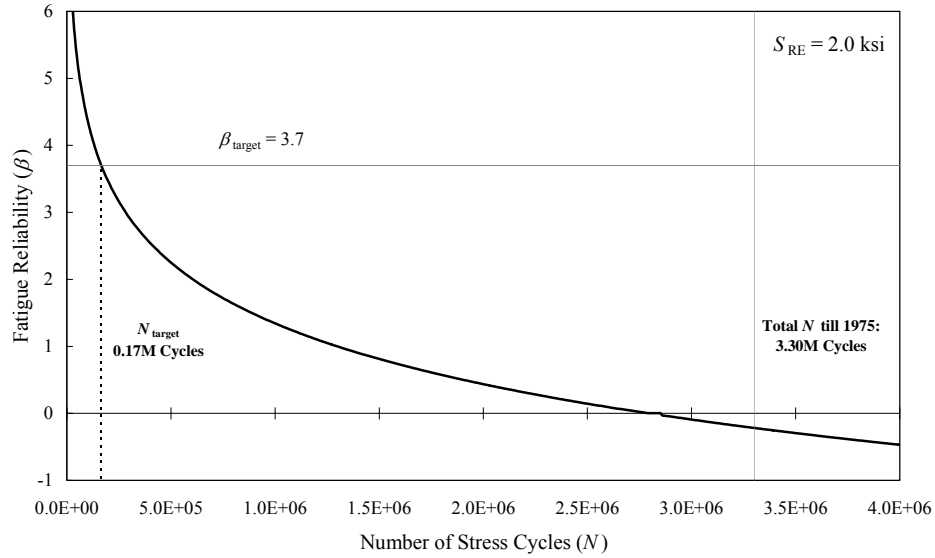


Figure 4.14: Fatigue Reliability of Gusset Plate-Transverse Stiffener Detail with an Initial Crack Size,  $a_0$ , of 0.39 in.

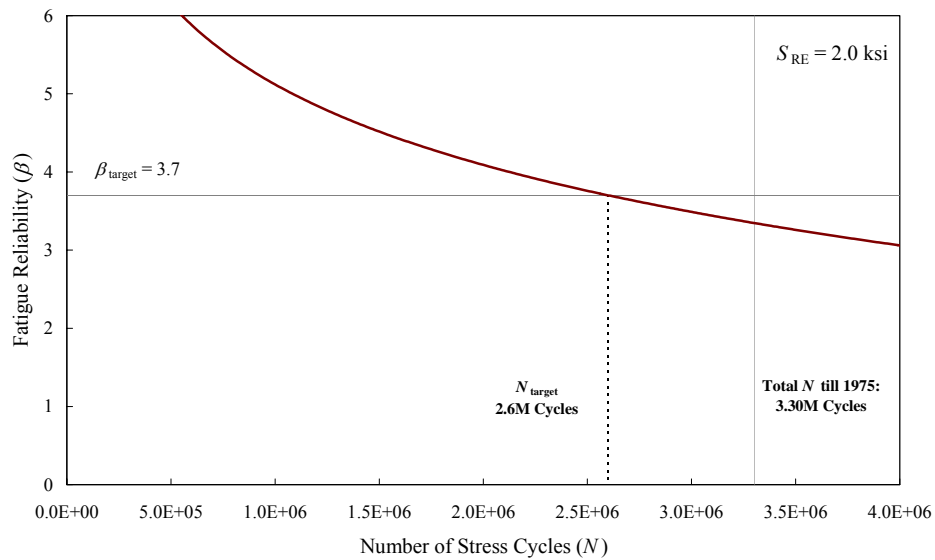


Figure 4.15: Fatigue Reliability of Gusset Plate-Transverse Stiffener Detail with a Lognormal Initial Crack Size,  $a_0$ , with a mean of  $3.937 \times 10^{-3}$  in. and a COV of 0.2.

#### 4.4 SUMMARY

Some key findings and conclusions from this chapter are summarized below:

- (1) The safety status of fracture-critical members (details) in steel bridges under fatigue loading can be represented by reliability analysis. Fatigue reliability analysis provides a convenient way of quantifying the fatigue deterioration of fracture-critical members in steel bridges. In contrast to deterministic procedures, fatigue reliability is directly related to the probability of fatigue failure. This allows for more advanced applications such as risk management, optimal fatigue design, and optimal inspection scheduling for fracture-critical members during the service life of a bridge. In Chapter 5, the application of fatigue reliability analysis to optimal inspection scheduling will be explored.
- (2) The fatigue reliability of a fracture-critical member can be assessed using AASHTO S-N curves or LEFM principles depending on the type of detail being studied. For details classified as belonging to one of the standard AASHTO fatigue categories, a limit state function expressed in terms of the number of stress cycles till failure based on Miner's rule is used to evaluate the fatigue reliability. For details not classified according to AASHTO fatigue categories, a limit state function related to crack size and growth rate is used to evaluate fatigue reliability.
- (3) The variables needed for fatigue reliability analysis in either the AASHTO or the LEFM approaches have been studied and statistics on these variables have been compiled in this chapter to assist in performing reliability analyses.
- (4) Three main factors – the number of stress cycles, the stress range, and the type/category of the detail – directly influence the fatigue reliability of a detail over time. In a direct way, an increase in the number of accumulated stress cycles leads to a lower fatigue reliability level (and a higher probability of fatigue failure). For

any type of detail, higher stress range levels will lower the fatigue reliability faster than smaller amplitude cycles. The more severe the fatigue category (e.g., AASHTO Category E is more severe than Category A), the lower the fatigue reliability will be for similar cyclic loads.

- (5) After obtaining the fatigue reliability index versus number of stress cycles (i.e.,  $\beta$  versus  $N$  curves), a comparison of the fatigue reliability with a target reliability index can provide useful information for planning inspection schedules. The number of stress cycles,  $N_{\text{target}}$ , that it takes for a detail to reach the selected minimum acceptable target reliability index (assumed to be 3.7 in the illustrations presented in this dissertation) can serve as a useful early warning point in time from which to consider more detailed inspections to avoid large cracks or fatigue failure.
- (6) It is important to note that though the fatigue reliability of a fracture-critical member might be higher than the target reliability (especially early on), this only means that the probability of fatigue failure is lower than the maximum acceptable level (i.e.,  $P_F$  is less than  $\Phi(-\beta_{\text{target}})$ ). Routine inspections are still needed for such details to detect cracks caused by unexpected events, perhaps not related to cyclic loading.
- (7) In the LEFM fatigue reliability approach, a case study was presented to show how the initial crack size can affect evaluation of the fatigue reliability of a detail in a direct manner. Without precise information of the initial crack size, an assumed initial crack size distribution based on available references (compiled in this chapter) can still yield an estimate of the fatigue reliability that can be used to determine a warning point associated with  $N_{\text{target}}$  accumulated cycles (see Item (5) above) after which, more detailed inspections of the detail might be considered.

The analysis procedures involved in the AASHTO fatigue reliability approach and in the LEFM reliability approach are summarized in Figures 4.16 and 4.17, respectively.



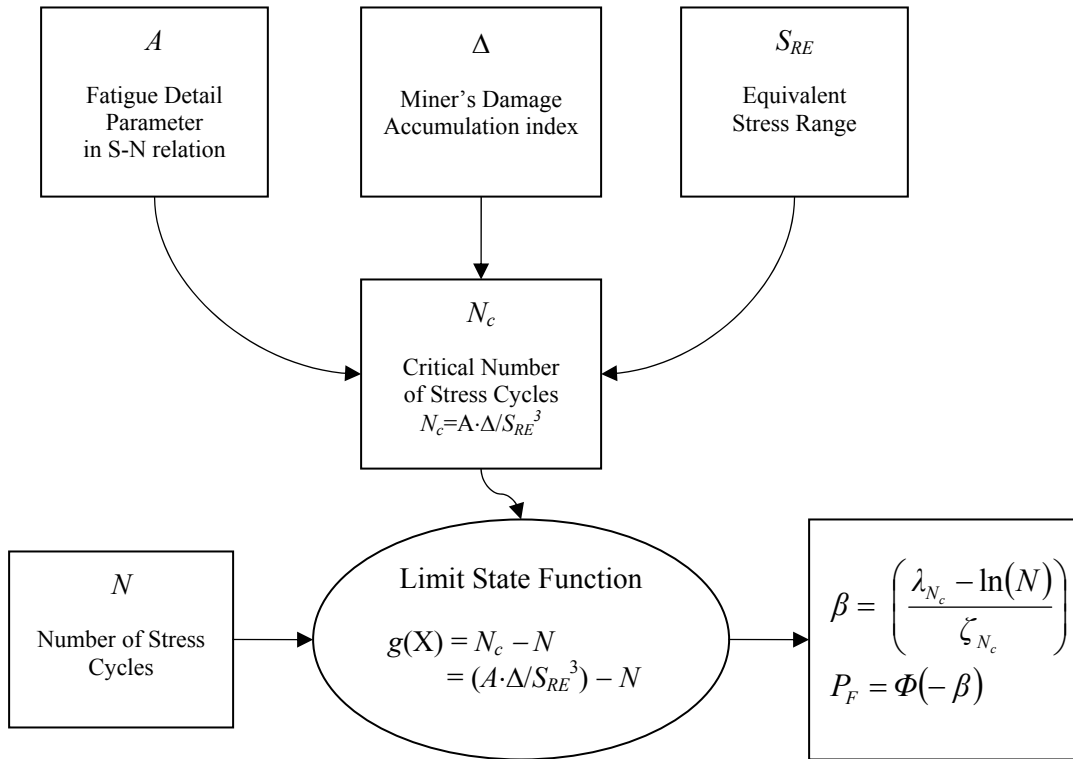


Figure 4.16: Flow Chart for the AASHTO Fatigue Reliability Analysis Approach.

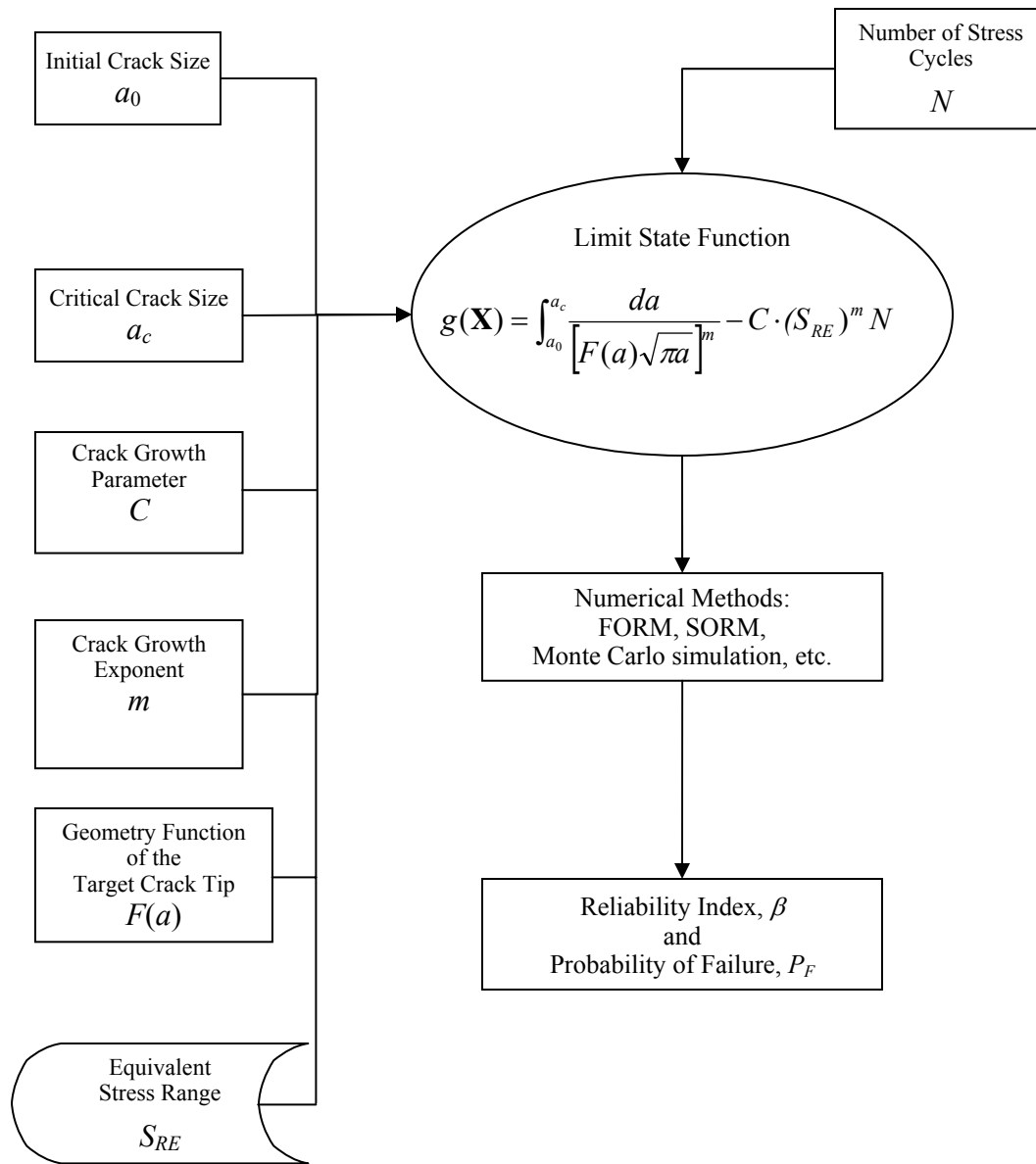


Figure 4.17: Flow Chart for the LEFM Fatigue Reliability Analysis Approach.

## **Chapter 5: RELIABILITY-BASED FATIGUE INSPECTION SCHEDULING FOR STEEL BRIDGES**

### **5.1 INTRODUCTION**

Currently, the scheduling of inspections to prevent steel bridges from fatigue failure is based on both a two-year periodic pattern required by the Federal Highway Administration (FHWA) and the responsible engineer's experience. However, since every steel bridge has its own specific geometric shape, design, and traffic conditions, fatigue is hard to predict. Furthermore, details may be classified into different categories and might experience quite different levels of stress ranges. This can result in different fatigue lives for each detail. Thus, a specific fixed inspection interval schedule may not meet the demands of all types of fatigue details in a steel bridge. Besides, a periodic inspection schedule leads to a fixed number of inspections over the service life of the bridge. This number of inspections may be more than necessary for some fatigue details and less for others. If the cost of an inspection is high, such as is the case for a fracture-critical inspection on a detail or member (which is usually expensive to perform) or if it causes traffic inconveniences, a fixed-interval periodic inspection schedule can place a burden on the transportation agency. Clearly, the present strategy of inspection scheduling may be not only uneconomical but also inadequate from a safety point of view. Therefore, this dissertation proposes a method of inspection scheduling for steel bridges based on reliability theory and optimization that seeks a balance of both economy and safety in the maintenance of steel bridges.

Reliability-based inspection scheduling has been applied in many areas of engineering. Thoft-Christensen and Sorensen (1987), Madsen et al. (1989) and Sorensen et al. (1991) applied such reliability-based inspection strategies to offshore

structures. Frangopol et al. (1997) utilized such inspection strategies for reinforced concrete bridges. For corrosion problems in steel girder bridges, Sommer et al. (1993) proposed a reliability-based strategy for inspection scheduling. The general approach in all such applications is to formulate the inspection scheduling problem as an optimization problem that seeks to minimize a cost function (the objective function) by adjusting inspection times within appropriate constraints while simultaneously maintaining safety.

The starting point for the reliability-based fatigue inspection scheduling procedure involves establishing the fatigue reliability curve (that describes the variation of the reliability index,  $\beta$ , versus number of accumulated stress cycles,  $N$ ) obtained from a fatigue reliability analysis (as was discussed in Chapter 4). Without any inspection or repair, this fatigue reliability curve will, in general, show a non-increasing trend of fatigue reliability with time in service for a detail. This is an indication of the deterioration in safety level of the detail under fatigue loading. Through inspections and possible repairs, the fatigue reliability of the detail can be raised to a higher level several times over the service life to prevent a decreasing reliability from falling below a specified target reliability level. Performing too many inspections and/or repairs to keep the detail at a very high level reliability over its service life might not be an economical way of scheduling inspections. As an example, consider three different inspection schedules (see Table 5.1) to be applied for a detail over its planned service life of 40 years. The three corresponding fatigue reliability curves associated with these three schedules might resemble those shown in Figure 5.1. Each upward adjustment in reliability at certain points in these curves corresponds to an improvement in fatigue reliability due to a repair that followed an inspection. Schedule I with four inspections every ten years is not a satisfactory inspection plan because four inspections are insufficient to prevent the fatigue reliability of the detail from falling below the target

reliability level. For schedule II, the ten inspections are effective in keeping the fatigue reliability above the target reliability throughout the planned service life; however, the frequent inspections increase the costs and make this schedule uneconomical. The objective of reliability-based inspection scheduling is to find an optimal schedule which will keep the fatigue reliability above the target reliability level over the service life. It allows for non-periodic inspections as well in order to yield the most economical program. Schedule III represents such an optimal schedule qualitatively for this illustrative example, which guarantees the lowest cost while not operating at unsafe levels. Such a solution needs to be obtained by optimization procedures.

Table 5.1: Three Inspection Schedules for an Example Detail.

Schedule	Number of Inspections	Inspection Interval (yrs)
I	4	10
II	10	4
III	Optimal Number	Optimum timing is determined. Intervals are non-uniform.

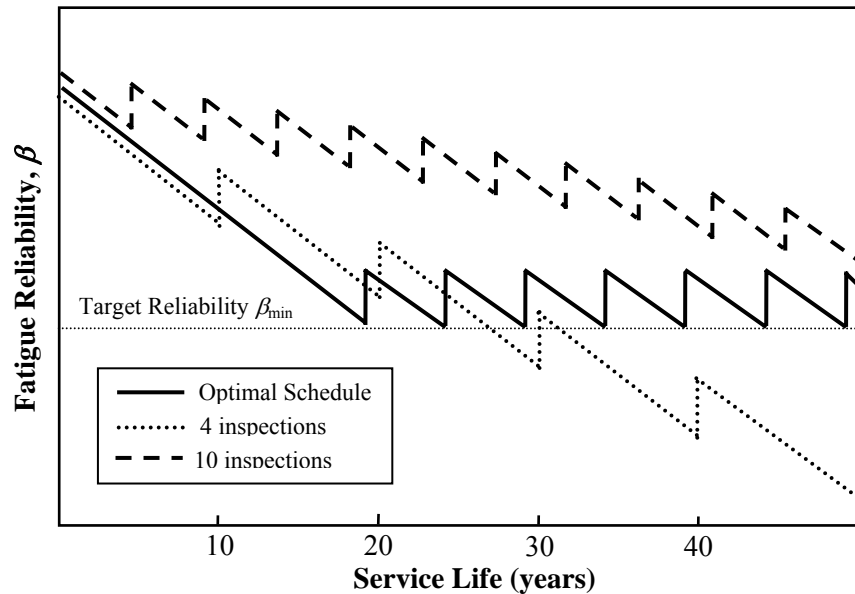


Figure 5.1: Fatigue Reliability for Three Illustrative Inspection Schedules.

The analyses involved in the reliability-based inspection scheduling procedure are described in detail in the following sections. The main features of the proposed procedure may be summarized as follows:

- (1) There is no need to define *a priori* the exact number of inspections and the exact inspection and repair times.
- (2) All possible inspection and repair scenarios are considered in an event tree analysis that will be presented in the following sections.
- (3) The occurrence probability of each inspection and repair scenario will be determined based on the likelihood of needing repair after each inspection. The updated fatigue reliability following each repair is always higher than the target reliability.
- (4) The optimal solution for establishing required inspection times takes into consideration all possible repair scenarios and minimizes total cost, which includes costs of inspections and expected costs of repairs and failure.

The event tree analysis that simulates all possible scenarios after inspection of a detail of interest is formulated based on an unknown number of inspections, an unknown set of inspection times, the fatigue reliability, and the likelihood of needed repairs during various points in time during the service life of the detail. With the event tree analysis, the cost function for the detail, which is composed of the costs of inspections, repairs, and fatigue failure is examined as part of the optimization procedure. The fatigue reliability and the likelihood of needed repairs may be determined with either the AASHTO approach or the LEFM approach depending on the type of the detail and then used in the event tree analysis and the search for the optimal schedule.

## 5.2 EVENT TREE ANALYSIS

In order to represent all the possible scenarios that might need to be considered after prospective inspections and repairs, an event tree analysis is needed. Some underlying assumptions that form the basis for the proposed procedure include the following:

- (1) that the fatigue reliability of a detail can be modeled as a non-increasing function of time,  $\beta(T)$ , to express the rate of deterioration of the detail over its service life;
- (2) that repair is considered by estimating the likelihood,  $P_R$ , that the detail will need repair (this quantity,  $P_R$ , will in turn be established as the probability of detecting a crack whose size exceeds some prescribed size that warrants repair);
- (3) that all detected cracks larger than the prescribed crack size in (2) are repaired immediately following the inspection;
- (4) that there are only two actions possible following each inspection: “repair” or “no repair;” and
- (5) that after a repair, the reliability of the detail is returned to its original level (i.e., an “as good as new” repair is guaranteed).

Based on the above five assumptions, an event tree analysis for a detail can be performed and will form part of the overall inspection scheduling procedure.

After every inspection of a fatigue detail, possible actions of “repair” and “no repair” are enumerated to construct the event tree for this detail over the service life. An example of an event tree, which is similar to one suggested by Frangopol et al. (1997), is shown in Figure 5.2. From the year  $T_0$  when the detail is assumed to be put into service until the year  $T_1^-$  when the first inspection is about to be performed, the detail is assumed not to have had any repair; so, a single horizontal branch can represent the status of the detail from  $T_0$  to  $T_1^-$ . The time spent during inspection is assumed to be negligibly short.

After the first inspection at  $T_1^+$ , a repair decision has to be made according to the inspection results for the fatigue detail. If a crack is detected and the crack size is over the size limit defined to be that needing repair, a repair action is assumed to be implemented immediately. The time spent during repair is also assumed to be negligibly short in this study but this assumption can easily be relaxed. If no crack is detected or the crack size can be tolerated (i.e., it is smaller than a size that warrants repair), no repair action should be taken. Hence, the original single horizontal branch modeling the fatigue detail's status at  $T_1$  is bifurcated into two branches; one branch models the detail status after repair from  $T_1^+$  to  $T_2^-$  (the time just preceding the second inspection) and the other branch models the status without any repair from  $T_1^+$  to  $T_2^-$ . In Figure 5.2, a branch designated "1" represents a repair action and a branch designated "0" represents a no-repair action. Both branches are bifurcated again at  $T_2^+$  just after the second inspection is completed to model the repair status of the detail. Continuing onward, each branch in the event tree will be bifurcated again and again immediately after every inspection is completed until the service life,  $T_f$ , is reached. Therefore, the event tree simulates all the possible repair realizations in all of the branches during the planned service life. If  $n$  inspections are performed during the service life of a detail,  $2^n$  branches will be generated at the end of the event tree, implying that  $2^n$  possible scenarios could happen in the future. Note that in the optimization problem to be formulated, we will be attempting to determine the number,  $n$ , of inspections and the times of these inspections,  $T_1, T_2, \dots, T_n$ .

The fatigue reliability, modeled as a decreasing function,  $\beta(T)$ , obtained based on the AASHTO approach or the LEFM approach for the fracture-critical detail of interest will be greatly affected by the repair realizations after each inspection. In this study, an assumption is made that the detail after repair will be as good as new. Thus, the fatigue



reliability at every inspection time will be raised (or updated) to the same level as that at the starting point,  $T_0$ , if a repair action is taken (i.e., on all “1” branches). Fatigue reliability patterns for all of the  $2^n$  branches are related to repair realizations for the detail. Figure 5.2 shows a schematic representation of the fatigue reliability patterns for every branch in a typical event tree when  $n$  equals 2. Note that the “as good as new” assumption may be modified to conditions where either the detail is “not as good as new” or is “better than new” when sufficient data are available for the repair procedure and the altered reliability of the repaired detail. Both the subsequent reliability curve following the repair and the associated costs might in general change for these assumptions relative to the “as good as new” case but such changes are easy to implement.

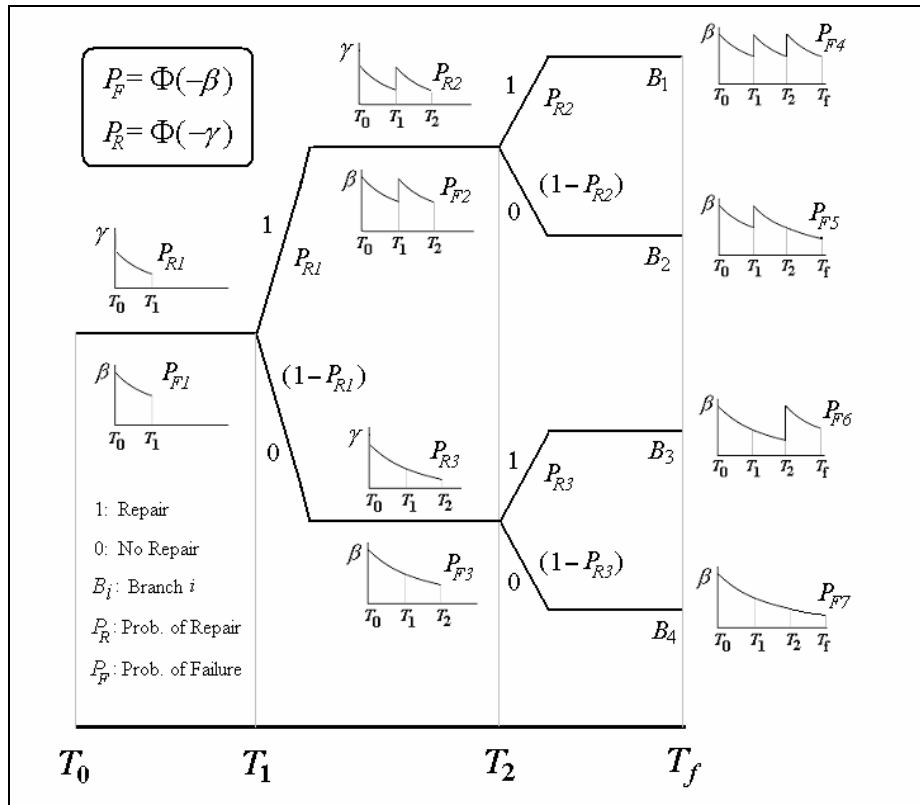


Figure 5.2: Representative Event Tree showing Inspection and Repair Realizations.

### 5.3 LIKELIHOOD OF NEEDED REPAIR

The decision of whether or not to repair as is made after every inspection can be interpreted in a probabilistic form. The likelihood of needed repair,  $P_R$ , will be employed to describe the decision made after every inspection. This likelihood may be thought to be the same as the probability of detecting a crack that exceeds a prescribed crack size that warrants repair in the detail. Due to differences in defining limit state functions for the AASHTO and the LFM fatigue reliability approaches, the definitions for the likelihood of needed repair,  $P_R$ , in these two fatigue reliability approaches are also different and are described in the following.

#### 5.3.1 AASHTO Approach

Since the limit state function,  $g(\mathbf{X})$ , employed for evaluating fatigue failure in the AASHTO approach is expressed in terms of the number of stress cycles, an associated limit state function,  $H(\mathbf{X})$ , for evaluating the likelihood of needed repair in the AASHTO approach may also be defined as a function related to number of stress cycles. Since the likelihood of needed repair is defined as the probability of detecting a crack size equal to or greater than a prescribed size,  $a_R$ , in the detail that warrants repair, a relationship between the number of stress cycles and crack size needs to be developed. Employing Equation 4.31, the number of stress cycles,  $N_R$ , associated with this prescribed crack size,  $a_R$ , can be expressed as:

$$N_R = \left\{ \int_{a_0}^{a_R} \frac{da}{[F(a) \cdot \sqrt{\pi a}]^m} \right\} / C \cdot (S_{RE})^m \quad (5.1)$$

or the number of years,  $Y_R$ , associated with  $a_R$  can be equivalently expressed as:

$$Y_R = \left\{ \int_{a_0}^{a_R} \frac{da}{[F(a) \cdot \sqrt{\pi a}]^m} \right\} / C \cdot (S_{RE})^m \cdot (365 \cdot ADTT_{SL} \cdot C_s) \quad (5.2)$$

The resistance term in the new repair-related limit state function,  $H(\mathbf{X})$ , can thus be set as  $N_R$  (or  $Y_R$ ), i.e., the number of stress cycles (or years) it takes for a crack to grow to a size,  $a_R$ ; while the load term in  $H(\mathbf{X})$  can be defined as the number of stress cycles accumulated (or years passed). Accordingly, the limit state function,  $H(\mathbf{X})$ , required for evaluating the likelihood of needed repair for AASHTO-type details can be defined as:

$$H(\mathbf{X}) = N_R - N \quad (5.3)$$

or, equivalently,

$$H(\mathbf{X}) = Y_R - Y \quad (5.4)$$

The likelihood of needed repair for the detail in question can then be related to an index,  $\gamma$ , as follows:

$$P_R = P(H(\mathbf{X}) \leq 0) = \Phi(-\gamma) \quad (5.5)$$

As can be seen in Equation 5.1, the geometry function,  $Y(a)$ , for the assumed crack type in the AASHTO-type detail and the equivalent initial flaw size (EIFS) defined in Chapter 4 for the uncracked detail are needed in order to evaluate the likelihood of needed repair. To facilitate practical implementation of the proposed procedure for inspection scheduling, the likelihood of needed repair in the AASHTO approach may be alternatively considered to be the same as the probability of first observation of a crack in the detail, which implies that a crack will be repaired as soon as it is first observed. With this definition, the resistance term in  $H(\mathbf{X})$  can be rewritten as the number of stress cycles until first observation of a crack. According to Fisher et al. (1970), this number of stress cycles until first observation of a crack was usually more than 75 percent of the number of cycles corresponding to the life of the AASHTO-type details they tested. Conservatively, then, the limit state function,  $H(\mathbf{X})$ , associated with the likelihood of needed repair can be represented as:

$$H(\mathbf{X}) = N_{0.75c} - N = 0.75N_c - N = \frac{0.75A \cdot \Delta}{S_{RE}^3} - N \quad (5.6)$$

where  $N$  is the number of stress cycles to which the detail is subjected, and  $N_c$  is the critical number of stress cycles leading to fatigue failure for the detail. Since the random variables,  $A$  and  $\Delta$ , have already been discussed in Chapter 4, the likelihood of needed repair can be easily evaluated based on Equation 5.5.

### 5.3.2 LEFM Approach

For the LEFM approach, the limit state function,  $H(\mathbf{X})$ , for evaluating the likelihood of needed repair for all non-AASHTO type details can be defined in terms of crack size in order to be consistent with the definition of the limit state function,  $g(\mathbf{X})$ , used for evaluating the probability of fatigue failure (Equation 4.33). The likelihood of needed repair may be regarded as the same as the probability of detecting a crack with a prescribed size,  $a_R$ , which may be considered as the maximum permissible size before repair is warranted. Replacing  $\psi(a_0, a_c)$  in Equation 4.33 by  $\psi(a_0, a_R)$ , the associated limit state function,  $H(\mathbf{X})$ , needed to evaluate  $P_R$  as proposed by Madsen (1989) is written as:

$$H(\mathbf{X}) = \psi(a_0, a_R) - \psi(a_0, a_N) \quad (5.7)$$

or

$$\begin{aligned} H(\mathbf{X}) &= \int_{a_0}^{a_R} \frac{da}{\left[ F(a) \sqrt{\pi a} \right]^m} - C(S_{RE})^m \cdot N \\ &= \int_{a_0}^{a_R} \frac{da}{\left[ F(a) \sqrt{\pi a} \right]^m} - C(S_{RE})^m \cdot (365 \cdot ADTT_{SL} \cdot C_s) \end{aligned} \quad (5.8)$$

With this limit state function,  $H(\mathbf{X})$ , defined for the LEFM approach, need for repair after an inspection corresponds to the event,  $H(\mathbf{X}) \leq 0$ . Hence, the likelihood of needed repair,  $P_R$ , for any non-AASHTO details can be evaluated using Equation 5.7 or 5.8. The index  $\gamma$  (see Equation 5.5 as well) associated with the likelihood of needed repair,  $P_R$ , can be evaluated as follows:

$$\gamma = \Phi^{-1}(1 - P_R) \quad (5.9)$$

### 5.3.3 Repair Realizations in the Event Tree

Considering the event tree branches as shown in Figure 5.2, it can be seen that the likelihood of needed repair at every inspection, i.e.,  $P_R(T_i)$ , depends on the elapsed time since the last repair. It is assumed that the likelihood of needed repair at the various inspection times are statistically independent, i.e.,  $P_R(T_i)$  and  $P_R(T_j)$  are statistically independent for  $i \neq j$ . The probability,  $P(B_i)$ , of any branch,  $B_i$ , that includes  $N_R$  repairs can be expressed as the product of  $N_R$  likelihood of needed repair terms and  $(N-N_R)$  complementary terms where repair is not needed.

## 5.4 COST FUNCTION

The various inspection and repair scenarios associated with any inspection schedule employed for a detail may be studied in an event tree analysis. As described in Section 5.2, such an event tree analysis can provide not only the probability of occurrence of each branch, but also the fatigue reliability associated with each branch for the inspection schedule considered. Hence, with the help of such an event tree approach, we can now define the cost of inspections, the cost of repairs, and the cost associated with failure of a specified detail. These costs can then be employed in the total cost function (objective function) for the optimization problem.

### 5.4.1 Cost of Inspections

For steel bridge details, nondestructive inspection methods might include visual inspection, ultrasonic inspection, radiographic inspection, magnetic particle inspection, dye penetrant inspection, acoustic emission inspection, etc. We consider cases where only one inspection technique is employed over the service life of a detail. In Chapter 6, selection between alternative inspection techniques is discussed.

Let  $K_I$  represent the cost of a single inspection of the specified detail. Then, the total cost of inspections over the service life,  $C_I$ , can be represented as:

$$C_I = \sum_{i=1}^n K_I = n \cdot K_I \quad (5.10)$$

where  $n$  represents the number of inspections.

### 5.4.2 Cost of Repairs

Let  $K_R$  represent the cost of a single repair of the specified detail. Because of the different repair realizations of the detail as shown in the event tree (see Figure 5.2), the cost of repair at the time  $T_i$  is the product of  $K_R$  and  $E[R_i]$ , the expected number of repairs at  $T_i$ . Let  $R_i$  denote a repair event at time,  $T_i$ , and  $B_j^i$  denote branch  $j$  of the event tree at time,  $T_i$ . The expected number of repairs at  $T_i$  can be expressed as:

$$E[R_i] = \sum_{j=1}^{2^{i-1}} P(R_i \cap B_j^i) \quad (5.11)$$

The total cost of repairs for the detail over the service life,  $C_R$ , with  $n$  inspections can be represented as:

$$C_R = \sum_{i=1}^n K_R \cdot E[R_i] \quad (5.12)$$

### 5.4.3 Cost of Failure

The cost of failure,  $C_F$ , is meant to represent the expected cost resulting from consequences of a failure. If the detail/member under consideration is fracture-critical, its failure could cause failure of the span where the detail is located or even failure of the entire steel bridge. Hence, the cost of failure should include the possible cost of rebuilding a span or the entire bridge, as appropriate, as well as costs due to lost use, injuries, fatalities, etc. – not all of which are easily and uncontroversially estimated. Nevertheless, all of these potential costs associated with a failure are summed to yield a quantity,  $K_F$ . The probability of failure on each of the branches in the event tree should be considered in the evaluation of the expected cost of failure. Let  $F$  denote the event that the detail in question fails and  $B_i$  denote branch  $i$  of the event tree. Then, the expected cost of failure for the specified detail over the service life may be defined as:

$$C_F = \sum_{i=1}^{2^n} \left\{ \frac{1}{T_f - T_0} \int_{T_0}^{T_f} K_F \cdot P(F \cap B_i) dT \right\} \quad (5.13)$$

Considering all the possible scenarios (branches) of the event tree for the detail, an expected tree reliability index  $E[\beta]$  can be represented as:

$$E[\beta] = -\Phi^{-1} \left( \sum_{j=1}^{2^n} P(F | B_j) \cdot P(B_j) \right) \quad (5.14)$$

Substituting Equation (5.14) into Equation (5.13), the cost of failure may finally be expressed as:

$$C_F = \frac{1}{T_f - T_0} \int_{T_0}^{T_f} K_F \cdot \Phi(-E[\beta]) dT \quad (5.15)$$

#### 5.4.4 Total Cost

With definitions of the cost of inspections, repairs, and failure for the specified detail, the total cost,  $C_T$ , may be represented as:

$$C_T = C_I + C_R + C_F \quad (5.16)$$

$$C_T = \left\{ \sum_{i=1}^n K_I \right\} + \left\{ \sum_{i=1}^n K_R \cdot E[R_i] \right\} + \left\{ \frac{1}{T_f - T_0} \int_{T_0}^{T_f} K_F \cdot \Phi(-E[\beta]) dT \right\} \quad (5.17)$$

where Equations 5.10, 5.12, and 5.15 have been used.

#### 5.5 CONSTRAINTS

The number of inspections,  $n$ , and the inspection times,  $T_1 \dots T_n$ , are variables for this optimization problem. One obvious constraint on the inspection times may be expressed as:

$$T_0 < T_1 < \dots < T_n < T_f \quad (5.18)$$

Usually, restrictions are placed on the time between inspections such that the inspection interval is neither too large (requiring an upper bound,  $T_{\max}$ , on time between inspections) nor too short (requiring a lower bound,  $T_{\min}$ ). Such constraints on the inspection interval may be required by local and state transportation agencies. Hence, a second constraint on inspection times for the optimization problem is:

$$T_{\min} \leq T_i - T_{i-1} \leq T_{\max}, \quad i = 1, 2, \dots, n \quad (5.19)$$

It is also usually necessary to keep the reliability (safety) for the selected detail above a specified level. This requirement can be achieved by defining a target reliability index,  $\beta_{\min}$ , which is the minimum acceptable safety level for the specified detail. Thus, an additional constraint to be included in our optimization problem may be defined as:

$$E[\beta(T_i)] \geq \beta_{\min}, \quad i = 1, 2, \dots, (n+1) \quad \text{where } T_{n+1} = T_f. \quad (5.20)$$



## 5.6 FORMULATION OF THE OPTIMIZATION PROBLEM

In summary, the optimization problem for inspection scheduling may be formulated as follows:

$$\min_{n, T_1, \dots, T_n} C_T = \left\{ \sum_{i=1}^n K_I \right\} + \left\{ \sum_{i=1}^n K_R \cdot E[R_i] \right\} + \left\{ \frac{1}{T_f - T_0} \int_{T_0}^{T_f} K_F \cdot \Phi(-E[\beta]) dT \right\} \quad (5.21)$$

$$\begin{aligned} \text{subject to} \quad & T_0 < T_1 < \dots < T_n < T_f \\ & T_{\min} \leq T_i - T_{i-1} \leq T_{\max}, \quad i = 1, 2, \dots, n \\ & E[\beta(T_i)] \geq \beta_{\min}, \quad i = 1, 2, \dots, (n+1) \end{aligned}$$

Minimizing the total cost, a set of inspection times,  $T_i$ , may be found. By changing the number of inspections,  $n$ , the total cost corresponding to a different number of inspections may be compared so as to finally yield the optimization solution.

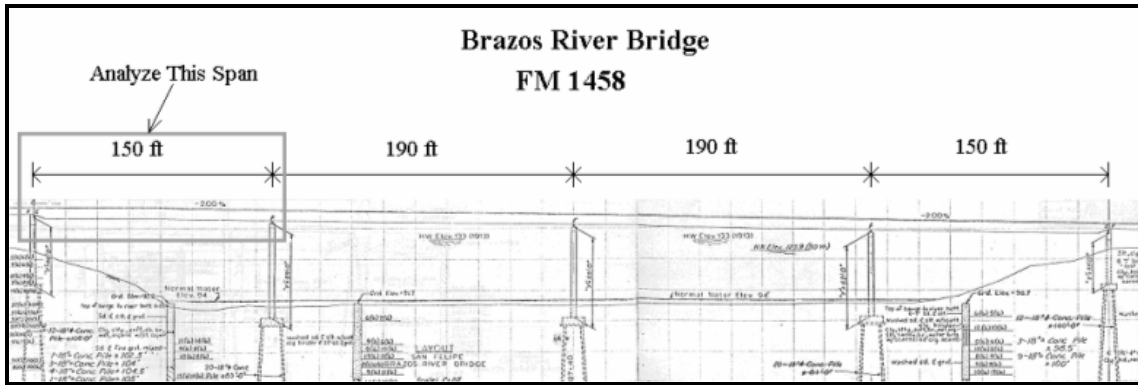
As described, the fatigue inspection scheduling problem becomes a mathematical optimization problem with reliability and inspection interval constraints that involves a search for a feasible set of optimization variables ( $n; T_1, T_2, \dots, T_n$ ) that yields the minimum total cost and an acceptable fatigue reliability for a detail over its service life. In theory, this optimization problem for inspection scheduling is a nonlinear optimization problem with constraints. Nonlinear optimization solvers such as NLPQL by Schittkowski (1985), GRG2 by Lasdon et al. (1978), SQP by Fan et al. (1988), DONLP2 by Spellucci (1998), and many others may be employed to solve this optimization problem. A FORTRAN program was developed to assist in solving the optimization problem of fatigue inspection scheduling in this study. The IMSL library routine, NCONF (Visual Numerics (1997)), was used to solve the general nonlinear programming problem using sequential quadratic programming and a finite-difference gradient. The routine, NCONF, is based on the subroutine, NLPQL, a FORTRAN code developed by Schittkowski (1985).

## 5.7 NUMERICAL EXAMPLES

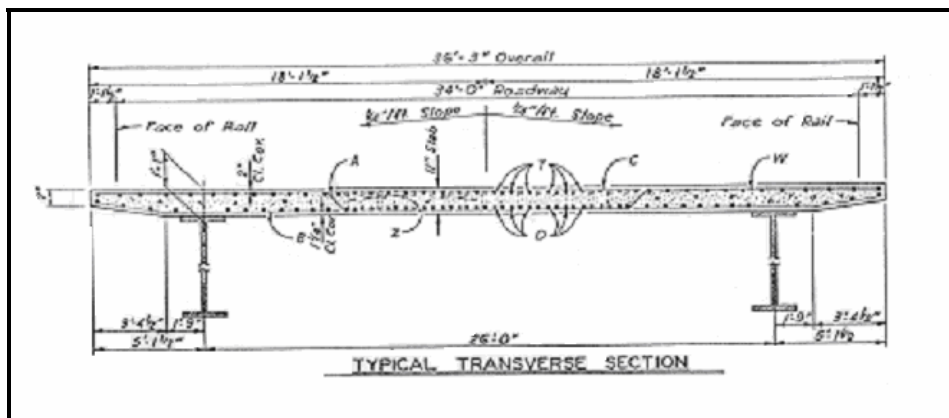
Two examples are presented here to illustrate application of the reliability-based optimal inspection scheduling procedure. The first example focuses on an AASHTO type detail in a plate girder bridge while the second example examines a non-AASHTO type detail in a box girder bridge. Both of these details are assumed to be located on fracture-critical members; hence, fatigue failure of the detail is expected to trigger collapse of the bridge span and result in considerable loss. The influence of relative costs of inspection, repair, and failure and the effect of variation in the models for daily truck traffic are discussed in these example studies.

### 5.7.1 Plate Girder Bridge Example

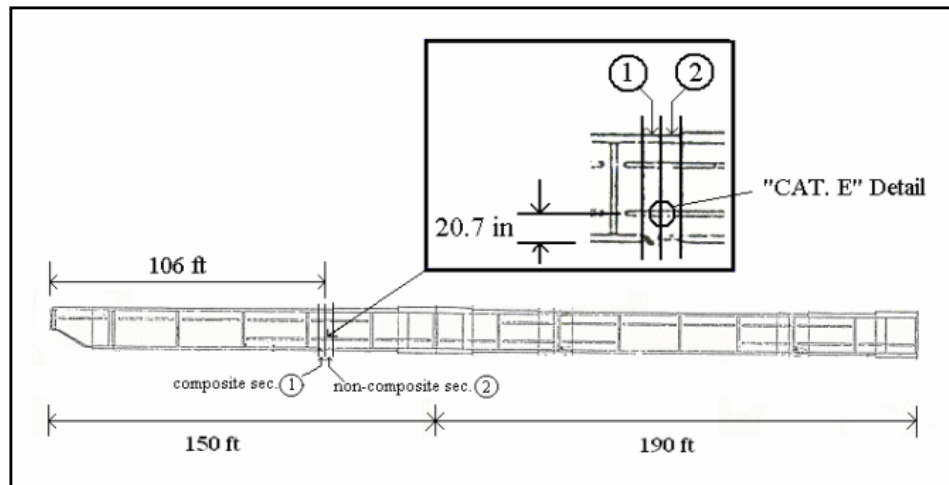
The example bridge studied here is the 680-ft long Brazos River Bridge in Texas, which was built in 1972. Figure 5.3 shows the layout of the bridge as well as a magnified view of the selected fatigue detail, which is classified as a Category E detail according to the AASHTO Specifications. This detail located in the leftmost 150-ft span is analyzed. A Rayleigh distribution is assumed for the stress ranges with distribution parameter,  $S_{R0}$ , equal to 6.13 ksi. This corresponds to an equivalent stress range,  $S_{RE}$ , of 9.53 ksi based on Equation 3.12, assuming a fatigue exponent,  $m$ , equal to 3. The target reliability  $\beta_{\min}$  for the detail is assumed to be 3.7, corresponding to a failure probability of approximately 1/10000. Two sets of relative costs of inspection, repair, and failure: (i)  $K_I : K_R : K_F = 1 : 1.3 \times 10^2 : 4 \times 10^5$ ; and (ii)  $K_I : K_R : K_F = 1 : 2.6 \times 10^2 : 4 \times 10^5$  are considered for illustration of the optimal inspection scheduling. The number of stress cycles per truck passage  $C_s$  and the Average Daily Truck Traffic  $ADTT$  are taken to be 1 and 84, respectively.



(a)



(b)



(c)

Figure 5.3: Brazos River Bridge showing (a) entire bridge in elevation; (b) a typical transverse section; and (c) a detail of interest for fatigue reliability.

After applying the AASHTO fatigue analysis approach, the fatigue reliability,  $\beta$ , of the specified detail over the service life is shown in Figure 5.4. The target reliability level,  $\beta_{\min}$ , of 3.7 is also shown in the figure. It can be seen that the fatigue reliability of the chosen detail is below the target reliability by the thirteenth year.

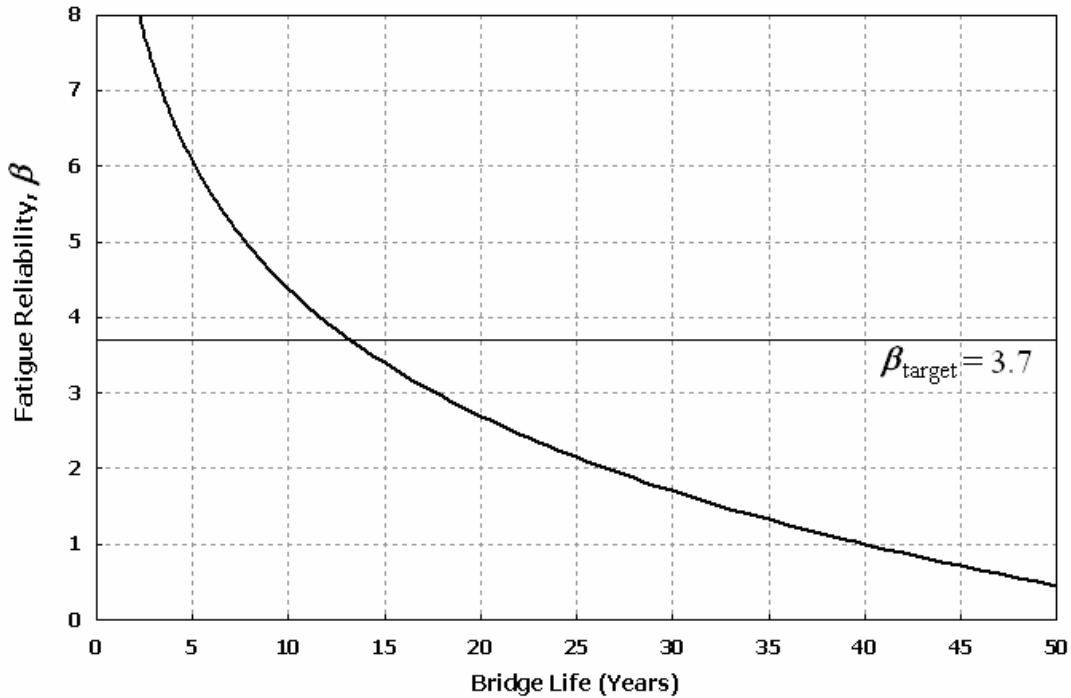


Figure 5.4: Fatigue Reliability of the chosen Category E Detail over 50 years.

First, we will assume that in the year 2002 (i.e., 30 years after 1972), no crack was found or that the crack in the detail was repaired to its original condition. To avoid too many inspections and to simultaneously meet the 2-year inspection interval required by the Federal Highway Administration (FHWA), the constraints on inspection intervals,  $T_{\min}$  and  $T_{\max}$ , are taken to be 0.5 and 2 years, respectively. Applying the optimization method proposed with an “as good as new” repair policy, and for the relative costs of  $K_I : K_R : K_F = 1 : 1.3 \times 10^2 : 4 \times 10^5$ , it is found in Fig. 5.5 that the optimal number of

inspections for the next twenty years is eleven and the associated optimal inspection schedule is as shown in Fig. 5.6 where, for comparison, an *ad hoc* periodic inspection schedule is also shown. Note that each discrete upward change in the reliability curve takes place at the time of an inspection and reflects the effect of a repair in raising the fatigue reliability.

The optimal inspection times in years are  $\mathbf{T} = (2.0, 4.0, 6.0, 8.0, 10.0, 12.0, 13.5, 14.0, 14.5, 15.0, 15.5) + 30$ . On comparing the optimal inspection schedule with the periodic two-year interval schedule, the total cost (162.7) of the optimal schedule is found to be less than the total cost (168.9) of the periodic schedule. Though the optimal schedule requires two more inspections than the periodic schedule, these additional inspections and the short interval between inspections after the bridge reaches 42 years of age reduce the risk of the detail's failure. This fact can be confirmed by the reduced cost associated with failure (in the total cost for the optimal schedule). Therefore, the optimal schedule clearly represents the preferred choice for inspecting this detail over its planned service life.

Upon releasing the upper-bound constraint on the inspection interval, i.e., when  $T_{max}$  is unbounded, it is found as shown in Fig. 5.7 that only five inspections are required to achieve the optimal schedule with an associated total cost of 157.6, which is less than the total cost (162.7) of the previous optimal schedule where  $T_{max}$  was equal to 2 years. The inspection times in years are  $\mathbf{T} = (13.2, 14.1, 14.6, 15.1, 15.6) + 30$ . Note that the reliability index,  $\beta$ , is equal to exactly 3.7 at  $T_1$  (43.2 yrs) and  $T_f$  (50 yrs). No inspections are needed before the reliability curve first hits the target reliability level at 43.2 yrs. Also, no inspections are needed after the bridge has completed 45.6 yrs of its planned life. Because of this, the total cost is lower than for the case where the constraint on  $T_{max}$  is included.

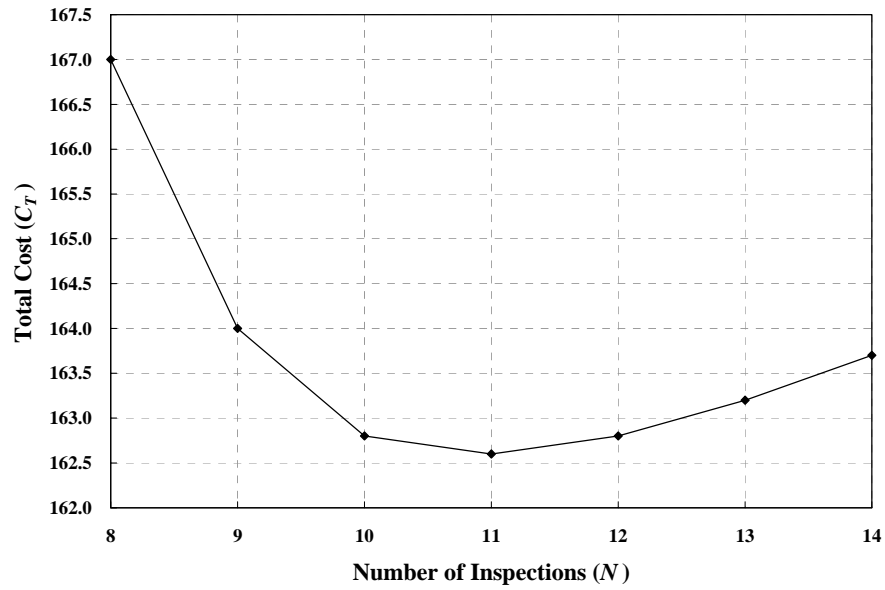


Figure 5.5: Optimal total cost as a function of the number of inspections for the chosen detail ( $K_I : K_R : K_F = 1 : 1.3 \times 10^2 : 4 \times 10^5$ ).

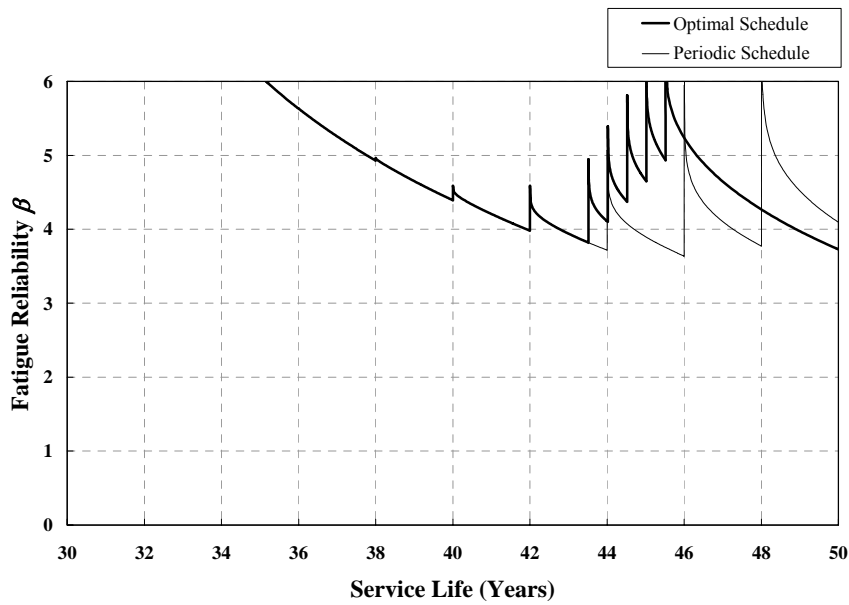


Figure 5.6: Optimal inspection schedule ( $T_{min} = 0.5$  yrs,  $T_{max} = 2$  yrs) for the repair cost case of  $K_I : K_R : K_F = 1 : 1.3 \times 10^2 : 4 \times 10^5$ ,  $C_T = 162.7$ .

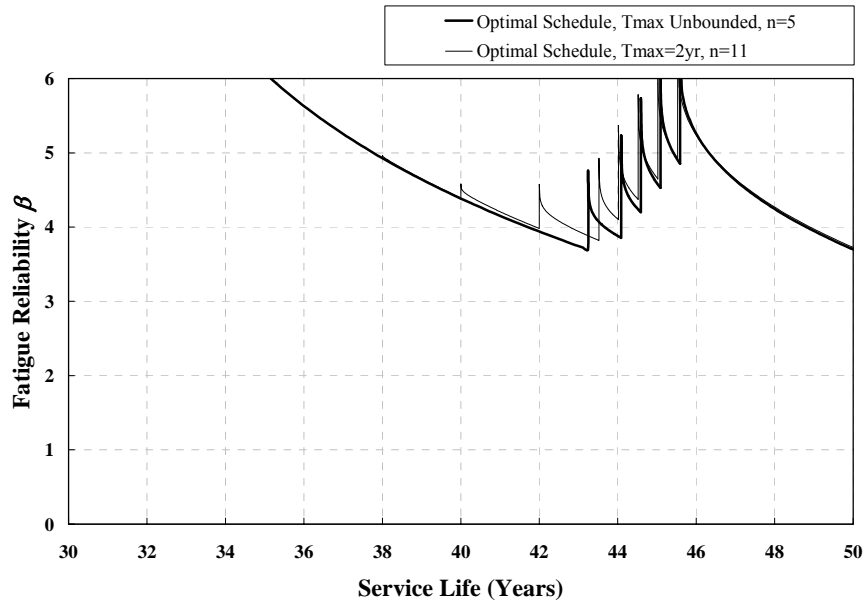


Figure 5.7: Optimal inspection schedule ( $T_{max}$  unbounded) for the repair cost case of  $K_I : K_R : K_F = 1 : 1.3 \times 10^2 : 4 \times 10^5$ ,  $C_T = 157.6$ .

For the second case with relative costs of  $K_I : K_R : K_F = 1 : 2.6 \times 10^2 : 4 \times 10^5$  and with inspection interval constraints of  $T_{min} = 0.5$  years and  $T_{max} = 2$  years, nine inspection times over the next twenty years are needed. The optimal inspection times in years are  $\mathbf{T} = (1.7, 3.4, 5.4, 7.4, 9.4, 11.4, 13.4, 15.1, 17.1) + 30$  as shown in Fig. 5.8 where again a two-year periodic inspection interval schedule is also shown. Though the number of inspections (nine) is the same as with the periodic schedule, the total cost (200.5) for the optimal schedule is still lower than the total cost (211.7) for the periodic schedule. After removing the upper-bound constraint ( $T_{max} = 2$  years) again, it is found in Fig. 5.9 that fewer (four) inspection times,  $\mathbf{T} = (10.8, 13.5, 15.1, 17.1) + 30$ , are needed to reach the optimal schedule with a total cost of 195.0, which, again, is lower than the total cost (200.5) for the optimal schedule with  $T_{max} = 2$  yrs.

From the results presented, it can be seen that the increase in the number of inspections,  $n$ , increases inspection and repair costs but typically decreases failure cost. The optimal result (or lowest cost) occurs at the number,  $n_{opt}$ , where the decrease in failure costs starts to become less than the increase in inspection and repair costs. From the two cases presented, it can be seen that removing the upper-bound constraint ( $T_{max}$ ) on inspection intervals leads to lower costs. Also, it found that when repair costs are larger, the optimal schedule generally involves fewer inspections. Clearly, the constraints on inspection intervals and the relative costs of inspection, repair, and failure affect the resulting optimal schedule for inspections in a very direct manner.

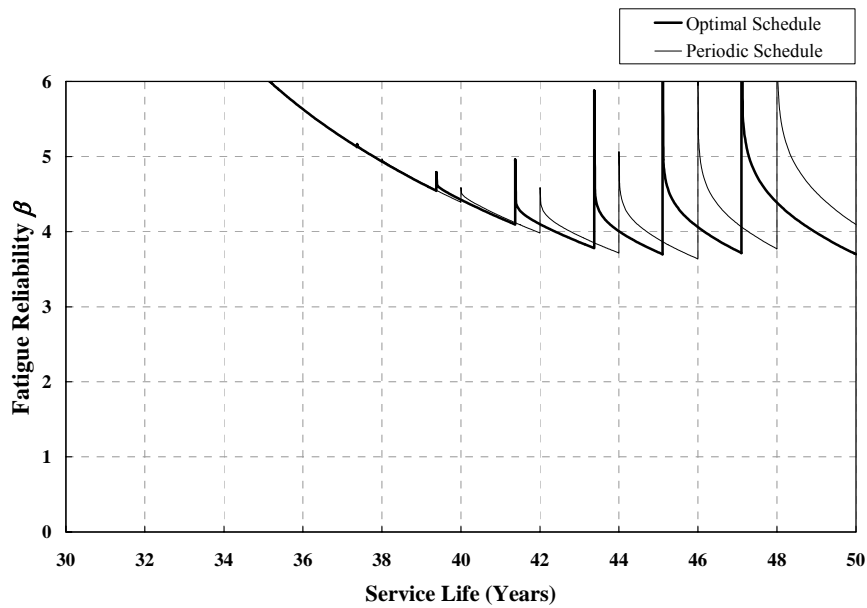


Figure 5.8: Optimal inspection schedule ( $T_{min} = 0.5$  yrs,  $T_{max} = 2$  yrs) for the repair cost case of  $K_I : K_R : K_F = 1 : 2.6 \times 10^2 : 4 \times 10^5$ ,  $C_T = 200.5$ .



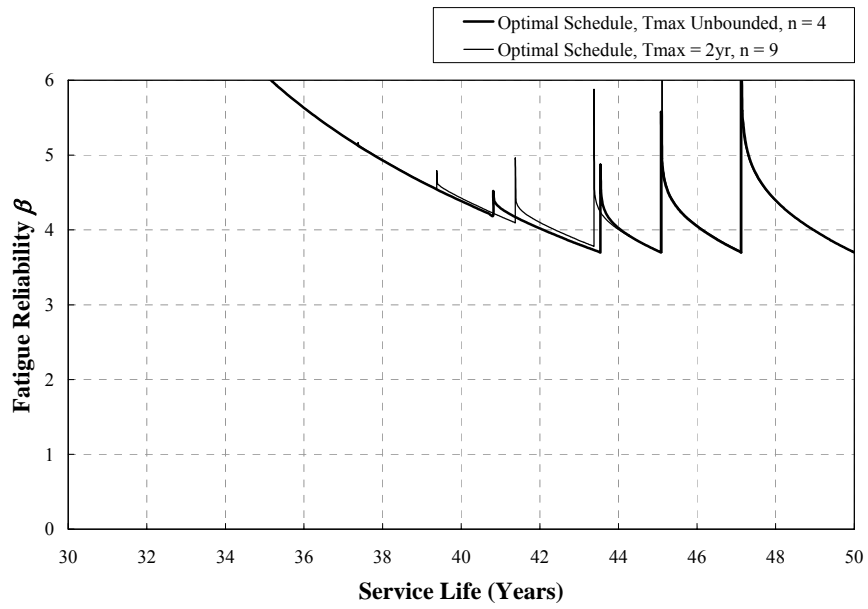


Figure 5.9: Optimal Inspection Schedule ( $T_{max}$  unbounded) for the repair cost case of  $K_I : K_R : K_F = 1 : 2.6 \times 10^2 : 4 \times 10^5$ ,  $C_T = 195.0$ .

### 5.7.2 Box Girder Bridge Example

A newly built bridge as shown in Figure 5.10 is considered. The bottom (tension) flange, with a width of 42 inches, is known to have a center-notched crack in the two full-penetration butt welds that run the entire width of the bottom flange. This example bridge is adapted from one described by Zhao et al. (1994) for which we seek an optimal inspection schedule for the next twenty years. For the traffic loading, the variables,  $C_s$  and  $ADTT$  are taken to be 1 and 300, respectively, in Equation 5.8. A Rayleigh distribution is assumed for the stress ranges with distribution parameter,  $S_{R0}$ , equal to 6.334 ksi. This corresponds to an equivalent stress range,  $S_{RE}$ , of 9.85 ksi assuming a fatigue exponent,  $m$ , equal to 3. The minimum (target) reliability index,  $\beta_{min}$ , is taken to be 3.7. Random variables related to the crack and its growth are listed in Table 5.2 and the geometry function for this crack geometry may be expressed according to Paris (1964) as:

$$F(a) = \frac{1 - 0.5(a/b) + 0.370(a/b)^2 - 0.044(a/b)^3}{\sqrt{1 - (a/b)}} \quad (5.22)$$

where  $2a$  is the crack size and  $2b$  is the width of the bottom flange plate.

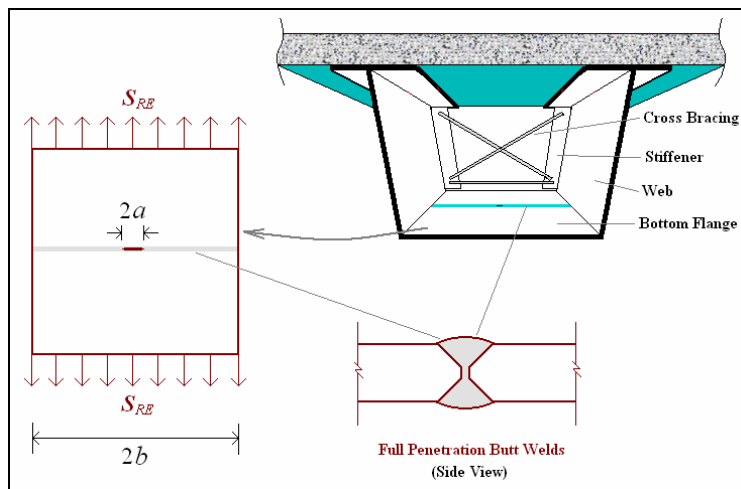


Figure 5.10: Center-Notched Crack in the Box Girder Bridge Example.

Table 5.2: Related Random Variables for Center Crack in Bottom Flange.

Variable	Type	Mean	COV
$a_0$ (initial crack size, in.)	lognormal	0.020 (in.)	0.500
$a_c$ (critical crack size, in.)	constant	2.000 (in.)	0.000
$a_R$ (crack size for repair, in.)	constant	0.200 (in.)	0.000
$C$ (fatigue growth parameter)*	lognormal	$2.05 \times 10^{-10}$	0.630
$m$ (fatigue growth exponent)	normal	3.000	0.100

\*  $C$  is assumed to have units consistent with crack size in inches and  $\Delta K$  in  $\text{ksi-in}^{1/2}$

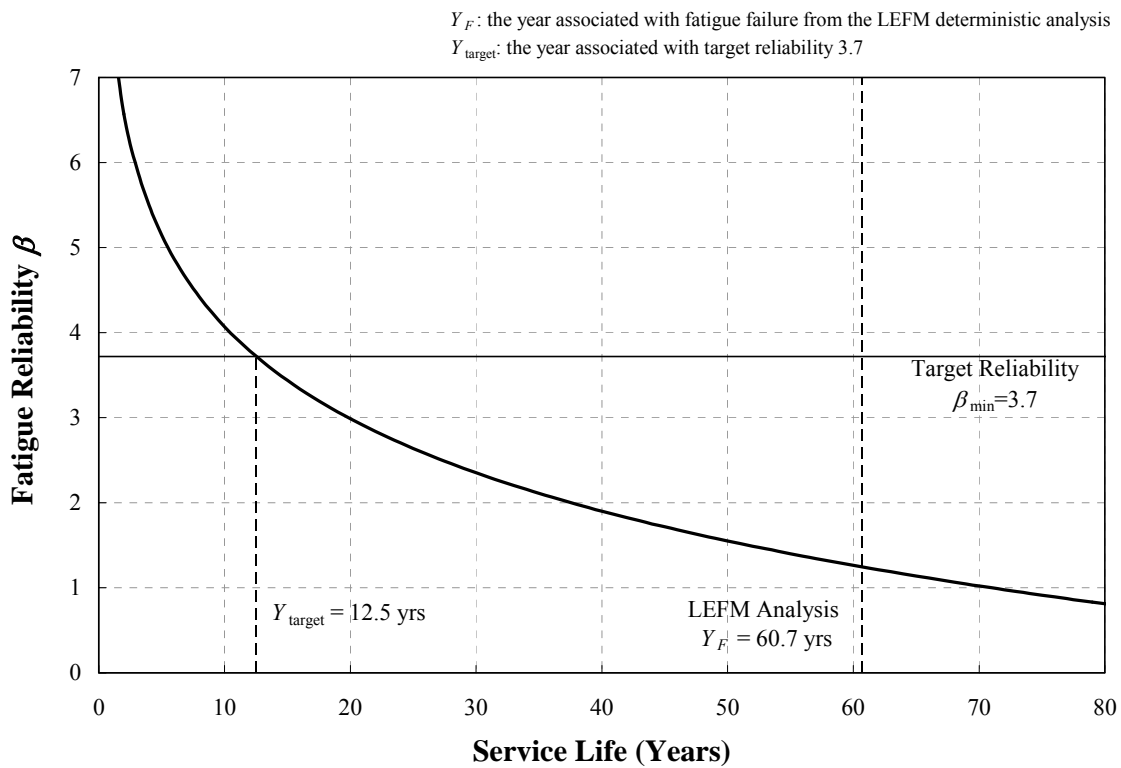


Figure 5.11: Fatigue Reliability of the Detail with Center-Notched Crack over 80 years.

### *Effects of Relative Repair and Failure Costs*

Three cases of relative costs of inspection, repair and failure: (i)  $K_I : K_R : K_F = 1 : 1 \times 10^1 : 1 \times 10^5$ ; (ii)  $K_I : K_R : K_F = 1 : 2 \times 10^1 : 1 \times 10^5$ ; and (iii)  $K_I : K_R : K_F = 1 : 1 \times 10^1 : 2 \times 10^5$  are considered here to focus on the relative effects of repair cost and failure cost on proposed optimal inspection scheduling plans. Since the detail shown in Figure 5.10 is not specifically defined in the AASHTO fatigue categories, the LEFM-based procedure described for non-AASHTO type details in Chapter 4 is applied and a fatigue reliability curve from a FORM (First-Order Reliability Method) computation leads to the time-dependent reliability curve shown in Figure 5.11. It can be seen that, without intervention or repair of some sort, the fatigue reliability of the chosen detail would fall below the target reliability of 3.7 after 12.5 years. Hence, an inspection schedule is needed for the detail in order to prevent failure due to fatigue. For each of the three cases, two optimal schedules are provided. One is the optimal schedule subject to the constraints,  $T_{min} = 0.5$  years and  $T_{max} = 2$  years, on inspection intervals to prevent overly frequent inspections and while still meeting the two-year inspection interval requirement by the FHWA. The other optimal schedule only requires the lower-bound constraint on  $T_{min}$  but leaves  $T_{max}$  unbounded.

For Case (i) using the relative costs of  $K_I : K_R : K_F = 1 : 1 \times 10^1 : 1 \times 10^5$ , reliability curves for the two optimal schedules with the different inspection interval constraints are shown in Figure 5.12. Again note, as in the plate girder example, that each discrete upward change in the reliability curve takes place at the time of an inspection and reflects the effect of a repair in raising the fatigue reliability. It may be seen that for the optimal schedule constrained by  $T_{max} = 2$  years, the optimal number of inspections is seven with a total cost of 35.7 and the inspection times in years,  $\mathbf{T} = (1.3, 3.3, 5.3, 7.3, 9.3, 11.3, 11.8)$ . Not unexpectedly, the optimal schedule without a  $T_{max}$  constraint requires fewer (three)

inspections and costs less (19.3); the associated inspection times in years,  $\mathbf{T} = (10.0, 10.5, 11.0)$ . Both optimal schedules result in lower costs than the total cost (47.2) for a two-year periodic inspection schedule that is required by the FHWA. Though the optimal schedule with  $T_{max} = 2$  years demands two fewer inspections than the periodic schedule, the optimal schedule still can maintain the fatigue reliability of the detail above the target reliability over the twenty years and also keep the costs lower than is the case with the periodic schedule. The two fewer inspections essentially reduce the inspection costs and possible repair costs in the future. For the optimal schedule with  $T_{max}$  unbounded, the reliability index,  $\beta$ , is approximately equal to 4.0 at  $T_1$  (10.0 yrs) and  $T_f$  (20 yrs). No inspections are needed before the reliability curve first drops to a level of 4.0 at 10.0 years. The schedule with unbounded  $T_{max}$  costs less (19.3) than that with  $T_{max} = 2$  years, where the costs were 35.7.

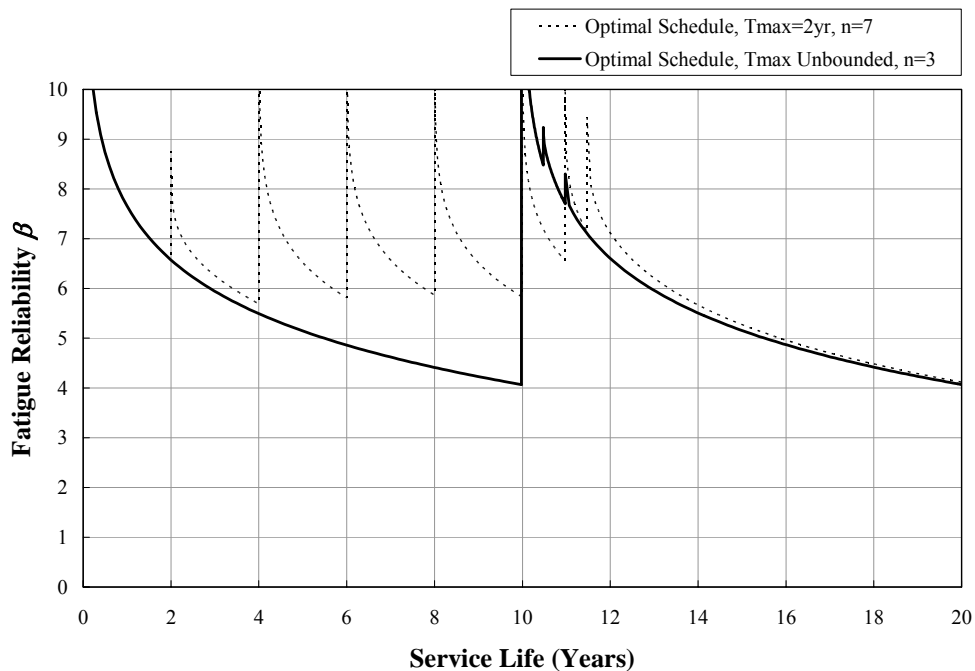


Figure 5.12: Optimal Inspection Schedules with  $T_{max} = 2$ yrs ( $C_T = 35.7$ ) and with unbounded  $T_{max}$  ( $C_T = 19.3$ ) for Case (i):  $K_I : K_R : K_F = 1 : 1 \times 10^1 : 1 \times 10^5$ .

For Case (ii) with higher repair costs than Case (i) (now,  $K_I : K_R : K_F = 1 : 2 \times 10^1 : 1 \times 10^5$ ), Figure 5.13 shows the two optimal inspection schedules. For the optimal schedule with  $T_{max} = 2$  years, six inspections over the next twenty years are needed and the optimal inspection times in years are  $T = (2.0, 4.0, 6.0, 8.0, 10.0, 10.6)$ . Because the number of inspections (six) is smaller than that with the two-year periodic schedule, the total cost (59.0) for this optimal schedule is lower than the total cost (85.2) with the periodic schedule. After removing the constraint on  $T_{max}$ , it is found that even fewer inspections (two) with  $T = (10.2, 10.7)$ , are needed to yield the optimal schedule with a total cost of 29.1, which is again lower than the total cost of 59.0 for the optimal schedule that has the constraint,  $T_{max} = 2$  years.

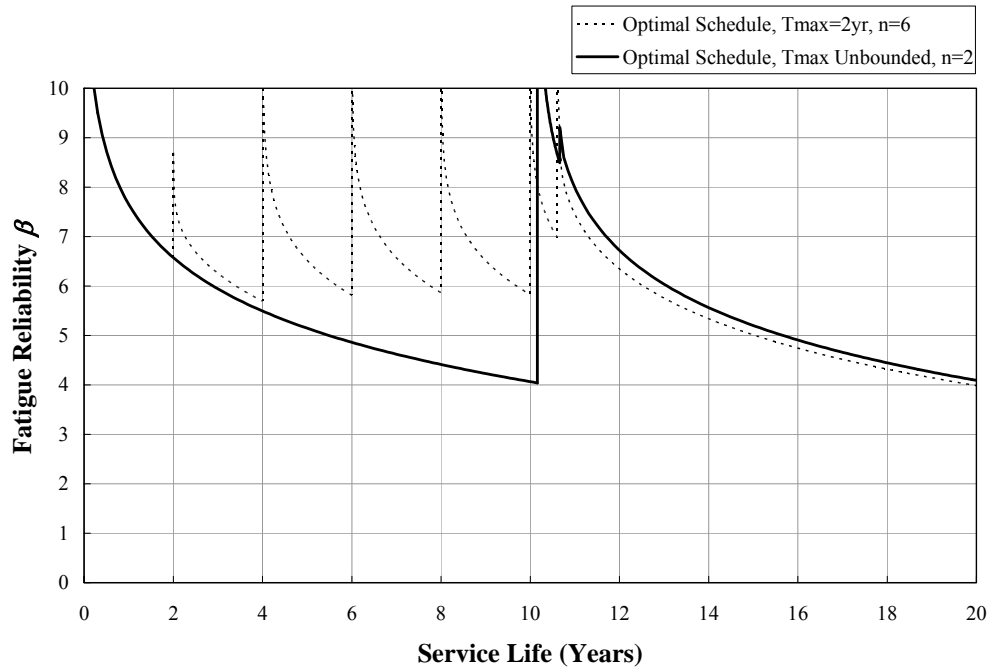


Figure 5.13: Optimal Inspection Schedules with  $T_{max} = 2$  yrs ( $C_T = 59.0$ ) and with unbounded  $T_{max}$  ( $C_T = 29.1$ ) for Case (ii):  $K_I : K_R : K_F = 1 : 2 \times 10^1 : 1 \times 10^5$ .

Comparing Cases (i) and (ii), it can be seen that the two optimal schedules in Case (ii) with the higher relative repair costs demand fewer inspections than the two corresponding schedules in Case (i). The increase in relative repair costs tends to decrease the number of inspections to arrive at the optimal schedule. This effect can be verified by comparing Figures 5.14 and 5.15, where the costs of various optimized inspection schedules in the two cases are presented. Note that at each abscissa value,  $n$  or Number of inspections, the costs shown are associated with the optimal schedule for that number,  $n$ . The overall optimal schedule that should be selected is that associated with the lowest cost after considering all possible values of  $n$ . It can be seen that the inspection and failure cost curves for both cases stay at roughly the same levels. However, the repair cost curve in Case (ii) with the higher relative repair costs, is approximately twice as high as the repair cost curve in Case (i). The total cost curve is controlled by the repair cost curve in Case (ii). The fewer the number of inspections, the lower the repair costs and total costs. However, fewer inspections increase the risk of failure and therefore raise the expected failure costs. Upon combining the effects of repair and failure costs with the number of inspections, the higher relative repair cost case (Case (ii)) yields an optimal schedule with relatively fewer inspections. Though Figures 5.14 and 5.15 only show optimal schedules with the constraint of  $T_{max} = 2$  years, the same effect of higher relative repair cost is found in the case where the constraint on  $T_{max}$  is removed. It should be noted that the failure cost curves in Figures 5.14 and 5.15 are at similar cost levels but are not exactly the same. This is because the same number of inspections in the two cases results in different optimized schedules over the planned period.

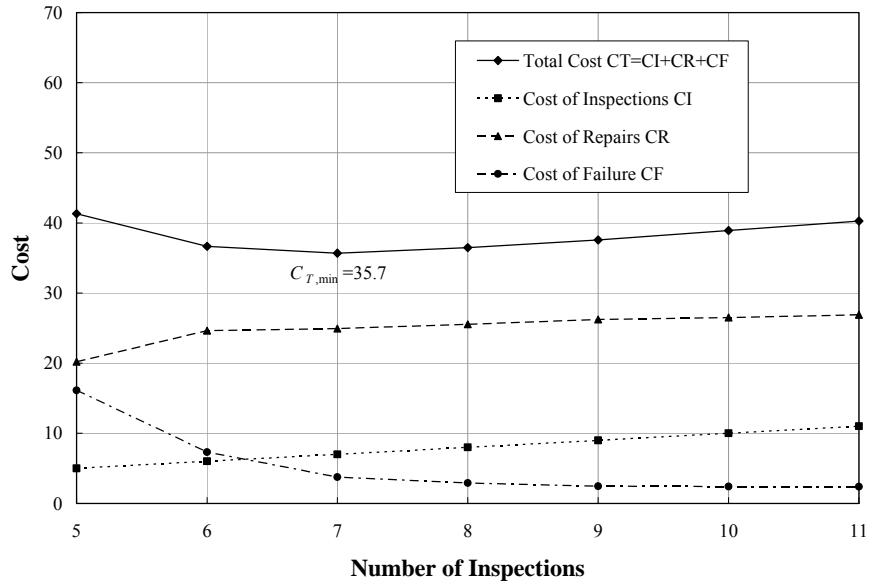


Figure 5.14: Costs of Various Optimized Inspection Schedules with  $T_{max} = 2$  yrs for Case (i):  $K_I : K_R : K_F = 1 : 1 \times 10^1 : 1 \times 10^5$ .

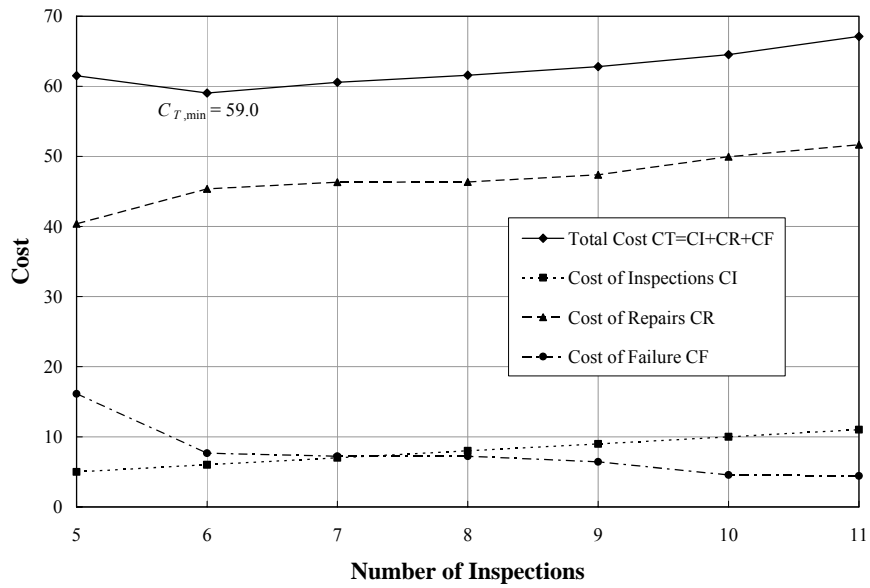


Figure 5.15: Costs of Various Optimized Inspection Schedules with  $T_{max} = 2$  yrs for Case (ii):  $K_I : K_R : K_F = 1 : 2 \times 10^1 : 1 \times 10^5$ .



For Case (iii) with the higher relative failure costs ( $K_I : K_R : K_F = 1 : 1 \times 10^1 : 2 \times 10^5$ ) compared to Case (i), the reliability curves for two inspection schedules with the different constraints are shown in Figure 5.16. The optimal schedule with no constraint on  $T_{max}$  requires fewer inspections (four) in twenty years and costs less (26.4) than the optimal schedule with  $T_{max} = 2$  years for which the number of inspections required is eight and cost, 38.7. The inspection times in years for the cases with  $T_{max} = 2$  years and with  $T_{max}$  unbounded are, respectively,  $\mathbf{T} = (1.5, 3.5, 5.5, 7.5, 9.5, 11.5, 12.0, 12.5)$  and  $\mathbf{T} = (0.5, 10.0, 10.5, 11.0)$ . Both optimal schedules result in lower costs than the total cost (47.5) for the two-year periodic inspection schedule required by the FHWA.

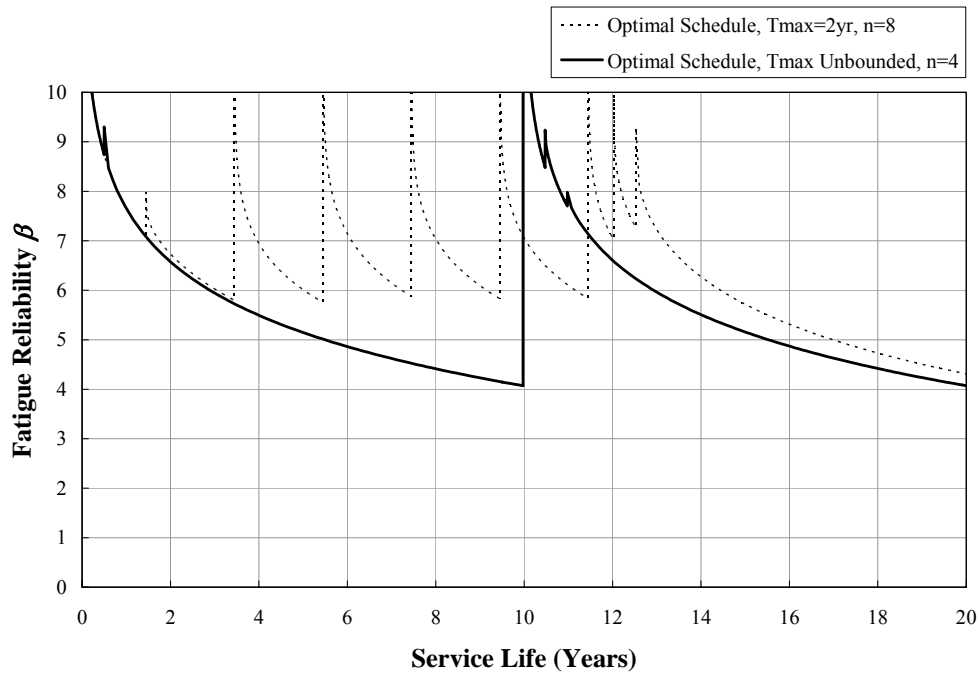


Figure 5.16: Optimal Inspection Schedules with  $T_{max} = 2$  yrs ( $C_T = 38.7$ ) and with unbounded  $T_{max}$  ( $C_T = 26.4$ ) for Case (iii):  $K_I : K_R : K_F = 1 : 1 \times 10^1 : 2 \times 10^5$ .

Comparing Cases (i) and (iii), it is found that the optimal schedules in Case (iii) (with higher failure cost case) requires more inspections than the optimal schedule in Case (i). With the  $T_{max}$  constraint set at 2 years, the higher failure cost case needs eight inspections while the lower failure cost case needs seven for lowest total cost. When  $T_{max}$  is unbounded, Case (i) requires three inspections while Case (iii) requires four. It is clear that an increase in relative failure costs,  $K_F$ , leads to an increase in the number of inspections in the optimal schedule. By studying Figures 5.17 and 5.18, it can be seen that for the optimal schedules with no  $T_{max}$  constraint, the increase in the relative failure cost (Case (iii)) essentially raises the failure cost curve about twice as high as the failure cost curve for Case (i) in Figure 5.17. The influence of different failure costs that is apparent in the increment in total cost can best be seen in the schedules with a small number of inspections. Repair and inspection cost curves are almost the same in both cases presented in Figures 5.17 and 5.18. In summary, higher relative failure cost raises the total cost curve more in schedules that involve fewer inspections. This is the reason why the Case (iii) schedule is associated with a larger number of inspections than Case (i). In the context of actual applications, this result is consistent with the fact that more critical details whose failures have greater consequences usually require more inspections to ensure adequate structural safety.

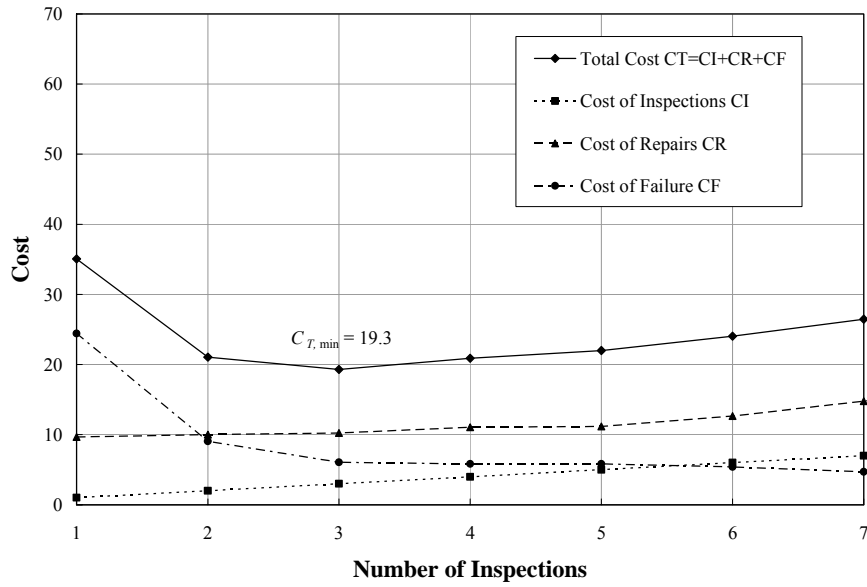


Figure 5.17: Costs of Various Optimized Inspection Schedules with  $T_{max}$  unbounded for Case (i):  $K_I : K_R : K_F = 1 : 1 \times 10^1 : 1 \times 10^5$ .

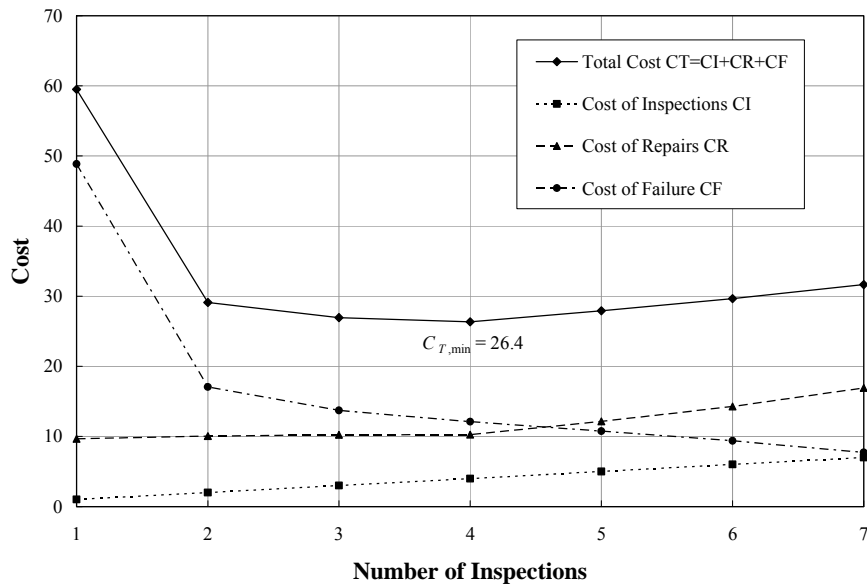


Figure 5.18: Costs of Various Optimized Inspection Schedules with  $T_{max}$  unbounded for Case (iii):  $K_I : K_R : K_F = 1 : 1 \times 10^1 : 2 \times 10^5$ .

### Effect of Average Daily Truck Traffic (ADTT) Models

Thus far, for convenience, all the analyses have been based on models with constant ADTT values (e.g., *ADTT* fixed at 300 in the cases studied). In reality, the ADTT value each year is not the same and should be treated as a random variable in the analysis. Moses et al. (1987) suggested using a lognormal distribution to model the random variable, ADTT. Hence, for the box girder example, lognormal ADTT models with a mean value of 300 and with COV values ranging from 0.1 to 0.4 are applied in order to assess the influence of ADTT uncertainty on fatigue reliability and on optimal inspection scheduling for the detail. Figure 5.19 shows variations in the fatigue reliability for the center crack detail with the different ADTT models. It can be seen that the fatigue reliability of the detail is lower for models with greater variability in ADTT. For the ADTT model with a COV of 0.4, the fatigue reliability falls below the target reliability by the ninth year, while with the constant ADTT model, it takes 12.5 years for this to occur.

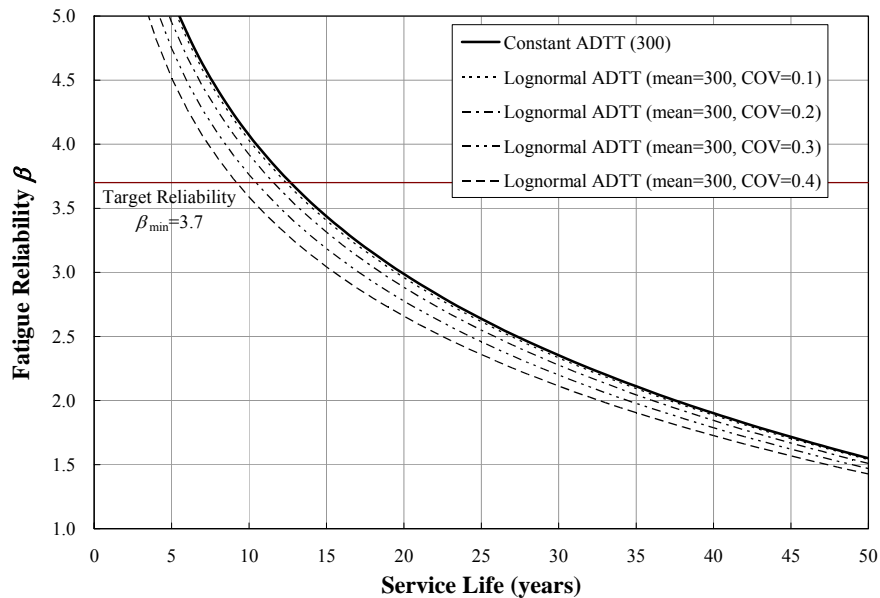


Figure 5.19: Fatigue Reliability for Various ADTT Models.

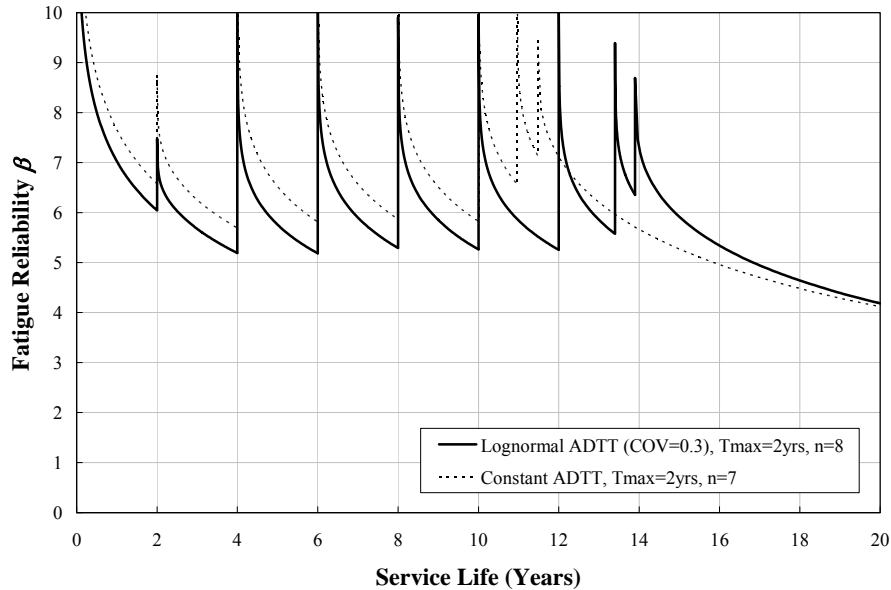


Figure 5.20: Optimal Schedules with Constant and Lognormal ADTT Models.

With a lognormal ADTT model (mean=300, COV=0.3), the optimization calculations are performed for Case (i) ( $K_I : K_R : K_F = 1 : 1 \times 10^1 : 1 \times 10^5$ ) to determine the influence of ADTT uncertainty on optimal inspection schedules. With the  $T_{max} = 2$  years constraint, the optimal schedule requires eight inspections with inspection times,  $\mathbf{T} = (2.0, 4.0, 6.0, 10.0, 12.0, 13.4, 13.9)$  and the total cost is 40.1. This optimal schedule demands one more inspection and costs more than the optimal inspection with the constant ADTT model ( $n = 7$  and  $C_T = 35.7$ ). Figure 5.20 shows a comparison of the schedules in these two cases. Due to ADTT uncertainty, the fatigue reliability with the lognormal ADTT model is lower than the fatigue reliability with constant ADTT. As a result, the constant ADTT model does not require any inspections after about 11.5 years, while the lognormal ADTT model requires inspections up to almost 14 years in order to keep the reliability above the target reliability level. This trend which suggests that an increase of ADTT uncertainty will require more inspections in an optimal schedule can

also be explained by comparing Figure 5.21 with Figure 5.14. Introducing uncertainty in ADTT leads to lower fatigue reliability of the detail, which in turn increases the risk of fatigue failure and associated failure costs. It can be seen that the failure cost curve in Figure 5.21 is significantly higher than the failure cost curve in Figure 5.14, especially for those schedules that involve a small number of inspections. Repair and inspection cost curves for the two cases are not very different. In summary, with the lognormal ADTT model, the combined effect of the failure, repair, and inspection costs results in an optimal schedule with a relatively larger number of inspections than with the constant ADTT model. Similar results can be found when the  $T_{max}$  constraint is removed. The optimal schedule with the lognormal ADTT model for unbounded  $T_{max}$  requires six inspections with inspection times,  $\mathbf{T} = (7.1, 7.6, 8.1, 13.6, 14.1, 14.6)$  and a total cost of 30.3. This optimal schedule again requires more inspections and costs more than the optimal schedule for the corresponding case with unbounded  $T_{max}$  and a constant ADTT model.

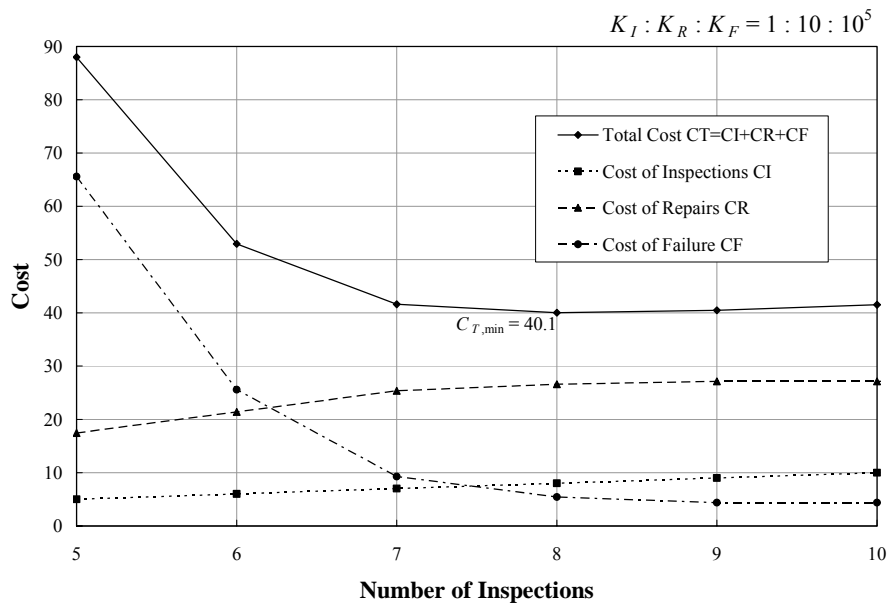


Figure 5.21: Costs of Various Optimized Inspection Schedules with  $T_{max} = 2$  yrs with a Lognormal ADTT Model (mean=300 and COV=0.3).

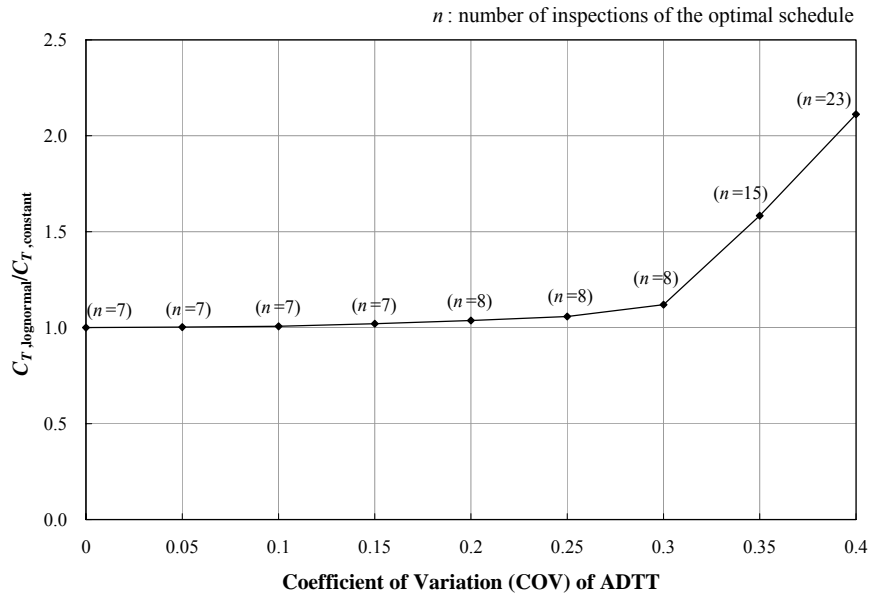


Figure 5.22: Normalized Costs for the Optimal Schedules with Various Lognormal ADTT Models.

Figure 5.22 shows normalized costs (indicated here as the ratio of cost with the lognormal ADTT model to that with constant ADTT) as a function of the COV assumed for ADTT. The number of required inspections is also indicated on the figure. It is seen that total costs increase with increase in the ADTT COV (or, equivalently, with increase in ADTT uncertainty). For low COV values up to about 0.3, the cost increases are small and at most one additional inspection is necessary when ADTT uncertainty is included, implying that ADTT uncertainty affects the overall scheduling problem to a limited extent. However, as ADTT uncertainty grows beyond 0.3, the cost and number of inspections required increase dramatically. As discussed earlier, greater uncertainty in ADTT implies lower fatigue reliability; the added inspections in the optimal schedules are needed to raise the fatigue reliability above the target reliability. Relating all of this to practical applications, the results summarized in Figure 5.22 suggest that greater

variability in the average daily truck traffic (ADTT) demands more inspections of bridge details to prevent failure due to fatigue. If the annual daily truck traffic does not fluctuate much, such as for saturated traffic condition in cities, the constant ADTT model can be adequate for use in optimal inspection scheduling. Moses et al. (1987) suggested a COV value of 0.1 for use with the lognormal ADTT model. As can be seen in Figure 5.22, the optimal schedule and total cost are not significantly affected by ADTT uncertainty associated with such a relatively low COV value.

#### *Effect of Constraint on Target Reliability, $\beta_{\text{target}}$*

Depending on the criticality of the detail and seriousness of failure consequences, the target reliability might sometimes need to be maintained at various specified high or low levels. Thus far, all the analyses for the box-girder example have been based on a target reliability,  $\beta_{\text{target}}$ , of 3.7, which corresponds to a probability of failure of  $10^{-4}$ . The effect of raising the  $\beta_{\text{target}}$  value to 4.2 (i.e.,  $P_F = 10^{-5}$ ) for Case (i) with  $K_I : K_R : K_F = 1 : 1 \times 10^2 : 1 \times 10^5$  is examined now in order to assess the influence of different target reliability constraints on optimization solutions. Upon analysis with the  $T_{\text{max}} = 2$  years constraint, it is found that the optimal schedule with the  $\beta_{\text{target}} = 4.2$  constraint requires seven inspections with a total cost of 35.7 and inspection times in years,  $\mathbf{T} = (1.3, 3.3, 5.3, 7.3, 9.3, 11.3, 11.8)$ , which is the same as the optimal schedule with the  $\beta_{\text{target}} = 3.7$  constraint. The reason the optimal schedule is unchanged is because the set of fatigue reliability index values,  $\boldsymbol{\beta} = (7.1, 5.8, 5.8, 5.9, 5.8, 5.8, 7.1, 4.2)$ , at the seven inspection times and at the end of the 20<sup>th</sup> service year meet even the higher reliability level of 4.2 as can be seen in Figure 5.12. Reliability constraints do not control the optimization solution; the inspection interval constraints do. The higher target reliability constraint of 4.2 eliminates a few infeasible schedules in the optimization process but results in the



same solution for lowest cost as that with the lower reliability constraint (of 3.7) as shown in Figure 5.23. It can be seen that schedules with fewer than seven inspections are infeasible for a target reliability of 4.2 because there are not a sufficient number of inspections to maintain the fatigue reliability as high as 4.2 over 20 years. The lowest cost for  $\beta_{\text{target}} = 4.2$  is associated with a feasible schedule and matches the solution for  $\beta_{\text{target}} = 3.7$ . Because the inspection interval constraints control the problem, the schedule for the lower reliability target leads to a safer than necessary schedule for that target reliability and even assures that higher target reliability levels can be met. Only when the desired target reliability rises to much higher levels will the optimal schedule shift to one requiring more inspections than that for a lower target reliability level. This is consistent with our expectation that more frequent inspections would be required to ensure a higher safety level for details.

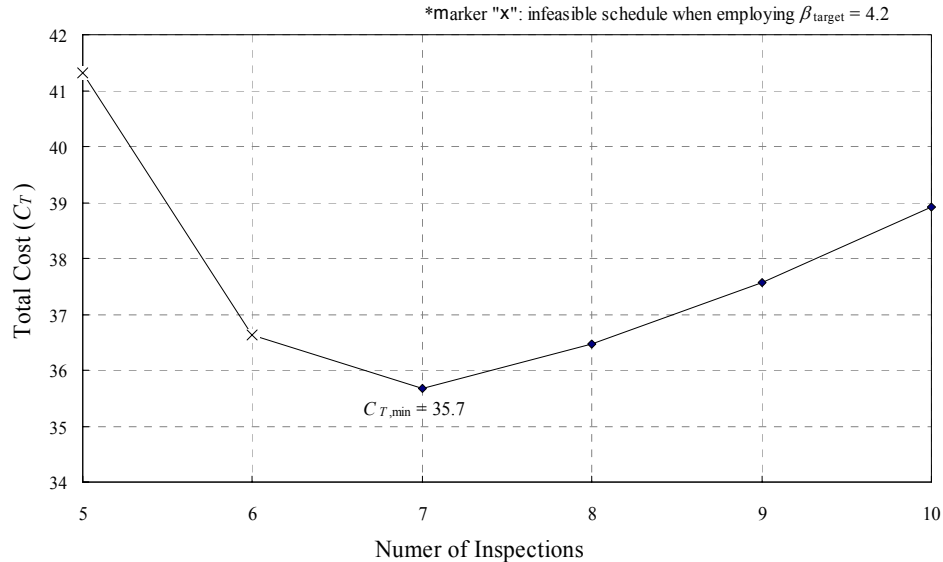


Figure 5.23: Optimal Total Cost as a Function of the Number of Inspections for the Butt-Welded Detail when  $\beta_{\text{target}} = 3.7$  or 4.2 for Case (i):  $K_I : K_R : K_F = 1 : 1 \times 10^1 : 1 \times 10^5$ .

Considering Case (i) again but with an unbounded  $T_{max}$  and  $\beta_{target} = 4.2$ , Figure 5.24 shows that the optimal schedule for this problem requires three inspections with inspection times,  $\mathbf{T} = (9.2, 9.7, 12.5)$  at a total cost of 22.3. Except for the number of inspections, this schedule is different from the optimal schedule under the  $\beta_{target} = 3.7$  constraint. It can be seen that the fatigue reliability of the detail over 20 years is above 4.2 and the total cost (22.3) of this schedule is higher than the total cost (19.3) for the optimal schedule with the lower target reliability constraint. Releasing the  $T_{max}$  constraint permits an optimal schedule with three inspections (i.e.,  $n=3$ ) which was not possible with the  $T_{max} = 2$  years constraint. Note that if the target reliability is raised to a level that is too high, the optimal schedule might not be one for which  $n = 3$  but will require more inspections, as expected.

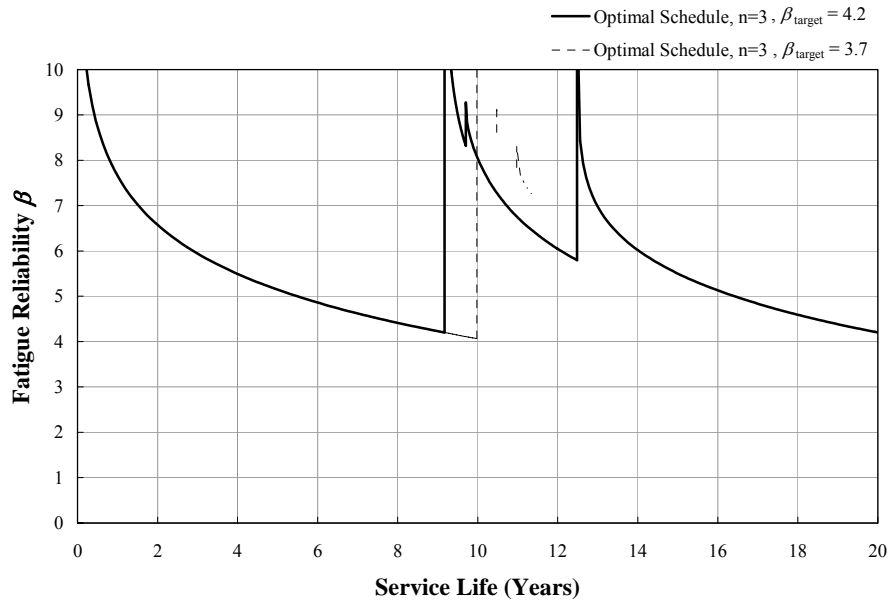


Figure 5.24: Optimal Inspection Schedules with  $\beta_{target} = 4.2$  ( $C_T = 22.3$ ) and with  $\beta_{target} = 3.7$  ( $C_T = 19.3$ ) for Case (i):  $K_I : K_R : K_F = 1 : 1 \times 10^1 : 1 \times 10^5$ .

## 5.8 CONCLUDING REMARKS

The key conclusions from this chapter may be summarized as follows:

- (1) Employing fatigue reliability analysis approaches presented in Chapter 4 along with means for determining the likelihood of needed repair, the use of event trees, and cost computations, the problem of fatigue inspection scheduling in bridge details can be modeled as a mathematical optimization problem. Through the proposed reliability-based inspection scheduling procedure, an optimal inspection schedule providing the number and times of planned inspection can be obtained that meets reliability and inspection interval constraints. Such an optimization procedure can, thus, yield not only the most economical inspection schedule (i.e., lowest cost), but also one that can maintain the inspected detail at prescribed safety levels.
- (2) The maximum time between inspections,  $T_{max}$ , is an important constraint that influences the number of inspections, the total cost, and the inspection strategy. When the inspection scheduling is constrained by  $T_{max}$ , a greater number of inspections will typically be necessary which raises the fatigue reliability of the detail and, thus, lowers the expected cost of failure. However, the cost of inspections and repairs increase, and the total cost grows as a result. When the constraint on  $T_{max}$  is removed, the schedule changes so as to require inspections only when the reliability curve gets close to the target reliability; this results in lower total costs.
- (3) As shown in the examples presented, the proposed scheduling method can be applied to both AASHTO and non-AASHTO type bridge details. The effects of relative repair cost ( $K_R$ ), relative failure cost ( $K_F$ ), ADTT uncertainty, and target reliability

( $\beta_{\text{target}}$ ) on inspection scheduling have all been studied. It is seen that all of these affect inspection scheduling in a direct manner as is summarized below.

- (4) An increase in relative repair costs tends to yield an optimal schedule with fewer inspections because the total costs are governed by the repair costs. A smaller number of inspections usually implies lower repair costs but potentially higher expected failure costs. The optimal schedule occurs at a number of inspections that balances increasing failure costs and decreasing inspection and repair costs.
- (5) An increase in failure costs tends to yield an optimal schedule with more inspections because total costs, especially when the number of inspections is small, are governed by failure costs. The fewer the inspections, the higher the failure costs. This result is consistent with real-life expectations that more important details (where failure consequences are greater) usually demand more inspections to avoid failures.
- (6) With regard to the influence of ADTT (traffic) uncertainty, it can be seen that with increasing variability in the average daily truck traffic, a larger number of inspections is required for the optimal schedule. Because uncertainty in ADTT leads to a lowering of the overall fatigue reliability of the detail, more inspections are needed to reduce the failure cost and, hence, the total cost to keep the fatigue reliability above the target reliability. However, only for steel bridges where the ADTT has a COV greater than about 0.30 will it be necessary to have significantly more inspections than is the case when a constant ADTT is assumed.
- (7) A higher target reliability constraint (i.e., more stringent safety requirement) tends to exclude schedules with very few inspections because such schedules cannot maintain the fatigue reliability of the detail above the higher target reliability over the planned service life. Higher target reliability levels typically require more inspections. This conclusion agrees with an expectation that a detail whose failure consequences

are greater will require more inspections to ensure the detail meets any imposed higher safety standards.

- (8) It is seen that a periodic two-year inspection schedule over the planned service life as is required by the FHWA for steel bridges will not be the optimal schedule for some details if one is interested in keeping costs low as well as maintaining safety. Though this periodic schedule has been shown to keep the fatigue reliability at a higher level than some optimal schedules obtained for the example bridges studied here, a larger number of inspections and repairs over the service life cause an increase in total cost. The reliability-based fatigue inspection strategy presented here yields the optimal inspection schedule while maintaining prescribed safety levels for lower costs.
- (9) The effect of including quality of inspection results using, for example, probability of detection (POD) measures for NDT techniques employed, has not been taken into consideration in the proposed reliability-based inspection scheduling method. In the results presented, this is valid as long as the prescribed crack size that warrants repair,  $a_R$ , is defined as being large enough to be detected by the planned non-destructive inspection (NDI) technique with certainty. Chapter 6 describes a probabilistic approach that considers the inspection quality of various NDI techniques and seeks to determine both a set of proper NDI techniques and an associated inspection schedule for a given detail that guarantees a prescribed reliability and keeps cost at a minimum.

## **CHAPTER 6: POD-BASED SELECTION OF NONDESTRUCTIVE INSPECTION TECHNIQUES FOR STEEL BRIDGES**

### **6.1 INTRODUCTION**

Steel bridges, an important part of the nation's transportation infrastructure, are vulnerable to fatigue deterioration because of the repetitive traffic loading that they experience. Non-destructive inspection (NDI) techniques, which can detect changes in material properties and/or flaws in structural details without impairing their use, are commonly used to detect and measure cracks in fracture-critical members of steel bridges. The various NDI techniques suggested for use on steel bridges in the FHWA Bridge Inspector's Training Manual (Hartle et al. (1995)) include Ultrasonic Inspection (UI), Magnetic Particle Inspection (MI), Penetrant Inspection (PI), Radiographic Inspection (RI), Acoustic Emission Inspection (AEI), and Visual Inspection (VI). For all of these techniques, inspection accuracy, accessibility, frequency, cost, and consequences of detection failures (misses) or false indications (false calls) must be considered when selecting the appropriate NDI technique. In Chapter 5, an optimization method was presented to solve the fatigue inspection scheduling problem using a reliability-based approach. Issues related to inspection quality were not considered in the proposed reliability-based scheduling method based on justifiable and reasonable assumptions. Though other reliability-based fatigue inspection scheduling methods in the offshore industry, such as the methods proposed by Sorensen et al. (1991), Faber et al. (1992a), and Cramer and Friis-Hansen (1992) include inspection quality in their analyses, it is not practical to calibrate the inspection quality coefficients and other parameters in their models so as to propose use of any single NDI technique (over

alternatives). Also, these methods generally demand complicated reliability algorithms or large numerical simulation studies to obtain optimal inspection results; this limits their applicability to bridge maintenance with associated tighter budgetary constraints.

An intuitive probabilistic approach for dealing with inspection quality is proposed in this chapter to select the most economical NDI method. On completion of each analysis that involves Monte Carlo simulations, the method recommends a single NDI technique and accompanied inspection schedule for fracture-critical members in a steel bridge that guarantees a specified acceptable safety level through the planned service life of the bridge. The actual Probability of Detection (POD) functions associated with the various NDI techniques are employed as the NDI detectabilities. By combining probability calculations based on the use of the POD functions together with Monte Carlo simulations of the crack growth for the fracture-critical member, a total cost function is formulated that includes the expected cost of inspections and failure that result with each alternative NDI technique and inspection schedule. The selection of an NDI technique with an associated inspection schedule for its use in the fracture-critical inspections is modeled as an optimization problem. The POD function corresponding to the NDI technique and the inspection interval are optimization variables for this problem. With appropriate constraints on inspection intervals and on a minimum (target) safety level, an optimal combination of NDI technique and inspection schedule that yields the minimum total cost and ensures the prescribed acceptable safety level for the specified detail can be obtained.

## **6.2 PROBABILITY OF DETECTION**

The four possible outcomes – true positive (hit), false negative (miss), false positive (false call) and true negative (correct accept) – of any NDI procedure are

illustrated in Table 6.1 The probability of detection (*POD*) of a crack of a given size is the conditional probability of a true positive call given that a crack with that size exists. Hence, from repeated inspections, an estimate of the *POD* can be obtained as follows:

$$P\hat{O}D = \frac{N_{TP}}{N_{TP} + N_{FN}} \quad (6.1)$$

where  $P\hat{O}D$  is the *POD* estimate for a specific crack size;  $N_{TP}$  is the number of true positive calls; and  $N_{FN}$  is the number of false negative calls. Correspondingly, the false call probability (*FCP*) can also be evaluated as:

$$F\hat{C}P = \frac{N_{FP}}{N_{FP} + N_{TN}} \quad (6.2)$$

where  $F\hat{C}P$  is the *FCP* estimate for a specific crack size;  $N_{FP}$  is the number of false positive calls; and  $N_{TN}$  is the number of true negative calls.

After introducing cracks of various sizes into test specimens and performing inspections, *POD* estimates for various crack sizes from different NDI techniques can be obtained. Based on the inspection results, generally, two analysis approaches – the Hit/Miss method and the Signal Response method – are employed to formulate the *POD* function,  $POD(a)$ , for any crack size,  $a$ , with any NDI technique.

Table 6.1: Four Possible Outcomes of NDI.

		Is Crack Detected by NDI?	
		Yes	No
Does Crack Exist?	Yes	True Positive (Hit or Correct Reject)	False Negative (Miss)
	No	False Positive (False Call)	True Negative (Correct Accept)



### 6.2.1 Hit/Miss Method

This method is applied when inspection data are recorded in terms of hits or misses (i.e., indicating whether or not a crack is detected). This is commonly used, for example, for data from penetrant inspection and visual inspection tests. The basic idea behind this method is to estimate the probability of detection  $P\hat{O}D$  for any given crack size from the hit and miss data by applying regression analysis or a maximum likelihood procedure. Berens and Hovey (1981) proposed that the log-logistic function can provide a satisfactory model for hit/miss inspection data. The log-logistic POD function can be expressed as:

$$POD(a) = \frac{\exp[\alpha + \beta \cdot \ln(a)]}{1 + \exp[\alpha + \beta \cdot \ln(a)]} \quad (6.3)$$

where  $a$  is the crack size while  $\alpha$  and  $\beta$  are statistical parameters to be estimated.

Because of the binomial property of hit/miss data, the  $P\hat{O}D$  estimate for a fixed crack size is essentially the sample proportion of hits. So, for a large number of inspections,  $M$ , performed for a particular crack size, the distribution of  $P\hat{O}D$  can be approximated by a normal distribution with mean and variance as follows:

$$E(P\hat{O}D) = POD \quad (6.4)$$

$$Var(P\hat{O}D) = \sqrt{\frac{POD(1-POD)}{M}} \quad (6.5)$$

In order to have a representative POD function for any NDI technique, reliable  $P\hat{O}D$  estimation for each crack size is necessary. Accordingly, confidence interval calculation may be used which involves establishing the required number of inspections,  $M_{req}$ , that will provide, say,  $100(1-\alpha)$  percent confidence that the error in using  $P\hat{O}D$  to estimate  $POD$  will be less than a specified level  $E$ . This required number of inspections,  $M_{req}$ , can be determined as follows (Miller and Freund, 1985):

$$M_{req} = \frac{1}{4} \left[ \frac{z_{\alpha/2}}{E} \right]^2 \quad (6.6)$$

where  $\alpha$  is the significance level;  $z_{\alpha/2}$  is the value of the standard normal variate with a cumulative probability level,  $(1-\alpha/2)$ . Let  $x$  be the number of true positive calls (hits) out of  $M_{req}$  inspections. Note that Equation 6.6 implies that if  $(x/M_{req})$  is used as an estimate for  $POD$ , we can assert with  $(1-\alpha)100$  confidence that the error will not exceed  $E$ .

### 6.2.2 Signal Response Method

This method is applied for inspection results recorded in terms of parameters  $\hat{a}$  indicating signal responses to stimuli (cracks), such as the inspection results produced by ultrasonic inspection and eddy current inspection. For  $\hat{a}$  values below the recording signal threshold,  $\hat{a}_{th}$ , no signal is recorded. For crack sizes exceeding the signal saturation limit,  $\hat{a}_{sat}$ , of the recording system, the corresponding  $\hat{a}$  values stay the same as  $\hat{a}_{sat}$ . However,  $\hat{a}$  values are displayed when they are greater than a specified decisive value,  $\hat{a}_{dec}$ . Between  $\hat{a}_{th}$  and  $\hat{a}_{sat}$ ,  $\hat{a}$  values can be expressed as the following regression relationship with crack size:

$$\ln(\hat{a}) = \beta_0 + \beta_1 \ln(a) + \varepsilon; \quad \hat{a}_{th} < a < \hat{a}_{sat} \quad (6.7)$$

where  $\beta_0$  and  $\beta_1$  are regression parameters and  $\varepsilon$  is normally distributed with a zero mean and a standard deviation  $\sigma_\varepsilon$ . As shown in Figure 6.1, the probability of detection function for a given crack size  $a$ ,  $POD(a)$ , can be expressed as:

$$POD(a) = P[\hat{a}(a) \geq \hat{a}_{dec}] = \int_{\hat{a}_{dec}}^{\infty} f_{\hat{a}|a}(\hat{a}) d\hat{a} = 1 - F_{\hat{a}|a}(\hat{a}_{dec}) \quad (6.8)$$

where  $f_{\hat{a}|a}(\hat{a})$  is the probability density function of the signal value,  $\hat{a}$ , for a given crack size,  $a$ ;  $F_{\hat{a}|a}(\hat{a})$  is the cumulative density function of the signal value,  $\hat{a}$ , for a given

crack size,  $a$ . Combining Equations 6.7 and 6.8, Berens (1989) suggested the POD function from the signal response method as follows assuming  $a$  is lognormal:

$$POD(a) = \Phi \left\{ \frac{\ln(a) - [\ln(\hat{a}_{dec}) - \beta_0] / \beta_1}{\sigma_\varepsilon / \beta_1} \right\} \quad (6.9)$$

In this study, the POD function from each considered NDI technique with respect to the detail of interest is taken as the NDI capability. The POD function representing the corresponding NDI technique and other factors such as cost of the proposed technique will affect the optimal inspection results.

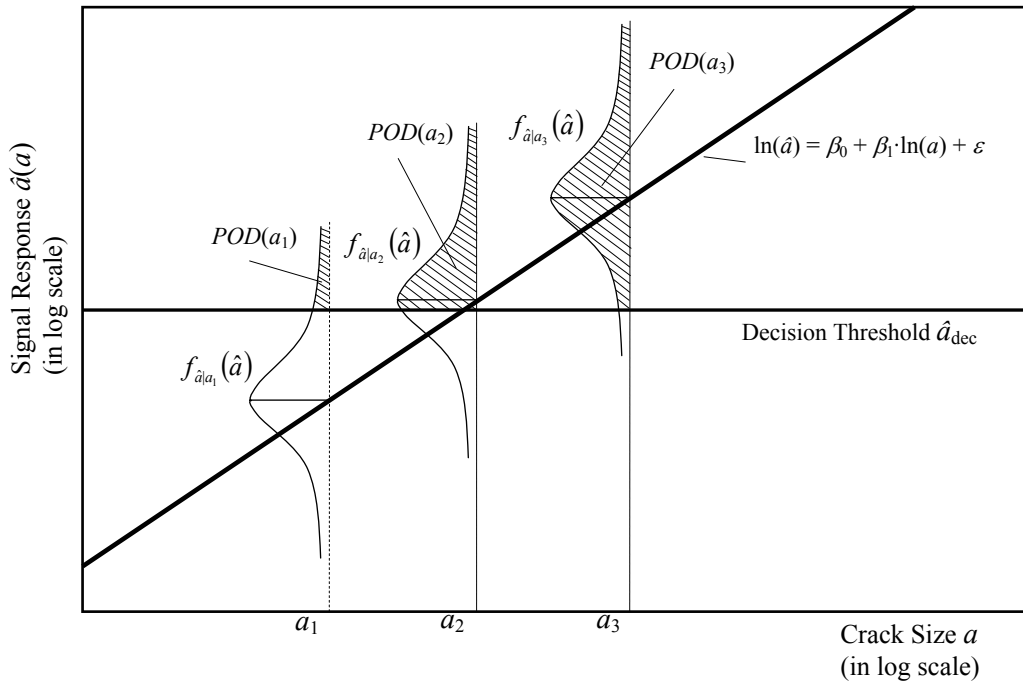


Figure 6.1: Probability of Detection Function,  $POD(a)$ , Calculation in Signal Response Method (Berens, 1989).

### 6.3 FATIGUE CRACK GROWTH MODEL

The basic fatigue crack growth model can be derived from the Paris and Erdogan relation (Paris' Law) and Linear Elastic Fracture Mechanics (LEFM). As described in Equation 4.31, the relation linking crack size and the number of stress cycles can be rewritten as:

$$\int_{a_0}^{a_N} \frac{da}{[F(a)\sqrt{\pi a}]^m} = C \cdot N \cdot S_{RE}^m \quad (6.11)$$

where  $a_0$  is the initial crack size and  $a_N$  is the crack size after  $N$  stress cycles. If  $\Psi(a)$  is defined as the indefinite integral form of the left side term of Equation 6.11, this equation can be rewritten as:

$$\Psi(a_N) - \Psi(a_0) = C \cdot N \cdot S_{RE}^m \quad (6.12)$$

The crack growth function can then also be represented as:

$$a_N = \Psi^{-1}[\Psi(a_0) + C \cdot N \cdot S_{RE}^m] \quad (6.13)$$

Generally, the material properties ( $C$  and  $m$ ) and initial crack size ( $a_0$ ) are described as random variables as was described in Chapter 4. The crack size,  $a_N$  is a function of the accumulated number of stress cycles ( $N$ ) while the equivalent stress range ( $S_{RE}$ ) for the detail can be evaluated as was described in Chapter 3. The geometry function  $F(a)$  for a specific fatigue detail in a steel bridge can be obtained from available stress intensity manuals or derived using fracture mechanics principles. In addition, the number of stress cycles ( $N$ ) can be associated with number of years in service ( $Y$ ) through Equation 4.13.

Consider a fracture-critical member in a steel bridge that has a constant geometry function and substitute Equation 4.13 into Equation 6.13. Upon integration, the crack growth function related to years in service,  $Y$ , for this detail may be expressed as follows (see Madsen et al. (1985)):

$$a(Y) = \left[ a_0^{\left(\frac{2-m}{2}\right)} + \left(\frac{2-m}{2}\right) \cdot \pi^{\left(\frac{m}{2}\right)} \cdot C \cdot S_{RE}^m \cdot (365 \cdot ADTT \cdot C_S \cdot Y) \right]^{\left(\frac{2}{2-m}\right)} \quad \text{for } m \neq 2 \quad (6.14)$$

$$a(Y) = a_0 \cdot \exp\left[\pi \cdot C \cdot S_{RE}^m \cdot (365 \cdot ADTT \cdot C_S \cdot Y)\right] \quad \text{for } m = 2 \quad (6.15)$$

According to LEFM, a crack will fracture when the stress intensity factor,  $K$ , of the crack exceeds the fracture toughness,  $K_c$ , of the material. In other words, the crack growth functions, such as Equations 6.13, 6.14 and 6.15, are valid only as long as the crack size is smaller than the critical crack size,  $a_{cr}$ , related to  $K_c$ .

#### 6.4 SIMULATION OF CRACK PROPAGATION AND INSPECTION SCENARIOS

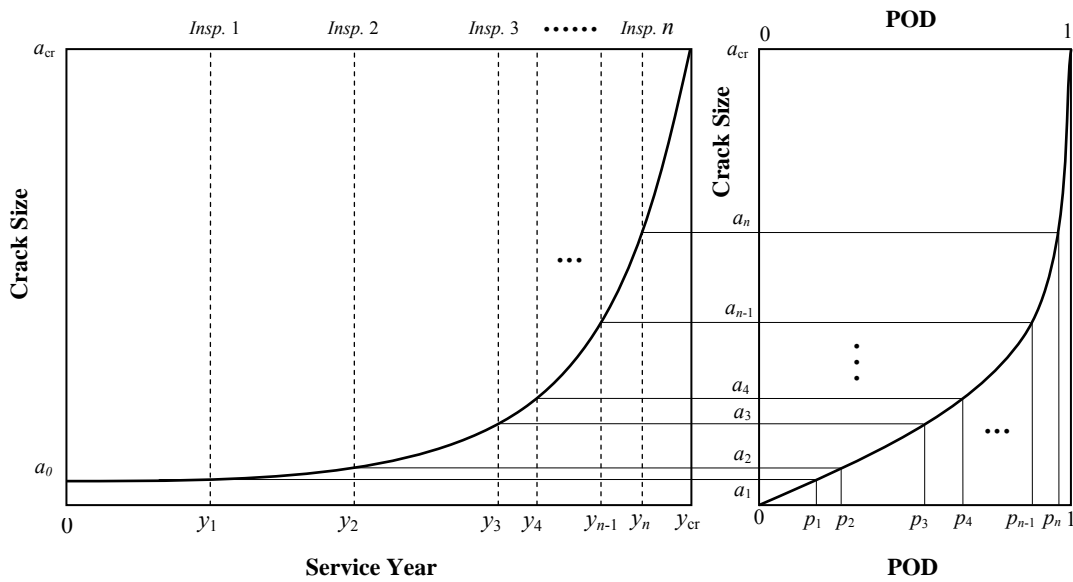


Figure 6.2: Probability of Detection Mapping.

Consider a situation where  $n$  nondestructive fatigue inspections are performed on a fracture-critical member of a steel bridge at fixed points in time,  $y_1, y_2, \dots, y_n$ . In each possible crack growth curve realization, the crack in the detail is assumed to reach its critical crack size at a time,  $y_{cr}$  (i.e.,  $a(y_{cr}) = a_{cr}$ ). By applying a crack growth model, the crack size,  $a_i$ , associated with each inspection time,  $y_i$ , can be obtained. By mapping each such crack size,  $a_i$ , onto the POD curve diagram related to the applied NDI technique, the probability of detecting the crack size,  $a_i$ , denoted as  $p_i$  can be determined. This mapping procedure is shown in Figure 6.2. Therefore, the probability of not detecting a crack,  $P_{nd}$ , and the probability of detecting a crack,  $P_d$ , before fracture can be expressed as:

$$P_{nd} = \prod_{i=1}^n (1 - p_i) \quad (6.16)$$

$$P_d = 1 - P_{nd} = 1 - \prod_{i=1}^n (1 - p_i) \quad (6.17)$$

where  $p_i$  is the probability of detection for a given crack size at the  $i^{\text{th}}$  inspection by applying the selected NDI technique; and  $n$  is the number of inspections before fracture. Fixed-interval inspection schedules are considered in this study in order to conform to practical application of such inspections for bridges. If the fixed inspection interval,  $y_{int}$ , for a schedule and time to fracture,  $y_{cr}$ , are known, the value of  $n$  can be determined without difficulty.

The initial crack size ( $a_0$ ), material properties ( $C$  and  $m$ ) for the detail, and traffic-related quantities ( $ADTT$ ,  $C_s$ , and  $S_{RE}$ ) are taken as random variables with specified probability distributions. Considering the resulting uncertainty in the crack growth model, the Monte Carlo method is applied to simulate possible crack growth curves as shown in Figure 6.3. Each crack growth simulation,  $i$ , provides two quantities of interest: one is the probability that a crack is not detected before fracture results,  $P_{nd,i}$ , and

the other is the number of inspections,  $n_i$ , before fracture. On accumulating the results of all the crack growth simulations, the expected probability of not detecting a crack,  $E(P_{nd})$ , before fracture and the expected number of inspections,  $E(n)$ , before fracture can be obtained as follows:

$$E(P_{nd}) = \frac{1}{N_{sim}} \sum_{i=1}^{N_{sim}} P_{nd,i} \quad (6.18)$$

$$E(n) = \frac{1}{N_{sim}} \sum_{i=1}^{N_{sim}} n_i \quad (6.19)$$

where  $N_{sim}$  is the number of simulations. By employing a sufficiently large number of simulations, converged estimates of  $E(P_{nd})$  and  $E(n)$  can be obtained. For the given POD curve associated with the selected NDI technique and the selected inspection schedule,  $E(P_{nd})$  represents a risk that the applied NDI technique will fail to detect the existing crack in a detail before a fracture occurs. Also,  $E(n)$  represents the expected number of inspections with the selected NDI method that may be performed during the fatigue life of the detail (i.e., before fracture occurs). It should be noted that the crack growth simulations here do not account for any repair activity.

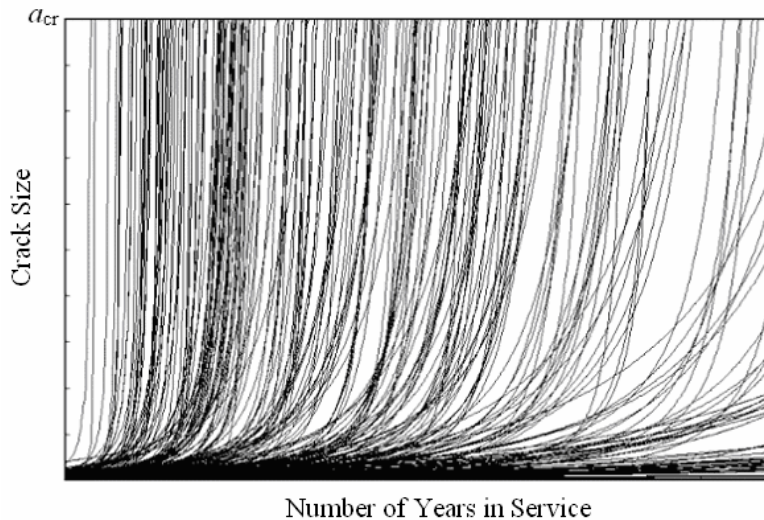


Figure 6.3: Crack Growth Curves from Monte Carlo Simulations.

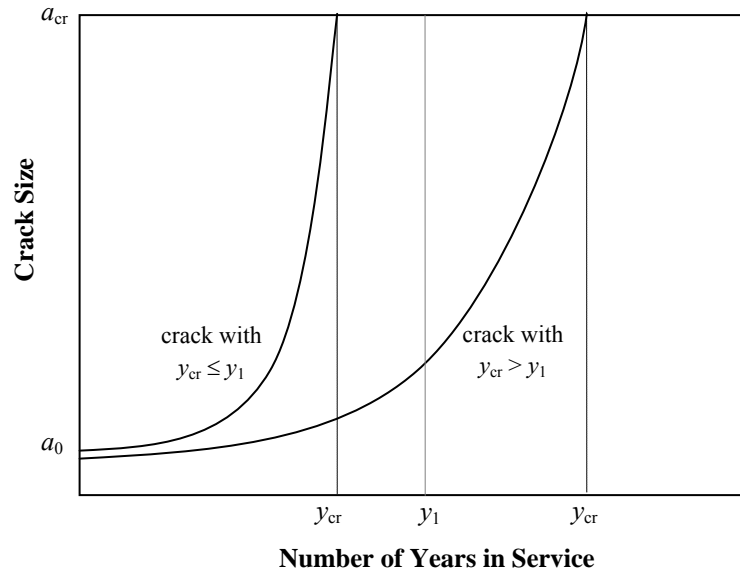


Figure 6.4: Crack Growth Models for  $y_{cr} \leq y_1$  and  $y_{cr} > y_1$ .

Because the crack growth curves are simulated randomly by the Monte Carlo method, it may be the case that the time till failure,  $y_{cr}$ , in a single simulation may be longer or shorter than the time,  $y_1$ , when the first inspection is performed as shown in Figure 6.4. For simulations with detail lives longer than the first inspection time, Equation 6.20 below can be employed to compute the expected probability of not detecting a crack. The expected number of inspections can also be determined correspondingly as indicated in Equation 6.21. Note that for simulations where the fatigue life is shorter than the time till the first inspection, the probability of not detecting a crack is 1 since no inspections are performed before  $a_{cr}$  is reached. The realizations of Monte Carlo simulations that enable computation of  $E(P_{nd})$  and  $E(n)$  are demonstrated in Figure 6.5 and the computations of  $E(P_{nd})$  and  $E(n)$  are expressed as follows:



$$\begin{aligned}
E[P_{nd}] &= E[P_{nd} | y_{cr} \geq y_1] \cdot P(y_{cr} \geq y_1) + E[P_{nd} | y_{cr} < y_1] \cdot P(y_{cr} < y_1) \\
&= \left( \frac{\sum_{i=1}^{N_1} P_{nd,i}}{N_1} \right) \cdot \left( \frac{N_1}{N_{sim}} \right) + \left( \frac{1 \cdot N_2}{N_2} \right) \cdot \left( \frac{N_2}{N_{sim}} \right) \\
&= \frac{\sum_{i=1}^{N_1} \left[ \prod_{j=1}^{n_i} (1 - p_j) \right] + N_2}{N_{sim}}
\end{aligned} \tag{6.20}$$

$$\begin{aligned}
E[n] &= E[n | y_{cr} \geq y_1] \cdot P(y_{cr} \geq y_1) + E[n | y_{cr} < y_1] \cdot P(y_{cr} < y_1) \\
&= \left( \frac{\sum_{i=1}^{N_1} n_i}{N_1} \right) \cdot \left( \frac{N_1}{N_{sim}} \right) + (0) \cdot \left( \frac{N_2}{N_{sim}} \right) \\
&= \frac{\left( \sum_{i=1}^{N_1} n_i \right)}{N_{sim}}
\end{aligned} \tag{6.21}$$

where  $N_1$  is the number of simulations that  $y_{cr} \geq y_1$ ;  $N_2$  is the number of simulations that  $y_{cr} < y_1$ ;  $N_{sim}$  ( $= N_1 + N_2$ ) is the number of total simulations; and  $n_i$  is the number of inspections in the  $i^{\text{th}}$  simulation.

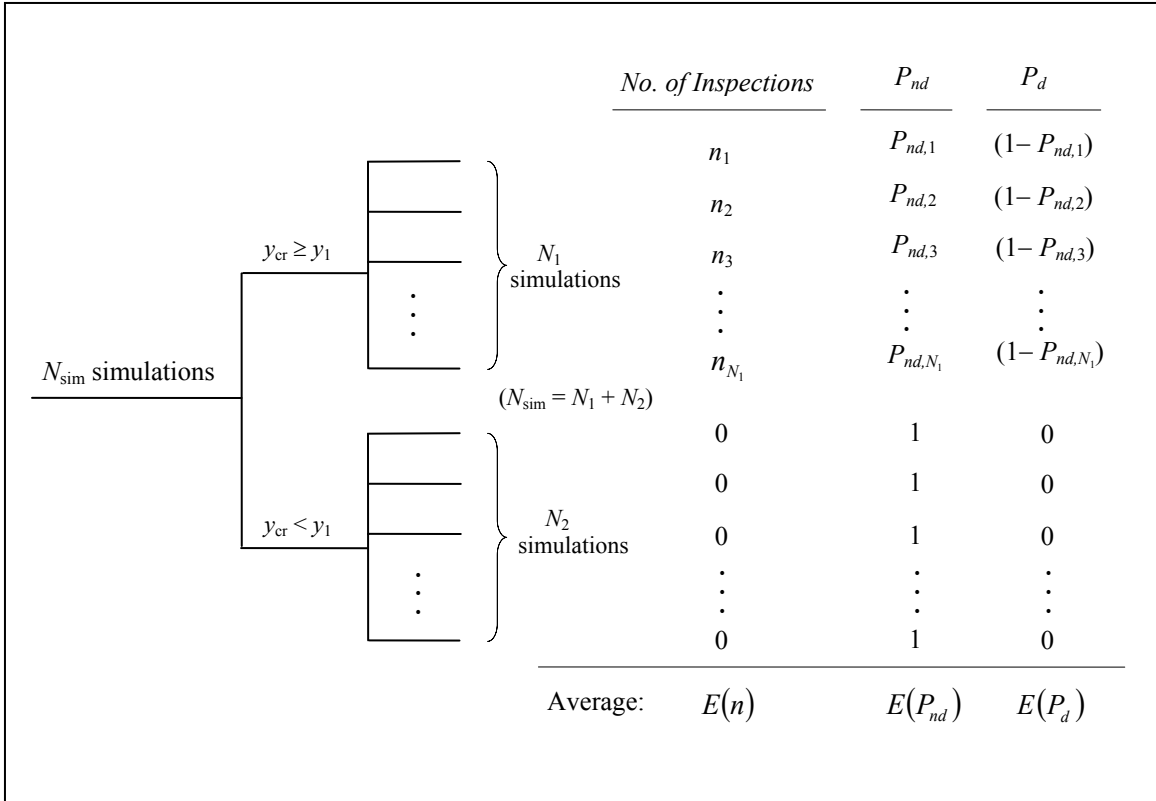


Figure 6.5: Monte Carlo Simulation Scenarios.

## 6.5 OPTIMAL NDI TECHNIQUE

Practical challenges for bridge inspectors include coming up with answers to questions such as “What kind of NDI techniques should I use and how often should I perform this NDI technique?” At present in the U.S., inspections for fracture-critical members in steel bridges are planned based on the FHWA two-year interval requirement and on the responsible engineer’s experience. As discussed in previous chapters, these schedules might not be optimal for all types of fatigue details on steel bridges. A rational method of selecting suitable NDI techniques for fatigue details in steel bridges can be useful. A probabilistic method is proposed for selection of an optimal NDI technique and associated inspection schedule for fracture-critical members using LEFM-based fatigue analysis, actual NDI detectabilities, and Monte Carlo simulations. This procedure is formulated so as to yield a balanced solution that takes into consideration both economy and safety.

### 6.5.1 Cost Function

To transform the problem of selection of a proper NDI technique to an optimization problem, a cost function needs to be defined that reflects the consequences of choosing a NDI technique and an associated inspection schedule for the detail or member under consideration. With the expected number of inspections,  $E(n)$ , and the expected probability of not detecting a crack,  $E(P_{nd})$ , using a selected NDI technique and inspection schedule, the cost function including the cost of inspections and the expected cost of failure can be easily assembled as is done in the following:

### *Cost of Inspections*

From the Monte Carlo simulation,  $E(n)$  represents the expected number of inspections for the specified detail if applying the selected NDI technique and the associated inspection schedule. Let  $K_I$  denote the cost of a single inspection of the specified detail. Then, the expected total cost of inspections over the service life,  $C_I$ , can be represented as:

$$C_I = K_I \cdot E(n) \quad (6.22)$$

### *Cost of Failure*

From the Monte Carlo simulations,  $E(P_{nd})$  represents the expected probability of not detecting a crack in the specified detail or member by the chosen NDI technique and schedule before failure. If, in the simulations, an NDI technique continuously fails to detect the growing crack in the detail, the expected fatigue failure probability will be high. Therefore,  $E(P_{nd})$  also gives an indication of the likelihood of fatigue failure for the detail over the service life as a result of failure to detect a growing by the selected NDI technique. The risk of fatigue failure for the specified detail that results from employing a specific NDI technique can be represented by estimating the (expected) cost of failure,  $C_F$ . If the detail/member under consideration is fracture-critical, its failure could cause failure of the span where the detail is located or even failure of the entire bridge. Hence, the cost of failure should include the possible cost of rebuilding a span or the entire bridge, as appropriate, as well as costs due to lost use, injuries, fatalities, etc. – not all of which are easily and uncontroversially estimated. Nevertheless, all of these potential costs are summed to yield a quantity,  $K_F$ , which represents the cost associated with a failure. The likelihood of such failures is the other term that should be included

in arriving at the expected cost of failure  $C_F$ . Hence, the expected cost of failure for the specified member or detail over the service life may be defined as:

$$C_F = K_F \cdot E(P_{nd}) \quad (6.23)$$

#### *Total Cost*

Using the definitions of the cost of inspections and failure in Equations 6.22 and 6.23 that result from selection of an NDI technique and its associated inspection schedule, the total cost,  $C_T$ , may be represented as:

$$C_T = C_I + C_F \quad (6.24)$$

$$C_T = K_I \cdot E(n) + K_F \cdot E(P_{nd}) \quad (6.25)$$

### **6.5.2 Optimization Variables**

The POD function corresponding to an NDI technique and the fixed interval,  $y_{int}$ , employed in an inspection program are two optimization variables in our optimization problem. The reason for employing a fixed-interval inspection schedule here is to conform with the practical realities of bridge inspections. The POD function for the chosen NDI technique directly affects the value of  $E(P_{nd})$  and the inspection interval,  $y_{int}$ , affects  $E(n)$  and  $E(P_{nd})$ . As a result, the total cost defined in Equation 6.25 is influenced by the POD function and the inspection interval,  $y_{int}$ , in a direct manner. By changing the POD function and the value of the fixed inspection interval,  $y_{int}$ , an optimal combination of POD function and  $y_{int}$  that yields the minimum cost can be found. This solution corresponds effectively to selection of an inspection plan that employs an NDI technique that provides the desired POD function and associated inspection schedule with the desired fixed-inspection interval.

### 6.5.3 Constraints

A target non-detection probability,  $P_{nd,max}$ , defined as the maximum allowable probability of not detecting a crack (i.e., the minimum acceptable safety level) for the NDI technique applied on the specified fatigue detail is applied as a constraint to exclude combinations of NDI techniques and inspection schedules that might be deemed unsafe because  $E(P_{nd})$  is too high. This constraint can be expressed as:

$$E(P_{nd}) < P_{nd,max} \quad (6.26)$$

Additionally, restrictions are placed on the time between inspections so that this inter-inspection interval is neither too large (upper bound,  $y_{max}$ ) nor too short (lower bound,  $y_{min}$ ). Such constraints on the inspection interval may be required by local and state transportation agencies. Hence, a second constraint on the inspection interval for the optimization problem is:

$$y_{min} < y_{int} < y_{max} \quad (6.27)$$

### 6.5.4 Formulation of Optimization Problem

In summary, the optimization problem for selecting an optimal NDI technique and associated inspection schedule may be formulated as follows:

$$\min_{POD, y_{int}} C_T = K_I \cdot E(n) + K_F \cdot E(P_{nd}) \quad (6.28)$$

optimization variables: POD function and inspection interval,  $y_{int}$

subjected to:  $E(P_{nd}) < P_{nd,max}$ ;  $y_{min} < y_{int} < y_{max}$

Upon minimizing the total cost, an optimum inspection interval,  $y_{int}$ , may be found. In addition, by changing the POD functions, i.e., changing the NDI technique, the total cost corresponding to the different POD functions may be compared so as to finally yield the optimization solution for the NDI technique and an associated inspection schedule.

To solve the optimization problem, the Monte Carlo Method is employed to calculate the expected probability of not detecting a crack,  $E(P_{nd})$ , and the expected number of inspections,  $E(n)$ , for a given NDI technique and an associated inspection schedule by treating the initial crack size ( $a_0$ ), crack growth parameter ( $C$ ), and crack growth exponent ( $m$ ) as random variables. After obtaining  $E(P_{nd})$  and  $E(n)$ , the total cost due to the given NDI technique and associated schedule can be evaluated. By changing the NDI technique and inspection schedule, several computations of total cost are obtained. The optimal choice comes from the NDI technique and schedule that lead to the minimum total cost. A flow chart describing this procedure is shown in Figure 6.6

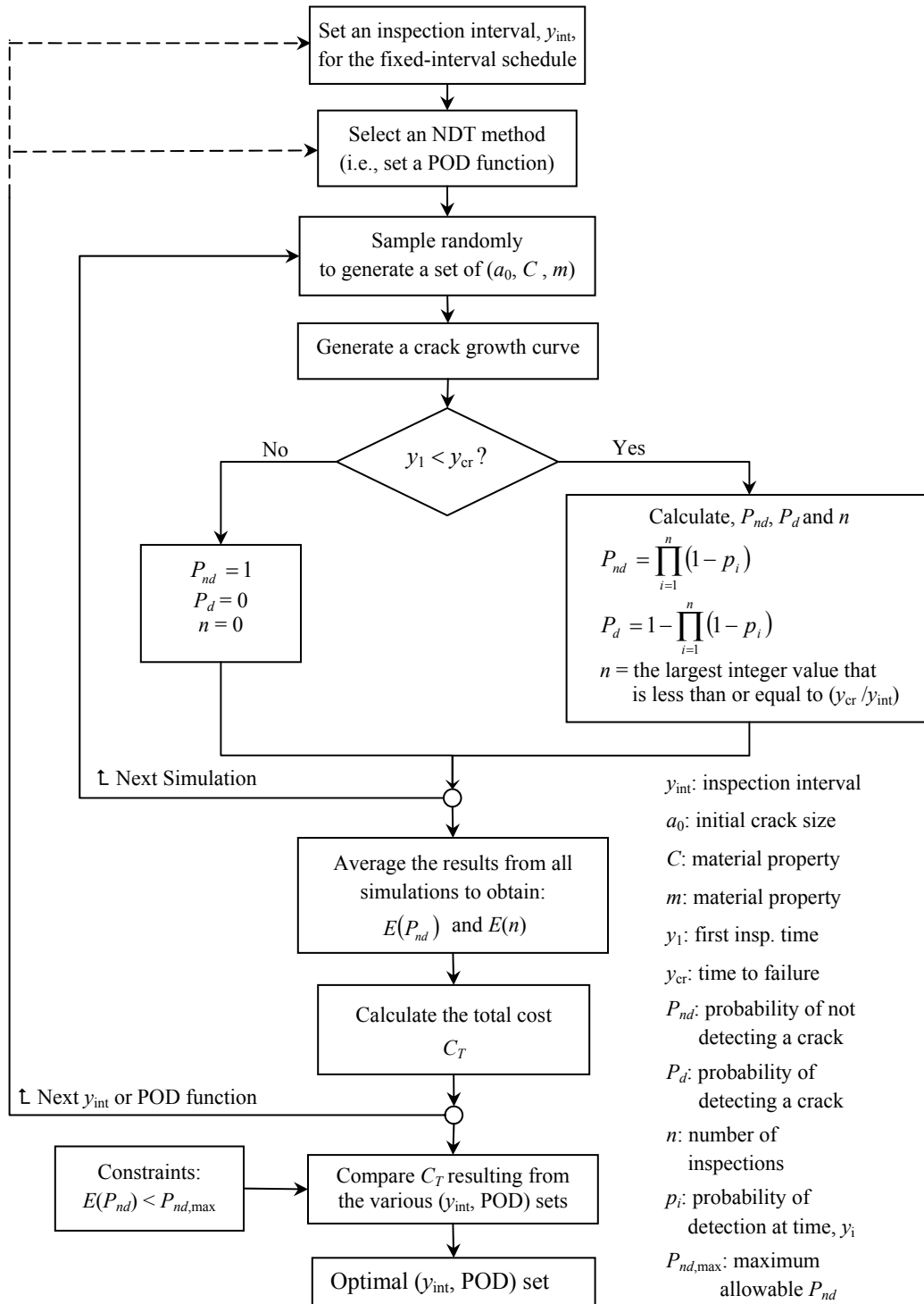


Figure 6.6: Flow Chart of Optimization Procedure.



## 6.6 NUMERICAL EXAMPLES

### 6.6.1 Box-Girder Example I

Two full-penetration butt welds in the bottom (tension) flange of a newly built steel box girder bridge, similar to the box girder example in Chapter 5, are studied in this example for which we seek an optimal NDI technique and an optimal inspection schedule for future service years. It is assumed that failure of the butt weld detail will result in collapse of the box-girder span. An inherent flaw is assumed to exist in the butt welds of the 60 in. width ( $w$ ) bottom flange as shown in Figure 6.7. The initial flaw size,  $a_0$ , is modeled as a lognormally distributed random variable with a mean value of 0.02 in. and a coefficient of variation of 0.5. The critical crack size,  $a_{cr}$ , is considered to be constant at 2 inches in this example. The fatigue growth parameter,  $C$ , is modeled as a lognormal variable with a mean value of  $2.05 \times 10^{-10}$  and a coefficient of variation of 0.63, assuming units of inches for crack size and  $\text{ksi-in}^{1/2}$  for fracture toughness. The fatigue growth exponent,  $m$ , is modeled as a normally distributed random variable with a mean value of 3.0 and a coefficient of variation of 0.1. The average daily truck traffic,  $ADTT$ , and the number of stress cycles per truck passage,  $C_s$ , for the box girder bridge are taken to be 600 and 1.0, respectively. A Rayleigh distribution is employed to model the stress range spectrum for the bottom flange of the bridge and  $S_{R0}$  is taken as 6.334 ksi for the stress range.

Three NDI techniques – ultrasonic inspection (UI), magnetic particle inspection (MI) and penetrant inspection (PI) – are considered here for the butt weld detail. The probability of detection (POD) functions for these three techniques, shown in Figure 6.8, are based on POD data from the flat plate testing results collected by Rummel and Matzkanin (1997) and are shown only for illustrative purposes. In practice, the POD

functions for the three NDI techniques ought to be obtained from numerous tests of similar butt weld details because the POD function of each NDI technique depends on the actual test object (form and material), the anomaly condition, the NDI procedure and the operator, as was observed by Rummel (1998). The three illustrative POD functions are described in Table 6.2. Two cases of relative costs of the three types of nondestructive inspections and of the cost of failure are considered here: (i)  $K_{I,PI} : K_{I,MI} : K_{I,UI} : K_F = 1.0 : 1.2 : 1.5 : 2.0 \times 10^4$ ; and (ii)  $K_{I,PI} : K_{I,MI} : K_{I,UI} : K_F = 1.0 : 1.2 : 1.5 : 4.0 \times 10^4$ . The maximum acceptable probability of not detecting a crack over the service life is taken to be 0.005, i.e.  $E(P_{nd}) < 0.005$  or  $P_{nd,max} = 0.005$ , in this example.

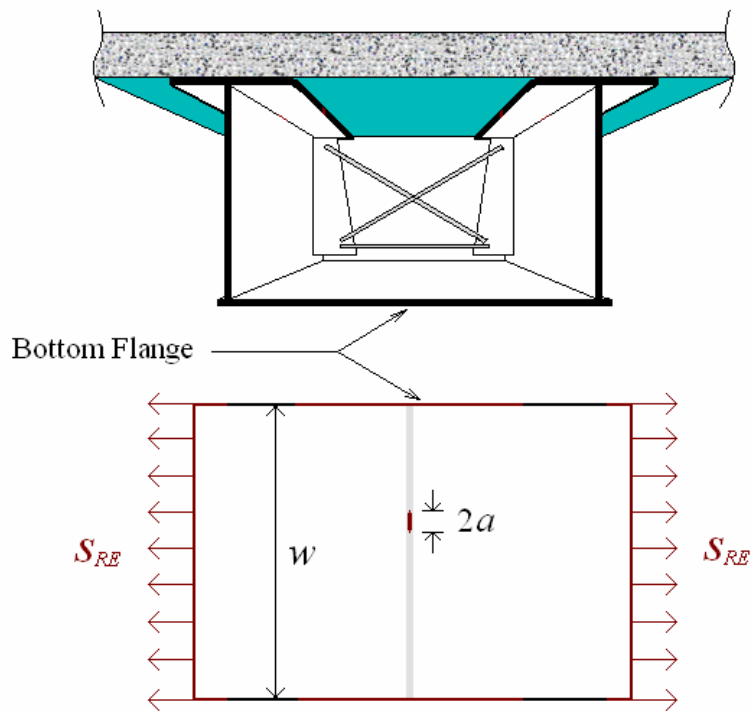


Figure 6.7: Detail in the Fracture-Critical Member of the Box Girder Bridge.

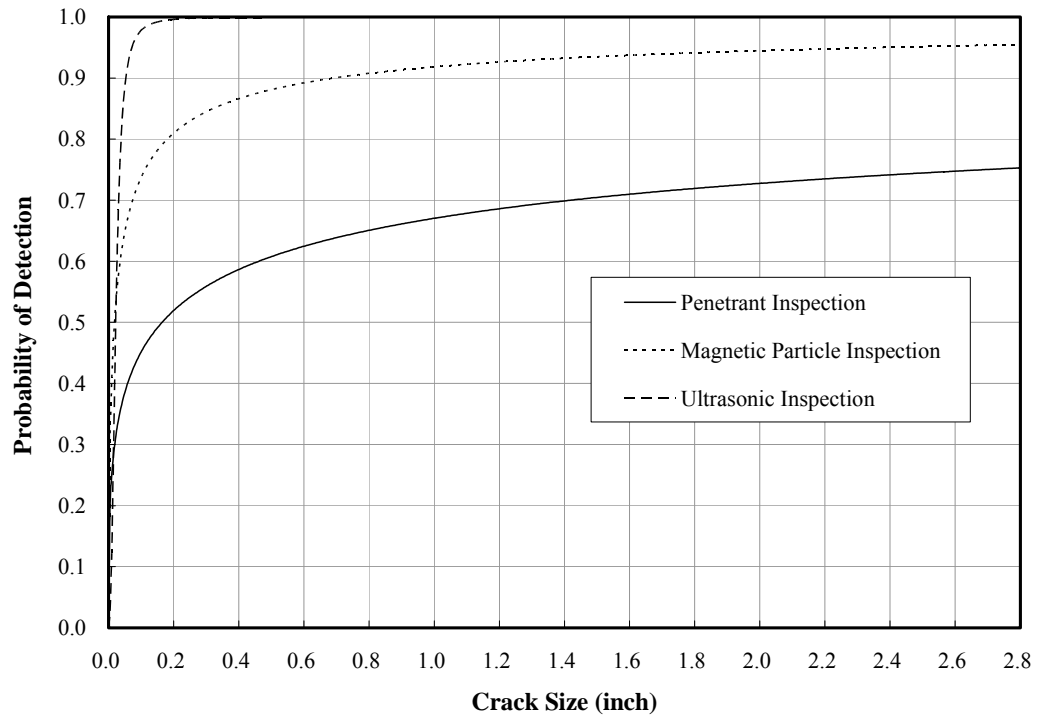


Figure 6.8: Probability of Detection (POD) Curves for Penetrant, Magnetic Particle, and Ultrasonic Inspections.

Table 6.2: POD Functions for Penetrant, Magnetic Particle, and Ultrasonic Inspections.

$POD(a) = \frac{\exp[\alpha + \beta \cdot \ln(a)]}{1 + \exp[\alpha + \beta \cdot \ln(a)]}$		
NDI technique	$\alpha$	$\beta$
UI	9.540	2.986
MI	2.420	0.604
PI	0.710	0.393
The form of the POD model used is proposed by Berens and Hovey (1981) where $\alpha$ and $\beta$ are estimated by the maximum likelihood method.		

Because the initial crack size,  $a_0$ , compared to the width of the bottom flange,  $w$ , is relatively small ( $a_0/w \approx 3.3 \times 10^{-4}$ ), the geometry function  $F(a)$  is taken to be unity for simplicity to model the stress intensity factor for the crack. Therefore, Equations 6.14 and 6.15 can be employed as the crack growth functions in our example. Figure 6.9 demonstrates the probability distribution of the fatigue life,  $Y_{cr}$ , for the considered detail over 250 years of the considered detail. Figure 6.10 shows 350 simulated crack growth curves for the detail under consideration based on the Monte Carlo method.

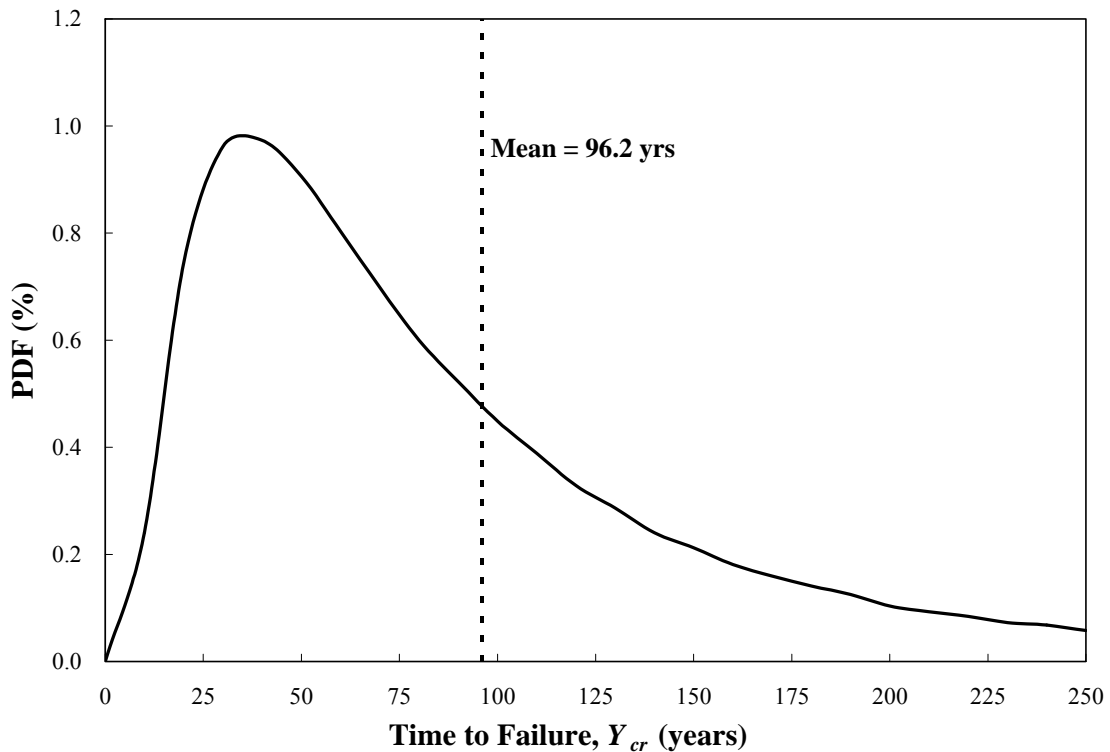


Figure 6.9: Probability Distribution of Time to Failure,  $Y_{cr}$ , from 0 to 250 Years.

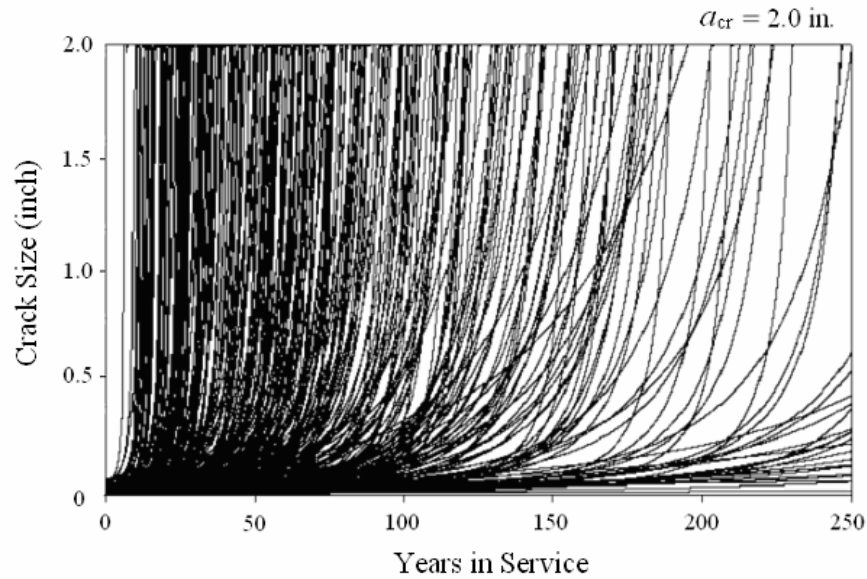


Figure 6.10: Crack Growth Simulations (350 simulations;  $a_{cr} = 2$  in.).

Five million Monte Carlo simulations are carried out in order to achieve stable results for the first case of the relative costs of the three nondestructive inspections and failure, namely,  $K_{I,PT} : K_{I,MT} : K_{I,UT} : K_F = 1.0 : 1.2 : 1.5 : 2.0 \times 10^4$ . Figures 6.11, 6.12 and 6.13 illustrate the costs for various fixed-interval schedules for the ultrasonic, magnetic particle, and penetrant inspections, respectively. It is noted, in these figures, that each inspection interval,  $y_{int}$ , on the abscissa essentially represents a schedule that employs  $y_{int}$  as inspection interval for the detail under consideration over the service life. The three figures show a tendency for inspections schedules with a longer fixed inspection interval to have a lower expected cost of inspections,  $C_I$ , but to simultaneously cause a higher expected cost of failure,  $C_F$ . On the other hand, schedules with a shorter inspection interval have higher expected cost of inspections,  $C_I$ , but lower expected cost of failure,  $C_F$ . The higher expected cost of inspections results from the increased

number of inspections expected for the detail due to the shorter inspection interval. The lower expected cost of failure results from the smaller likelihood of failing to detect the crack before fracture occurs. The combined effect of  $C_I$  and  $C_F$  for different inspection intervals results in an optimal inspection interval,  $y_{\text{int,opt}}$ , that yields the lowest total cost,  $C_{T,\text{min}}$ , and the optimal schedule with  $y_{\text{int,opt}}$  for each NDI technique as shown in the three figures. Before comparing the optimal inspection intervals,  $y_{\text{int,opt}}$ , for each of the three nondestructive inspections to obtain the optimal inspection schedule for the detail, the constraint  $E(P_{nd}) < 0.005$  needs to be verified first to identify the feasible schedules as shown in Figure 6.14. For the ultrasonic inspection, feasible schedules are all those where the fixed inspection interval is less than or equal to 5 years. For the magnetic particle inspection, the maximum feasible inspection interval is 4 years. Finally, for the penetrant inspection, the maximum feasible inspection interval is only 2 years. After eliminating the infeasible schedules, the most economical schedule with the ultrasonic method is to perform inspections every 3 years, which yields a total cost of 63.9 (see Figure 6.11). For the magnetic particle inspection, the most economical schedule is to inspect every 2.5 years, which yields a total cost of 66.1 (see Figure 6.12). Finally, as seen in Figure 6.13, inspecting every 1.5 years, which results in a total cost of 95.4, is the best choice for the penetrant inspection. Combining Figures 6.11, 6.12, 6.13 and the constraint on  $E(P_{nd})$ , Figure 6.15 shows total costs for the feasible and infeasible schedules with the three NDI techniques. Note that each marker “x” in Figure 6.15 indicates an infeasible schedule that fails to meet the constraint,  $E(P_{nd}) < 0.005$ . It can be seen that the optimal schedule is to perform ultrasonic inspections every 3 years. As shown in Table 6.3, even though a single ultrasonic inspection is more expensive than a single magnetic particle or penetrant inspection ( $K_{I,PT} : K_{I,MT} : K_{I,UT} : K_F = 1.0 : 1.2 : 1.5$ ), the less frequent inspections and the higher flaw detectability with the UI technique

together yield lower total costs than that resulting from use of the other two NDI techniques. Both, the magnetic particle and the penetrant inspection, have lower single inspection costs, but the greater number of inspections and the higher probability of failing to detect a crack resulting from a lower flaw detectability cause higher total costs than with the ultrasonic inspections.

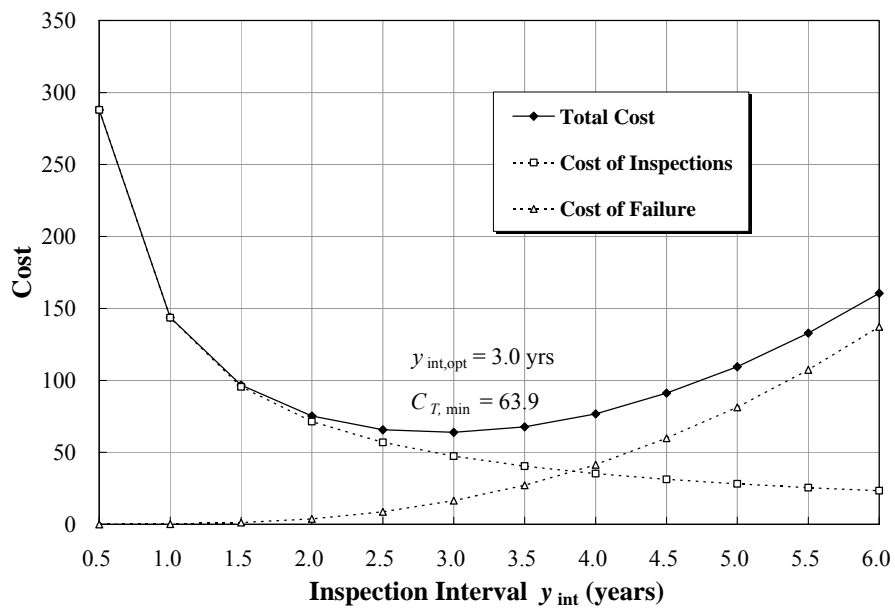


Figure 6.11: Costs of Ultrasonic Inspections for Various Fixed-Interval Schedules for  $K_{I,UI} : K_F = 1.5 : 2 \times 10^4$ .

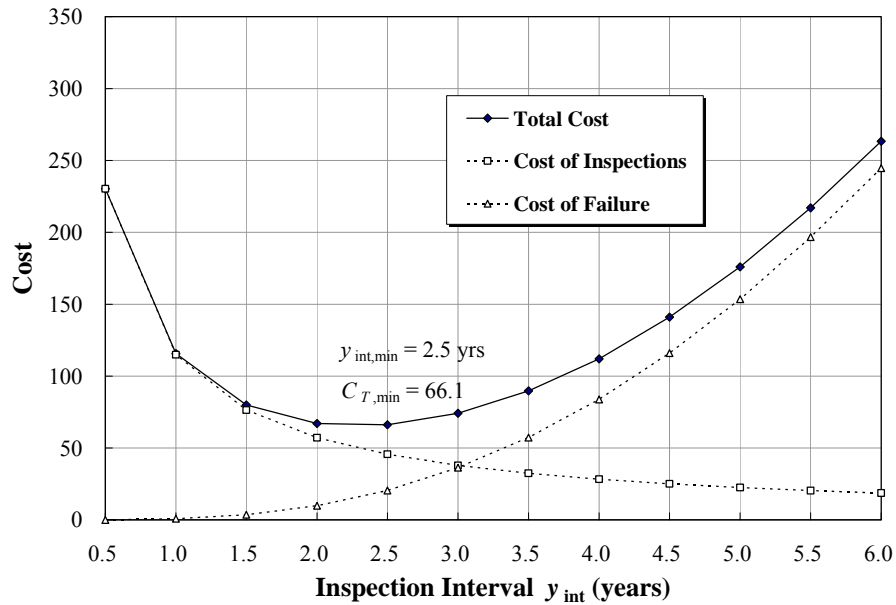


Figure 6.12: Costs of Magnetic Particle Inspections for Various Fixed-Interval Schedules for  $K_{L,MI} : K_F = 1.2 : 2 \times 10^4$ .

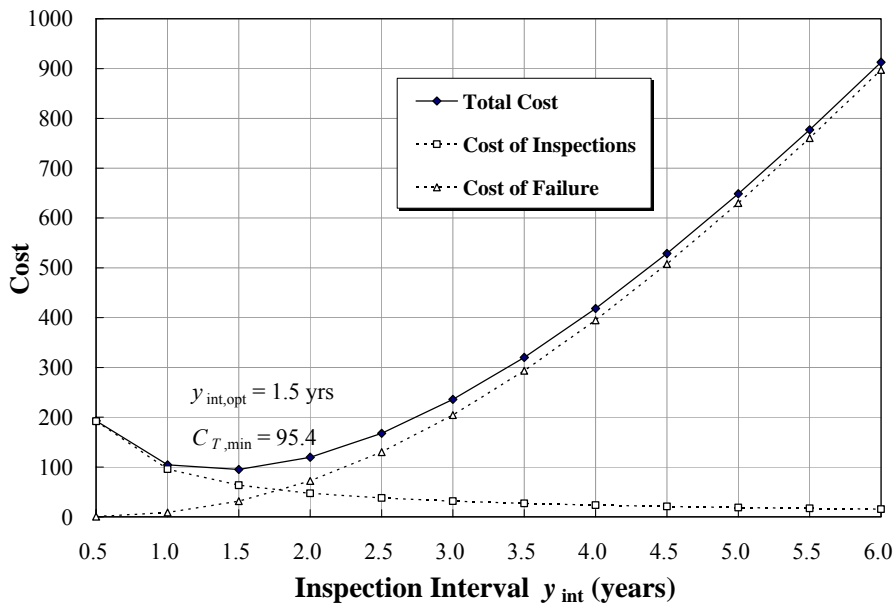


Figure 6.13: Costs of Penetrant Inspections for Various Fixed-Interval Schedules for  $K_{L,PI} : K_F = 1.0 : 2 \times 10^4$ .



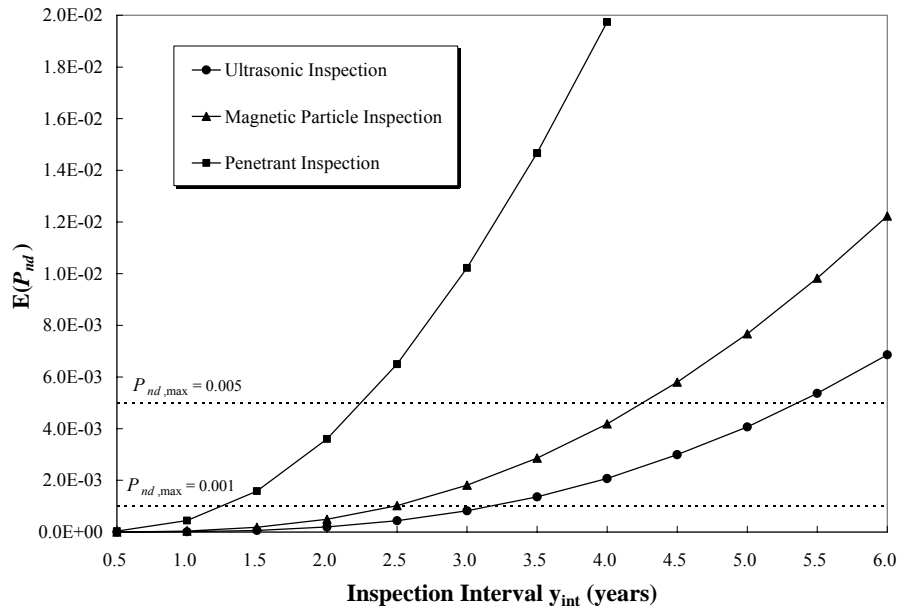


Figure 6.14: Expected Probabilities of Failing to Detect the Growing Crack,  $E(P_{nd})$ , for the UI, MI and PI Techniques Compared with the Maximum Acceptable Probability of Non-Detection,  $P_{nd,max}$ .

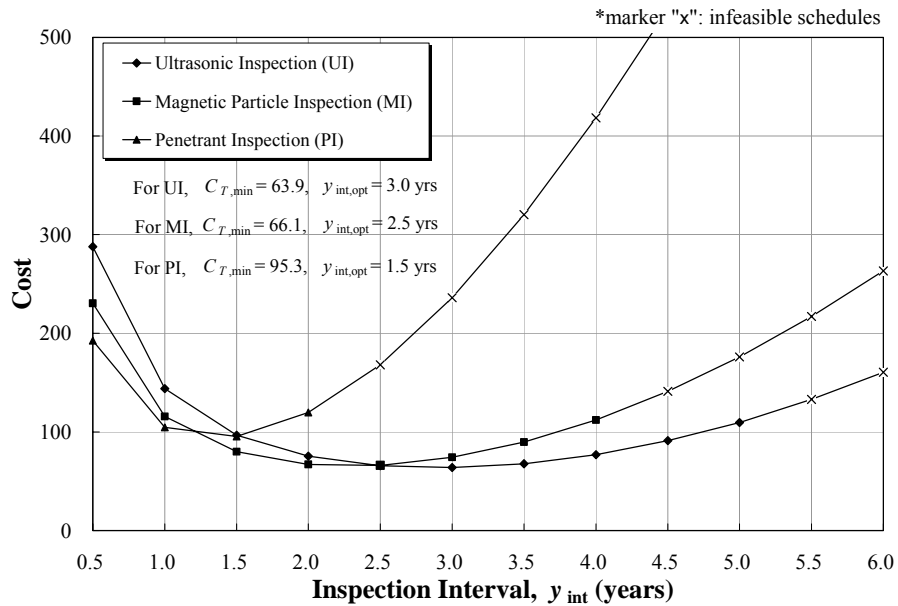


Figure 6.15: Cost Comparison of UI, MI and PI in Various Fixed-Interval Schedules for  $K_{I,PI} : K_{I,MI} : K_{I,UI} : K_F = 1.0 : 1.2 : 1.5 : 2 \times 10^4$  with the Constraint,  $P_{nd,max} = 0.005$ .

Table 6.3: Optimal Results for the UI, MI and PI Techniques with the Constraint,  $P_{nd,max} = 0.005$ .

NDI Technique	$E(n)$	$E(P_{nd})$	$y_{int,opt}$ (years)	$C_{T,min}$
Ultrasonic	31.2	$8.26 \times 10^{-4}$	3.0	63.9
Magnetic Particle	38.0	$1.02 \times 10^{-3}$	2.5	66.1
Penetrant	63.6	$1.59 \times 10^{-3}$	1.5	95.3

The constraint,  $P_{nd,max} = 0.005$  (i.e.,  $E(P_{nd}) < 0.005$ ), eliminates some infeasible inspection schedules, typically those schedules with long inspection intervals. A relatively larger number of schedules are eliminated for any NDI technique that has lower detectability, such as PI. From Figure 6.15, it can be seen that the optimal schedule for the case where  $P_{nd,max}$  is 0.005 can be directly identified from the local minima of the three NDI curves so that the  $P_{nd,max}$  constraint virtually does not affect the optimization solution in this case. However, when a stricter constraint,  $P_{nd,max} = 0.001$  (i.e.,  $E(P_{nd}) < 0.001$ ), is applied to the same problem, it is obvious that a greater number of schedules become infeasible as shown in Figure 6.16. As a result, the optimal inspection interval for PI changes from 1.5 years ( $C_T = 95.3$ ) to 1.0 year ( $C_T = 104.6$ ), and the corresponding optimal inspection interval for MI changes from 2.5 years ( $C_T = 66.1$ ) to 2 years ( $C_T = 67.0$ ). Both these NDI methods therefore demand more frequent inspections to satisfy the stricter  $P_{nd,max}$  constraint which, hence, result in higher total costs. Because the schedule yielding the minimum total cost ( $C_T = 63.9$ ) in the ultrasonic inspection is not yet affected by the stricter constraint, the optimal schedule with the stricter constraint remains unchanged from the case when  $P_{nd,max}$  was 0.005.

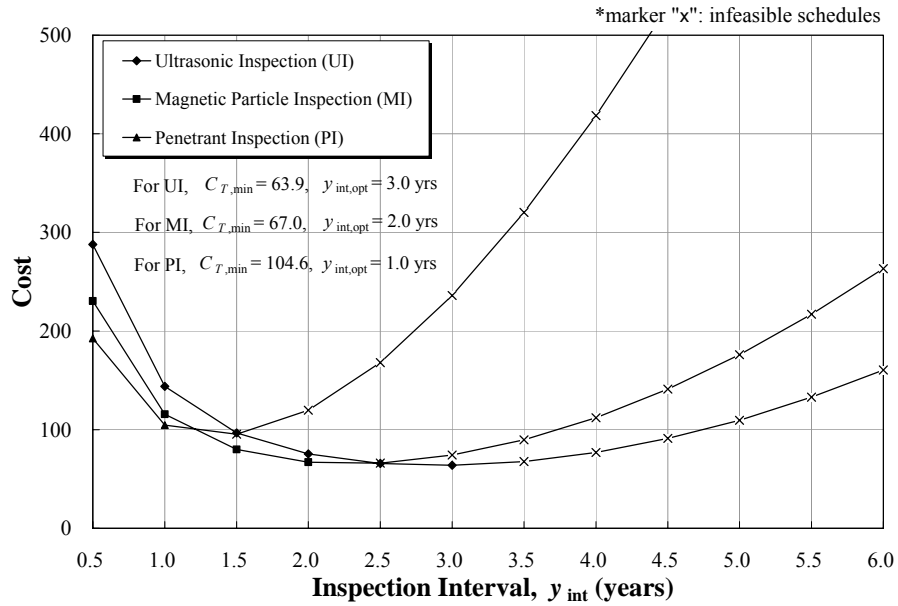


Figure 6.16: Cost Comparison of UI, MI and PI in Various Fixed-Interval Schedules for  $K_{I,PI} : K_{I,MI} : K_{I,UI} : K_F = 1.0 : 1.2 : 1.5 : 2 \times 10^4$  and with the Constraint  $P_{nd \max} = 0.001$ .

For the higher relative failure cost case (ii) where  $K_{I,PT} : K_{I,MT} : K_{I,UT} : K_F = 1.0 : 1.2 : 1.5 : 4.0 \times 10^4$  and with the constraint,  $P_{nd,\max} = 0.005$ , the  $E(n)$  and  $E(P_{nd})$  values from the Monte Carlo simulations remain the same as in the lower failure cost case, but the higher relative failure cost,  $K_F$ , raises the failure cost curve twice as high as the failure cost in the lower relative failure cost case. This in turn results in higher total costs for each of the three NDI techniques, especially for those schedules having large  $E(P_{nd})$  values (see Figures 6.17, 6.18 and 6.19). Compared to the lower relative failure cost case, the higher total cost curve shifts the schedule with the minimum cost to one with shorter inspection intervals for each NDI technique. Comparing Figures 6.15 and 6.20, the schedule with the minimum total cost for UI changes from a 3-year inspection

interval (with  $C_T = 63.9$ ) to a 2.5-year interval (with  $C_T = 74.5$ ). The 3-year periodic schedule in the higher failure cost case has a total cost of 80.4 for UI and is therefore no longer the best schedule. For MI, the schedule changes from a 2.5-year inspection interval (with  $C_T = 66.1$ ) to a 2-year interval (with  $C_T = 76.8$ ), and, for PI, the schedule changes from a 1.5-year inspection interval (with  $C_T = 95.3$ ) to a 1-year interval (with  $C_T = 113.4$ ). Finally, the optimal schedule in the higher relative failure cost case is to employ UI techniques for inspections every 2.5 years. The increase in the relative failure cost,  $K_F$ , affects the optimization solution in a direct manner. In the proposed POD-based optimization procedure, higher  $K_F$  values tend to yield an optimal strategy that demands more frequent inspections and higher NDI detectability. This tendency is evident in the optimization results and is consistent with the expectation that more important details or members should require more frequent and precise inspections.

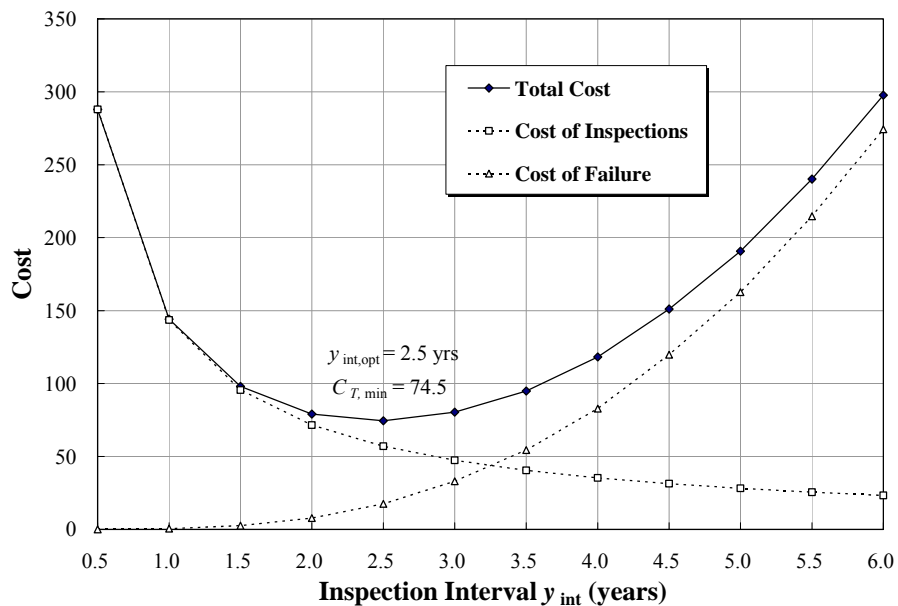


Figure 6.17: Costs of Ultrasonic Inspections for Various Fixed-Interval Schedules for  $K_{I,UI} : K_F = 1.5 : 4 \times 10^4$ .

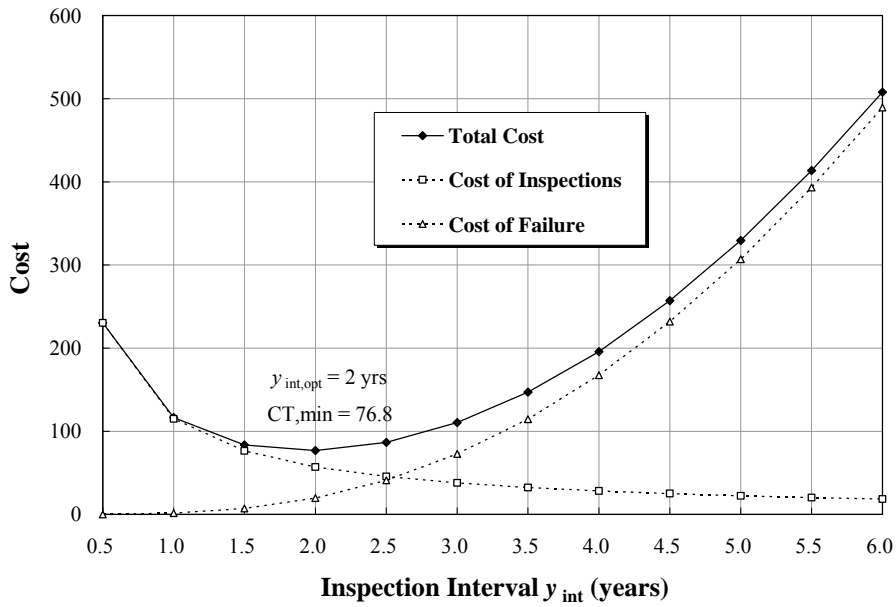


Figure 6.18: Costs of Magnetic Particle Inspections for Various Fixed-Interval Schedules for  $K_{L,MI} : K_F = 1.2 : 4 \times 10^4$ .

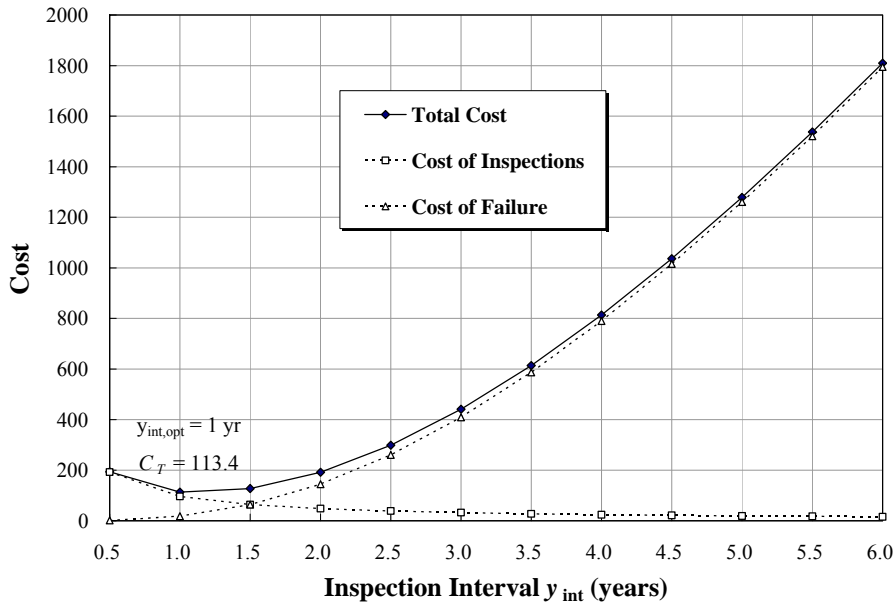


Figure 6.19: Costs of Penetrant Inspections for Various Fixed-Interval Schedules for  $K_{L,MI} : K_F = 1.2 : 4 \times 10^4$ .

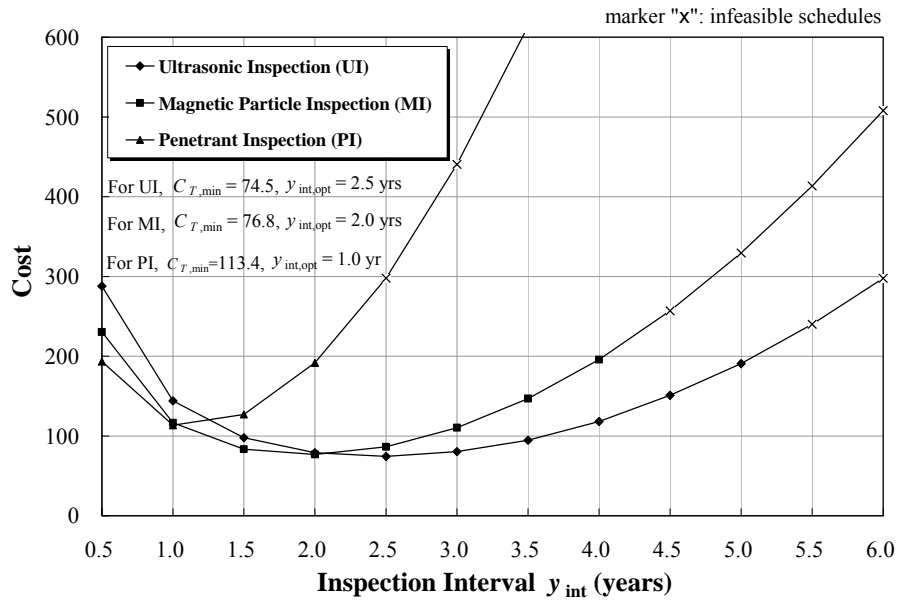


Figure 6.20: Cost Comparison of UI, MI and PI in Various Fixed-Interval Schedules for  $K_{I,PI} : K_{I,MI} : K_{I,UI} : K_F = 1.0 : 1.2 : 1.5 : 4 \times 10^4$  with the Constraint  $P_{nd \max} = 0.005$ .

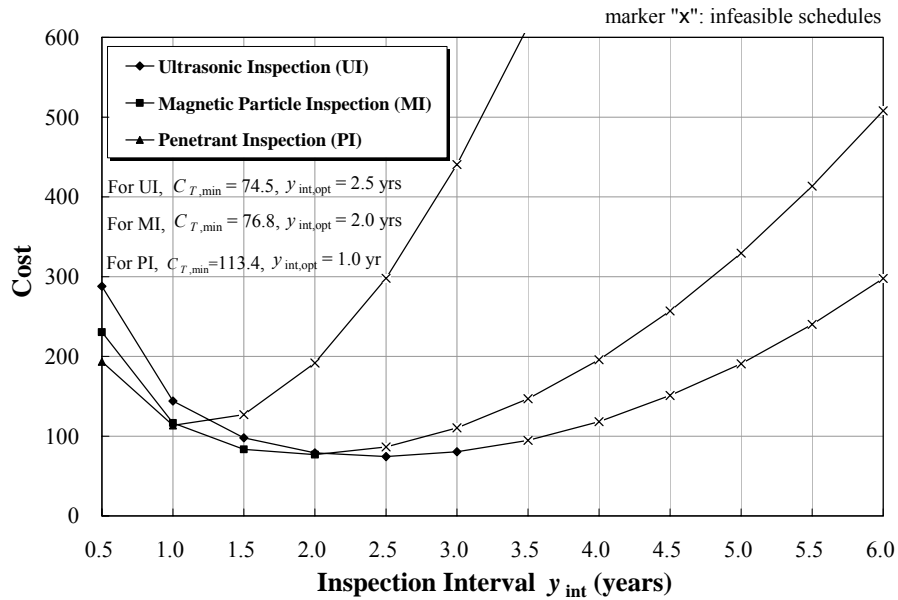


Figure 6.21: Cost Comparison of UI, MI and PI in Various Fixed-Interval Schedules for  $K_{I,PI} : K_{I,MI} : K_{I,UI} : K_F = 1.0 : 1.2 : 1.5 : 4 \times 10^4$  with the Constraint  $P_{nd \max} = 0.001$ .

Since the  $E(P_{nd})$  values for all schedules in the three NDI techniques remain the same as the values in Figure 6.14, because they are not affected by the higher relative failure cost,  $K_F$ , the infeasible schedules for the three NDI techniques under the constraint,  $P_{nd,max} = 0.001$ , are the same as the infeasible schedules in the lower relative failure cost case with the same  $P_{nd,max}$  constraint (see Figure 6.16). The schedules for UI, MI, and PI with a fixed-inspection interval greater than and equal to 3.5 years, 2.5 years, and 1.5 years, respectively, are identified as infeasible. It can be seen in Figure 6.21 that the constraint,  $P_{nd,max} = 0.001$ , does not influence the schedule with the minimum total cost for each NDI technique so that the optimal NDI technique and the associated strategy is still to carry out ultrasonic inspections and every 2.5 years.

In addition, as the results have shown in the two cases discussed, the present two-year periodic inspection required by the FHWA may not be the optimal schedule for the butt weld detail inspected by any of the three NDI techniques. Except for the two-year periodic MI schedule in the higher failure cost case (ii), the two-year periodic schedules using the other two NDI techniques result in higher total costs than the optimal schedule.

### 6.6.2 Box-Girder Example II

Two optimal fatigue inspection schedules, generated using the reliability-based scheduling method of Chapter 5 and the POD-based method of Chapter 6 for the same box-girder example in Section 5.7.2, are compared in this example. The same three NDI techniques (UI, MI, and PI) and their associated POD functions described in Section 6.6.1 (i.e., Box-Girder Example I) are utilized in this example as well. The relative costs of the three NDI techniques and of failure are  $K_{I,PI} : K_{I,MI} : K_{I,UI} : K_F = 1.0 : 1.2 : 1.5 : 1 \times 10^5$ . The relative cost of repair,  $K_R$ , considered in the reliability-based scheduling method is taken as 10 times that of  $K_{I,PI}$ . With respect to safety constraints, the reliability-based scheduling method employs a target reliability index,  $\beta_{\text{target}}$ , of 3.7, and the POD-based method employs a maximum allowable probability of not detecting a crack,  $P_{nd,\text{max}}$ , equal to 0.005. The POD-based method is suitable for seeking the optimal schedule from among all schedules with fixed inspection intervals. Hence, for comparison purposes, the reliability-based method is altered so that the search for the optimal schedule is carried out with uniform intervals only. Due to the different total cost ( $C_T$ ) formulations in the two methods, these costs cannot be compared directly with each other. However, schedules for the lowest costs with each method may be compared.

Based on a prescribed crack size warranting repair,  $a_R$ , the reliability-based scheduling approach usually assumes an ideal inspection quality for the employed NDI technique. In this example, this prescribed crack size for repair is assumed to be 0.2 in, which can be detected by the ultrasonic inspection (UI) technique with almost 100% certainty, as shown in Figure 6.8. Hence, the optimization results from the reliability-based scheduling method can be thought to represent the optimal schedule for the given



UI technique. With the pre-defined relative costs of inspection (UI), repair, and failure ( $K_{I,UI} : K_R : K_F = 1.5 : 10 : 10^5$ ) in the proposed reliability-based scheduling approach, Figure 6.22 illustrates the total costs for various fixed-interval schedules. It can be seen that the optimal fixed-interval schedule analyzed by the reliability-based method for the detail suggests performing ultrasonic inspections every 5 years. The planned service life does not affect the optimization result for the reliability-based approach as can be seen in Figure 6.22.

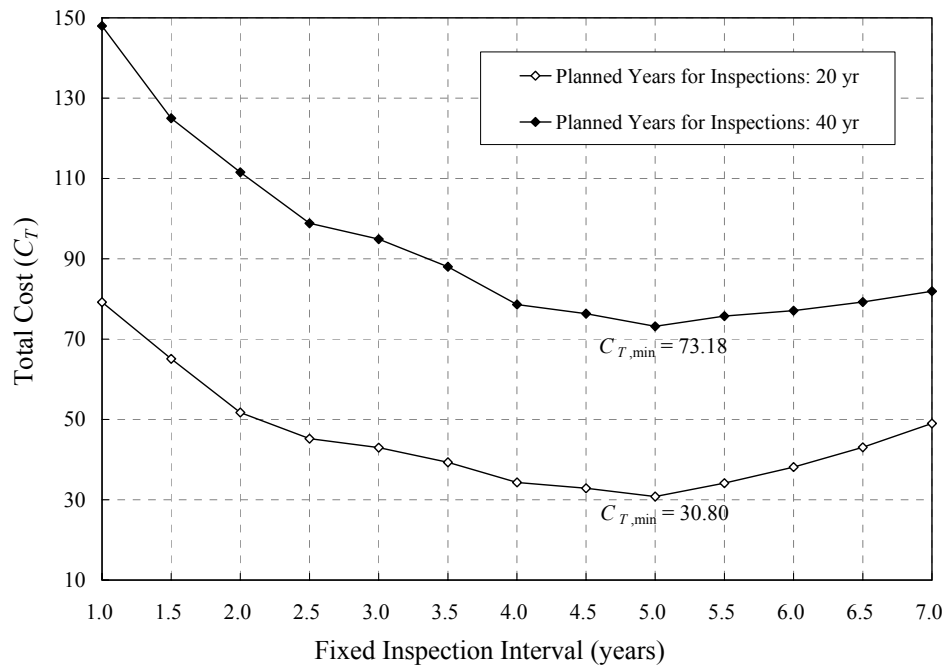


Figure 6.22: Total Costs of Various Fixed-Interval Schedules using the Reliability-Based Scheduling Method ( $K_{I,UI} : K_R : K_F = 1.5 : 10 : 10^5$ ).

With the relative costs of PI, MI, UI, and of failure ( $K_{I,PI} : K_{I,MI} : K_{I,UI} : K_F = 1.0 : 1.2 : 1.5 : 10^5$ ) in the POD-based scheduling approach, the total costs for the various fixed-interval schedules with each given NDI technique are shown in Figure 6.23. It

can be seen that the best schedule for the UI technique requires inspections on the detail every 4 years, which yields a total cost of 90.7. For the MI technique, a 3-year periodic inspection schedule for the detail, which yields a total cost 94.3, is optimal. For the PI technique, inspecting the detail every 2 years, which produces a total cost of 140.0, is the optimal schedule. As can be seen, NDI techniques with lower crack detectabilities require shorter intervals between inspections in the optimal schedule. Using the POD-based method, the UI technique with a 4-year periodic inspection schedule, which yields the lowest total cost of 90.7, provides an optimal inspection scheduling strategy for the detail.

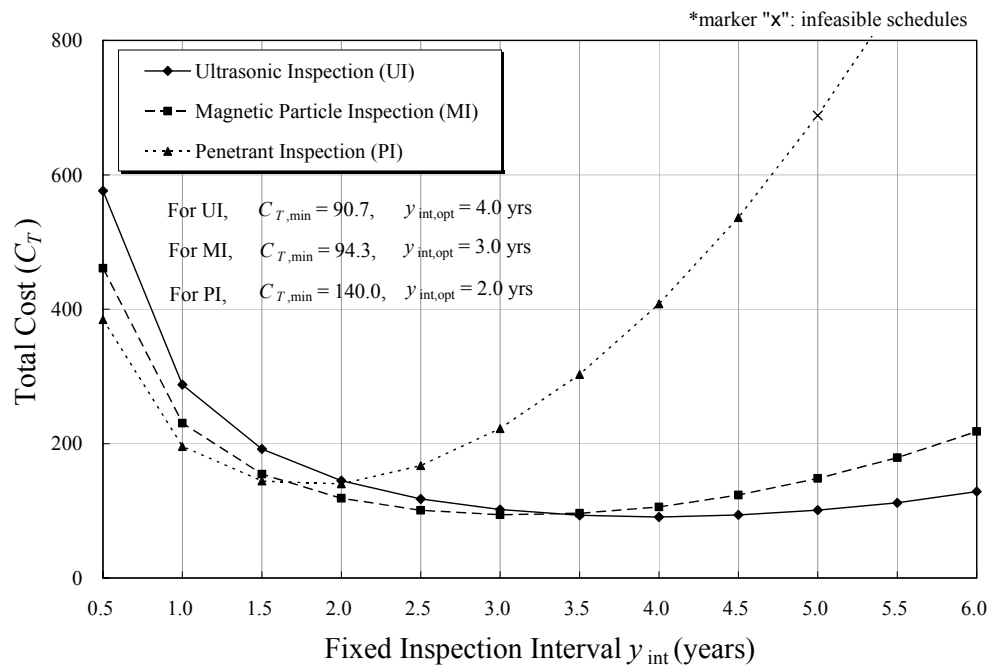


Figure 6.23: Total Cost Comparison of UI, MI and PI in Various Fixed-Interval Schedules using the POD-Based Scheduling Method for  $K_{I,PI} : K_{I,MI} : K_{I,UI} : K_F = 1.0 : 1.2 : 1.5 : 10^5$  with the Constraint,  $P_{nd,max} = 0.005$ .

Comparing the results from the reliability-based method and the POD-based method, it is found that, for the same detail and using the same UI technique, these two methods recommend different optimal schedules. The reliability-based method suggests that the optimal strategy with the UI technique should employ a 5-year periodic inspection schedule. However, the POD-based method recommends a more conservative 4-year inspection interval schedule. The reason that the two methods yield different optimal schedules is due to the different assumptions implicit in the two optimization approaches. Through the event tree analysis, the reliability-based method considers possible repair effects on a detail after each inspection, and thus takes into account the possible extended service life of the detail due to the possible repair scenarios modeled. The POD-based method, on the other hand, does not include any repair effects during the crack propagation process, and therefore does not consider any extended service life that might result when repairs are carried out. When scheduling a detail without considering any possible plan of fatigue life extension due to repairs, the POD-based method rationally will yield a more conservative schedule than the optimal schedule derived by using the reliability-based method in which the extended fatigue life of the detail is explicitly taken into consideration.

## 6.7 SUMMARY

A probabilistic approach for selecting an optimal NDI technique and an associated inspection schedule for fracture-critical members in steel bridges has been presented. The method builds upon LEFM fatigue analysis and the actual detection capabilities of NDI techniques for the fracture-critical member of interest, and then employs the probability of detection information in Monte Carlo simulations to formulate an optimization problem. Solution of this optimization problem yields the most suitable NDI technique and associated inspection schedule for the detail. The findings of this chapter can be summarized as follows:

- (1) As can be seen in the cost- $y_{\text{int}}$  (cost vs. inspection interval) diagrams presented, for a given NDI technique, the total cost is controlled by the cost of inspections for schedules with short inspection intervals (i.e., the schedules involving frequent inspections). The shorter the fixed inspection interval employed in the schedule, the greater will be the cost of inspections for that schedule. For schedules with longer inspection intervals, the total cost is governed by the cost of failure. The longer the fixed inspection interval in the schedule, the greater will be the cost of failure for that schedule. Hence, a valley-shaped total cost curve is generated. After applying the  $P_{nd,\text{max}}$  constraint to eliminate some infeasible schedules, the optimal schedule for an NDI technique can usually be found at the bottom of the valley-shaped total cost curve.
- (2) Comparing NDI techniques (as was done in Table 6.3), an NDI technique with a lower crack detectability will normally demand more inspections ( $E(n)$ ) than an NDI technique with a higher crack detectability to achieve the schedule with the minimum total cost (i.e., the optimal schedule for the NDI technique). This result

is consistent with the practical experience where more inspections are needed for an NDI technique with a low crack detectability to ensure inspection quality.

- (3) From the results of the numerical examples presented, it is seen that the two-year periodic inspection schedule required by the FHWA over the service life may not be the optimal (lowest-cost) schedule for some NDI techniques and details. The optimal schedule for a specified fracture-critical member needs to consider the NDI technique applied and the fatigue performance of the member. The POD-based method presented here yields a more rational inspection strategy than an arbitrarily specified two-year inspection schedule.
- (4) The optimization results are affected by the NDI detectabilities (i.e., POD functions), the constraint on the expected probability of not detecting a crack,  $E(P_{nd})$ , and the relative costs of inspection and failure.
- (5) Regarding the effect of crack detectability, it can be seen from the examples presented (such as in Figure 6.14), that the NDI technique with the higher detectability for cracks tends to yield a lower  $E(P_{nd})$  especially for schedules with a longer inspection interval. This lower  $E(P_{nd})$  contributes in turn to lower costs of failure in the total cost. However, an NDI technique with a higher crack detectability is usually more expensive and involves higher inspection costs.
- (6) Regarding the effect of the  $P_{nd,max}$  constraint, it is found that by lowering the  $P_{nd,max}$  value (i.e., raising the safety level of a detail), schedules with longer fixed inspection intervals tend to be excluded because these schedules usually cause higher  $E(P_{nd})$  values than the prescribed value of  $P_{nd,max}$ . Therefore, upon decreasing the  $P_{nd,max}$  value, the optimal schedule adjusts to a shorter inspection interval. This trend in the proposed model agrees with reality where higher safety levels required by a

detail generally demand more frequent inspections (i.e., a shorter inspection interval).

- (7) Regarding the effect of relative cost of failure,  $K_F$ , as can be seen in cases (i) and (ii) studied, the higher relative cost of failure,  $K_F$ , has the tendency to require an optimal schedule with a shorter fixed inspection interval. Comparing Figures 6.11 and 6.17 for example, it can be seen that the higher  $K_F$  lifts the failure cost curve in the cost- $y_{\text{int}}$  diagram. The longer the fixed inspection interval employed in the schedule, the higher is the cost of failure. The  $K_F$  value does not affect the number of inspections  $E(n)$  of each schedule; hence, the inspection cost curve remains the same when  $K_F$  is changed. Thus, the total cost curve is governed by the failure cost curve. The raised total cost curve due to the increased failure cost curve, therefore, shifts the optimal schedule to one with a relatively shorter inspection interval. In addition, when a higher  $K_F$  is considered, the optimal NDI technique usually is one with a higher crack detectability. This is because such an NDI technique with a higher crack detectability will usually yield a lower failure cost for inspection schedules.
- (8) From the demonstrated box-girder example II, the proposed reliability-based scheduling method of Chapter 5 and the POD-based method presented in Chapter 6 compared for a given ultrasonic inspection technique. It is found that, for the same fracture-critical member, the proposed POD-based method tends to yield a more conservative optimal inspection schedule than the schedule generated using the reliability-based method. This is because, conservatively, the POD-based method does not consider possible future repair actions, which may extend the fatigue life of the detail/member.

## **Chapter 7: SUMMARY AND CONCLUSIONS**

Fatigue is a random and complex process that can affect the performance of all steel bridges. It can bring about localized failure in a single detail or overall failure of the entire bridge. The disadvantage of estimating the fatigue life of a bridge detail using a deterministic approach is that the uncertainty in external and internal factors such as in the vehicle-induced fatigue loading, the aggressiveness of environmental conditions, the material characteristics, and structural geometry are not treated in a rational manner. Accounting for these uncertainties in deterministic approaches can lead to very conservative estimates of fatigue lives for the details. Even when a detail is subjected to constant-amplitude stress cycles, the fatigue life of that detail is random. This observation can be verified by the considerable amount of scatter in fatigue test data that are employed to establish the design S-N curves in the AASHTO specifications.

As an alternative to using deterministic approaches, probabilistic approaches involving fatigue reliability analysis can be used to help characterize the safety and performance of a steel bridge detail subjected to cyclic loading. For details clearly defined under standard AASHTO categories, the AASHTO fatigue reliability approach, which employs a limit state function related to number of stress cycles, may be utilized for the fatigue reliability calculations. Variability in the truck-induced fatigue loading and uncertainty in internal factors (such as material properties and detail geometry) are taken into consideration in the model. For non-AASHTO type details, the fatigue reliability is evaluated by using an approach based on Linear Elastic Fracture Mechanics (LEFM) principles and a limit state function related to crack size. Uncertainties related to initial crack size, fatigue-related parameters in Paris' law as well as in the random fatigue loading are taken into consideration in this model. In both reliability analysis

approaches, the variable-amplitude vehicle-induced fatigue loading is modeled by using an equivalent stress range.

Three methods for modeling variable-amplitude fatigue loadings in steel bridges were presented in Chapter 3. These included the stress spectrum analysis, the assumed distribution analysis, and the fatigue truck analysis methods. The objective of each of these three methods was to derive the equivalent stress range for a given bridge detail.

In Chapter 4, the fatigue reliability approaches to be used with an S-N curve approach (for AASHTO details) and an LEFM-based approach (for non-AASHTO details) were presented. Fatigue reliability analysis provides a convenient way of quantifying the fatigue deterioration of fracture-critical details in steel bridges. Variables needed for fatigue reliability analysis with the AASHTO and the LEFM approaches were studied and statistics on these variables have been compiled in Chapter 4 to assist in performing reliability analyses. After obtaining the fatigue reliability index versus number of stress cycles (i.e.,  $\beta$  versus  $N$  curves), a comparison of the fatigue reliability with a target reliability index can provide useful information for planning inspection schedules. The number of stress cycles,  $N_{\text{target}}$ , that it takes for a detail to reach the selected minimum acceptable target reliability index (assumed to be 3.7 in the illustrations presented in this dissertation) can serve as a useful early warning point in time from which to consider more detailed inspections to avoid large cracks or fatigue failure. This was demonstrated with two case studies. In the study involving use of the LEFM fatigue reliability approach, it was showed how even without precise information of an initial crack size, assumed initial crack size distributions based on available references (compiled in Chapter 4) can help to estimate the fatigue reliability which can then be used to determine a warning point associated with  $N_{\text{target}}$  accumulated cycles after which, more detailed inspections of the detail might be considered. More



importantly, the approaches presented in Chapter 4 were developed in sufficient detail to enable their use in the optimal inspection scheduling discussed in Chapter 5.

Employing fatigue reliability analysis techniques along with means for determining the likelihood of needed repairs, the use of event trees, as well as cost computations, the problem of fatigue inspection scheduling in bridge details was formulated as a mathematical optimization problem. Through the proposed reliability-based inspection scheduling procedure, an optimal inspection schedule providing the number and times of planned inspection can be obtained that meets reliability and inspection interval constraints. Such an optimization procedure can, thus, yield not only the most economical inspection schedule (i.e., lowest cost), but also one that can maintain the inspected detail at prescribed safety levels. In light of the FHWA imposed two-year interval between inspections, a study of more rational treatment of inspection times was undertaken. The maximum time between inspections,  $T_{max}$ , was found to be an important constraint that influences the number of inspections, the total cost, and the inspection strategy. When the inspection scheduling is constrained by  $T_{max}$ , a greater number of inspections will typically be necessary which raises the fatigue reliability of the detail and, thus, lowers the expected cost of failure. As shown in the examples presented, the proposed scheduling method can be applied to both AASHTO and non-AASHTO type bridge details. The effects of relative costs of repair, inspection, and failure that make up the total cost, the influence of ADTT uncertainty, and the effect of different target reliability levels on inspection scheduling were all studied in detail in Chapter 5.

An increase in relative repair costs tends to yield an optimal schedule with fewer inspections because the total costs are governed by the repair costs. An increase in

failure costs tends to yield an optimal schedule with more inspections because total costs, especially when the number of inspections is small, are governed by failure costs.

With regard to the influence of ADTT (traffic) uncertainty, it was shown that with increasing variability in the average daily truck traffic, a larger number of inspections is required for the optimal schedule. However, only for steel bridges where the ADTT has a COV greater than about 0.30 is it necessary to have significantly more inspections than are required for the case when a constant ADTT is assumed.

A higher target reliability constraint (i.e., more stringent safety requirement) tends to exclude schedules with very few inspections because such schedules cannot maintain the fatigue reliability of the detail above the higher target reliability over the planned service life. This conclusion is in agreement with an expectation that a detail whose failure consequences are greater will require more inspections to ensure the detail meets any imposed higher safety standards.

Importantly, it was seen that a periodic two-year inspection schedule over the planned service life as is required by the FHWA for steel bridges will not be the optimal schedule for some details if one is interested in keeping costs low as well as maintaining safety. Though such periodic schedule can often keep the fatigue reliability at a higher level than some optimal schedules, the larger number of inspections and repairs needed over the service life cause an increase in total cost. The reliability-based fatigue inspection strategy presented here yields the optimal inspection schedule while maintaining prescribed safety levels for lower costs.

When the quality of nondestructive inspection (NDI) techniques is taken into consideration in fatigue inspections, a probabilistic approach based on actual probability of detection (POD) estimates for selected NDI techniques and an LEFM analysis of crack propagation can be used to select the optimal NDI technique and associated schedule for

a fracture-critical bridge member of interest. This is demonstrated in Chapter 6 where the procedure formulated models the NDI selection problem as a different optimization problem (from the one in Chapter 5) in which only inspection and failure costs are considered. Through Monte Carlo simulation schemes, the solution of this optimization problem, which is constrained by the maximum allowable probability of not detecting a crack ( $P_{nd,max}$ ), and by upper and lower bounds on inspection intervals, yields the most economical and risk-controlled NDI technique along with an associated schedule for the bridge detail of interest. In the numerical examples presented, it was found that an NDI technique with a lower quality normally demands more inspections than one with a higher quality to achieve the schedule with the minimum total cost. Also, by decreasing the  $P_{nd,max}$  value (i.e., raising the safety level), the optimal schedule tends to adjust to a schedule with a relatively shorter inspection interval because the higher safety level demanded for the detail generally requires more frequent inspections.

When the POD-based scheduling approach and the reliability-based scheduling approaches are compared, it was found that, for a fracture-critical member, the proposed POD-based method was found to provide a more conservative optimal schedule than the reliability-based scheduling method because possible future repair actions on the detail are not considered in the POD-based approach.

In summary, this dissertation has provided methods to evaluate the fatigue performance as well as the risk of fatigue failure for fracture-critical members in steel bridges. Two rational methods – one based on reliability analysis and the other on NDI-related quality (probability of detection) information – have been proposed to permit rational inspection and maintenance strategies for steel bridges. Applying these methods to various types of details, bridge authorities can optimally allocate their maintenance budgets in an efficient manner without compromising safety.

- Future research of the presented work can be extended to the following directions:
- (1) The POD-based selection method for NDI techniques only suggests an optimal schedule with a uniform inspection interval for the detail of interest. From experience with the reliability-based scheduling method, a fixed-interval schedule may not provide the optimal schedule with the lowest total cost for the detail. Hence, the POD-based method can be extended to find an optimal schedule that allows for non-uniform inspection intervals. This extended research will demand more advanced simulation and optimization techniques.
  - (2) The reliability-based inspection scheduling method proposed in this dissertation considered only an “as-good-as-new repair” or “no repair” after each inspection, so that a basic two-branch event tree analysis (i.e., 2<sup>nd</sup> tree analysis) could be utilized. When the repair policy is changed to permit multiple repair actions, the proposed scheduling model can be extended to employ a multi-event tree analysis in the optimization process.
  - (3) Corrosion effects can be incorporated into the proposed reliability-based scheduling method to deal with corrosion–fatigue inspection problems in steel bridges.
  - (4) The reliability-based scheduling method or the POD-based NDT selection method can be extended for use with other degrading civil infrastructure systems.

## Appendix A

### A.1 DERIVED PROBABILITY DISTRIBUTIONS FOR A FUNCTION OF RANDOM VARIABLES

Consider a function,  $Y = g(X_1, X_2, \dots, X_n) = g(\mathbf{X})$ , where

$Y$  is a response variable;

$\mathbf{X}$  is a random variable vector composed of  $X_1, X_2, \dots$ , and  $X_n$ ;

$g(\mathbf{X})$  is a response model,

then  $F_Y(y) = \iint \dots \int_{g(\mathbf{x}) \leq y} f_{X_1, X_2, \dots, X_n}(x_1, x_2, \dots, x_n) dx_1 dx_2 \dots dx_n$ , where

$F_Y(y)$  is the CDF of  $Y$ ;  $f_{X_1, X_2, \dots, X_n}(x_1, x_2, \dots, x_n)$  is the joint PDF of  $X_1, X_2, \dots$ , and  $X_n$ .

In many cases, an analytical result of  $F_Y(y)$  can be derived as shown in Table A.1.

Table A.1 Basic Random Variable Transformations for  $Y = g(\mathbf{X})$ .

<i>Function <math>Y = g(\mathbf{X})</math></i>	<i>Probability Distribution for <math>X_i</math></i>	<i>Probability Distribution for <math>Y</math></i>
$Y = \sum_{i=1}^n a_i X_i + b$	<p>Normal(<math>\mu_{X_i}, \sigma_{X_i}</math>)</p> <p><math>COV(X_i, X_j) = \rho_{i,j} \sigma_{X_i} \sigma_{X_j}</math></p>	<p>Normal(<math>\mu_Y, \sigma_Y</math>)</p> <p><math>\mu_Y = \sum_{i=1}^n a_i \mu_{X_i} + b</math></p> <p><math>\sigma_Y = \sqrt{\sum_{i=1}^n \sum_{j=1}^n a_i a_j COV(X_i, X_j)}</math></p>
$Y = b \prod_{i=1}^n X_i^{a_i}$	<p>Lognormal(<math>\lambda_{X_i}, \zeta_{X_i}</math>)</p> <p><math>COV[\ln(X_i), \ln(X_j)] = \rho_{i,j} \zeta_{X_i} \zeta_{X_j}</math></p>	<p>Normal(<math>\lambda_Y, \zeta_Y</math>)</p> <p><math>\lambda_Y = \sum_{i=1}^n a_i \lambda_{X_i} + \ln(b)</math></p> <p><math>\zeta_Y = \sqrt{\sum_{i=1}^n \sum_{j=1}^n a_i a_j COV(\ln(X_i), \ln(X_j))}</math></p>

Table A.1 (Continued) Basic Random Variable Transformations for  $Y = g(\mathbf{X})$ .

<i>Function <math>Y = g(X)</math></i>	<i>Probability Distribution for <math>X_i</math></i>	<i>Probability Distribution for <math>Y</math></i>
$Y = \sum_{i=1}^n X_i^2$	Normal(0,1) $\rho_{i,j} = 0$ for all $i \neq j$	Chi Square ( $f$ ), $f = n$ $\mu_Y = f$ ; $\sigma_Y = \sqrt{2f}$
$Y = \sqrt{\sum_{i=1}^n X_i^2}$	Normal(0,1) $\rho_{i,j} = 0$ for all $i \neq j$	Chi ( $f$ ), $f = n$ $\mu_Y = \sqrt{2} \left\{ \frac{\Gamma[(f+1)/2]}{\Gamma(f/2)} \right\}$ $\sigma_Y = \sqrt{f-2} \left\{ \frac{\Gamma^2[(f+1)/2]}{\Gamma^2(f/2)} \right\}$
$Y = \frac{X_1}{X_2/\sqrt{f}}$	$X_1$ is Normal( $\mu_{X_1}, \sigma_{X_1}$ ) $X_2$ is Chi( $f$ ) $\rho_{1,2} = 0$	Student's T( $f$ ) $\mu_Y = 0$ $\sigma_Y = \sqrt{\frac{f}{f-2}}$ , $f > 2$
$Y = \frac{X_1/\sqrt{f_1}}{X_2/\sqrt{f_2}}$	$X_1$ is Chi( $f_1$ ) $X_2$ is Chi( $f_2$ ) $\rho_{1,2} = 0$	F Distribution ( $f_1, f_2$ ) $\mu_Y = \frac{f_2}{f_2-2}$ , $f_2 > 2$ $\sigma_Y = \sqrt{\frac{2f_2^2(f_1+f_2-2)}{f_1(f_2-2)^2(f_2-4)}}$
$Y = \sum_{i=1}^n X_i$	Poisson( $\nu_{X_i}$ ) $\rho_{i,j} = 0$ for all $i \neq j$	Poisson( $\nu_Y$ ) $\nu_Y = \sum_{i=1}^n \nu_{X_i}$
$Y = \max(X_1, \dots, X_n)$	$F_{X_i}(x) = F_X(x)$ for all $i$ $\rho_{i,j} = 0$ for all $i \neq j$	$F_Y(y) = [F_X(y)]^n$
$Y = \min(X_1, \dots, X_n)$	$F_{X_i}(x) = F_X(x)$ for all $i$ $\rho_{i,j} = 0$ for all $i \neq j$	$F_Y(y) = 1 - [1 - F_X(y)]^n$

## Appendix B

### B.1 RACKWITZ-FIESSLER ALGORITHM IN THE FIRST-ORDER RELIABILITY METHOD

The Rackwitz-Fiessler algorithm for the First-Order Reliability Method (FORM) can be described using the following steps:

- (1) Normalize the basic random variables,  $\mathbf{X}$ , so as to obtain the independent standardized normal variables,  $\mathbf{U}$ .
- (2) Transform the limit state function,  $g(\mathbf{X})$ , to  $g(\mathbf{U})$ .
- (3) Guess a design point,  $\mathbf{x}^*$  (original variables), and transform it to standard normal space as  $\mathbf{u}^*$ . For uncorrelated variables, the design point in U-space can be obtained as follows:

$$u_i^* = \frac{x_i^* - \mu_i^N}{\sigma_i^N} \quad (\text{B.1})$$

where  $\mu_i^N$  and  $\sigma_i^N$  are the mean and standard deviation, respectively, of an equivalent normal distribution of  $X_i$  if  $X_i$  is non-normal. For correlated non-normal variables, the Rosenblatt transformation is required to obtain  $u_i^*$ .

- (4) Evaluate  $g(\mathbf{u}^*)$  and check if  $|g(\mathbf{u}^*)| < \varepsilon$ , where  $\varepsilon$  is specified.

- (5) Evaluate gradients  $\left( \frac{\partial g}{\partial u_i} \right)_{\mathbf{u}^*}$  in the current iteration.

- (6) Obtain an updated vector for  $\mathbf{u}_{up}^*$  using the following recursive formula:

$$\mathbf{u}_{up}^* = \mathbf{u}_{(k+1)}^* = \frac{1}{|\nabla g(\mathbf{u}_{(k)}^*)|^2} \left[ \left( \nabla g(\mathbf{u}_{(k)}^*) \right)^T \cdot \mathbf{u}_{(k)}^* - g(\mathbf{u}_{(k)}^*) \right] \cdot \nabla g(\mathbf{u}_{(k)}^*) \quad (\text{B.2})$$

- (7) If  $|g(\mathbf{u}_{up}^*)| > \varepsilon$  and the  $\mathbf{u}_{up}^*$  is different from that of step (3), go back to step (3) using  $\mathbf{x}_{up}^*$  as the new design point, where

$$x_{i,up}^* = u_{i,up}^* \sigma_i^N + \mu_i^N \quad (\text{B.3})$$

(8) Repeat Steps (3) to (7) until  $|g(\mathbf{u}^*)| < \varepsilon$  and  $\mathbf{u}^*$  does not change significantly.

(9) The reliability index  $\beta$  can be computed as follows:

$$\beta = [\mathbf{u}^T \cdot \mathbf{u}]^{1/2} \quad (\text{B.3})$$



## Appendix C

### C.1 RAINFLOW COUNTING METHOD FOR STRESS CYCLES

Once strain time history data have been collected for any detail, a stress-time history plot for the detail can be obtained. Rotate this stress-time history plot so that the stress axis is oriented horizontally and the time axis increases downward so that the Rainflow Count Method can now applied. The Rainflow Counting Method proposed by Matsuishi and Endo (1968) comes from the idea of letting “rain” drip down and fall on the rotated stress-time history line and then employing a stress cycle counting procedure by following specified “rain dripping rules.” Rain is allowed to flow from the top of the stress-time history line and must stop flowing in the following three situations summarized by Bannantine et al. (1990):

- (1) Rainflow that starts at a local maximum point and falls toward a local minimum point must stop flowing at a time point where another local maximum point is greater than the local maximum point where the rain flow begins.
- (2) Rainflow that starts at a local minimum point and falls toward a local maximum point must stop flowing at a time point where another local minimum point is less than the local minimum point where the rain flow begins.
- (3) Rain cannot flow over a “wet” stress-time history segment, which means rain cannot encounter a previous rainflow.

For the example shown in Figure C.1, the first rainflow begins from point 1 and stops at point A because point 5 is less than point 1 (Rule (2)). The second rainflow starts from point 2 stops at point B because point 4 is greater than point 2 (Rule (1)). The third rainflow that initiates from point 3 ends at point C due to Rule (3). The fourth rainflow starts from point 5 and ends at point D by Rule (2). The fifth rainflow begins

from point 6 and stops at point E due to rule (3). Each rainflow corresponds to a half of a stress cycle and needs to be paired with another half cycle to form a complete stress cycle. With the five rainflows identified in Figure C.1, it is evident that the half cycle 2-B can be paired with the half cycle 3-C and the half cycle 5-D can be paired with the half cycle 6-E. As can be seen in the figure, some rainflows (half cycles) still cannot be paired with others so as to form complete cycles. A technique of moving the portion of the stress history that occurs before the absolute maximum point to the end of the stress history can resolve the problem of unpaired half cycles. This modification to the Rainflow Counting Method is illustrated in Figure C.2.

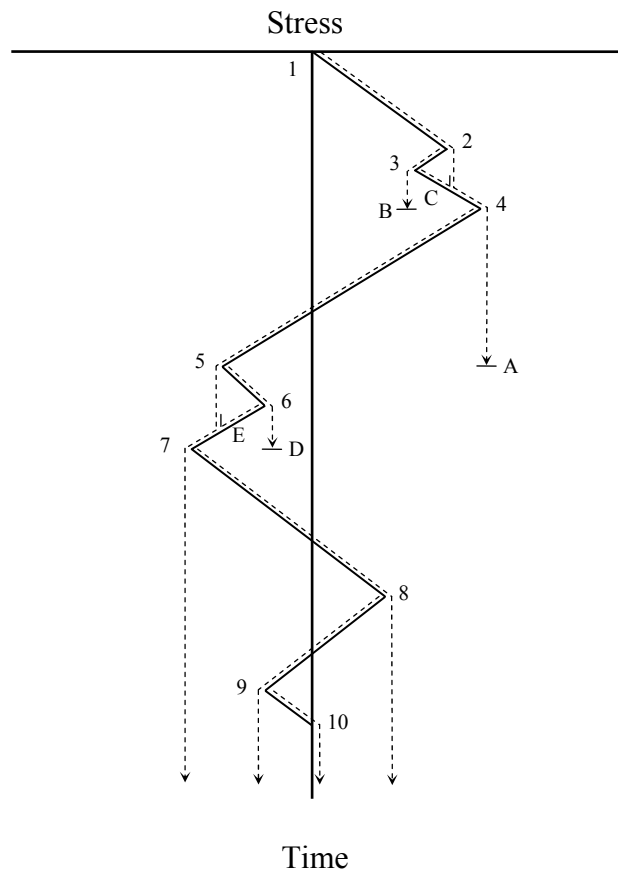


Figure C.1 Rainflow Counting Method for a Variable-Amplitude Stress History (Hoadley et al., 1982).

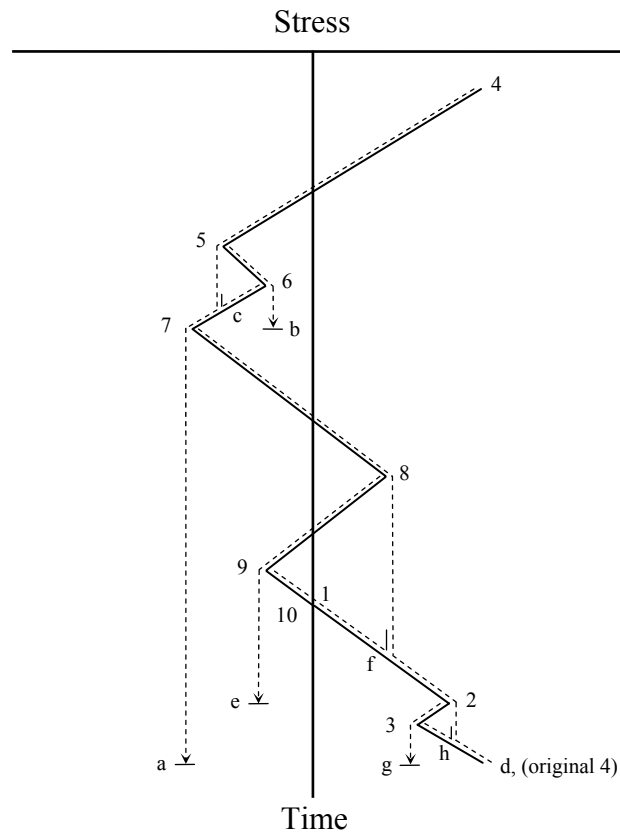


Figure C.2 Modified Rainflow Counting Method for a Variable-Amplitude Stress History (Hoadley et al., 1982).

As shown in Figure C.1, point 4 is the absolute maximum point so the portion 1-4 of the stress history is shifted downward so as to connect point 10 with point 1 of the original history. A new rainflow counting can now proceed. By Rule (1), rainflows 4-a, 8-e and 2-g can be obtained. Also, according to Rule (2), rainflows 5-b and 7-d can be obtained. Finally, rainflows 6-c, 9-f and 3-h are identified. Hence, four complete cycles are formed by the paired cycles which are (4-a, 7-d), (5-b, 6-c), (8-e, 9-f), and (2-g, 3-h). No half cycles are left in the modified Rainflow Counting Method.

## References

- Aaghaakouchak, A., Glinka, G. and Dharmavasan, S. (1989). "A Load Shedding Model for Fracture Mechanics Analysis of Fatigue Cracks in Tubular Joints." *Proceedings of the 8<sup>th</sup> International Conference on Offshore Mechanics and Arctic Engineering*, ASME, Vol. 2, The Hague, Netherlands, pp. 159-166.
- AASHTO Guide Specifications for Fatigue Evaluation of Existing Steel Bridges* (1990), American Association of State Highway and Transportation Officials, Washington, D. C.
- AASHTO LRFD Bridge Design Specifications* (1998), American Association of State Highway and Transportation Officials, Washington, D. C.
- Aker Offshore Partner A. S (1999). "Review of Probabilistic Inspection Analysis Methods." *Offshore Technology Report 061*, Health and Safety Executive, UK.
- Albrecht, P. A. and Yamada, K. (1977). "Rapid Calculation of Stress Intensity Factors." *Journal of Structural Division*, ASCE, Vol.103, No. ST2, pp. 377-389.
- Albrecht, P. and Yazdani, N. (1986). "Risk Analysis of Extending Bridge Service Life." Report No. FHWA/MD. 84/01, Dept. of Civil Engineering, University of Maryland, College Park, MD.
- Ang, A. H.-S. and Munse, W. S. (1975). "Practical Reliability Basis for Structural Fatigue." *Proceedings of ASCE National Structural Engineering Conference*, New Orleans, Louisiana.
- Ang, A. H.-S. and Tang, W. H. (1984). "*Probability Concepts in Engineering Planning and Design; Volume II – Decision, Risk, and Reliability.*" John Wiley & Sons, Inc.
- ASCE Committee on Fatigue and Fracture Reliability, (1982a). "Fatigue Reliability: Introduction." *Journal of the Structural Division*, Proceedings of the American Society of Civil Engineers, ASCE, Vol. 108, No. ST1, pp. 3-23.
- ASCE Committee on Fatigue and Fracture Reliability, (1982b) "Fatigue Reliability: Quality Assurance and Maintainability." *Journal of the Structural Division*, Proceedings of the American Society of Civil Engineers, ASCE, Vol. 108, No. ST1, pp. 25-46.
- ASCE Committee on Fatigue and Fracture Reliability, (1982c) "Fatigue Reliability: Variable Amplitude Loading." *Journal of the Structural Division*, Proceedings of the American Society of Civil Engineers, ASCE, Vol. 108, No. ST1, pp. 47-69.

- ASCE Committee on Fatigue and Fracture Reliability, (1982d) "Fatigue Reliability: Development of Criteria for Design." *Journal of the Structural Division*, Proceedings of the American Society of Civil Engineers, ASCE, Vol. 108, No. ST1, pp. 71-87.
- Bannantine, J. A., Comer, J. J. and Handrock, J. L. (1990). *Fundamentals of Metal Fatigue Analysis*, Prentice Hall, Englewood Cliffs, New Jersey.
- Barsom, J. M. (1973). "Fatigue Crack Growth under Variable-Amplitude Loading in ASTM A514 Grade B Steel." *ASTM STP 536*, American Society for Testing and Materials, Philadelphia.
- Barsom, J. M. and Novak, S. R. (1977). "Subcritical Crack Growth in Steel Bridge Members." *National Cooperative Highway Research Program Report 181*, Transportation Research Board, National Research Council, Washington, D.C.
- Barsom, J. M. and Rolfe, S. T. (1999). *Fracture and Fatigue Control in Structures: Applications of Fracture Mechanics*, 3<sup>rd</sup> Edition, Butterworth-Heinemann, Massachusetts, USA.
- Basquin, O. H. (1910). "The Exponential Law of Endurance Test." *Proceedings of the American Society of Testing and Materials*, 10, pp. 625-630.
- Berens, A. P. and Hovey, P. W. (1981). "Evaluation of NDE Reliability Characterization." *AFWAL-TR-81-4160*, Vol. 1, Air Force Wright-Aeronautical Laboratory, Wright-Patterson Air Force Base.
- Berens, A. P. (1989). *NDE Reliability Analysis*. In: *Metals Handbook*, Vol. 17. 9<sup>th</sup> ed. ASM International, pp. 689-701
- Berge, S. and Eide, D. I. (1981). "Residual Stress and Stress Interaction in Fatigue Testing on Welded Joints." Norwegian Institute of Technology, Trondheim.
- Bokalrud, T. and Karlsen, A. (1982). "Control of Fatigue Failure in Ship Hulls by Ultrasonic." Norwegian Maritime Research No. 1.
- British Standard Institution (BSI), (1991). "Guidance on Methods for Assessing the Acceptability of Flaws in Fusion Welded Structures." *British Standard PD6493*, London, UK.
- British Standard Institution (BSI), (1997). "Guide on Methods for Assessing the Acceptability of Flaws in Fusion Welded Structures." *British Standard BS7910*, London, UK.

- Coffin, L. F. (1954). "A Study of the Effects of Cyclic Thermal Stresses on a Ductile Metal." *Transactions of the American Society of Mechanical Engineers*, 76, pp. 931-950.
- Cortie, M. B. and Garrett, G. G. (1988). "On the Correlation Between C and m in the Paris Equation for Fatigue Crack Propagation." *Engineering Fracture Mechanics*, Vol. 30, No. 1, pp. 49-58.
- Cramer, E. H. and Friis-Hansen, P. (1992). "Reliability Based Optimization of Multi-Component Welded Structures." *Proceedings of the 11<sup>st</sup> International Conference on Offshore Mechanics and Arctic Engineering*, ASME, Vol. 2, Calgary Canada, pp. 265-271.
- Cremona, C. (1996). "Reliability Updating of Welded Joints Damaged by Fatigue." *International Journal of Fatigue*, Vol. 18, No. 8, pp. 567-575.
- Dharmavasan, S., Faber, M. H., Dijkstra, O. D., Cervetto, D. and Manfredi E. (1994). "Reliability Based Inspection Scheduling for Fixed Offshore Structures." *Proceedings of the 13<sup>th</sup> International Conference on Offshore Mechanics and Arctic Engineering*, ASME, Vol. 2, Houston USA, pp. 227-235.
- DNV, (1984). *Fatigue Strength Analysis for Mobile Offshore Units: Classification Notes No. 30.2*, Det Norske Veritas, Høvik, Norway.
- DNV, (1988). *Recommended Practices*, DNV-RP-404, Det Norske Veritas, Høvik Norway.
- Dowling, N. E. (1993). *Mechanical Behavior of Materials*, Prentice Hall, Englewood Cliffs, New Jersey.
- Engesvik, K. M. and Moan, T. (1983). "Probabilistic Analysis of the Uncertainty in the Fatigue Capacity of Welded Joints." *Engineering Fracture Mechanics*, Vol. 18, No. 4, pp. 743-762.
- Faber, M. H., Sorensen, J. D. and Kroon, I. (1992a). "Optimal Inspection Strategies for Offshore Structural Systems." *Proceedings of the 11<sup>st</sup> International Conference on Offshore Mechanics and Arctic Engineering*, ASME, Vol. 2, Calgary Canada, pp. 145-151.
- Faber, M. H., Sorensen, J. D., Rackwitz, R., Thoft-Christensen, P. and Bryla, P. (1992b). "Reliability Analysis of an Offshore Structure: A Case Study 1." *Proceedings of the 11<sup>st</sup> International Conference on Offshore Mechanics and Arctic Engineering*, ASME, Vol. 2, Calgary Canada, pp. 449-455.

- Fan, Y., Sarkar, S. and Lasdon, L. S. (1988). "Experiments with Successive Quadratic Programming Algorithms." *Journal of Optimization Theory and Applications*, Vol. 56, No. 3, pp. 359-383.
- Fisher, J. W., Frank, K. H., Hirt, M. A and McNamee, B. M. (1970). "Effect of Weldments on the Fatigue Strength of Steel Beams." *National Cooperative Highway Research Program Report 102*, Transportation Research Board, National Research Council, Washington, D. C.
- Fisher, J. W. (1984). *Fatigue and Fracture in Steel Bridges: Case Studies*, John Wiley & Sons, Inc.
- Frangopol, D. M., Lin, K. Y. and Estes, A. (1997). "Life-Cycle Cost Design of Deteriorating Structures." *Journal of Structural Engineering*, ASCE, Vol. 123, No. 10, pp. 1390-1401.
- Fujita, M., Schall, G. and Rackwitz, R. (1989). "Adaptive Reliability-Based Inspection Strategies for Structures Subject to Fatigue." *Proceedings of the 5<sup>th</sup> International Conference on Structural Safety and Reliability*, pp. 1619-1626.
- Garbatov, Y. and Soares, C. G. (1998). "Fatigue Reliability of Maintained Welded Joints in the Side Shell of Tankers." *Journal of Offshore Mechanics and Arctic Engineering*, ASME, Vol. 120, pp. 2-9.
- Gurney, T. R. (1983). "Fatigue Tests under Variable Amplitude Loading." *Report No. 220/83*, The Welding Institute, Cambridge, UK.
- Hartle, R. A., Amrhein, W. J., Wilson III, K. E., Bauhman, D. R. and Tkacs, J. J. (1995). "Bridge Inspector's Training Manual 90." *FHWA-PD-91-015*, Federal Highway Administration, Washington, D. C.
- Hasofer, A. M. and Lind, N. C. (1974). "Exact and Invariant Second-Moment Code Format." *Journal of Engineering Mechanics Division*, ASCE, Vol. 100, pp. 111-121.
- Hertzberg, R. W. (1995). "On Calculation of Closure-Free Fatigue Crack Propagation Data in Monolithic Metal Alloys." *Materials Science and Engineering A*, Vol. 190, pp. 25-32.
- Hirt, M. A. and Fisher, J. W. (1973). "Fatigue Crack Growth in Welded Beams." *Engineering Fracture Mechanics*, Vol. 5, pp. 415-429.
- Hoadley, P. W., Frank, K. H. and Yura, J. A. (1982), "Estimation of the Fatigue Life of A Test Bridge from Traffic Data." *Research Report No. 247-4*, Center of Transportation Research, The University of Texas at Austin, Texas.

- Holmes, R. and Kerr, J. (1982). "Fatigue Strength of Welded Connections Subjected to North Sea Environment and Random Load Condition." *Proceedings of the 3<sup>rd</sup> International Conference on Behavior of Offshore Structures*, Vol. 2, BOSS, Boston, MA.
- Hong, H. P. (1997). "Reliability Analysis with Nondestructive Inspection." *Structural Safety*, Vol. 19, No. 4, pp. 383-395.
- Hovde, G. O. and Moan, T. (1994). "Fatigue Reliability of TLP Tether System Considering the Effect of Inspection and Repair." *Behavior of Offshore Structures*, Vol. 3, pp. 85-100.
- Hovde, G. O. and Moan, T. (1997). "Fatigue Reliability of TLP Tether System." *Journal of Offshore Mechanics and Arctic Engineering*, ASME, Vol. 119, pp. 53-60.
- Iman, R. L. and Conover, W. J. (1980). "Small Sample Sensitivity Analysis Techniques for Computer Models, with an Application to Risk Assessment." *Communications in Statistics: Theory and Methods*, A9, No. 17, pp. 1749-1842.
- Jiao, G. and Moan, T. (1990). "Methods of Reliability Model Updating Through Additional Events." *Structural Safety*, Vol. 9, No. 2, pp. 139-153.
- Jiao, G. (1992). "Reliability Analysis of Crack Growth with Inspection Planning." *Proceedings of the 11<sup>st</sup> International Conference on Offshore Mechanics and Arctic Engineering*, ASME, Vol. 2, Calgary Canada, pp. 227-235.
- Keating, P. B. and Fisher, J. W. (1986). "Evaluation of Fatigue Tests and Design Criteria on Welded Details." *National Cooperative Highway Research Program Report 286*, Transportation Research Board, National Research Council, Washington, D.C.
- Kirkemo, F. (1988). "Applications of Probabilistic Fracture Mechanics to Offshore Structures." *Applied Mechanics Review*, Vol. 42, No. 2, pp. 61-84.
- Klingerman, D. J. and Fisher, J. W. (1973). "Threshold Crack Growth in A36 Steel." *Fritz Engineering Laboratory Report No. 386.2*, Lehigh University, Bethlehem, Pennsylvania.
- Koiter, W. T. (1965). "Note on the stress intensity factor for sheet strips with cracks under tensile load." *Report No. 134*, University of Technology, Laboratory of Engineering Mechanics, Delft, Netherlands.
- Kountouris, I. S. and Baker, M. J. (1989). "Defect Assessment: Analysis of Defects Detected by MPI in an Offshore Structure." *CESLIC Report No. OR6*, Dept. Civil Engineering, Imperial College, London, UK.



- Laman, J. A. and Nowak, A. S. (1996). "Fatigue-Load Models for Girder Bridges." *Journal of Structural Engineering*, ASCE, Vol. 122, No. 7, pp. 726-733.
- Lanning, D. and Shen, M. H. H. (1996). "Reliability of Welded Structures Containing Fatigue Cracks." *Journal of Offshore Mechanics and Arctic Engineering*, ASME, Vol. 118, pp. 300-306.
- Lanning, D. and Shen, M. H. H. (1997). "Fatigue Reliability of Structures Containing Short Cracks." *Proceedings of the 16<sup>th</sup> International Conference on Offshore Mechanics and Arctic Engineering*, ASME, Vol. 2, Yokohama Japan, pp. 229-235.
- Lasdon, L. S., Waren, A. D., Jain, A., and Ratner, M. (1978). "Design and Testing of a Generalized Reduced Gradient Code for Nonlinear Programming." *ACM Transactions on Mathematical Software*, Vol. 4, No. 1, pp. 34-50.
- Liu, W. K., Chen, Y. and Belytschko, T. (1996). "Three Reliability Methods for Fatigue Crack Growth." *Engineering Fracture Mechanics*, Vol. 53, No. 5, pp. 733-752.
- Lotsberg, I., Sigurdsson, G. and Wold, T. P. (1999). "Probabilistic Inspection Planning of the Asgard A FPSO Hull Structure with Respect to Fatigue." *Proceedings of the 18<sup>th</sup> International Conference on Offshore Mechanics and Arctic Engineering*, ASME, Vol. 2, St. John's Canada, pp. 259-266.
- Lukic, M. and Cremona, C. (2001). "Probabilistic Assessment of Welded Joints versus Fatigue and Fracture." *Journal of Structural Engineering*, ASCE, Vol. 127, No. 8, pp. 145-160.
- Madsen, H. O., Krenk, S. and Lind, N. C. (1985). *Methods of Structural Safety*, Prentice-Hall Inc., Englewood Cliffs, New Jersey.
- Madsen, H. O., Sorensen, J. D. and Olesen, R. (1989). "Optimal Inspection Planning for Fatigue Damage of Offshore Structures." *Proceedings of the 5<sup>th</sup> International Conference on Structural Safety and Reliability*, pp. 2099-2106.
- Manning S. D., Yang, J. N. and Rudd, J. L. (1986). "Durability Analysis of Aircraft Structures." *Probabilistic Fracture Mechanics and Reliability*, Chapter 5, American Society of Testing and Materials, Special Technical Publication.
- Manson, S. S. (1954). "Behaviour of Materials under Condition of Thermal Stress." *National Advisory Commission on Aeronautics*, Report 1170, Lewis Flight Propulsion Laboratory, Cleveland.
- Massarelli, P. and Baber, T. (2001). "Fatigue Reliability of Steel Highway Bridge Details." *Final Report VTRC 02-R4*, Virginia Transportation Research Council, Charlottesville, Virginia.

- Matsuishi, M. and Endo, T. (1968). "Fatigue of Metals Subjected to Varying Stress." paper presented to Japan Society of Mechanical Engineers, Fukuoka, Japan.
- Mayfield, M. E. and Maxey, W. A. (1982). "ERW Weld Zone Characteristics." NG-18 Report No. 130, American Gas Association, Arlington, Virginia.
- Melchers, R. E. (1989). "Improved Importance Sampling for Structural Reliability Calculation." *Proceedings of the 5<sup>th</sup> International Conference on Structural Safety and Reliability*, pp. 1185-1192.
- Miller, I. and Freund, J. E. (1985). *Probability and Statistics for Engineers*, 3<sup>rd</sup> Edition, Prentice-Hall Inc., Englewood Cliffs, New Jersey.
- Miner, M. A. (1945). "Cumulative Damage in Fatigue." *Journal of Applied Mechanics*, Vol. 12, No. 3, pp. 159-164.
- Moan, T., Hovde, G. O. and Blanker, A. M. (1993). "Reliability-Based Fatigue Design Criteria for Offshore Structures Considering the Effect of Inspection and Repair." *Proceedings of Offshore Technology Conference*, pp. 591-600.
- Moan, T., Vardal, O. T., Hellevig, N. C. and Skjoldli, K. (1997). "In-Service Observations of Cracks in North Sea Jackets: A Study on Initial Crack Depth and POD Values." *Proceedings of the 16<sup>th</sup> International Conference on Offshore Mechanics and Arctic Engineering*, ASME, Vol. 2, Yokohama, Japan, Paper 1335.
- Moses, F., Schilling, C. G. and Raju, K. S. (1987). "Fatigue Evaluation Procedures for Steel Bridges." *National Cooperative Highway Research Program Report 299*, Transportation Research Board, National Research Council, Washington, D. C.
- Nolte, K. G. and Hansford, J. E. (1976). "Closed-Form Expressions for Determining the Fatigue Damage of Structures Due to Ocean Waves." *Proceedings of Offshore Technology Conference*, Vol. 2, Houston Texas, pp. 861-870.
- Onoufriou, T. (1999). "Reliability Based Inspection Planning of Offshore Structures." *Marine Structures*, Vol. 12, pp. 521-539.
- Ortiz, K. and Kiremidjian, A. (1984). "A Fatigue Reliability Model for Offshore Structures." *Proceedings of the 4<sup>th</sup> ASCE Specialty Conference on Probabilistic Mechanics and Structural Reliability*, Berkeley California, pp. 363-366.
- Paris, P. C. (1964). "The Fracture Mechanics Approach to Fatigue." *Fatigue – An Interdisciplinary Approach*, Syracuse University Press, Syracuse, New York, pp. 107-132.

- Paris, P. C. and Erdogan, F. (1963). "A Critical Analysis of Crack Propagation Laws." *Journal of Basic Engineering*, ASME, Vol. 85, pp. 528-534.
- Pederson, C., Madsen, H. O., Nielson, J. A., Ribler, J. P. and Krenk, S. (1992). "Reliability Based Inspection Planning for the Tyra Field." *Proceedings of the 11<sup>st</sup> International Conference on Offshore Mechanics and Arctic Engineering*, ASME, Vol. 2, Calgary, Canada, pp. 255-263.
- Rackwitz, R. and Fiessler, B. (1978). "Structural Reliability under Combined Random Load Sequences." *Computers and Structures*, Vol. 9, pp. 484-494.
- Righiniotis, T. D. and Chryssanthopoulos, M. K. (2003). "Probabilistic Fatigue Analysis under Constant Amplitude Loading." *Journal of Constructional Steel Research*, Vol. 59, pp. 867-886.
- Righiniotis, T.D. (2004). "Influence of Management Actions on Fatigue Reliability of a Welded Joint." *International Journal of Fatigue*, Vol. 26, No. 3, pp. 231-239.
- Rippling, E. R. and Crosley, P. B. (1983). *Narrative Summary on Fracture Control in Relation to Bridge Design*, Federal Highway Administration, Washington, D. C.
- Roberts, R., Irwin, G. R., Fisher, J. W., Chen, G., Chakravarti, P., Ma, Z. Z. and Yen, B. T. (1986). "Corrosion Fatigue Characteristics of Bridge Steels." Vol. 1: Executive Summary, *Report FHWA/RD-86/165*, Federal Highway Administration, Washington, D.C.
- Rudd, J. L. and Gray, T. D. (1977). "Quantification of Fastener Hole Quality." *Proceedings of the 18<sup>th</sup> AIAA/ASME/SAE Structures, Structural Dynamics and Materials Conference*.
- Rudd, J. L., Yang, J. N., Manning, S. D. and Garver, W. R. (1982a). "Durability Design Requirements and Analysis for Metallic Airframe." *Design of Fatigue and Fracture Resistant Structures*, ASTM STP 761, pp. 133-151.
- Rudd, J. L., Yang, J. N., Manning, S. D. and Yee, B. G. W. (1982b). "Damage Assessment of Mechanically Fastened Joints in the Small Crack Size Range." *Proceedings of the 9<sup>th</sup> US National Congress of Applied Mechanics*.
- Rudd, J. L., Yang, J. N., Manning, S. D. and Yee, B. G. W. (1982c). "Probabilistic Fracture Mechanics Analysis Methods for Structural Durability." *Proceedings of AGARD Meeting on Behavior of Short Cracks in Airframe Components*.
- Rummel, W. D. and Matzkanin, G. A. (1997). *Nondestructive Evaluation Capabilities Data Book*, Nondestructive Testing Information Analysis Center, Austin, Texas.

- Rummel, W. D. (1998). "Probability of Detection as a Quantitative Measure of Nondestructive Testing End-to-End Process Capabilities." *Materials Evaluation*, Vol. 56, No. 1, pp. 29-35.
- Schilling, C. G., Klippstein, K. H., Barsom, J. M., and Blake G. T. (1974). "Fatigue of Welded Steel Bridge Members under Variable-Amplitude Loadings." *Research Results Digest No. 60*, Highway Research Board, Washington, D. C.
- Schilling, C. G., Klippstein, K. H., Barsom, J. M., and Blake G. T. (1978). "Fatigue of Welded Steel Bridge Members under Variable-Amplitude Loadings." *National Cooperative Highway Research Program Report 188*, Transportation Research Board, National Research Council, Washington, D. C.
- Schittkowski, K. (1985). "NLPQL: A Fortran Subroutine for Solving Constrained Nonlinear Programming Problems." *Annals of Operations Research*, Vol. 5, pp. 485-500.
- Schütz, W. (1979). "The Prediction of Fatigue Life in the Crack Initiation and Propagation Stages – A State of Art Survey." *Engineering Fracture Mechanics*, Vol. 11, No. 2, pp. 405-421.
- Shetty, N. K. and Baker, M. J. (1990). "Fatigue Reliability of Tubular Joints in Offshore Structures: Reliability Analysis." *Proceedings of the 9<sup>th</sup> International Conference on Offshore Mechanics and Arctic Engineering*, ASME, Vol. 2, Houston, USA, pp. 223-230.
- Shetty, N. K. (1992). *System Reliability of Fixed Offshore Structures under Fatigue Deterioration*, PhD Dissertation, Imperial College, UK.
- Shin, Y. S. and Lukens, R. W. (1983). "Probability Based High Cycle Fatigue Life Prediction." *Random Fatigue Life Prediction*, ASME, Vol. 72, New York, pp. 73-88.
- Shinozuka, M. (1979). "Durability Methods Development." Vol. 4: Initial Quality Representation, *AFFDL-TR-79-3118*.
- Skjong, R. and Bitner-Gregersen, E. M. (2002). "Cost Effectiveness of Hull Girder Safety." *Proceedings of the 21st International Conference on Offshore Mechanics and Arctic Engineering*, ASME, Vol. 2, Oslo Norway, pp. 583-590.
- Snyder, R. E., Likins, G. E. and Moses, F. (1985) "Loading Spectrum Experienced by Bridge Structures in the United States." *Report FHWA/RD-85/012*, Bridge Weighing Systems, Inc., Warrensville, Ohio.

- Sommer, A. M., Nowak, A. S. and Thoft-Christensen, P. (1993). "Probability-Based Bridge Inspection Strategy." *Journal of Structure Engineering*, ASCE, Vol. 119, No. 12, pp. 3520-3536.
- Sorensen, J. D., Faber, M. H., Rackwitz, R. and Thoft-Christensen, P. (1991). "Modelling in Optimal Inspection and Repair." *Proceedings of the 10<sup>th</sup> International Conference on Offshore Mechanics and Arctic Engineering*, ASME, Vol. 2, Stavanger Norway, pp. 281-288.
- Spellucci, P. (1998). "A SQP Method for General Nonlinear Programs Using Only Equality Constrained Subproblems." *Mathematical Programming*, Vol. 82, No. 3, pp. 413-448.
- Suwan, S. (2002). "Analysis of Structural Plate Mechanical Properties: Statistical Variability and Implications in Structural Reliability." M. S. Thesis, Department of Civil Engineering, University of Texas at Austin.
- Suwan, S., Manuel, L. and Frank, K. H. (2003). "Statistical Analysis of Structural Plate Mechanical Properties." PMFSEL Report No. 03-1, Phil M. Ferguson Structural Engineering Laboratory, The University of Texas at Austin.
- Tada, H., Paris, P. C. and Irwin, G. R. (1973). *The Stress Analysis of Crack Handbook*, 1<sup>st</sup> ed. Del Research Corporation, Hellertown, PA.
- Tada, H., Paris, P. C. and Irwin, G. R. (1985). *The Stress Analysis of Crack Handbook*, 2<sup>nd</sup> ed. Paris Productions Incorporated, St. Louis, MO.
- Tang, J. P. and Yao, J. T. P. (1972). "Fatigue Damage Factor in Structural Design." *Journal of the Structural Division, Proceedings of the American Society of Civil Engineers*, ASCE, Vol. 98, No. ST1, pp. 125-134.
- Thoft-Christensen, P. and Sorensen, J. D. (1987). "Optimal Strategy for Inspection and Repair of Structural Systems." *Civil Engineering System*, Vol. 4, pp. 94-100.
- Visual Numerics (1997). *IMSL – FORTRAN Subroutines for Mathematical Applications*, Math/Library Volume 2.
- Wirsching, P. H. (1979). "Fatigue Reliability in Welded Joints of Offshore Structures." *Proceedings of Offshore Technology Conference*, Vol. 1, pp. 197-202.
- Wirsching, P. H. (1980). "Fatigue Reliability in Welded Joints of Offshore Structures." *International Journal of Fatigue*, Vol. 2, No. 2, pp. 77-83.
- Wirsching, P. H. (1984). "Fatigue Reliability for Offshore Structures." *Journal of Structural Engineering*, ASCE, Vol. 110, No. 10, pp. 2340-2356.

- Wirsching, P. H. and Chen, Y. N. (1987). "Fatigue Design Criteria for TLP Tendons." *Journal of Structural Engineering*, ASCE, Vol. 113, No. 7, pp. 1398-1414.
- Wirsching, P. H., Ortiz, K. and Chen, Y. N. (1987). "Fracture Mechanics Fatigue Model in a Reliability Format." *Proceedings of the 6<sup>th</sup> International Symposium on OMAE*, Houston Texas, pp. 331-337.
- Wirsching, P. H. and Chen, Y. N. (1988). "Consideration of Probability-Based Fatigue Design for Marine Structures." *Marine Structures*, Vol. 1, pp. 23-45.
- Wirsching, P. H. and Torng, Y. (1989). "Optimal Strategies for Design, Inspection, and Repair of Fatigue Sensitive Structural Systems Using Risk-Based Economics." *Proceedings of the 5<sup>th</sup> International Conference on Structural Safety and Reliability*, pp. 2107-2114.
- Ximenes, M. C. C. and Mansour, A. E. (1991). "Fatigue System Reliability of TLP Tendons Including Inspection Updating." *Proceedings of the 10<sup>th</sup> International Conference on Offshore Mechanics and Arctic Engineering*, ASME, Vol. 2, Stavanger Norway, pp. 203-211.
- Yamada, K. and Albrecht, P. (1976). "Fatigue Design of Welded Bridge Details for Service Stresses." *Transportation Research Record 607*, Transportation Research Board, Washington, D. C.
- Yang, J. N. and Trapp, W. J. (1974). "Reliability Analysis of Aircraft Structures under Random Loading and Periodic Inspection." *AIAA Journal*, Vol. 12, No. 12, pp. 1623-1630.
- Yang, J. N. (1980). "Statistical Estimation of Economic Life for Aircraft Structures." *Journal of Aircraft AIAA*, Vol. 17, No. 7, pp. 528-535.
- Yang, J. N., Manning, S. D., Rudd, J. L. and Hsi, W. H. (1985). "Stochastic Crack Propagation in Fastener Holes." *Journal of Aircraft*, AIAA, Vol. 22, No.9, pp. 810-817.
- Yao, J. T. P. (1974). "Fatigue Reliability and Design." *Journal of the Structural Division*, Proceedings of the American Society of Civil Engineers, ASCE, Vol. 100, No. ST9, pp. 1827-1836.
- Yao, J. T. P. and Furuta, H. (1986). "Probabilistic Treatment of Fuzzy Events in Civil Engineering." *Journal of Probabilistic Engineering Mechanics*, Vol. 1, No. 1, pp. 58-64.
- Yazdani, N. (1984). *Risk Analysis of Extending Bridge Service Life*, PhD Dissertation, University of Maryland.

- Yazdani, N. and Albrecht, P. (1987). "Risk Analysis of Fatigue Failure of Highway Steel Bridges." *Journal of Structural Engineering*, ASCE, Vol. 113, No. 3, pp. 483-500.
- Yazdani, N. and Albrecht, P. (1989). "Crack Growth Rates of Structural Steel in Air and Aqueous Environments." *Engineering Fracture Mechanics*, Vol. 32, No. 6, pp. 997-1007.
- Zhang, R. and Mahadevan, S. (2000). "Model Uncertainty and Bayesian Updating in Reliability-Based Inspection." *Structural Safety*, Vol. 22, No. 2, pp. 145-160.
- Zhang, R. and Mahadevan, S. (2001). "Fatigue Reliability Analysis Using Nondestructive Inspection." *Journal of Structural Engineering*, ASCE, Vol. 127, No. 8, pp. 957-965.
- Zhao, Z., Haldar, A. and Breen, F. (1994a). "Fatigue-Reliability Evaluation of Steel Bridges." *Journal of Structural Engineering*, ASCE, Vol. 120, No. 5, pp. 1608-1623.
- Zhao, Z., Haldar, A. and Breen, F. (1994b). "Fatigue Reliability Updating through Inspection for Steel Bridges." *Journal of Structural Engineering*, ASCE, Vol. 120, No. 5, pp. 1624-1642.
- Zhao, Z. (1995). *Primary and Deformation-Induced High and Low Cycle Fatigue Reliability of Infrastructure with Updating Through Non-Destructive Inspection*, PhD Dissertation, the University of Arizona.
- Zhao, Z. and Haldar, A. (1996). "Bridge Fatigue Damage Evaluation and Updating Using Non-destructive Inspections." *Engineering Fracture Mechanics*, Vol. 53, No. 5, pp. 775-788.
- Zheng, R. and Ellingwood, B. R. (1998). "Role of Nondestructive Evaluation in Time-Dependent Reliability Analysis." *Structural Safety*, Vol. 20, No. 4, pp. 303-408.

## **Vita**

Hsin-Yang Chung was born in Miaoli, Taiwan to Nien-Hao Chung and Chun-Mei Chen on February 25, 1972. After graduating from Taipei Municipal Chien-Kuo High School in June 1990, he entered National Chen Kung University in Tainan, Taiwan that same fall. In June of 1994, he received a Bachelor of Science degree in Civil Engineering with highest distinction and was ranked first in his class. Soon after graduation he was admitted to the graduate program of structural engineering in the same department. He received his Master of Science degree in Civil Engineering in June 1996. After two-year mandatory military service as a second lieutenant in the army, he was employed as a teaching assistant in Department of Civil Engineering at Tamkang University in Tamsui, Taiwan in 1998. In August of 2000, he enrolled in the doctoral program in civil engineering at the University of Texas at Austin. During his doctoral studies, he worked as a research assistant at the Phil M. Ferguson Structural Engineering Laboratory and a teaching assistant in Civil Engineering Department.

Permanent address: 1<sup>st</sup> Floor, No. 1 Her-Pyng Road  
Miaoli 360, Taiwan

This dissertation was typed by the author.